Sathish-Kumar Kamaraj
Arun Thirumurugan
Shanmuga Sundar Dhanabalan
Samuel A. Hevia *Editors*

Microscopic Techniques for the Non-Expert

Springer

Microscopic Techniques for the Non-Expert

Sathish-Kumar Kamaraj
Arun Thirumurugan
Shanmuga Sundar Dhanabalan
Samuel A. Hevia
Editors

Microscopic Techniques for the Non-Expert

Springer

Editors
Sathish-Kumar Kamaraj
Departamento de Ingeniería
Instituto Tecnológico El Llano
Aguascalientes (ITEL)/Tecnológico
Nacional de México (TecNM)
Aguascalientes, Mexico

Shanmuga Sundar Dhanabalan
School of Engineering
RMIT University
Melbourne, VIC, Australia

Arun Thirumurugan
Sede Vallenar
Universidad de Atacama
Vallenar, Chile

Samuel A. Hevia
Institute of Physics
Pontifical Catholic University of Chile
Casilla 306, RM - Santiago, Chile

ISBN 978-3-030-99541-6 ISBN 978-3-030-99542-3 (eBook)
https://doi.org/10.1007/978-3-030-99542-3

This Springer imprint is published by the registered company Springer Nature Switzerland AG
The registered company address is: Gewerbestrasse 11, 6330 Cham, Switzerland

Preface

In the era of nanotechnology, microscopic techniques are playing a vital role in any technological advancement of various multidisciplinary research area. Behind the scenes, nature always resides its secrets in a different form. One of the classical examples in the physical world is electromagnetic radiation (EM). We have known long before that EM radiation is like a wave, capable of showing interference and diffraction. The latter finding reveals one more additional property which is the particle nature of light composed of massless photons having discrete energy and momentum. This turns the two fold nature of light, the particle-wave duality. The light source and corresponding frequency levels are used to magnify the objects in the Microscope. The classical light source microscopes reported in the seventeenth century were able to increase the magnification by adjusting the depth of focus which could magnify as high as 1000 times of specimens. This could further lead to the origin of Microbiology field. The resolving powers of the light microscope are limited by 400 and 700 nm wavelength sources that are able to produce 200 manometers (0.2 microns, 0.2 μ meters). In the early 1930s, the introduction of the source of the electron beam as a magnifying source with the aid of a magnetic lens under the high vacuum resulted in the possibility of magnifying 100,000 times of specimens. The resolving power of electron microscope is capable of 0.1 nm is due to a few thousand of electron volt beam source. In 2014, the Nobel Prize in Chemistry was awarded to Eric Betzig, Stefan W. Hell, and William E. Moerner for having bypassed the limitation of optical microscopy resolution better than 0.2 mm. With the aid of fluorescent molecules, two separate techniques such as stimulated emission depletion (STED) microscopy and single-molecule microscopy are exploited to improve the resolution. Stimulated emission depletion (STED) microscopy—were used two laser beams, first stimulates to glow the fluorescent molecules, the second one selects the fluorescent with the nanometer-sized volume. While scanning the specimen by nanometer range, yields an image with a greater resolution which is better than the Abbe's stipulated limit. Single-molecule microscopy—this method helps to switch on individual fluorescence and scans the same area multiple times, each time scattered molecules glow. The final superimposed images, yields a dense super resolved image at the nano scale level. The implement of frequency modulation technique provides a high-resolution image even at the atomic level along with the chemical structure and surfaces of various samples. That is called scanning probe microscopy technique in the general category. It is based upon

scanning the probe on the surface of the samples, while it monitors some interaction between the probe and the surface. There are two state-of-the-art of interaction monitoring named as scanning tunnelling microscopy (STM) and atomic force microscopy (AFM). The STM can monitor the interaction between the metallic tip and a conducting sample surface to find the tunnelling current under the non-physical contact mode. AFM is capable of monitoring the van der Waals force between the tip and the surface. This could either function in contact mode (short range of repulsive force) or non-contact mode (long range of attractive force). Exploration of this technique is not only limited to the atomic scale resolution of visualization and manipulation of atoms but also able to study the biological important functional molecules (DNA, RNA, and proteins) interactions at the nanoscale domain. The notorious speech by Richard Feynman in 1959 at the California Institute of Technology (Caltech) accelerated toward the finding of the nanoscale dimension. Norio Taniguchi was the first to coin the term "Nanotechnology" ("Nano" means "dwarf" in Greece) in 1974. The progress of new microscopy technologies over the present technologies would lead to the expansion of new field of investigation associated with the technological development in the diverse field. This promotes invading of several technologically advanced processes in various disciplines like energy, environments, and health. Hence, it is mandatory for non-experts to know about the advancement of microscopy techniques. We hope this book would be helpful for us not only in the introductory level but also provide advancements in microscopy techniques to the non-experts.

Aguascalientes, Mexico — Sathish-Kumar Kamaraj
Copiapó, Chile — Arun Thirumurugan
Melbourne, Australia — Shanmuga Sundar Dhanabalan
Casilla 306, Chile — Samuel A. Hevia

Acknowledgment

First of all, we thank the almighty for providing us with good health and a valuable opportunity to complete this book successfully. In our journey toward this book, we express our heartfelt thanks to the series editor and advisory board for accepting our book and for their support and encouragement. We extend our sincere thanks to all authors and reviewers for their valuable contribution and genuine support to complete this book. We have great pleasure in acknowledging various publishers and authors for permitting us the copyright to use their figures and tables.

Kamaraj Sathish-Kumar would like to express his gratitude to Ernesto Lugo Ledesma, Director of Technology Institute of El Llano Aguascalientes (ITEL) and Enrique Fernández Fassnacht Director General of National Technology Institute of México (TecNM) for their constant support and facilities, which made the promotion of research activities possible. Further extensions to the funding agency of the National Council for Science and Technology (CONACyT—México), IT19F245-TecNM, and Secretary of Public Education (SEP-México) for their constant support.

Arun Thirumurugan would like to thank ANID-SA77210070, Chile for the financial support and would like to express his gratitude to Dr. R. Kanagadurai (Presidency College, Chennai, India), Dr. Justin Joseyphus (NIT-T, India), Dr. A. Chandra Bose (NIT-T, India), Dr. T. Srinivasa Rao (NIT-T, India), Prof. P.V Satyam (IOP, India), Dr. K. Ravichandran (AVVM College, TN, India), Dr. Ali Akbari-Fakhrabadi (FCFM, University of Chile, Chile), Prof. Mangala Raja (University of Concepcion, Chile) for their guidance and support. Also, Arun Thirumurugan would like to thank Dr. Prakash (University of Glasgow, UK), Dr. Ganesh Babu (VIT, India), Dr. Udaya Bhaskar Rednam, Dr. Mauricio J. Morel, Dr. Cesar Echeverria E and Yerko Reyes Caamaño (University of ATACAMA, Chile), Mrs. Divya, and Mrs. Silviya Illanes Godoy for their support.

Shanmuga Sundar Dhanabalan would like to express his sincere thanks to Prof. Sivanantha Raja Avaninathan (Alagappa Chettiar Government College of Engineering and Technology, Karaikudi, Tamil Nadu, India), Prof. Marcos Flores Carrasco (FCFM, University of Chile, Chile), Prof. Sharath Sriram, and Prof. Madhu Bhaskaran (Functional Materials and Microsystems, RMIT University, Australia) for their continuous support, guidance, and encouragement.

Samuel A. Hevia would like to thank the Chilean National Agency for Research and Development (ANID) for FONDECYT grant 1201589 and the MINECON-Chile through project Millennium Nucleus MULTIMAT.

Contents

About the Editors

Sathish-Kumar Kamaraj is a research professor and Bio-Nano Interface Technology for Sustainable Energy and Environment research group leader at the Technological Institute of El Llano Aguascalientes, (ITEL)/National Technological Institute of Mexico (TecNM). He received his B.Sc. in Botany (Spln. Industrial Microbiology), Master's in Microbiology, and Postgraduate Diploma in Chemical Information Technology from Madurai Kamaraj University, Tamil Nadu, India. He obtained a Doctorate in Nanoscience and Nanotechnology (2010–2014) at the Center for Research and Advanced Studies of the National Polytechnic Institute (CINVESTAV-IPN), CDMX, Mexico, with the scholarship from the General Directorate of International Relations-Secretary of Public Education Mexico (SEP-Mexico). During the academic period, he received the Best Student Competition Award at Battelle's Second International Symposium on Bioremediation and Sustainable Environmental Technologies (2013), in Jacksonville, Florida, USA. His thesis won the Best Ph.D. Thesis Award from the Mexican Hydrogen Society. His passion for sustainable natural systems triggers him to integrate his knowledge of various fields to address the problems in the area of Energy, Environment, and Health. He believes that the sustainable balance in the environment would lead to the wellness of the living being. He registered various patents in the Mexican Institute of Industrial Property (IMPI) and technology transfer to the industries. He also has relationships with the Government agencies and private sector for circumstantial decision-making. He served as a guest editor and reviewer in international journals.

Arun Thirumurugan is an assistant professor at the Universidad de Atacama, Chile working on the development of nanomaterial for energy and environmental applications. He has completed his Ph.D. (2010–2015) from the National Institute of Technology, Tiruchirappalli, India. He has worked as a postdoctoral fellow (2015–2017) at the Institute of Physics, Bhubaneswar, India, and then worked as a FONDECYT postdoctoral fellow (2017–2020) at the University of Chile, Santiago, Chile. He has vast experience in handling microscopes such as scanning, environmental, and transmission electron microscopes (FESEM, ESEM, TEM, and HRTEM). He has published 68 research articles and 9 book chapters in reputed

international publishers. He is also serving as guest editor for various publications (Springer, Frontiers, and MDPI). He is a life member of the Electron Microscope Society of India and the Magnetics Society of India.

Shanmuga Sundar Dhanabalan works as a researcher at Functional Materials and Microsystems Research Group, School of Engineering, RMIT University, Melbourne, Australia. He received his Ph.D. degree in Flexible Electronics from Anna University, Chennai, in 2017. After working as an Assistant Professor in reputed engineering colleges in India, he has been awarded CONICYT-FONDECYT Postdoctoral Fellowship by the University of Chile, Santiago, Chile, in 2018–2021. He received a project fund of $81,624,000 CLP from FONDECYT (Chilean government) for the project titled "Fabrication of Flexible Siloxane-Based Organic Light Emitting Diodes" as a Principal Investigator at the University of Chile, Santiago, Chile. He serves as a guest editor in reputed international journals of IEEE, Elsevier, and Springer. He has published around 20 papers in the reputed indexed international journals and 6 book chapters. He has participated/presented his works in many national and international conferences. He delivered special lectures, keynote talks in FDP, STTP, workshops, and seminars in various prestigious institutions. He is a fellow member of the Optical Society of India, International Association of Engineers, and Indian Society of Systems for Science and Engineering.

Samuel A. Hevia is an Associate Professor in the Faculty of Physics and Director of Physics Research in the Research Center for Nanotechnology and Advanced Materials, CIEN-UC, at Pontificia Universidad Católica de Chile. He received his Ph.D. in Physics from the Universidad Técnica Federico Santa María in 2009. In 2010, he was a Postdoctoral Fellow in the University of California, San Diego, in the group of the Distinguished Prof. Dr. Ivan K. Schuller. His interests encompass solid-state physics and materials science for application in energy, sensors, and neuromorphic computing. Dr. Hevia has technical expertise in fabrication and characterization of surfaces, thin-films, and nanostructures. He has authored more than 30 publications in international journals, 2 books, and 80+ contributions to scientific congress. He has been advisor to 7 bachelors, 4 masters, 6 Ph.D. students, and 6 postdoctoral fellows. He has participated in 17 grants and in 13 of them as a Principal Investigator.

A Beginner's Guide to Different Types of Microscopes

1

Wilgince Apollon, Sathish-Kumar Kamaraj, Juan Antonio Vidales-Contreras, Humberto Rodríguez-Fuentes, Héctor Flores-Breceda, Juan Arredondo-Valdez, and Alejandro Isabel Luna-Maldonado

Abstract

The microscope has been a great tool for the Scientifics since Zacharias Janssen was invented around 1600. The microscope is very helpful to study morphology and structural features (molecules to atomic) of the microorganisms (Virus, Bacteria, Fungi, and Algae), cell biology, and materials science. Over time, the microscope has evolved, with the aid of different sources of the electromagnetic spectrum that opens new avenues for visualizing seemingly invisible things from cell organelles to atomic resolution. Hence, it is vital to know about the different types of microscopy depending on the field of interest to use. In this chapter, we review the characteristics of the main microscopes. We focus on the types of emitting light sources, such as incandescent lamps, laser light, arc or flash lamps, and LED light. We also present the specifications of image (resolution, magnification, formation) as well as, the classification of microscopes (Compound, Electron and Scanning Probe Microscopes) and a comparison of various of their characteristics. In addition, we show a comparison of various characteristics of the microscopes. We review recent advances that leverage microscopy for robust image analysis.

Wilgince Apollon (✉) · Juan Antonio Vidales-Contreras · Humberto Rodríguez-Fuentes · Héctor Flores-Breceda · Juan Arredondo-Valdez · Alejandro Isabel Luna-Maldonado
Universidad Autónoma de Nuevo León, Facultad de Agronomía, Departamento de Ingeniería Agrícola y de los Alimentos, Nuevo León, México
wilgince.apollon@uanl.edu.mx

Sathish-Kumar Kamaraj
TecNM-Instituto Tecnológico El Llano Aguascalientes (ITEL), Laboratorio de Medio Ambiente Sostenible, El Llano Ags, México
e-mail: alejandro.lunaml@uanl.edu.mx

S.-K. Kamaraj et al. (eds.), *Microscopic Techniques for the Non-Expert*,
https://doi.org/10.1007/978-3-030-99542-3_1

Keywords

Compound microscope · Emitting light sources · Image formation · Scanning probe microscope

1.1 Introduction to the Microscopic World

Microscopes were created to be able to see the smallest living beings and structures on the planet, far smaller than the human eye is capable of seeing unaided. The technology has, of course, developed much over time and today, the presence of modern optical instruments in laboratories dedicated to microbiological studies not only facilitates research but also allows us to obtain very precise results. Before using one of these powerful instruments, however, it is important to know a little about their functionality, as well as learn how to best use them. A microscope has three main functions: (i) to create a large image of the sample, (ii) to provide distinctly and, as far as possible, unequivocal information within the image obtained, and (iii) to make this information visible so that the human eye can comfortably see it, in order to make sense of it.

From its ancient origins with simple lenses over 4000 years ago to the invention of the first so-called compound microscope said to be by Dutch father-and-son team Hans and Zacharias Janssen in 1590, taking into account Galileo's discoveries on the way, the technology used to see the useable has developed with the desire to see evermore. Famously, Robert Hooke was the first to conduct experiments in which he magnified insects and sketched them, publishing Micrographia in 1665 [1] (Fig. 1.1). The microscope he used was lit by a kerosene lamp and used a spherical tank filled with water, a rudimentary microscope by today's standards and yet the images still a delight. Ever since these important, microscopic, milestones, scientists have not stopped observing the world through these, increasingly powerful, scientific instruments. Today, scientists can visualize not only the structures but also the dynamic processes within living cells and all of this in breathtaking detail. Modern microscopes are capable of revealing everything from insulin secretion to chemical crossfire in sections of biological tissue. However, modern microscopes still owe much to the compound microscope the Dutch spectacle makers, Janssen and Janssen developed all those years ago (Fig. 1.2); it consists simply of a pipe (tube) with a glass (lens) at each end. But how did the instrument work? Well, transforming the space between the glasses also modified the amplification. In the Fig. 1.1, we can see the basic concepts of the microscopic world seen in one of Hooke's compound microscopes.

1.1.1 Types of Emitting Light—Sources

Depending on the class of microscope being used, and the reason for using it, several options may present themselves when looking for a light source today. In the

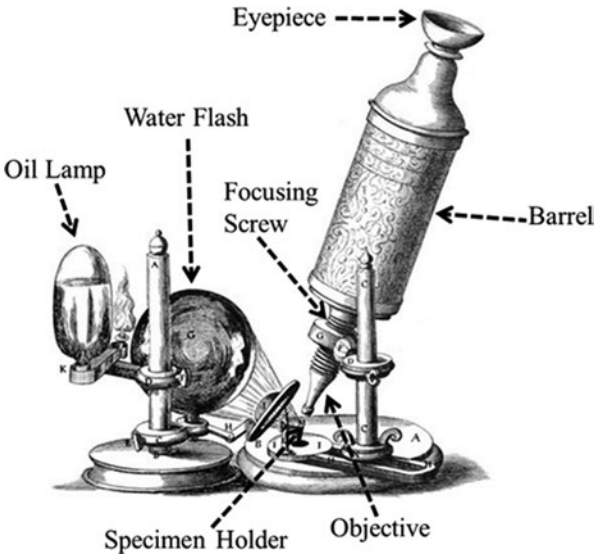

Fig. 1.1 Diagram of a compound microscope designed in 1660s by Robert Hooke. This image was taken and modified from Welcome Library, London; Copyrighted work available under Creative Commons Attribution licence CC BY 4.0: https://creativecommons.org/licenses/by/4.0/

past, ambient light from lamps and the sun were used to provide an external source of illumination, which were very effective in their day. Early microscopists commonly used ingenious methods of collecting and focussing light, using, for example, the reflection from a large whiteboard. However, a more reliable source of illumination was needed and thusly many alternatives have been developed over time.

The incandescent light bulb is still the most common light source for modern microscopes and is made of tungsten-halogen that is placed in a pensive casing, projecting illumination via the collecting lens and toward the subplate's condenser. To control the electric potential of the lamp, a resistor is used, which is incorporated into the microscope holder. The halogen tungsten lamp (bulb), consumes a constant current (CC) (voltage of 12 volts), which generates power of 100 volts. The DC power supply serves as a voltage controller for the lamp, commonly constructed into the microscope lodging, with a potentiometer controlled using an electric potential actuator button installed elsewhere on the microscope stand. Lightbulbs generally produce a great deal of heat throughout the microscope's operating period; however, the casing (made up of many layers of heat sinks) functions by dissipating the excess heat. Below, we present three types of emitting light sources.

1.1.1.1 Incandescent Lamps

As stated, these lamps are the main source of illumination used in modern microscopes; which are different from those used for investigations of fluorescence microscopy. These types of lamps transmit an uninterrupted spectrum of

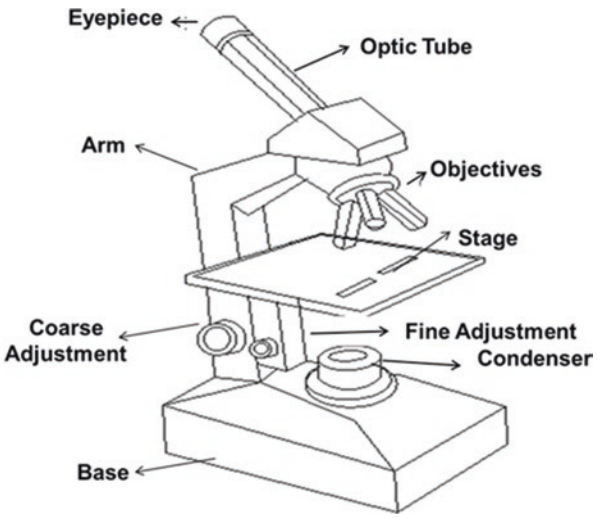

Fig. 1.2 Compound microscope design

illumination which ranges from 300 to more than 1200–1400 nanometers (nm). During the transmission of illumination's spectrum, most of the wavelength intensity is centralized between the ranges of 600 to 1200 nm area. Both the configurations, the construction and the operation of these lamps are very simple. They consist of a closed-lens light bulb stuffed with an inactive gas containing a wire filament made of tungsten fed with an electric current from direct current (DC). During operation, bulbs generate a lot of heat and light, yet this light represents only 5% of energy generation. The color, heat, and luminosity of these categories of lamps vary with the requested voltage, however, the average values are in a range between 2200°K and 3400°K [2].

1.1.1.2 Laser Light Sources

In the past few decades, the use of lasers, such as the argon-ion laser, which has a high emission capacity at 488 and 514 nm, has increased considerably. Lasers are very useful in laser scanning confocal microscopy, despite their high cost. The compact 405 nm violet lasers (VLs) were designed to replace expensive Ultraviolet lasers (UVLs) for most biological studies. The best performance of a laser is obtained when the maximum excitation wavelength of the dye is nearby to the wavelength of the laser. Other types of lasers are (i) Red Lasers (633 nm), and (ii) Green Lasers (543 nm), both consisting of helium-neon. In contrast, with these lasers, the maximum wavelength of the laser might not exactly match the maximum excitation of a given dye [3].

In addition, supercontinuum white light lasers are other categories of light sources that have been used in the past decades. In a comprehensive review on technology and applications of supercontinuum white light lasers, the author reported that those technologies could wide spectral coverage from 400 to 2400 nm [4].

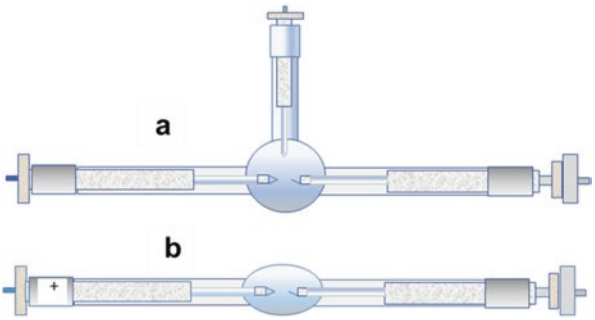

Fig. 1.3 Illustration of (**a**) a type of constructed lamp by the vapour of mercury (Hg) which is furnished with a lighter electrode, and (**b**) a contemporary small flash lamp (HBO 200-watt mercury) feeding with alternate energy via an outward power supply. This image was modified from Wikimedia Commons, copyrighted work available under Creative Common licence CC-BY-SA-4.0. https://commons.wikimedia.org/wiki/Category:CC-BY-SA-4.0

Supercontinuum white light lasers have great potential and the right characteristics to replace conventional light sources, due to their spatial beam profile, as well as their brightness and wavelength tuning combination.

1.1.1.3 Arc or Flash Lamps

According to Lagunas-Solar [5], flash lamps are also an important category in which mostly a gas discharge filled with xenon (Xe) is used. In order to function, an electric current must be employed to a compressed gas of up to 30 atm, allowing the passage of electric current and generating a brilliant wideband radiation emission, e.g., illumination. The spectrum emission of arc lamps includes (a) visible light, (b) alongside some infrared radiation, as well as (c) a significant band of radiation. Nitrogen (N) for vacuum UV can also be exploited to produce various spectra emissions to other UV bands. Arc lamps are built using fused quartz or glass tubes to avoid the absorption of so-called UV photons; Tungsten metal electrodes must also be used at both ends of these lamps.

In addition, mercury vapor-arc lamps (Fig. 1.3a) are another type of valuable light source for expert categories of microscopy [6]. Like arc lamps (Fig. 1.3b), they are also controlled by external lighting sources, which are designed to meet electrical requirements such as turning on the lamp first and then providing the proper current, while maintaining constant illumination. Flash lamps have an average life span of approximately 200 h, whereas most external energy sources are supplied with a timer allowing the microscopist to have control of the elapsed time.

1.1.1.4 LED Light Source

During the last decade, LED light sources have been applied frequently with the main objective of replacing traditional light sources, such as the traditional lamp. LEDs are promising emerging technologies used exclusively for illumination in light microscopy. These versatile semiconductor technologies possess all the desirable characteristics that traditional lamps lack. LEDs have been used because of

their high luminous efficiency, as well as their longer life span and excellent performance in terms of color. These light sources are widely used today. For example, if we want to work in different categories of fluorescent molecules, these are the best option as long as they are chosen with their appropriate spectrum at the time of their installation in the microscopes. Since its implementation, LEDs have been applied in Colibri lighting systems [7] and fluorescence microscopes [8]. Furthermore, LEDs have been used in the detection of individual molecules [9]. Some of the advantages that LEDs have are: their low cost, small size, improved the illumination of the images, provide a spectrum of multiple wavelengths; which are combined with a digital camera system [10]. Finally, LEDs are efficient enough to run on low voltage batteries, and this makes them very economical compared to other light sources.

1.1.2 Microscope Image

1.1.2.1 Image Resolution

The resolution of a person's sight is known to be 200 μm (0.2 mm), compared to a light microscope which has a high-definition capacity and can amplify images up to 1000× to illuminate details down to 0.2 μm [11]. The smallest distinguishable distance between objects (minimum resolvable distance) is known as the resolution limit. The resolution restriction of human sight is around 200 μm. However, the use of a light microscope allows the same items to be seen as two different entities, due to the light microscope's ability to easily distinguish distances of less than 200 μm. This indicates that there is a proportional relationship between the minimum resolvable distance and the resolution of an optical microscope, i.e., the shorter the distance value is, the larger the resolution of the microscope [12]. In Fig. 1.4, we present the different parts of a Light Microscopy.

1.1.2.2 Image Magnification

Theoretically, image enlargement is the process by which the resolution of the image is virtually increased in sequence to highlight details that are implicit in the original image, but not obvious [13]. Image enlargement has different applications. These include, (i) the analysis of satellite images [14], (ii) the visualization of medical images, and (iii) the coincidence of images captured with different sensors. Generally, this type of image requires a large amount of memory (high capacity) to be constituted employing a bidimensional matrix of pixel worth. When using various encoding schemes, the memory demand for warehousing for transmitting is reduced. Furthermore, the bandwidth requirement depends on both (a) the dimension of the image and (b) the type of procedure utilized for encoding. Ideally, it will continue expanding the image by improving the magnification [11]. However, it is difficult to reveal new information of consistent quality on a piece (object) just by enhancing the magnification. For this reason, before applying the technical magnification to any encoded image, it must be transformed to regular form across the decoding procedure, which incurs a few computer-based costs. Additionally, clear

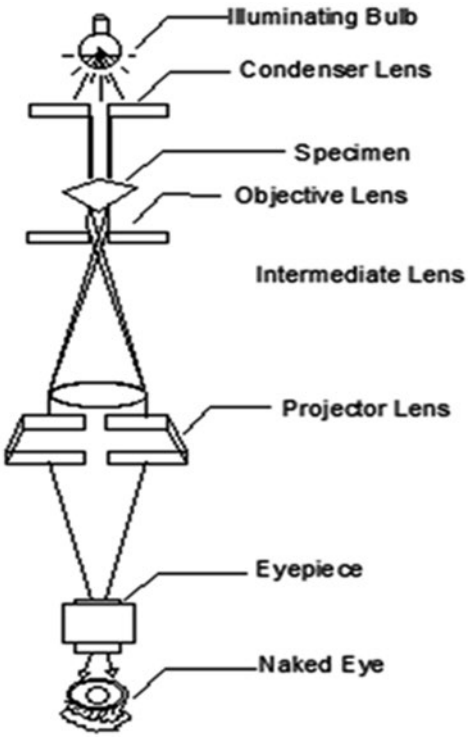

Fig. 1.4 Shematic diagram of a Light Microscopy

Table 1.1 Dimension of the image components through different amplifications for 2000 × 2000-pixel picture or image settlement and 20 × 20 cm exhibit magnitude

Magnitude of image component on the sample	Magnification
10×	10×
1.0 μm	100×
100.0 nm	1000×
10.0 nm	10,000×
2.0 nm	50,000×
1.0 nm	100,000×
0.10 nm	1,000,000×

Note: This table was modified from Ul-Hamid [11] with permission of Springer Nature (Licence number: 5201530877446)

information in an image cannot be determined beyond a certain amplification (magnification); because of the restrictions imposed by both the solving energy of the imaging technique and those of human sight. According to UI-Hamid [11], the magnitude of the image component can be heightened by using a smaller size. Table 1.1 shows the magnification during imaging.

1.1.2.3 Image Formation

The illumination from the optical microscope flashlight moves, by way of the condenser, throughout the sample (specimen), some of the illuminations cross around and some are received via the sample, having been calmed on its way. These types of illuminations are known as deflected, or direct illumination (light). During the image formation, the electron pipe located in the highest area of the column produces an electron beam with power in the range of between approximately 100 eV to 30,000 eV. This is concentrated on a fine probe through so-called electromagnetic glasses (lenses), found inside the column.

In addition, the light diffracted by the sample is focused in different places located on a similar image plane. This diffracted light then causes harmful interference, reducing the power and outcome even in less obscure regions. During the imaging process, the electron ray penetrates the specimen in a teardrop form, expanding with values from100 nm to 5 μm which depend not only on the density of the sample but also on the energy of the beam. Another aspect to consider in this process is the fact that there is an interaction between both the beam and the specimen, producing several indicators including electrons and backscattered X-rays [11, 15]. These are self-possessed and utilized to determine the basic creation of the material sample, as well as producing the images. Figure 1.5 indicates the connection established, one by one, between the points on the display screen and the impact points of the beam on the sample surface.

Furthermore, electrons expanding from a separate position are identified with the support of a kind of detector as an indicator with a determined intensity. This way, from each end (point), where the electron ray relates to the sample and also generates an indicator (signal), it connects the corresponding end on the display monitor; it is displayed as an intensity (I).

Finally, the type of lens is a key factor in image formation. Modern microscope lenses are capable of obtaining real-time images of the samples with the minimum

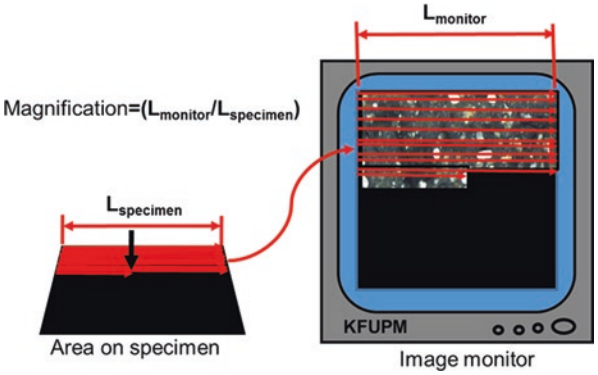

Fig. 1.5 Illustration of the one-to-one connection between the beam locations on the points on the monitor and the specimen (Modified from UI-Hamid [11] with permission of Springer Nature; Licence number: 5201530877446)

possible margin of error. There are different types of microscopes and lenses that are used by researchers in laboratories today. These include (i) the objective lens which helps in the magnification strength needed, (ii) the eyepiece lens that researchers use to view the samples on the slide, (iii) the condenser lens that focuses the light source from the microscope onto the sample (condenser lens can obtain 400× magnification), and (iv) oil-immersion lens which is different with respect to the other lenses. This difference is because you have immersion oil between the lens and the glass slide. In addition, light microscopes are made up of two ocular lenses (5× and 10×) and three objective lenses (5×/10×, 40×, and 90/100×) [16]. Unlike light microscopes, electron microscopes use objective lenses, as well as projector lenses, convergence lenses, intermediate lenses, and eyepieces. Therefore, we can argue that the type of lens affects both the design and the operation of the microscope. The efficiency of a microscope is proportional to the type of lens used.

1.2 Classification of Microscope

Compound microscopes are manufactured to supply an expanded (magnified) bidimensional image, which can be centered radially on consecutive focal planes, thereby, allowing a thorough scan of a specimen's fine structural formation in both 2D and 3D [17]. Various categories of microscopes have been designed, configured, developed, and applied throughout numerous fields of science and technology (Fig. 1.6); however, the vast majority of microscopes could be classified into three

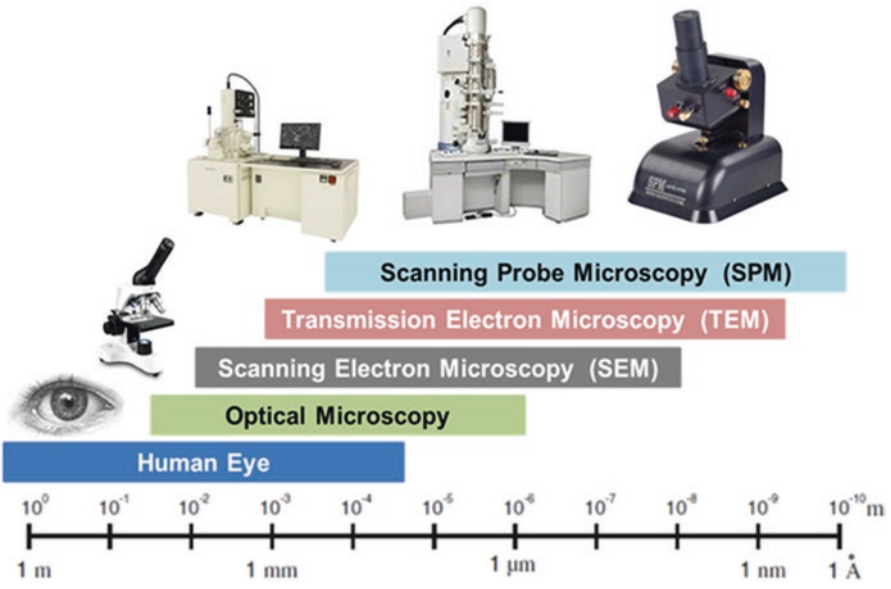

Fig. 1.6 Range of images for different microscopes

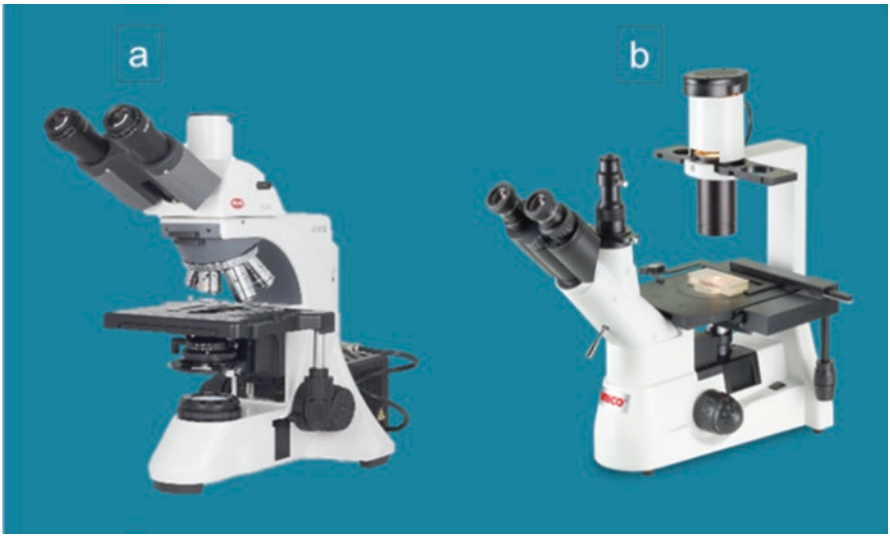

Fig. 1.7 Upright microscope (**a**) and inverted microscope (**b**)

classes: (1) electron microscopes, (2) fluorescence microscopes, and (3) optical microscopes [18].

The human eye can discern objects down to approximately 0.2 mm. Optical microscopes reveal minute objects that could not be seen in any other way and all by using the age-old method of enlarging them with the aid of a combination of glass lenses.

Microscopes can also be classified based on their construction. An upright microscope (Fig. 1.7a) that observes a specimen from above is by far the most well-known and has a seemingly endless number of applications. A reversed microscope (Fig. 1.7b), on the other hand, with its illumination source and capacitor on the top, observes a specimen from below.

An electron microscope with an enlarging lens processes an image of the object from above. Specimen magnifying glasses, however, are biconvex, meaning they are denser at the center than at the edge. The image is seen by the eye as if it was at 25 cm.

1.2.1 Optical Microscope (Light Microscope)

The optical microscope creates a magnified image of a specimen and serves three basic functions, (a) modifying an amplification (magnification), (b) sharpening an image, (c) bringing it into focus, and (d) obtaining clarity. This is also known as an Observation Optical System. The function of illuminating a sample consists of three fundamental roles (i) modifying illumination power, (ii) collecting illumination, and (iii) supplying illumination. It is also known as a Light Optical System. In

addition, a specimen can be projected throughout an optical system [19] and result in a protrusion image to the eyes or a pick-up apparatus such as a CCD (charge-coupled device). Nevertheless, the brightness of the said optical system, is in fact, a result of accumulated illumination emitted from the illumination source and gives the subject the brightness needed to enlighten it. Furthermore, for an inverted microscope, the arrangement liaison between those types of optical systems is, of course, reversed at the center of a sample as compared to an upright microscope. In a system of optical microscopy, monitoring at high heat is accomplished employing a UV CCD camera and UV light while radiant heat is cut off by a UV illumination transference filter [20].

1.2.2 Fluorescence Microscope

This category makes use of a very elevated intensity illumination source that moves a fluorescent source over a useful specimen. These fluorescent sources transmit a low-power illumination of a longer perception which generates the amplified image instead of the initial illumination source. The assimilation and retransmission (reradiation) of illumination by organic and inorganic samples is usually the consequence of a permanent physical occurrence, outlined as being fluorescence. When radiation persists long after the agitation illumination has been put out, the phenomenon is said to be phosphorescence [21].

According to Slavík [22], a fluorescence microscope (FM) is an instrument that authorizes the dynamic acquisition of detail based on the spectroscopic characteristics of fluorescent reporter molecules, at very small degrees of resolution, which can be seen by the naked eye. Furthermore, Fluorescence Lifetime Imaging Microscopy (FLIM) has become a potent and widely used instrument to monitor inter and intramolecular dynamics of fluorophore-labelled proteins inside living cells [23]. FM is a widely used study device deployed throughout disciplines in both biomedical and biological sciences [24]. Finally, FM is the main instrument with which to observe cell physiology [25].

In addition, when reflected illumination, and backdrop fluorescence are passed through this category of microscopy, the targeted parts of a particular specimen can be observed in 3D (Fig. 1.8). This is achieved by way of the application of strong illumination sources, like lasers, that can be focused precisely. This process is carried out frequently across specimens.

In most instances, the specimen in question is treated with a well-known fluorescent material such as a fluorophore and is then illuminated through the lens using an improved power source. The importance of fluorophore is to label cells, tissues, and proteins by using a fluorescent marker for analysis by FM [26]. The illuminating light is then assimilated by the fluorophores and leads them to release a prolonged smaller power frequency illumination. This fluorescent illumination can be separated from the surrounding radiation emission with filters created for that specific wavelength, permitting the observer to see exclusively what is fluorescing [27]. Most of the FM employed in biology nowadays are known as epi-fluorescence

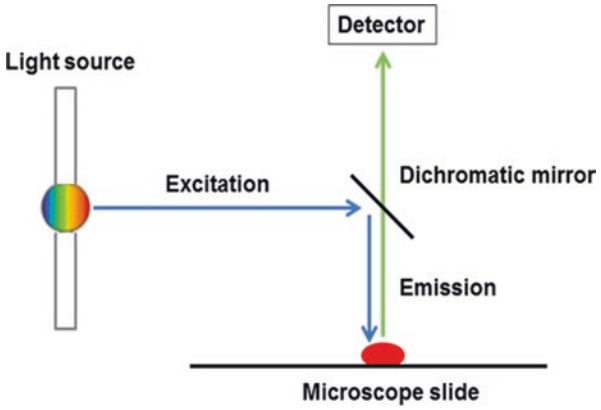

Fig. 1.8 Fundamentals of a fluorescence microscopy

microscopes, meaning that both the agitation and the monitoring (observation) of the fluorescence take place on the specimen. Most FMs use a Xe or Hg arc dismissal (discharge) flashlight for their lighting, as these categories produce a highly intense illumination source. Another class of microscope, corresponds to Total Internal Reflection Fluorescence (TIRF) microscopy, which produces an illuminated light source (e.g., in the range between 50 and 100 nm) located at the interface of the slide itself; this greatly reduces out-of-focus light and improves the ability to identify fluorescent molecules. It has proved to be a critical method in living cell imaging.

1.3 Electron Microscope

Optical microscopes are not able to differentiate any small-scale structure other than the frequency of illumination. For this reason, engineers such as Ernst Ruska and Max Knoll have invented the Electron Microscope (EM). This kind of microscope uses an electron beam as the source of illumination in place of light [28]. This allows for the discerning of the disposition of atoms in materials and obtains atomic level information by way of an electron beam.

1.3.1 Scanning Electron Microscope

An Scanning Electron Microscope (SEM) makes use of a centered beam of high-powered electrons to produce a diversity of indicators on the area of solid samples. Signals are generated from the liaisons between electrons and the specimen, then release the previously unseen details of the said specimen [29].

Figure 1.9 represents a field emission SEM that operates both in variable pressure mode, as well as high vacuum mode; the two functions both use a resolution of

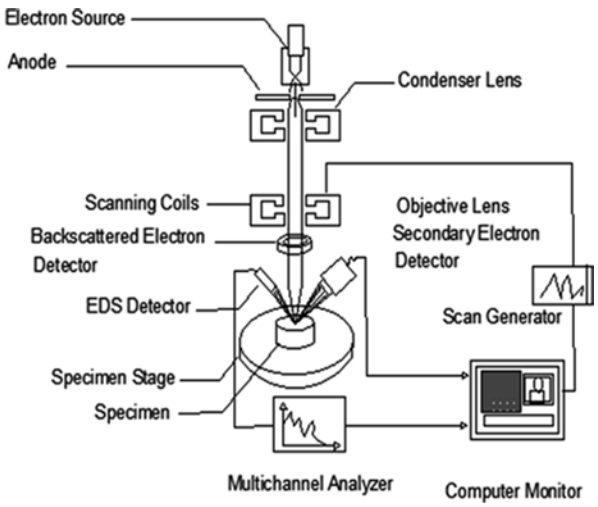

Fig. 1.9 Schematic of a Scanning Emission Microscope

~10 nm. This type of microscope has its characteristics, i.e., it is equipped with (a) an electron detector placed on the lens, (b) an X-ray spectroscopy system made up of the so-called energy dispersion (EDS) that contains drift detectors of Dual silicon (each with an area of 60 mm^2 and a resolution of 123 eV), (c) a cathodoluminescence detector (CL) and (d) with secondary and backscattered electron detectors. In an SEM, images are obtained by scanning the beam showing the signal from an electron detector on a personal computer monitor [30].

An SEM is composed of (a) lenses, a sample chamber, detectors, and a search coil. Secondly, by (b) a source of electrons. For instance, Field Emission Gun (FEG) is made of cerium hexaboride (CeB6) or lanthanum hexaboride (LaB6), and tungsten electron filament (W). Other components of SEMs are Secondary Electron Detector (SED); Energy Scattering Spectroscopy (EDS), and Electron Backscatter Detector (BSD).

One of the characteristics SEMs share is that they always have at least one detector, which is generally of the secondary electron type. Also, most of these instruments have additional detectors. It is understood that the specific abilities of any instrument depend on the detectors that are adapted.

When planning to prepare a specimen for further analysis, its provenance (acquisition) must first be taken into account and of course, its size and whether it will fit into the SEM chamber itself. Secondly, any adjustments are taken into account to avoid charge accumulation in electrically insulating specimens.

Almost all electrically insulating specimens are covered with a significant thin layer of either carbon, gold, or some other metals. In cases in which the elemental analysis of a specimen is crucial or, indeed, a priority, carbon is the most desirable. However, electrically insulating specimens coated with a layer of metal (e.g., gold)

are more effective or safer for applications such as high-resolution electronic imaging. Furthermore, one of the advantages of the electrically insulating specimen is that it can be examined without the use of a conductive coating in an instrument capable of low vacuum operation.

In summary, among the capabilities that these instruments are the following: electrical and metallurgical material failure analysis, polymer and life science, semiconductor design, material identification, forensic science, etc.

1.3.2 Transmission Electron Microscope

A Transmission Electron Microscope (TEM) is an analytical tool permitting visualization and analysis of samples from the lands of micro space (1 μm = 10^{-6} m) to nano space (1 nm = 10^{-9} m). A TEM discloses levels of information and intricacy unreachable by light microscopy due to the fact that it employs a centered beam of high-power electrons. It permits precise microstructural assessment via high-resolution as well as high amplification imaging [31].

The main use of TEM is to process images from a specimen by enlightening the specimen with electrons inside a void and discovering the electrons that are transferred by way of the specimen. By using a TEM, we are able to see all of an atom's column present in crystalline specimens.

A TEM produces a bright-field image (conventional image) of a specimen which can be likened to that of shadow puppetry. For its operation, TEM makes use of a beam of extremely energetic electrons instead of the light of a torch. During operation, through to the specimen being processed, portions of the material deflect or detain electrons more than other portions. Electrons are gathered from below the sample using a phosphorescent monitor (screen). In areas where electrons do not pass through the specimen, the displayed image is obscure, while where electrons cross, the image is brilliant and a range of grays are observed in the middle; which depends greatly on how the electrons interact and are scattered through the sample (Fig. 1.10).

Amplifications of up to 1,000,000× and resolution under 1 nm are commonly reached. Another aspect to consider is that quantitative and qualitative elemental analyses can be provided based on characteristics as minuscule as 1 nm. For instance, for a crystalline stage both the crystal structure, as well as the restrictions of the lattice and the orientation of the specimen can be determined. To our knowledge, inside an atom, there are negatively charged particles called electrons (e−). These, at the same time, cannot be focused with glass lenses compared to photons, which are used by so-called "electromagnets" to focus electrons.

1.4 Scanning Probe Microscope

An Scanning Probe Microscope (SPM) is a tool employed for examining surfaces at a nanoscale level [32]. SPM is employed to produce an exclusive likeness of nanoscale structures and surfaces or maneuvre atoms to displace them in particular

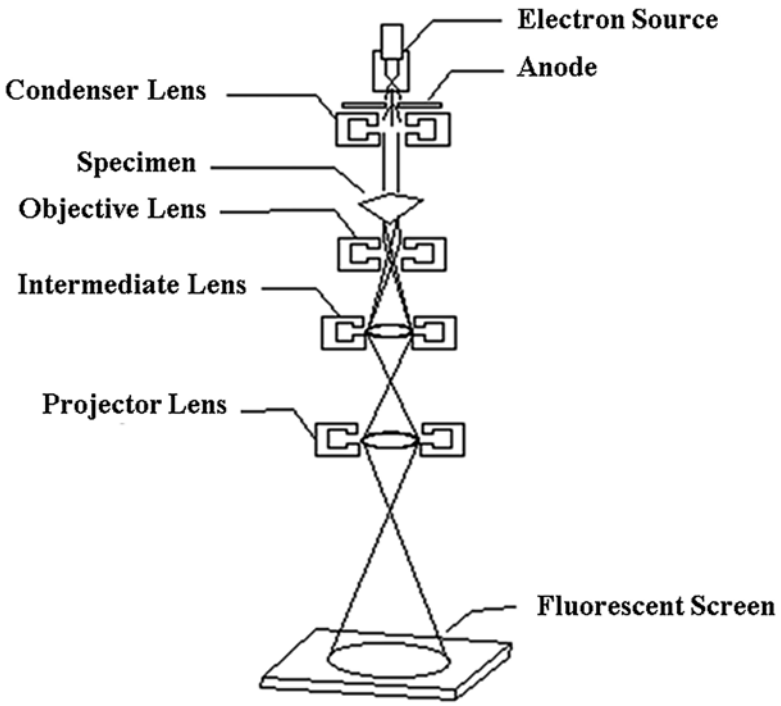

Fig. 1.10 Transmission electron microscope. This figure was modified from Wikimedia Commons: copyrighted work available under Creative Commons Attribution licence CC-BY-2.5 in https://commons.wikimedia.org/wiki/Category:CC-BY-2.5

patterns. It requires a physical probe that examines above the area of a sample collecting details that are employed to create the image or also exploit the atoms.

Generally, the SPM technique has the ability to capture images of surface structures through the use of atomic resolution without harming the specimen. SPMs also offer images in a three-dimensional form. In addition, SPMs can operate without a vacuum, compared to other types of microscope such as optical and electronic microscopes that have that feature or function; instead, they can measure different physical effects. These comprise things such as electrical properties as in magnetic force properties (MFP) or Kelvin probe force microscopy (KPFM).

The SPM possesses a cutting probe point on the final part of a cantilever, which can examine or scan the facet of the sample. The point can even be as narrow as a single atom. A force diverts the cantilever when the point finds near to the facet of the specimen, which may be estimated by a laser thrown back through the cantilever within photodetectors. The tip moves both forward and backward, respectively, in a very controlled manner and the probe can be moved, atom by atom. Deflections originate from various forces such as (a) electrostatic forces, (b) chemicals, (c) van der Waals, (d) capillaries, and (e) mechanical joints.

The details achieved by the laser contemplations identified by the photodetectors are merged to produce an image on a PC. The processed image is colorless as which is a portrayal of characteristics rather than illumination, though they are generally given color by the PC program to aid in distinguishing diverse characteristics of the sample. The conductor does not have a direct view of the area, however, an image constitutes the form of the area. They are extremely strong and could receive a very high definition of until a nanometer.

SPMs form images ordinarily gained as a bidimensional (two-dimensional) grid of data points and displayed as a PC image. In 1982, researchers like Heinrich Rohrer and Gerd from the IBM Research Laboratory in Zurich developed the Scanning Tunnel Microscope (STM); which was the first SPM of its kind. This technology was the first to be acknowledged for having atomic resolution capacity. An STM utilizes an electrical current at the heart of the scanning tip, i.e., of the microscope and the specimen to fabricate an image of the facet of the specimen.

Furthermore, there are diverse methods developed within SPM technology, depending on the aim of the research. SPM can be placed to connection mode, which entails an unchanged force among both the surface of the sample and the cantilever tip. This kind of mode permits perception of the area to be generated quickly. Otherwise, the microscope can be regulated to a tapping manner, and that entails vibration of the cantilever so that the point connects the surface of the sample sporadically. This is most helpful when the research or examine specimen has a squashy surface.

Two main categories of SPM exist: 1) Atomic Force Microscopes (AFMs) and 2) Scanning Tunneling Microscopes (STMs). In both STMs and AFMs, an image is recorded by the automatic movement of a fine tip like a sensor placed near the surface (close to the surface) in lines throughout the specimen; in this respect, the specimen is effectively being scanned. When we talk about a fine tip for these classes of the microscope, we mean a tip with a radius in the minute range between 1 and 10 nm. When placed near the surface, this means at an interval of just a few nanometers. Throughout a scan, the surface is detected and from this detail appears an image of the surface. In the case of scanning transportation, either the specimen or the tip can be displaced. As such, we talk about both a Probe Scanner; and then a Specimen Scanner, respectively [33].

1.4.1 Scanning Tunnelling Microscope

This type of microscope (Scanning Tunnelling Microscope, STM) is based on the straightforward notion of conducting a specimen. The tips are metallic and the specimens are linked to a voltage supply (Fig. 1.11). Then the tip of the STM is brought very close to the specimen until there is a flow of current, called a tunnel current. It should be noted that there is an exponential connection between the flow of the current and the tip at the distance from the specimen. Throughout a scanning process, the point is shifted up and down to keep up a steady current; thus, the point is displacing at an invariable distance from the surface. The underpass energy, in charge

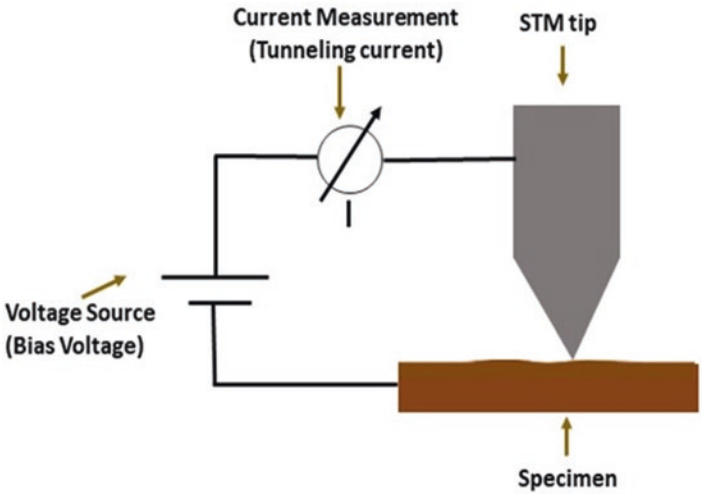

Fig. 1.11 Scanning Tunnelling Microscope

of the imaging passes all over the atom at the tip, which is nearest to the specimen surface. Consequently, when using a tip cut simply, using a normal couple of pincers, atomic resolution can frequently be attained [34].

The voltages employed for STM calculations are commonly under 1 V, therefore, the tip created by the fine tip and the electric field between the specimens is relatively large. When taking into account the atmosphere, it is solely practicable to gain atomic resolution for determining specimens. The simple atomic grid to detect is that of a Highly Oriented Pyrolytic Graphite (HOPG) specimen considering that the top layer from such a specimen may be eliminated using a segment of adhesive tape, disclosing for a short period an atomically clean area.

STMs are generally mainstreamed within an extremely firm scan platform, and the utmost scan zone is approximately in the range between 0.5 and 10 μm. Frequently, STMs are employed in Ultra High Vacuums (UHV), so that a prepared specimen surface might stay untouched for a longer period.

Additionally, to the topography, SPMs may also measure other physical parameters, e.g., in parallel with a scan-type AFM, an energy flux can be measured, or the stage movement of the cantilever oscillation as well as various other physical properties. It is also feasible to register U/I curve, spectrums, as well as all points on the surface, or other details selected. Furthermore, it is feasible to maneuvre the surface. Another example of an extended AFM is the Scanning Near-field Optical Microscope (SNOM). During its operation, additional to the topography is also electromagnetic details (i.e., light) which can be registered. Considering the datasheets of the SPM manufacturers, several abbreviations are observed, which are exclusively three letters long. This indicates that there are various measurement methods. Finally, it is likely to calculate a large number of physical variables (parameters) using both an electrically conductive material and a flexible tip.

1.4.2 Atomic Force Microscope

This kind of microscope uses electrical energy between the microscope's scanning tip and the specimen to obtain an image from the specimen's surface, which must be conductive or semi-conductive, restricting the substances (materials) that can be explored. These restrictions among others have driven the creation of the first Atomic Force Microscope (AFM) [35].

Today, there are AFMs capable of rapid scanning without the loss of either force control or loss of definition. All of this, without additional operating costs or additional complexity. This type of AFM attains instantaneous AFM images with the projected high-definition of a high-efficiency AFM, and they can also scan at >125 Hz when observing a specimen to discover the area of interest, or at duration rates of 1-s/image frame in the air or a liquid.

The AFMs possess a sensor from a fine point at the interface, known as a cantilever. A laser beam is concentrated over the upper part of the cantilever and mirrored over a position detector. In this manner, it is likely to monitor the flexing of the cantilever, even though the thickness is exclusively a few microns, and so very scarcely force is indispensable to flex the cantilever. This force assessment may be employed for a mechanical scanning of the specimen area.

Generally, most AFMs currently function in different modes such as AC or Tapping Mode. A cantilever is agitated through its resonance frequency, which is always oscillating. The sensor voltage, as well as the laser beam, are also oscillating, and it is practicable to estimate a current indicator corresponding to the mechanical oscillation magnitude of the cantilever. The forces take place at both the specimen and the cantilever which are here, one to two orders of dimension littler than for communication manner or mode (i.e., app. 0.1 nN). This outcome in fewer impacts on the specimen's area and longer life of the cantilever tip. The effect on the resolution of this manner of operation has proved to be insignificant and for this reason, it has become the most used mode.

Calculations from a cantilever in AC mode, require that resonance frequency should be determined. Accordingly, the oscillation magnitude at diverse frequencies (i.e., the frequency spectrum) is monitored. The resonance frequency is perceived in the frequency spectrum as a peak at a particular height and width. Therefore, each cantilever possesses numerous resonance frequencies because it might oscillate in various ways and various directions. The scanner sensitivity is improved with a very high Q factor (i.e., the correlation between the width and the resonance of the peaks) of the actual resonance frequency.

Almost all SPMs can resolve all height steps of the atoms. AFMs can also achieve a sideward atomic resolution. In the same manner, in normal atmospheric conditions, each surface contains some soaked up particles concealing the authentic surface of the AFM point. Just a few areas permit sideward atomic resolution in the air. In this way, the STMs possess the advantage because through the tunnel current constantly moves immediately above the following atom on the specimen area. This type of "self-focusing" does not happen with an AFM. AFMs with the sideward atomic resolution is merely employed for specific occurrences, where reaching a

sideward atomic resolution is further crucial than the loss of flexibility, brought on by the higher stability of the total set arrangement. Typical AFMs have been designed for approximate, large scan regions (e.g., in the range between 50 and 200 μm), and also the scanner phases allow for the research of diverse categories and magnitudes of the specimen.

Traditional AFMs composed of a piezoelectric tube scanner need data levelling, due to their inherent arced or curved motion. Nevertheless, this levelling might distort a specimen's micro-surface structure, as well as its Z value. The more recently developed AFMs are equipped with a flexure-based scanner that allows well-controlled raster scans along with *X* and *Y* directions only. As an outcome, this up-to-date scanner design may successfully eradicate background curvatures in extensive scan regions and enhance the accuracy of AFM calculations.

The AFMs employ a very fine tip for checking and mapping the morphology of a surface. Nonetheless, with an AFM, there is no need for the specimen to be conductive, nor is it indispensable to calculate a current between the tip and specimen to generate an image. AFMs use the probe, or tip, at the termination of a microfabricated cantilever with a small spring steady to calculate the tip-specimen forces as the tip presses (either constantly or sporadically) contrary to the specimen. The forces among the point and the specimen area cause the cantilever to deflect, or curve, like the tip, is being scanned above the specimen. The cantilever deviation is monitored, and the calculations produce a map of surface topography.

Some applications of STM are as follows: (a) Organic Material Thin Films and Adsorbate Particles in Air, (b) Quartz Microbalance Study of Molecularly Thin Water Layers, (c) Explorations of Alcohol/Alkane Mixtures Adsorbed on Graphite Surfaces, (d) Carbon nanotubes, (e) Chemical-Vapor Deposited Diamond Films, and (f) Porous Silicon-Based Surfaces Conducting Polymer Film, etc.

1.5 Comparison of Various Characteristics of the Microscopes

In the case of an optical microscope, it is highly challenging to explore the area structure of a specimen. For the measurement of a surface profile applying maximum resolution, it is necessary to dissect the specimen. The users of a scanning probe microscope do not see the sample surface directly, instead, they see an image that represents the surface of the sample.

The principal difference between both electron and light microscopes is that either a beam of electrons is employed for amplifying the image of an item or discernible illumination is employed to amplify images of the small-scale region of mediums or biological samples respectively. Regarding an optical microscope, the electron microscope reaches significant definition and amplification by exploiting the signal characteristic of electrons. The wavelength of electrons is generally 1/100,000 that of discernible radiation.

Furthermore, in a scanning probe microscope, the surface of the specimen might be conductive or semi-conductive, restricting the materials which can be investigated. These restrictions and others of scanning probe microscopes led to the invention of the first atomic force microscope [36]. Atomic force microscopes may likewise achieve a sideward atomic resolution. This places serious restrictions on the point geometry, nevertheless, and means it is very complicated to reach with usual cantilevers with a point radius of 10 nm.

In the case of an electron microscope, the principal difference between SEM and TEM is that SEMs generate an image by detecting reflected electrons, while TEMs employ transmitted electrons to produce an image. In the case of TEMs, which need the firmness of the scan stage, this exclusively permits little specimen proportions and heights.

The STM and the AFM are scanning probe microscopes with a high capacity to resolve surface information at an atomic level. The STMs have even been employed to enhance magnetic recording heads and standard diffraction gratings. The potential of STMs, which do not need a conductive specimen. A tight combined atomic force and STM may carry out unchanged height monitoring and reach atomic definition in both STM and AFM on different specimens [37].

1.6 Advantages and Limitations

Among the greatest advantages that microscopes have, we can firstly cite the convenience and simplicity of these instruments. Secondly, using a compound light microscope is not only very easy, but it is also very easy to store (it is relatively small) and it also has its illumination source. Thirdly, compound light microscopes can disclose a considerable deal of information in specimens, i.e., due to their multiple lenses. Light microscopes are capable of providing a high level of experimental quality, and also are unaltered by electromagnetic fields and are highly adaptable to the needs of the experiment. While one of the biggest limitations of having an optical microscope is that they have a lower resolution. Other limitations include: (i) these instruments require the person to have an expectation of what they want to find, (ii) difficulty in visualizing living internal structures, (iii) light microscopes do not scale to the level of its alternatives, for instance, low magnification [38].

On the other hand, fluorescence microscopy has the following advantages:

- Samples can be fixed before adding a fluorophore.
- They allow very detailed measurements of the observed sample.
- They are able to trace the path of an individual protein during their life cycle.
- They have a high degree of specificity.

Meanwhile, some of fluorescence microscopy limitations are:

- Its dependence on probes.
- Inability to observe unexpected structures without initial identification.

- The presence of autofluorescent biomolecules causes interactions that detract from the effectiveness of each probe used in microscopy.
- It requires a lot to carry out the process of fixing the fabric and washing.

Like light microscopy, SEM is easy to use and works fast too. Another advantage of this type of microscope is the generation of data in digital form in real-time. Most SEM samples used require minimal setup actions. However, SEMs are very expensive and need to be in an area free from electrical interference. These microscopes are very complicated in terms of use; e.g., preparing the samples involves a great deal of training. Besides, when using SEM we are exposed to radiation, which is associated with electrons scattering from below the surface of the specimen. Finally, SPM allows us to widely observe samples using the same microscope and sample in the short term. The SPM provides fast and highly efficient images with little effort and modification. However, one of the main limitations of SPM is that the images provided are in black and white. This sometimes causes confusion about the original or real size of a specimen evaluated.

Acknowledgment WA extends his thanks for the PhD grant from the National Council for Science and Technology (CONACYT, for its acronym in Spanish), as well as the Universidad Autónoma de Nuevo León (UANL) through the Subdirectorate of Postgraduate Studies of the Faculty of Agronomy (FA-UANL, for its acronym in Spanish) for his acceptance in the PhD Program. WA, also, thanks in a particular way his Doctoral Thesis Committee. In addition, AILM and WA thank PAICYT (Programa de Apoyo a la Investigación Científica y Tecnológica)-(CT1519-21) from Universidad Autónoma de Nuevo León for their support. Finally, KSK would like to acknowledge the Proyectos de Desarrollo Tecnológico e Innovación-2021-TecNM-Instituto Tecnológico El Llano Aguascalientes-(IT19F245).

References

1. Hooke R (1665) Micrographia, or, some physiological descriptions of minute bodies made by magnifying glasses: with observations and inquiries thereupon. Printed by J. Martyn and J. Allestry, London. http://hdl.loc.gov/loc.rbc/Rosenwald.1511.1
2. Gendre MF (2017) Incandescent lamps. In: Handbook of advanced lighting technology, pp 1013–1064. https://doi.org/10.1007/978-3-319-00176-0_2
3. Ladouceur AM, Brown CM (2021) Fluorescence microscopy light source review. Curr Protoc 1(10):e304. https://doi.org/10.1002/cpz1.304
4. Granzow N (2019) Supercontinuum white light lasers: a review on technology and applications. In: Proc. SPIE 11144, photonics and education in measurement science, 1114408. https://doi.org/10.1117/12.2533094
5. Lagunas-Solar MC (2014) Food technologies: pulsed ultraviolet radiation processing. In: Encyclopedia of food safety, vol 3, pp 225–238. https://doi.org/10.1016/B978-0-12-378612-8.00261-4
6. Kumar A, Sagdeo A, Sagdeo PR (2021) Possibility of using ultraviolet radiation for disinfecting the novel COVID-19. Photodiagn Photodyn Ther 34:102234. https://doi.org/10.1016/j.pdpdt.2021.102234
7. Hohman B (2008) LED light source: major advance in fluorescence microscopy. Microsc Today 16:28–29. https://doi.org/10.1017/S1551929500061733

8. Kuo T-C, Ding T-J, Lin J-H, Ma S-H (2019) Optical design of an LED lighting source for fluorescence microscopes. Appl Sci 9(21):4574. https://doi.org/10.3390/app9214574
9. Gerhardt I, Mai L, Lamas-Linares A, Kurtsiefer C (2011) Detection of single molecules illuminated by a light-emitting diode. Sensors 11:905–916. https://doi.org/10.3390/s110100905
10. Cybulski J, Clements J, Prakash M (2014) Foldscope: origami-based paper microscope. PLoS One 9:e98781. https://doi.org/10.1371/journal.pone.0098781
11. Ul-Hamid A (2018) Contrast formation in the SEM. In: A beginners' guide to scanning electron microscopy. Springer, Cham, pp 77–128. https://doi.org/10.1007/978-3-319-98482-7_3
12. Chiarini-Garcia H, Parreira GG, Almeida FR (2011) Glycol methacrylate embedding for improved morphological, morphometrical, and immunohistochemical investigations under light microscopy: testes as a model. In: Light microscopy. Humana Press, Totowa, NJ, pp 3–18. https://doi.org/10.1007/978-1-60761-950-5_1
13. Mitra SK, Murthy CA, Kundu MK (2000) A technique for image magnification using partitioned iterative function system. Pattern Recogn 33(7):1119–1133. https://doi.org/10.1016/S0031-3203(99)00108-9
14. Chavez PS Jr (1986) Digital merging of landsat TM and digitised NHAP data for 1: 24000 scale image mapping. Photogrammetric Eng Remote Sens 52:1637–1646. http://pubs.er.usgs.gov/publication/70015329
15. Mualla F, Aubreville M, Maier A (2018) Microscopy. In: Maier A, Steidl S, Christlein V et al (eds) Medical imaging systems: an introductory guide [internet]. Springer, Cham (CH). https://doi.org/10.1007/978-3-319-96520-8_5
16. Equipment. (1998) Microbiological analysis of food and water, pp 51–85. https://doi.org/10.1016/B978-044482911-5/50022-9
17. Srinivasan S (2021) Three-dimensional (3D) visualization for intraocular surgery: necessity or nicety. J Cataract Refract Surg 47(3):287–288. https://doi.org/10.1097/j.jcrs.0000000000000595
18. Chen X, Zheng B, Liu H (2011) Optical and digital microscopic imaging techniques and applications in pathology. Anal Cell Pathol 34(1, 2):5–18. https://doi.org/10.3233/acp-2011-0006
19. Golomingi R, Haas C, Dobay A, Kottner S, Ebert L (2021) Sperm hunting on optical microscope slides for forensic analysis with deep convolutional networks – a feasibility study. Forensic Sci Int Genet 56:102602. https://doi.org/10.1016/j.fsigen.2021.102602
20. Dong Y, Kakisawa H, Kagawa Y (2013) Optical system for microscopic observation and strain measurement at high temperature. Meas Sci Technol 25(2):025002. https://doi.org/10.1088/0957-0233/25/2/025002
21. Herman B (1987) Fluorescence microscopy, 2nd edn. Garland Science. https://doi.org/10.1201/9781003077060
22. Slavík J (1996) Fluorescence microscopy and fluorescent probes. Plenum Press, New York. https://doi.org/10.1007/978-1-4899-1866-6
23. Engelborghs Y, Visser AJWG (2016) Fluorescence spectroscopy and microscopy. Humana. https://doi.org/10.1007/978-1-62703-649-8
24. Sanderson J (2020) Fundamentals of microscopy. Curr Protocols Mouse Biol 10(2):e76. https://doi.org/10.1002/cpmo.76
25. Sanderson MJ, Smith I, Parker I, Bootman MD (2014) Fluorescence microscopy. Cold Spring Harb Protoc 2014(10). https://doi.org/10.1101/pdb.top071795
26. Jensen EC (2012) Use of fluorescent probes: their effect on cell biology and limitations. Anat Rec Adv Integr Anat Evol Biol 295(12):2031–2036. https://doi.org/10.1002/ar.22602
27. Riddell N, Crewther SG, Murphy MJ, Tani Y (2021) Long-wavelength–filtered light transiently inhibits negative lens-induced axial eye growth in the Chick myopia model. Transl Vis Sci Technol 10:38. https://doi.org/10.1167/tvst.10.9.38
28. Rez P, Singh A (2021) Lattice resolution of vibrational modes in the electron microscope. Ultramicroscopy 220. https://doi.org/10.1016/j.ultramic.2020.113162
29. Novikov YA (2021) Calibration of a scanning electron microscope: 2. Methods of signal processing. J Surf Investig 15:987–998. https://doi.org/10.1134/S102745102105013X

30. Reed SJB (2005) Electron microprobe analysis and scanning electron microscopy in geology. Cambridge University Press. https://doi.org/10.1017/CBO9780511610561
31. Carter CB, Williams DB (eds) (2016) Transmission electron microscopy: diffraction, imaging, and spectrometry. Springer. https://doi.org/10.1007/978-3-319-26651-0
32. Cocker TL, Jelic V, Hillenbrand R, Hagmann FA (2021) Nanoscale terahertz scanning probe microscopy. Nat Photon 15:558–569. https://doi.org/10.1038/s41566-021-00835-6
33. Jensen AT, Neto WS, Ferreira GR, Glenn AF, Gambetta R, Gonçalves SB et al (2017) Synthesis of polymer/inorganic hybrids through heterophase polymerizations. In: Recent developments in polymer macro, micro and Nano blends: preparation and characterisation, pp 207–235. https://doi.org/10.1016/B978-0-08-100408-1.00008-X
34. Sahare S, Ghoderao, Prachi, Khan SB, Chan Y, Lee S-L (2020) Recent progress in hybrid perovskites solar cells through scanning Tunneling microscopy and spectroscopy. Nanoscale. https://doi.org/10.1039/D0NR03499A
35. Binnig G, Quate CF, Gerber C (1986) Atomic force microscope. Phys Rev Lett 56(9):930–933. https://doi.org/10.1103/physrevlett.56.930
36. Main K, Provan JI, Haynes PJ, Wells G, Hartley JA, Pyne A (2021) Atomic force microscopy-a tool for structural and translational DNA research. APL Bioeng 5(3):031504
37. Pürckhauer K, Maier S, Merkel A, Kirpal D, Giessibl FJ (2020) Combined atomic force microscope and scanning tunneling microscope with high optical access achieving atomic resolution in ambient conditions. Rev Sci Instrum 91(8):083701. https://doi.org/10.1063/5.0013921
38. Robson AL, Dastoor PC, Flynn J, Palmer W, Martin A, Smith DW, Woldu A, Hua S (2018) Advantages and limitations of current imaging techniques for characterizing liposome morphology. Front Pharmacol 9:80. https://doi.org/10.3389/fphar.2018.00080

Principles of Light and Fluorescence Microscopy

2

Laura E. Zavala-García, Ramón Carriles, Mercedes G. López, and Lino Sánchez-Segura

Abstract

This chapter provides an overview of light and fluorescence microscopy, beginning from the basic principles of optics such as transmission, absorption, diffraction, refraction, and behavior electromagnetic theory. To understand the concepts of magnification and resolution, this chapter explores the theory of formation of real and virtual images and some properties of the lenses that compound the optical system of a microscope, including the aberration problems and corrections applied in the objectives. On the other hand, this chapter explores the concepts of Abbe resolution and the difference with the magnification of the optical system in the microscope. The description of the mechanical components and light sources of optical and fluorescence microscopes allow understanding of the difference between microtechniques applied to each of these microscopes and utilization in biology and materials science. These basic principles of microscopy will allow nonexpert users to contextualize the first results of observations in the microscope. The main limitations in the microscopist formation are the high cost of the equipment and the unavailability of the expert users to teach, it is for these reasons we consider that the training should begin with a rapid guide of basic microscopy concepts.

Laura E. Zavala-García
Centro de Desarrollo de Productos Bióticos, Instituto Politécnico Nacional, Morelos, Mexico
email: elizavala1993@gmail.com

Ramón Carriles
División de Fotónica, Centro de Investigaciones en Óptica, A.C., León, Guanajuato, Mexico
email: ramon@cio.mx

MercedesG.López
Departamento de Bioquímica y Biotecnología, Centro de Investigación y de Estudios Avanzados del Instituto Politécnico Nacional Carretera Irapuato-León, Guanajuato, Mexico
email: mercedes.lopez@cinvestav.mx

LinoSánchez-Segura
Departamento Ingeniería Genética Centro de Investigación y de Estudios Avanzados del Instituto Politécnico Nacional, Carretera Irapuato-León, Guanajuato, Mexico
email: lino.sanchez@cinvestav.mx

S.-K. Kamaraj et al. (eds.), *Microscopic Techniques for the Non-Expert*,
https://doi.org/10.1007/978-3-030-99542-3_2

Keywords

Microscopy · Light · Fluorescence · Wavelength · Sample holder

2.1 Introduction

Fluorescence microscopy is considered an advanced visualization technique for biological samples due to the flexibility offered by the equipment, to sample preparation procedures that can target specific cell organelles and to the information gained from the observed fluorescent structures, among other factors. Moreover, an understanding of the principles involved in fluorescence microscopy sets the basis to understand confocal and multiphoton microscopy. In this chapter, we will explore the optical principles of light microscopy, fluorescence microscopy, theory of light–matter interactions, and the sample preparation and visualization of several samples with fluorescence.

Microscopy in biological science has been used to identify and describe, from basic morphology of unicellular organisms to complex organization of several tissues of the human body. Moreover, histological and histochemical staining techniques allow the association of chemical compounds with morphological structures and can help to describe the function of the cells in the tissue of live organisms. Meanwhile, in biomaterial science, microscopy allows the recognition of morphological patterns and the quantification of the morphometry in the structures associated with physicochemical changes. However, the main difficulty posed by these microtechniques is that they require an extensive and individual training as well as cycles of experimentation in the laboratory. In order to make the best use of the available microscopy resources and to advance novel microscopy techniques it is mandatory to understand the basic optical and physical principles behind the operation of a light microscope and image formation.

2.2 Generalities About Light

We are all familiar with light and therefore we could tend to believe that we understand what it is and its basic properties; however, for technical applications, it is required to understand some fundamental optical concepts about light. In this section we will explore, in an extremely simplified way, some of the required concepts related to microscopy and used later in the text.

As we know, optics is the branch of Physics devoted to the study of light and its interactions with matter as well as the instruments used to manipulate it. Within optics, there are several different levels of sophistication and generality, that depend on the underlying assumptions made. The most basic level is geometrical optics, where light is considered as rays that propagate in a straight line across space; as its name implies, it is useful to study the direction of propagation. Then we have what is called physical optics, here light is studied as a wave phenomena and leads to new

aspects such as interference and diffraction. This level of approximation is needed when a more detailed description of the propagation is needed; for example, to determine the resolution limit of an optical system. A more general approach that actually encompasses the two previous descriptions as limit cases, is to invoke electromagnetic theory. One of the most striking consequences of Maxwell's equations is to recognize that light is just an electromagnetic wave vibrating with a particular range of frequencies. Under this description, we can appreciate that visible light is just a part (where our eyes happen to be sensitive) of what is called the electromagnetic spectrum which contains other regions such as ultraviolet (UV), infrared (IR), X-rays, microwaves, radio waves, radar waves, and TV waves. The only difference between these sections of the electromagnetic spectrum is the frequency at which the waves vibrate; the reason that these sections seem to behave so differently is because the properties of materials (absorption, scattering, index of refraction, etc.) interacting with electromagnetic waves with different frequencies vary enormously across the spectrum. Finally, if we incorporate quantum mechanical effects into electromagnetic theory, we enter into the realms of quantum optics, which might be considered as the most complete description of light that we have. Please understand that each one of these descriptions is different approximations to the same phenomena, and therefore all of them are useful under the appropriate circumstances; there is no need to invoke quantum optics to describe the everyday observed behavior of a lens or microscope. On the other hand, there are some phenomena that cannot be described within some of the approximations; for example, geometrical optics cannot account for diffraction, or electromagnetism cannot account for the quantum phenomenon known as entanglement.

A microscope can mainly be described using geometrical and physical optics; although, as we will find later in connection with nonlinear optical properties, the description of some phenomena is better understood using a quantum mechanical description. Another point that needs to be understood, and perhaps just accepted, is that light has a dual nature: sometimes it behaves as a wave and others as a particle (photon). Historically, this was one of the observations that led to the development of quantum mechanics in the first part of the last century. In this text, we will refer mainly to the wave nature of light, although at some point we will invoke photons; therefore, let us start by reviewing some very general characteristics of light as a wave.

An electromagnetic wave is a spatial and temporal periodic (meaning that it repeats itself over space and time) disturbance that can propagate even in vacuum. This disturbance has a well-defined direction of propagation (light propagates in a straight line) and consists of electric and magnetic fields that oscillate in time and space and that are mutually perpendicular to one another and to the direction of propagation. The specific direction in which the electric field point is called the polarization state of light. Since we are talking about a periodic event, it must repeat itself after some time, this time is called the period of the wave (T, measured in seconds, s) and its inverse is known as the frequency ($\upsilon = 1/T$, measured in Hertz, Hz, which are s^{-1}). When a wave propagates from one medium to another, its frequency does not change. The frequency of light is responsible for the "color" of

light, obviously, we can only call it color in the visible part of the spectrum; however, it is much more frequent to use the wavelength to specify the color. The wavelength describes the distance that is needed for the wave to repeat itself, in a way is the spatial concept analogous to the period in time; it is related to the frequency by $\lambda = c/\upsilon$, where c is the speed of light in vacuum (299,792,458 m/s) and λ is the wavelength (measured in units of distance, for visible light typically in nm). One last attribute of an electromagnetic wave is its amplitude, which is related to how large is the electric field of the wave. The square of the amplitude is proportional to the intensity of the light (typically measured in Watts/area, W/cm^2, or W/m^2). In a description of light in terms of photons, the intensity is related to the total number of photons present in the beam of light, each photon having specific energy given by $E = h\upsilon$, where h is the so-called Planck's constant ($h = 6.626 \times 10^{-34}$ Joules second, Js).

What we have described so far mainly refers to light in vacuum; however, in order to "control" light, i.e., redirect it, measure it, detect it, and use it in general, we must make it interact with materials. As the reader is most likely aware, existing materials offer an enormous variety of properties that can vary widely from one to another. From the optics point of view, we could divide materials into transparent and opaque; transparent materials are typically used to form lenses, filters, windows, etc., while detectors, screens, mirrors, etc. are typically opaque. The most important property of a transparent material is its index of refraction, $n = c/v$, where n is the index of refraction (unitless) and c is the speed of light in vacuum. Among many other things, n tell us how much an incident beam of light will deviate from its original trajectory after changing from one medium to another; the relation is called Snell's law of refraction. This deviation is central to microscopy because that is the principle of operation of a lens, which is a fundamental optical element of any microscope. One very important detail of n is that its numerical value depends on the specific color of the light involved, i.e., n is a function of λ; in optics, dispersion refers to a material property that depends on λ, so the index of refraction is dispersive. This has deep consequences, for example, a lens will focus on different colors at different points because each color experiences a slightly different n, this is called chromatic aberration.

To start making connections with samples in microscopy and appreciate how different optical phenomena intervene in a microscope, let us imagine we want to see a cell within a tissue. When light propagates from one medium to another (say tissue to cell), due to the differences in indices of refraction there would be some amount of light that will be transmitted (in the direction given by Snell's law) and another part, typically smaller, that will be reflected (for example, when you look at your reflection in a transparent window). So, in principle, we could form an image of the cell using the transmitted light (the microscope would be working in transmission) or by using the reflected light (we would have a microscope working in reflection geometry, sometimes called epi-imaging). The transmitted light will propagate through the new medium (the cell) but it could be transmitted without change or it can be absorbed (either partially, as in a tinted window, or completely, as in an opaque material), or scattered (for example,

when you look at something through frosted glass). Scattering occurs when light propagating inside a medium encounters particles that make it deviate from its original trajectory, in our example we could think about some cell organelles that can scatter light or also we can imagine that after the light left the cell we want to observe, it encounters other cells that change the trajectory of the propagating light. As we will see later, scattering is a major challenge in microscopy because it makes the acquired images to look blurry, as if they were out of focus, which is not desirable.

All this very basic description of light and some of its properties play an important role in different aspects of microscopy, as we will try to show in the next sections. Keep in mind that since this is an introductory level book, we cannot develop many of these aspects but the reader is encouraged to explore more in the many sources available.

2.3 Lenses

The lens is a usually circular piece composed of refracting and transparent material; this implies that induces a discontinuity in the prevailing medium and a reconfiguration of the transmitted energy distribution. This effect is caused by the deviation (refraction) suffered by a ray of light when crossing an interface between two media and applies to any wave phenomena; for instance, UV, visible or IR light, microwaves, radio waves, or even sound waves. A convex lens refracts parallel rays of light incident on its surface and changes their trajectory so that they emerge from the lens to converge to one point, called focus. The convex lens is thicker at its midpoint than at its edges; on the other hand, a concave lens is thinner in the middle than at the edges. Converging lenses are known as positive lenses and can form a real image. On the other hand, a concave lens, called a negative lens, will make a bundle of parallel rays diverge from a point or center line known as the focus.

Actually, there are several different lens shapes and a microscope requires many of these different types; the difference between them is the basic curvature patterns of their surfaces (Fig. 2.1). There are also compound lenses consisting of two or even three lenses, typically made of materials with different indexes of refraction, glued together; these lenses are used to avoid chromatic distortions, i.e., to avoid different colors of light to take different paths. A brief classification of the basic lenses is described below:

The biconvex lens: This lens is convergent with the capacity to change the trajectory of rays dependent upon the curvature angle of its faces (Fig. 2.1a). Higher angles of curvature produce shorter focal lengths. This symmetrical shape reduces the spherical aberration. These lenses are typically used for focusing and image magnification [1].

The plano-convex lens: A plano-convex lens is characterized by having one positive hemispherical side and one flat side (Fig. 2.1b). This lens is convergent, focusing parallel rays of light to a focal point. This lens can form real images, which can be corrected by filters and finally projected. The characteristically asymmetry of

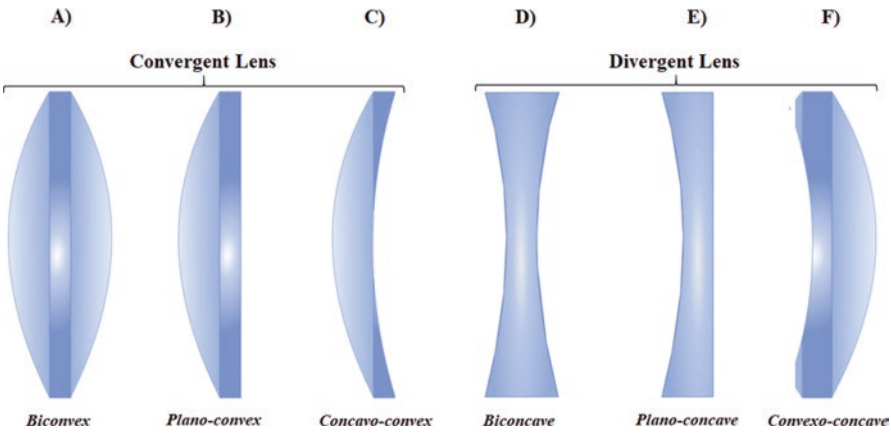

Fig. 2.1 The internal optics of microscopy have two basic groups of lenses, the convergent lenses and the divergent lenses. (**a**) Biconvex. (**b**) Plano-convex. (**c**) Concavo-convex. (**d**) Biconcave. (**e**) Plano-concave. (**f**) Convexo-concave

plano-convex lenses minimizes spherical aberration in applications where the object and image lie at unequal distances from the lens. When the curved surface of the lens is oriented toward the object, the sharpest possible focus is achieved. Plano-convex lenses are useful for collimating diverging beams of light.

The concavo-convex lens: The main characteristic of this lens is that it produces convergence of the rays, for this property it is considered a positive lens, and due to its asymmetric shape it is commonly known as a meniscus lens. One of its faces is in a convex hemispherical shape, while the other is slightly concave (Fig. 2.1c). The meniscus lenses are usually coupled with other lenses to produce an optical system with a longer or shorter focal length than the original single lens. Positive meniscus lenses have a greater curvature radius on the concave side of the lens than on the convex side, which enables the formation of a real image [1].

The biconcave lens: This lens is a divergent lens used to produce image reduction, as well as increasing system focal length and collimating converging light beams. It is also called double-concave lens. It shows a capacity to refract parallel input rays so that they diverge away from the optical axis on the output side of the lens but form a negative focal point in front of the lens (Fig. 2.1d). The biconcave lens is coupled with other lenses in order to reduce the focal length of an optical system.

The plano-concave lens: This lens shows divergent properties, which results in a negative focal point and produces a virtual image (Fig. 2.1e). The main optical characteristics of the plano-concave lens are to form a divergent beam when a collimated light beam is incident on the curved surface of the lens. Plano-concave lenses are used to expand light beams or to increase the focal length in optical dispositive.

The convex-concave lens: This lens is classified as negative and is characterized by having a concave surface with a lower curvature radius than its convex surface, it is more commonly called a meniscus lens, and the light rays that emanate from

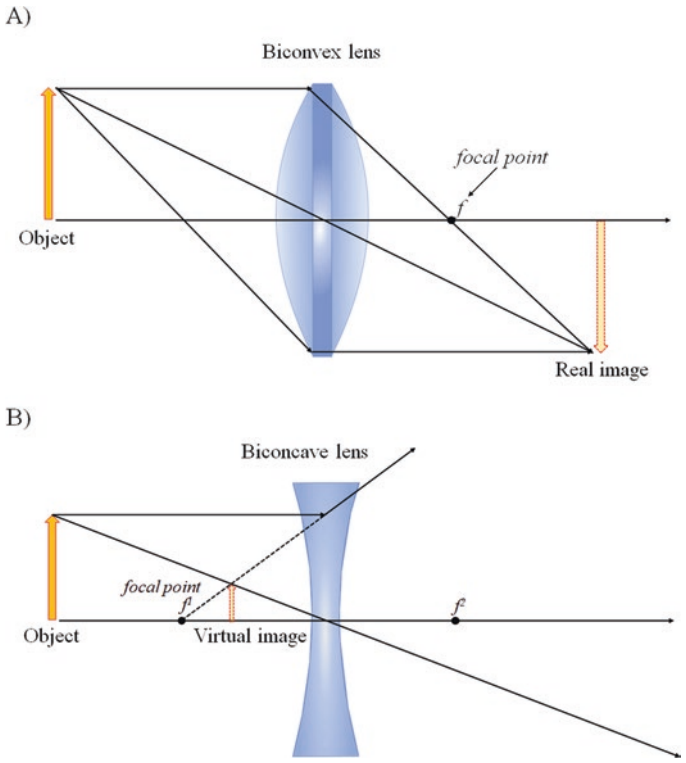

Fig. 2.2 Diagram of the optics formation of images, differences between convergent and divergent lenses. (**a**) Formation of the real image with the biconvex lens. (**b**) Formation of the virtual image with the biconcave lens

this lens are divergent (Fig. 2.1f). The convex–concave lens is used to reduce or eliminate spherical aberration in optical devices and can be combined with other lenses to improve the resolution of a system.

As aforementioned, the shape of the lens determines the angles of refraction of light that crosses the lens and therefore the image position and size. The convex lens and its variants show an important property, the possibility to project *real images* of objects into surfaces such as screen, film, or retina (Fig. 2.2a). However, some geometric conditions must be met in order to produce a *real image*, the distance between the object and the lens must be greater than the focal length of the lens. Otherwise, if the object is closer to the convergent lens, under the focal distance of the lens, the lens will produce an increased image with the impression of being at a longer distance of the real object, this image is called *virtual image* (Fig. 2.2b). To produce *virtual images*, the concave lens and its variants are used because an image formed by a diverging lens is not real and cannot project onto a surface.

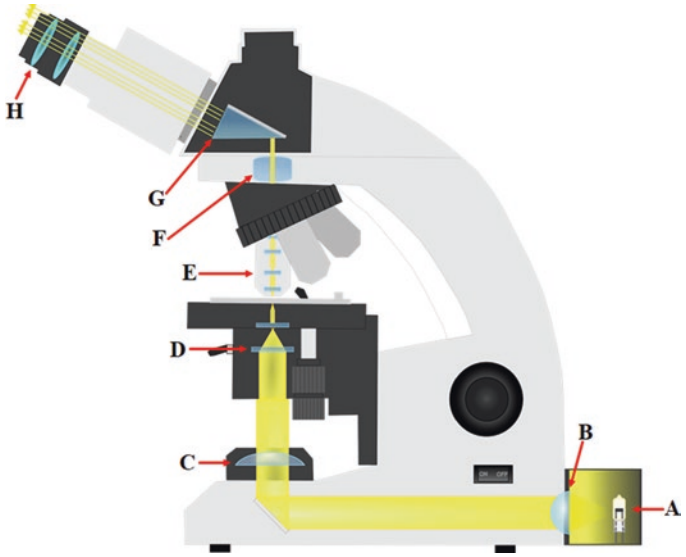

Fig. 2.3 Electrical and optical diapositives that compound an optical bright-field microscope. (**a**) Lamp. (**b**) Collector lens. (**c**) Field diaphragm. (**d**) Condenser. (**e**) Objective. (**f**) Tube lens (**g**) Beamsplitter. (**h**) Eyepiece

2.4 Basic Concept of Light Microscopy

In optical bright-field microscopy, the source of light is a tungsten-halogen incandescent bulb (Fig. 2.3a) installed in a reflective case that projects the rays through the collector lens (Fig. 2.3b). The off-center rays are led to the field diaphragm (Fig. 2.3c), used to regulate the beam broadening by closing or opening the diaphragm; this aperture controls the angle of the light rays reaching the specimen (seen as intensity of light in the image). Subsequently, the light is captured by the substage condenser (Fig. 2.3d). The condenser aperture diaphragm must be adjusted according to the aperture of the objective, this operation is critical to obtain the full potential of the objective. This procedure is known as the Khöler illumination condition. The photons that cross the sample mounted in the stage are captured by the objective (Fig. 2.3e). The objective is the most important piece of the microscope, composed of a group of lenses (front lens, meniscus, single, double or triple group of lenses, rear lens, and objective lens); this dispositive is responsible for the magnification and resolution of the images. To understand the basic features of an objective and the conditions under which it can be used, it is necessary to correctly interpret the parameters printed in the external case of the objective: numerical aperture, magnification, optical tube length, degree of aberration correction, compatibility with fluorescence, and immersion medium information. The light emerges from the objective and goes to the tube lens (Fig. 2.3f). The tube lens has the function of forming a virtual image (inverted and magnified) at the object plane of the eyepiece lens. The light emerges from the tube lens and arrives to the beamsplitter

(Fig. 2.3g), which is a component utilized to divide the light beam into two parts, each one of these parts goes to the eyepieces or camera port. The beamsplitter is composed of two right-angle prisms that are coated by partially reflective material with capacity to change the trajectory of the light at 90° angle. The eyepieces are responsible to form a real image of the specimen and also play a role in the final magnification and brightness of the image (Fig. 2.3h) [2].

2.5 Geometry of the Image Formation

The operation of a microscope involves the manipulation of light from the sample using lenses. One way to understand the function of the lens is to follow the trajectory of light across the lens. When a set of parallel rays of light travel through a convergent lens, they suffer a change of trajectory due to the curvature of the lens surface and converge to a point, denominated focus (Fig. 2.4a) [3, 4]. The distance between focus and lens is called the focal distance (*f*) and constitutes the main

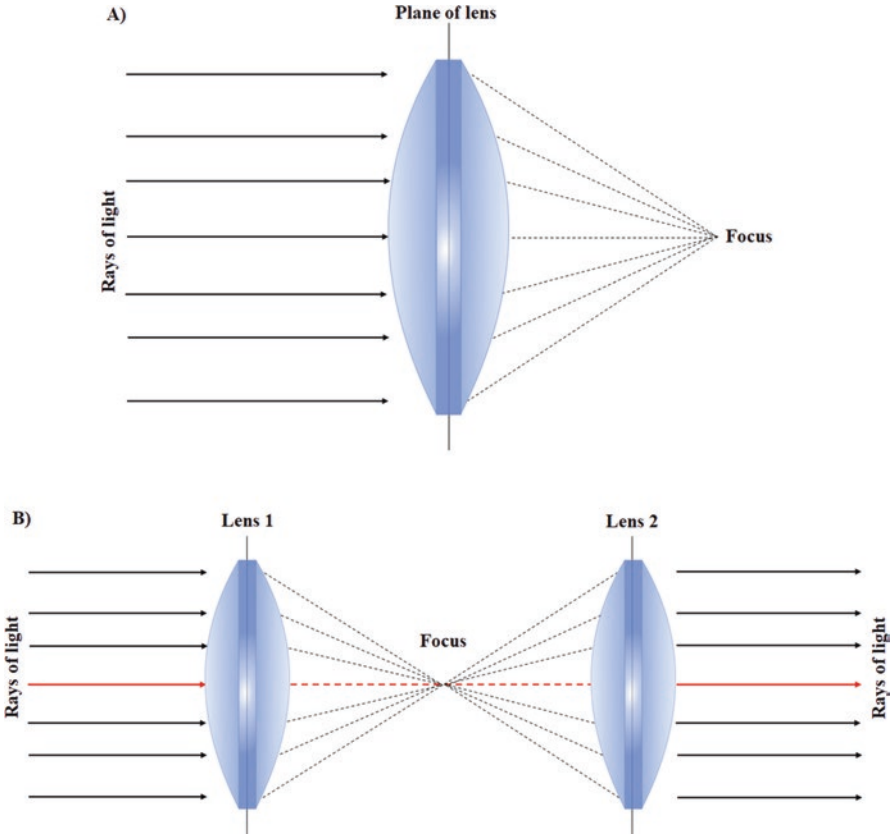

Fig. 2.4 (**a**) Most changes the trajectory of parallel light rays into a focus point. (**b**) Contrary effect, the light rays emerged from a point source, such as the focus of a lens, leave the secondary lens in as parallel rays

defining parameter of a lens [5]. Analogously, when a point source of light is placed at a focal length from a lens, it will emerge collimated after the lens (Fig. 2.4b). For a given lens, with a fixed *f*, and a given distance from the object to the lens, there will be a point where an image will be formed. By changing the object to lens distance, one can control the image position. This is the principle behind focusing on a sample. The optics inside a microscope are more complex than a single lens; as described before, just the objective can contain several lenses inside. When we have a system of lenses, the image from the first lens will be the object for the second and similarly for the following lenses.

2.6 Microscope Objectives

For the beginner user of any microscopy equipment, the correct choice of microscope objectives is the main barrier to overcome during the operation of the microscope. The microscope objectives are the most important components of an optical microscope because they are responsible for primary image formation and are a decisive factor to obtain good quality images. The objectives are manufactured according to the type of sample and microtechnique used to analyze a sample.

Understanding the large list of objectives manufactured by several companies is almost an impossible work; however, their main characteristics can be summarized in a simple classification in classes according to their functionality such as aberration, correction, and application. Also, due to the various qualities of materials and production processes employed in objective fabrication and the incorporation of proprietary technologies, there is a slight importance in the manufacturing company [6]. In order to understand the function of the objectives and to obtain the maximal performance, it is important to explain some artifacts that occur in microscopes, for example, chromatic aberration.

When white light rays cross a lens that has a different refraction index with respect to the incident medium, a phenomenon called material dispersion occurs in which different wavelengths in the white light experience a slightly different index of refraction. This leads to chromatic aberration, meaning that different colors will be separated and converge to different focal points (Fig. 2.5a). There are two types of chromatic aberration: *axial or longitudinal chromatic aberration* and *lateral chromatic aberration*. In the *longitudinal chromatic aberration*, an axial white light point source will be imaged as a continuous axial gradient of identical images, each of a different color, forming a blurry composite image of the object [5]. The main visible symptom to recognize the axial aberration is the formation of different images out of focus and showing a halo of a single color; while the *lateral chromatic aberration* occurs when the white light source is placed off-axis. The visible symptom is recognized by the formation of ghost images (overlapping images) with different magnifications due to the lenses having different focal lengths for different wavelengths of light.

To correct these problems, the lenses inside the objectives are arranged so that one cancels the chromatic aberration from another. This can be done at several

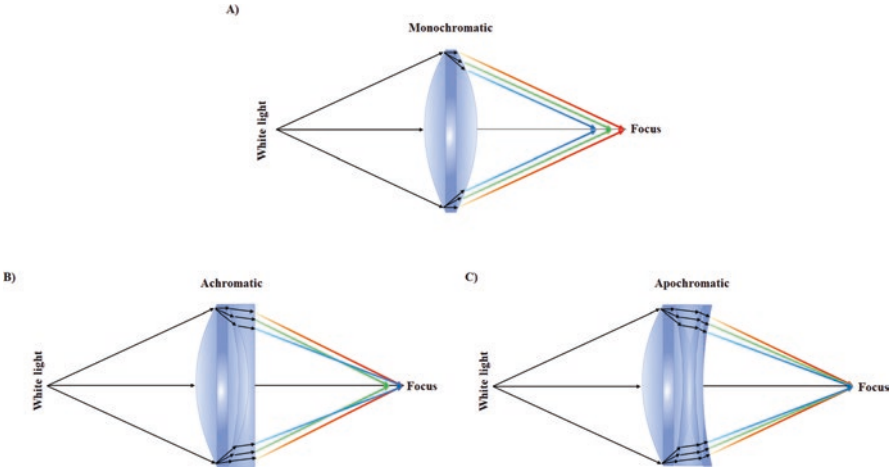

Fig. 2.5 (**a**) Monochromatic aberration, the blue, green, and red colors show a different focal point. (**b**) Achromatic aberration, the blue and red colors are corrected, the green color shows a different focal point. (**c**) Apochromatic correction, three colors are corrected in the same focal point

levels of correction to satisfy the needs of different applications in laboratory, but at the cost of increasing objective complexity and therefore its price. Most objectives can be classified in the following ways according to their chromatic aberration properties:

Achromate: These are the most used objectives in a scholarly laboratory. The main disadvantage of this dispositive is the lack of correction for the flatness of field (or field curvature). The advantage is the correction of axial chromatic aberration for blue (486 nm) and red (656 nm) wavelength, i.e., both rays converge into a single common focal point. The disadvantage is that they show spherical aberration for green wavelength (546 nm) (Fig. 2.5b).

Semi-apochromate or Fluorite: These objectives are chromatically corrected for red–green–blue in the focal point. Moreover, they are spherically corrected for blue and green. This objective shows better performance for samples with higher contrast than achromatic objectives.

Apochromatic: These objectives show an excellent performance for fluorescence. Their longitudinal chromatic aberration is corrected for four colors (near UV, blue, green, and red) and they are spherically corrected for UV, blue, and sometimes green. Typically, the apochromate is corrected from g- to c-line (Fig. 2.5c).

Plan: These objectives produce a flat image across the field of view. The three objectives discussed above produce a distortion of image (curved image). A plan-achromat, plan-fluorite, or plan-apochromat is corrected for this aberration.

The important parameters to understand the functionality of the microscope objectives are the numerical aperture (NA) and working distance (WD). The NA of a microscope objective is the measured capacity to acquire light through collection of the light cone between the principal lens of the objective and the sample. The NA

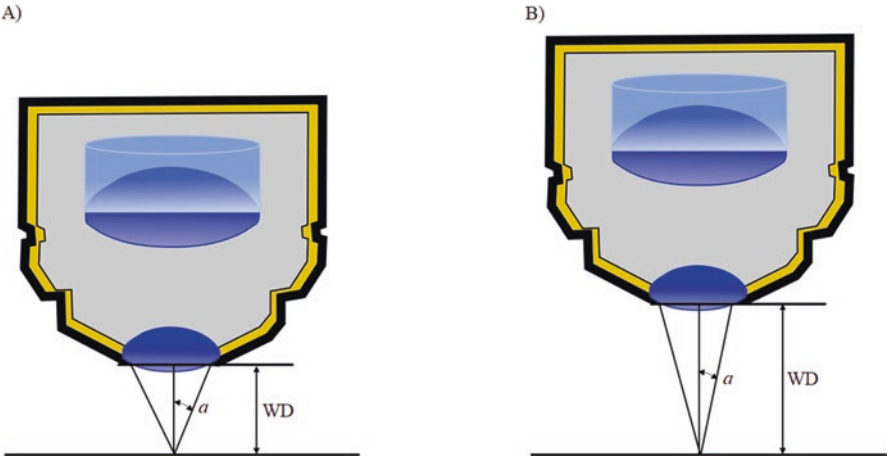

Fig. 2.6 (**a**) The numerical aperture (NA) of a microscope objective is defined by the semi-angle of the light cone between the principal lens of objective and the sample. (**b**) The working distance (WD) is the separation between objective and sample; it affects the NA of the objective

is also the parameter that determines the minimum resolvable feature discernible with a given objective, i.e., the resolution. The higher the NA of an objective, the finer the specimen detail it can resolve (Fig. 2.6a) [5].

The numerical aperture and its physical implications in the resolution of an optical system were studied by Ernest Abbe when he worked for Zeiss, the mathematical equation that defines the NA is:

$$\mathrm{NA} = n\mathrm{sin}\mathrm{sin}a \tag{2.1}$$

where, NA is the numerical aperture, n is the refractive index of the medium between the objective and the specimen, and a is one-half of the angular aperture. The numerical aperture is an important factor to consider to maximize image brightness. The objectives with higher numerical aperture have a capacity to collect more light from the sample because the light-concentrating power of the objective (serving as a condenser) is proportional to the square of the numerical aperture $(\mathrm{NA})^2$, and the light gathering power of the objective is also proportional to $(\mathrm{NA})^2$. Thus, for all but the highest NA objectives, brightness varies as $(\mathrm{NA})^4$ [2].

The working distance (WD) is measured in millimeters and specifies the distance between the front edge of the objective lens and the specimen surface, including the cover glass in case of immersion objective lenses, when the specimen is focused (Fig. 2.6b). Increasing the WD results in lower NA or additional complexity due to the need to correct spherical and chromatic aberrations, which is very challenging with high NAs [6].

2.7 Köhler Illumination

To achieve a higher performance and obtain high-quality images in the microscope, the Köhler illumination calibration must be applied routinely. The objective of this process is to optimize the optical system of the microscope with respect to the light. Köhler illumination allows to illuminate the specimen uniformly without artifacts, i.e., the beam diameter of the light source must be similar to the collecting area of the objective. To reach light uniformity in the sample, the optics should be adjusted in sequential steps. The collector lens on the field diaphragm collects light from the lamp and focuses it at the front focal plane of the condenser lens. The light crosses the condenser lens and illuminates the specimen. In this step, the condenser must be adjusted to allow the light beam to fill the aperture and thus illuminate the specimen with a solid cone of homogeneous light. Correct illumination of the visualization area decreases image degrading by light scattering. A practical summary to achieve Köhler illumination is described below:

1. The specimen should be in focus.
2. The field diaphragm (the iris located nearest to the light source) must be closed up to the point where one can see just the edges of the diaphragm appearing in the field of view.
3. The edges of the iris must be in focus, do this by changing the focal plane (moving the condenser focusing knob). Both, the sample and the iris edge, should be in focus.
4. The image of the iris must be centered with respect to the sample image. This is achieved by using the condenser-centering screws that control the *x*-*y* movement of the condenser.
5. Once centered and focused, the hexagonal plane of the iris must be opened so the edges lie just outside the edges of the field of view.
6. The contrast of the image must be adjusted by opening or closing the field diaphragm of the condenser. The optimum opening depends on the type of specimen observed; for plant and animal tissues the change of contrast with aperture is of lower magnitude as compared to the change in free cells samples.
7. Finally, the light intensity must be adjusted to a convenient level to improve the image contrast. This can be done either by regulating the power in the light source or by using neutral density filters placed after the light source.

As aforementioned, the Köhler illumination calibration must be done frequently due to possible mechanical shifts of the microscope; these changes can result in poor performance of the optical system. Moreover, the Köhler optimization is a prerequisite for advanced visualization methods.

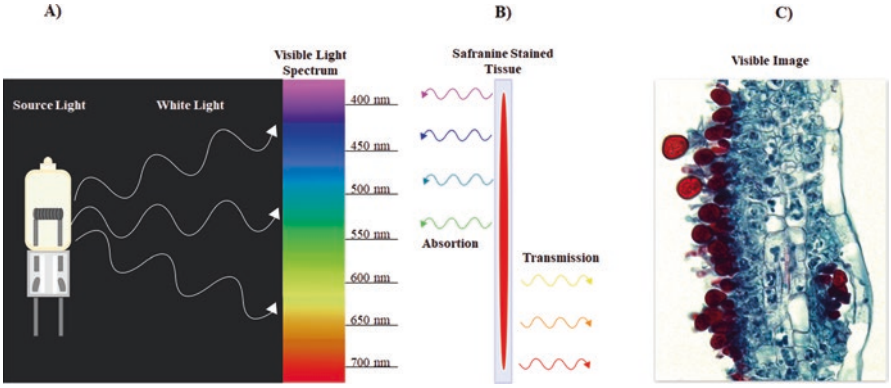

Fig. 2.7 Image contrast induced by staining in optical bright-field microscopy. (**a**) Tungsten bulb produces white light containing all the visible spectrum. (**b**) Safranine dye absorbs a part of the spectrum and transmits the yellow, orange, and red wavelengths. (**c**) Image shows chlamydospores of fungi (sexual structures) with high affinity to safranine (red color)

2.8 Contrast in Biological Samples by Staining

Biological samples consist mainly of water; this represents a challenge for their visualization since there is almost no contrast between their components. Different contrast agents and techniques are in use in modern microscopy. A widely used scheme to provide contrast in images is through staining; for example, in many histological techniques, tissue is cleared and stained with several dyes formed or made by one pigment or a mix of pigments with *mordant* metal salts that function as the fixative colors [5, 7]. Pigments are constituted of molecules called chromophores and are classified by their reactive functional group in the transition $n \rightarrow \pi$ and $\pi \rightarrow \pi$ that produce the color. Some common chemical groups of chromophores are azo and anthraquinone dyes [8] with extended conjugations. Chromophores show a higher capacity to link to hydroxyl (OH), carboxyl (COOH), and amino (NH_2) functional groups of the structural biomolecules of cells due to the auxochrome domain of dyes making possible the coupling to the tissue [7].

In classic staining for histology, the combination of dyes with different colors does not produce a new color [5]. The color of the dye is produced by the absorption of light in specific regions of the visible light spectrum. For example, safranine staining shows an intense red color in plant and animal tissues; this color is observed under white light illumination (light that contains all the visible colors) after the stained tissue absorbs the green, cyan, and violet components of the incident light and allows only the transmission of colors corresponding to an intense red (Fig. 2.7). In a microscope, the contrast balance of an image is regulated by the aperture of the condenser diaphragm; while the brightness is adjusted by modulating the light intensity of the source through the use of filters that attenuate the light.

2.9 Fluorescence Microscope

In 1838, David Brewster discovered a new optical phenomenon that was further studied by Sir George G. Stokes in 1852 who described some experiments that revealed "refrangible radiations" from many biological materials; this phenomenon is what we now know as fluorescence, which involves the capacity of some substances to emit visible light when they are illuminated with ultraviolet (UV) light. The implementation of fluorescence in microscopy can be attributed to studies by Stokes, who designed the first excitation and emission filters and used sunlight as the source of UV. The excitation filter was elaborated with a solution of cuprammonium (cupric hydroxide in ammonia water) to hold back the visible light of the spectrum and project the UV light onto the sample; while the emission yellow barrier filter was a compound of potassium dichromate to allow the fluorescence to be separated from the background [9].

The incorporation of fluorescence into a microscope requires an engineering adjustment to the equipment. In 1903, Henry Friedrich Wilhem Siedentopf and Richard Adolf Zsigmondy developed the slit ultramicroscope for the Carl Zeiss company. Siedentopf manufactured a dark-field condenser that blocked the incident light from the microscope objective, thereby improving the specimen contrast [10]. However, Siedentopf reported that the UV light produced spots of fluorescence from the sample. In the case of Siedentopf microscope, the fluorescence was a problem due to the reduction of the contrast of the sample.

At the same time, improved quartz monochromatic UV objectives were developed by Moritz von Rohr and subsequently the mathematical explanation, improvements to the construction of microscopes and photographic acquisition equipment were apported by August Köhler in 1904 [9]. Using ultraviolet light in microscopy can increase its resolution, since according to a fundamental describing resolution equation, discovered by Ernest Abbe (Eq. 2.2), the best resolution that can be achieved with a given optical microscope depends on the wavelength of the exciting light [10]. The shorter the wavelength, the smaller the minimum resolvable feature on the sample.

$$d = \frac{\lambda}{\mathrm{lnlnsin} \propto} = \frac{\lambda}{l\mathrm{NA}} \tag{2.2}$$

In this formula, λ represents the wavelength of light, l is a geometrical factor of order 1, n is the index of refraction of the medium, α is the half-angle of the focused cone of light after the objective of the microscope and NA is the numerical aperture.

2.10 Physical Principles of Fluorescence

Quantum mechanically, light can be thought of as a wave or as a particle, it actually has this dual character just as other particles. The intensity of a beam of light is related to the number of photons that make up that beam, but each individual photon has energy determined by its frequency, ν, by the formula $E = h\nu$ (h is Plank's

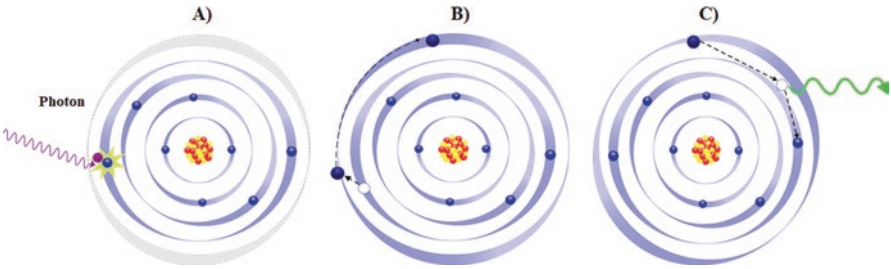

Fig. 2.8 The excitation and fluorescence emission are a quantum effect. (**a**) Energy transfer from a photon to an electron in an atom. (**b**) The excited electron jumps to a higher state of energy. (**c**) The loss of energy during transition to a basal orbital produces a photon in a visible spectrum

constant). Fluorescence is the emission of light by an atom or molecule after it is excited with light of higher photon energy than the emitted photon. When light is incident on a fluorescent material it is absorbed (Fig. 2.8a) resulting in the annihilation of one of the incident photons and a valence electron making a transition to a higher energy level (Fig. 2.8b), it is said that the electron is in its excited state. The energy difference between the excited and ground electron levels must be equal to the energy provided by the photon. After "arriving" at the high energy level, the electron loses some of its energy giving it to the "bulk" of the material and relaxes back to the lower energy level that is occupied at the beginning, the excess energy is emitted as a photon with lower energy than the originally absorbed photon (Fig. 2.8c) [2, 7, 11].

Any given fluorophore will be excited with efficiency dependent on the colors of the exciting light, this information is codified in an absorption spectrum. The intensity of the fluorescence as a function of the color of the emitted light is recorded in an emission spectrum (Fig. 2.9a) [8]. In a fluorescence microscope, the excitation of the fluorochrome (*Ex*) is induced by a narrow range of wavelengths determined by the excitation filter (Fig. 2.9b). The fluorescence emitted by the excited molecule is the emission (*Em*) which is collected by the objective and is visualized after passing through a dichroic mirror and an emission filter installed in the microscope [5]. The broad range of emission wavelengths that reach the eyes or the photodetector (camera) is represented in a spectral curve of the intensity of fluorescence displaced to the lower energy region of spectral wavelength (Fig. 2.9b).

2.11 Lamp

The lamp is an electric device used to generate intense radiant power within a given wavelength range [12]. Robert W. Wood in 1903, developed an arc lamp with a dye solution of nitrosodiumethylaniline efficiently producing ultraviolet light between 300 and 400 nm [9, 10]. The first fluorescence microscopes showed poor performance due to a low number of photons reaching the eyes. The incorporation of an efficient source of UV light solved the problem, this was possible with the

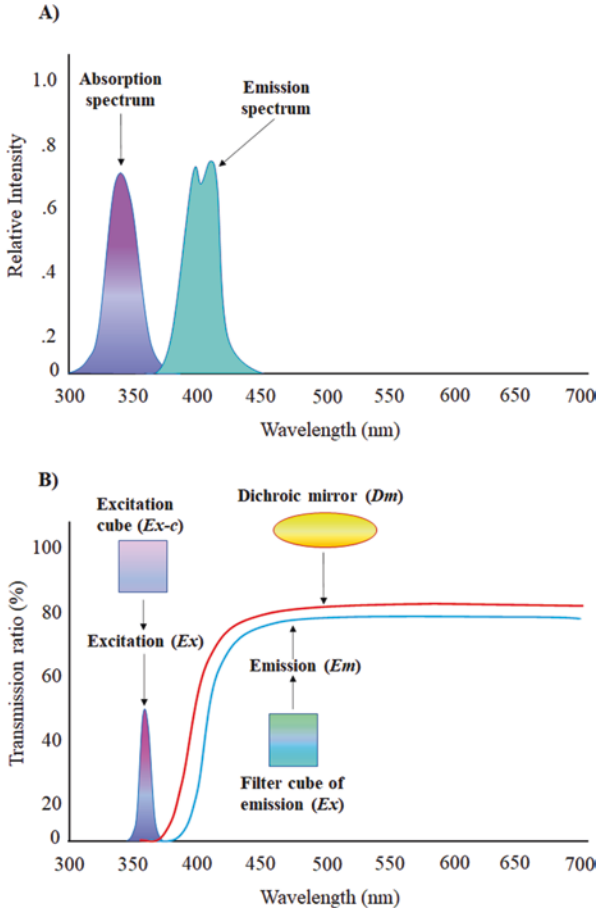

Fig. 2.9 Spectral curves of a hypothetical fluorochrome. (**a**) Conceptualization of the fluorescent dye, emission–absorption curves. (**b**) In fluorescence microscopy, the spectra of emission–excitation curves change according to the used filter cubes

development of the vapor mercury lamp. Mercury lamps contain two electrodes sealed under high pressure in a quartz glass bulb that also contains vaporized mercury. When the electrical energy is switched on, a continuous high voltage is established between the electrodes, ionizing the mercury gas leading to an efficient emission of UV light. After 3–5 minutes of use, the emission stabilizes when the voltage shows a reduction because the ionized gas acts as a bridge and generates a plasma between the electrodes. The mercury vapor lamp produces plenty of ultraviolet light but a lower intensity in the visible spectrum region. The emitted light did not have a continuous spectral profile, it showed peaks of high intensity at 313, 334, 365, 406, 435, 546, and 578 nm and is used with the majority of commercial fluorophores [13]. Another problem with this type of lamp is that its efficiency of UV light production decreases with time.

The luminous efficiency of a lamp, expressed in lumens per watt, is a measure of how efficiently a lamp converts electrical power, expressed in watts, to light expressed in lumens [12]. Image brightness in fluorescence microscopy is dependent on optical as well as technical factors. Optical factors include the numerical aperture of the objectives (the higher the aperture, the brighter the image) due to the higher light concentration. Another optical factor is the brightness, which is dependent on the magnification steps; multiple magnification sequences lead to reduced intensity in the final image; the brightness of the image is inversely proportional to the square of the eyepiece magnification [2]. On the other hand, some technical factors are the concentration of the fluorophore used to stain the sample since this affects the brightness, incubation time of the fluorophore sample, dilution of the buffer, molarity and pH of the buffer used to wash, mounting medium, degasification, and stabilization of samples after mounting.

2.12 Filters for Excitation and Emission

In fluorescence microscopy, the goal is to produce highly efficient illumination onto the sample and to capture sufficient fluorescence emission spectrally separated from the excitation wavelength to produce a clear image. In modern microscopy equipment, the use of excitation filters allows the illumination of the sample at a specific wavelength, producing an excitation within a well-defined range (Fig. 2.10) [2]. Dichroic mirrors are a filter with double functions. One side reflects excitation light from the UV source to the sample and the other side allows emission wavelengths to pass from the sample to the detector or ocular. The dichroic mirrors are positioned at 45° from the emission filter and excitation filter (Fig. 2.10). The fluorescence of the sample is visualized using a barrier or emission filter opaque to the excitation wavelength but transmissive to the longer wavelengths emitted from the sample (Fig. 2.10) [14]. These filters are mounted in an optical block or carcass manufactured in plastic or metallic material with several shapes that depend on the brand and model of the microscope.

As aforementioned, the first filters used during development of the fluorescence microscope were solutions of metallic salts in different stages of oxide reduction that showed a capacity to adsorb energy and transmit fluorescence. These first developed filters consisted of glass pieces stained with dyes or the combination of two filters to form band-pass filters [14]. Nowadays, commercial filters for fluorescence analysis consist of two types: colored glass filters and thin-film coated filters [15].

Colored glass filters attenuate light by absorption; therefore, the spectral performance is dependent on the thickness of the glass. Some advantages of these filters are the relatively low cost of production, stability, durability, and that their spectral performance is independent of the angle of incidence of the beam. Among their disadvantages, the following can be mentioned, limited versatility in their fabrication, high autofluorescence, low heat dispersion (leading to mechanical stress and

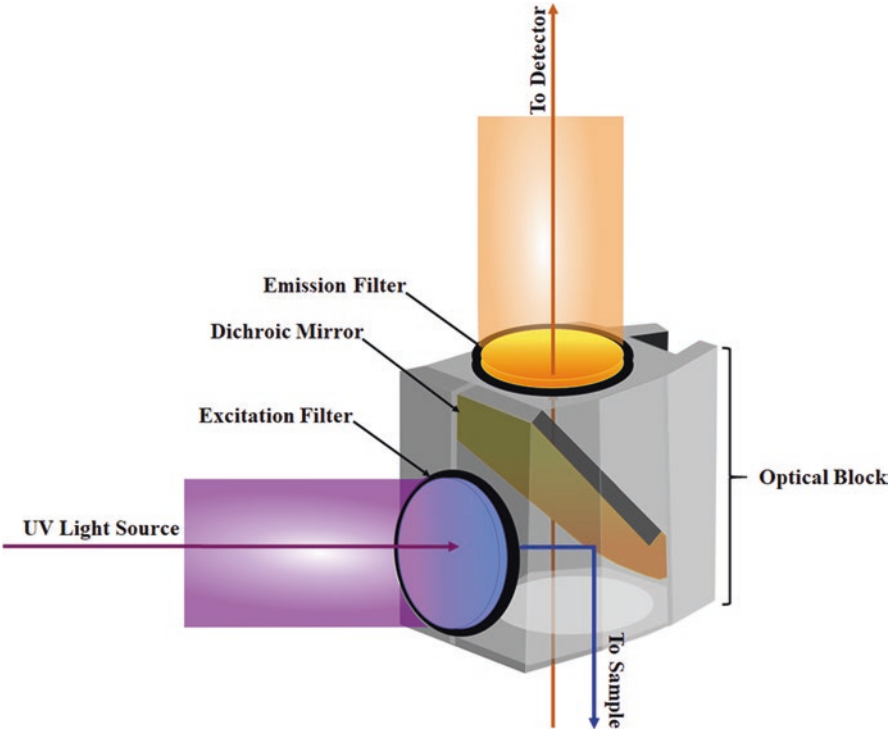

Fig. 2.10 Filter cubes for fluorescence microscope are composed of excitation filter, dichroic mirror, and emission filter, under optical block or carcase

breakage), band-pass filters of this type show relatively poor performance and low peak transmittance [15].

On the other hand, thin-film coated filters have two subtypes, metallic coatings and thin-film interference coatings. The filters manufactured with metallic coatings are more used in microscopy as reflective mirrors and neutral density filters (used to control the intensity of light). The interference coatings are composed of a stack of nanometric thin layers formed by sputtering metals, each with a thickness on the order of a wavelength of light, approximately 1/10,000 of a millimeter in thickness [15]. Different types of filters can be fabricated with this mechanism, such as band-pass, shortpass, longpass, or dichroic beamsplitters. Some limitations observed in these filters are that the characteristic blocking performance only holds within a finite wavelength range, the coating materials are limited in their range of transparency, and that interference coatings are sensitive to the angle of incidence. Some solutions to these problems are adding an absorption glass that increases the blocking range between interference coatings or changing some sensitive materials. However, this solution might lead to secondary effects, for example, reduction in transmission (show lower brightness of fluorescence in images) or increasing the thickness of glass.

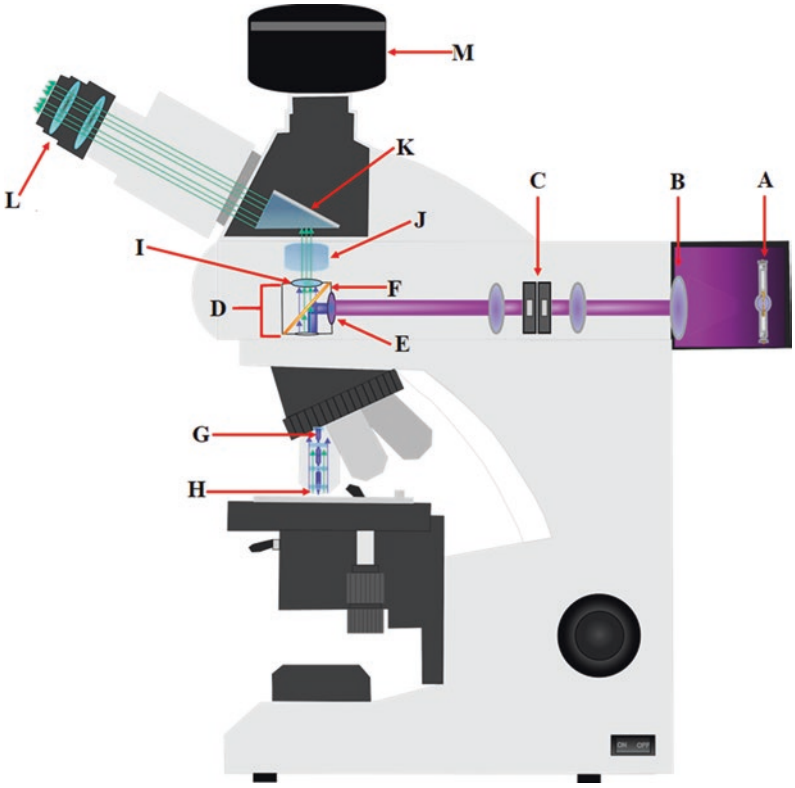

Fig. 2.11 Electrical and optical devices that conform a fluorescence microscope. (**a**) Mercury lamp. (**b**) Collector lens. (**c**) Condenser and field diaphragms. (**d**) Filter cube. (**e**) Filter emission glass. (**f**) Dichroic mirror. (**g**) Objective. (**h**) Lens objective. (**i**) Emission glass filter. (**j**) Tube lens. (**k**) Beamsplitter. (**l**) Oculars. (**m**) Camera

2.13 Components of the Fluorescence Microscope

The mechanical statives of a fluorescence microscope (Fig. 2.11) and an optical bright-field microscope are similar (Fig. 2.3); however, as it has been mentioned in previous sections, the source of UV light and the need for excitation and emission filters are of great importance and require appropriate accommodation. It has been found that it is advantageous to install these components in a reflected light vertical illumination geometry, with the illumination source interposed between the observation viewing tubes and the nosepiece carrying the objectives. A universal configuration is typically implemented in the following way: the source of light is a vapor mercury lamp (Fig. 2.11a) installed in a reflective case that concentrates the UV

light and efficiently dissipates heat. The UV light is collimated by the collector lens (Fig. 2.11b) and aligned and centered with an intermedial dispositive called aperture and field diaphragms, respectively (Fig. 2.11c) to satisfy the Köhler illumination condition for fluorescence. The UV beam arrives at the excitation filter cube (Fig. 2.11d), where the broad UV spectrum from the lamp is decreased to the excitation wavelength required by the sample through the excitation filter glass (Fig. 2.11e). The filtered excitation light is reflected by a dichroic mirror (a mirror able to reflect some wavelengths and transmit others, Fig. 2.11f) to change its trajectory by 90-degrees and send it to the objective. The objective is used to focus the light into the sample and as a correcting condenser of the trajectory of the rays because the microscope objective is always in correct alignment (Fig. 2.11g). Once the excitation light arrives to the sample, it is absorbed and induces fluorescence which is emitted over a 4π solid angle; some of the fluorescence rays reach the front lens of objective and are collected (Fig. 2.11h), the collection efficiency depends on the numerical aperture (NA) of the objective. The objective allows for correction of the trajectory of the rays collected producing a collimated transmitted fluorescence beam. The fluorescence, overlapped with reflected excitation light, returns to the dichroic mirror that, in this step, acts as a barrier filter (as aforementioned excitation wavelengths are reflected but longer wavelengths are transmitted). The emission glass filter has a double function, to isolate the fluorescence emission with maximum sensitivity and to enable image formation on a dark background (Fig. 2.11i). The image formation is done by the tube lens (Fig. 2.11j), which forms a virtual image. Finally, the fluorescence signal is reflected and divided into two parts in the beamsplitter (Fig. 2.11k) and sent to the eyepieces (Fig. 2.11l) or camera detection system to form the final image (Fig. 2.11m).

2.14 Fluorescence in Biological Samples

Some biological tissues show autofluorescence, this can be a major problem when preparing certain experimental protocols for animal tissues since the emitted autofluorescence can represent an undesired background. However, in plants the autofluorescence can sometimes be used to identify some biopolymers associated with a specific structure, i.e., Fig. 2.12, shows a slice of *Zea mays* root. The UV light interacts with some biomolecules, i.e., suberin, lignin, and cellulose, in the *Zea mays* roots that are able to produce fluorescence. The suberin compound is formed by monomeric aliphatic (ω-hydroxycarboxylic acids, 1, ω-dicarboxylic acids, carboxylic acids, and alcohols with chain lengths ranging from C_{16} up to C_{32}) and an aromatic domain covalently cross-linked hydroxycinnamic acid-derived matrix [16]. While, the lignins are racemic heterobiopolymers derivated from three hydroxycinnamyl alcohol monomers with three degrees of methoxylation to produce ρ-hydroxyphenyl, guaiacyl, and syringyl [17]. Although this example shows

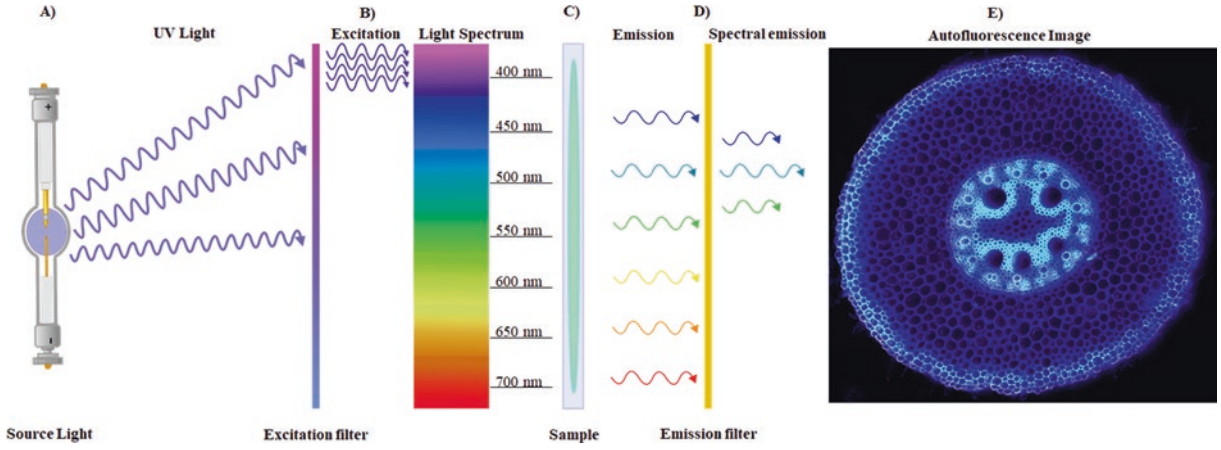

Fig. 2.12 In the fluorescence microscope, the color in a biological sample can be due to photoexcitation of endogenous molecules or artificial molecules added to the sample (fluorochromes). (**a**) The UV lamp produces light with several UV peaks. (**b**) The light crosses the excitation filter glass. (**c**) The light in the spectral region 350–360 nm interacts with biomolecules such as cellulose and lignin in the *Zea mays* root, producing fluorescence. (**d**) The emission of fluorescence is recovered by the objective of the microscope and crosses through the emission glass filter. (**e**) The fluorescence signal from the sample is used to produce an image by a capture media, like a digital camera

that for some specific systems autofluorescence can help to identify a chemical compound associated with a specific tissue structure, this is not generally true. In general, fluorescence cannot be used to identify specific chemical compounds; however, this can be accomplished with fluorochromes attached to antibodies and other cellular markers, fluorescent proteins, or using some more sophisticated techniques such as Raman microscopy.

In order to visualize nonfluorescent samples, it is necessary to use external fluorescent dyes or fluorochromes that show high capacity to emit light at different spectral ranges from the ultraviolet, through the visible, to the near infrared. There are several fluorescent dyes; however, for them to be most useful they must satisfy some requirements such as producing a specific color, a high molar extinction coefficient and, most importantly, a high quantum yield [8]. The λ_{max} of the emission spectrum of a dye is typically ~20–50 nm longer than that of its absorption; however, the separation of the maxima of the excitation and emission spectra (*Stokes shift*), can range from <10 to >100 nm [14].

2.15 Fluorochromes

Nowadays, there exist multiple alternatives of fluorochromes in the market for staining; several of these chemical compounds can have an affinity to locate themselves in specific cellular organelles or in the microstructure of biomaterials. However, before mounting an experiment, the microscopist must consider some points to obtain the best image, among them the type of UV source installed in the microscope, excitation and emission ranges of the filter cubes, and characteristics of the sample, i.e., if the analysis of the sample is in vivo or previously preserved by chemical fixation, if the fixation process is soft or hard, if the sample can be analyzed in one piece or if it can be cut in thin slices.

In a biology research laboratory, the uses of fluorescence microscopy are plentiful; it is used to visualize differentiation of cellular organelles, growth process, delimitation of some structures during development, compartmentalization of metabolites, cell and death response to administration of drugs, response and localization of damage during pathogen attack and visualization of the biological interactions as symbiotic relations in eukaryotic cells, among many other applications. On the other hand, in biomaterial research the interest changes, the fluorescence microscope is used to describe the presence or absence of some materials, the morphology and morphometric characteristics of materials, modifications before and after chemical of physical treatments, chemical composition and its alteration in relation to sample processing, to mention some.

To study the physical changes or biological processes of interest, the microscopist has a wide variety of fluorochromes within his/her reach. In Table 2.1, the most

Table 2.1 Fluorochrome classification by excitation and emission filter and molecular affinity

UV excitation	Fluorochrome	Affinity	Organelle
Excitation 365/10 Emission 420LP Dichroic Mirror 400LP	DAPI	DNA stain	Nucleus
	Hoechest 33258–33342	DNA stain	Nucleus
	Alexa Fluor 350 Hydrazide	Aldehydes or ketones in polysaccharides or glycoproteins	Cytoplasm
	Calcofluor	Cellulose and chitin	Cell walls of yeast, fungi and some parasitic organism
	LysoTracker Blue DND-22	Acidic organelles	Lysosome
Blue excitation			
Excitation 480/20 Emission 520LP Dichroic Mirror 505LP	FITC	Immunolabeling of peptides, proteins, tracers, or amplification substrates	Several organelles
	EGFP	Molecular biology as label	Several organelles
	Alexa Fluor 488	Immunolabeling of peptides, proteins, tracers, or amplification substrates	Several organelles
	Acridine Orange	DNA or RNA	Lysosomal, death/live and cell-cycle
Green excitation			
Excitation 535/30 Emission 580LP Dichroic Mirror 565LP	TRITC (Tetramethylrhodamine)	Immunolabeling of peptides, proteins, tracers, or amplification substrates	Several organelles
	Rhodamine	Cationic molecules	Active mitochondria
	RFP	Molecular biology as label	Several organelles
	Alexa Fluor 546	Immunolabeling of peptides, proteins, tracers, or amplification substrates	Several organelles
	Alexa Fluor 568	Immunolabeling of peptides, proteins, tracers, or amplification substrates	Several organelles
	Cy3	DNA stain	Nucleus
	EtBr		
	Mito-Tracker Red	Functional group Thiol	Mitochondria, previously fixed
	PI	All genetic material (DNA and RNA)	Death cells
Green excitation for special dyes			
Excitation 535/50 Emission 645/75 Dichroic Mirror 565LP	EthD-1	High-affinity nucleic acid	Death cells
	Nile Red	Neutral lipids	Lipid droplets
	FM 4-64	Polar lipids	Vacuoles

common fluorochromes are classified by a spectral band of excitation–emission and chemical affinity.

In order to measure the capacity to generate fluorescence and compare the efficiency between fluorochromes, a quantity called quantum yield (Φ) is defined as:

$$\$ = \frac{\text{Number of quanta emitted}}{\text{Number of quanta absorbed}} \tag{2.3}$$

This index is determined by relative rates of fluorescence emission and adsorbed exciting light and measures how efficient is the fluorochrome in converting incident light into fluorescence [8]. The activation of the excited state of the fluorochrome molecule depends on the environmental conditions; for example, when the fluorochrome fluorochrome is diluted in a high viscosity solvent the quantum yield increases, reaching a higher efficiency (Φ ca. 1.0 = 100%). While fluorochromes dissolved in low-viscosity solvents such as used in some protocols of staining, the quantum yield is often low and the efficiency of the fluorochrome is considered poor (Φ ca. 0.1 = 10%).

2.16 Classification of the Light Microscopes

In recent years, microscope manufacturers have reached great advances in the technologies applied to improve the optical and digital resolution and velocity of detection of biological molecules. In some cases, the magnifications of light microscopes have reached tens of nanometers of resolution, these systems are called superresolution microscopes and are available commercially. There are also hybrid systems, such as scanning probe microscopes (SPM) and atomic force microscopes (Fig. 2.13) that can have even atomic resolution by taking advantage of so-called near field effects.

For microscopy nonexpert users, there could be some confusion regarding the classification of light microscopes. When we refer to light microscopy, from the most basic to the most advanced equipment, the source of illumination is always light (photons), typically in some spectral range within UV-visible-near IR. On the other hand, when we talk about electron microscopy, the illumination source is not light but an electron beam, while for scanning probe microscopy it is the electrostatic forces between the probe tip and the studied surface. To understand the types of light microscopes, in Fig. 2.13 we offer a summary of the classification of microscopes based on the illumination source.

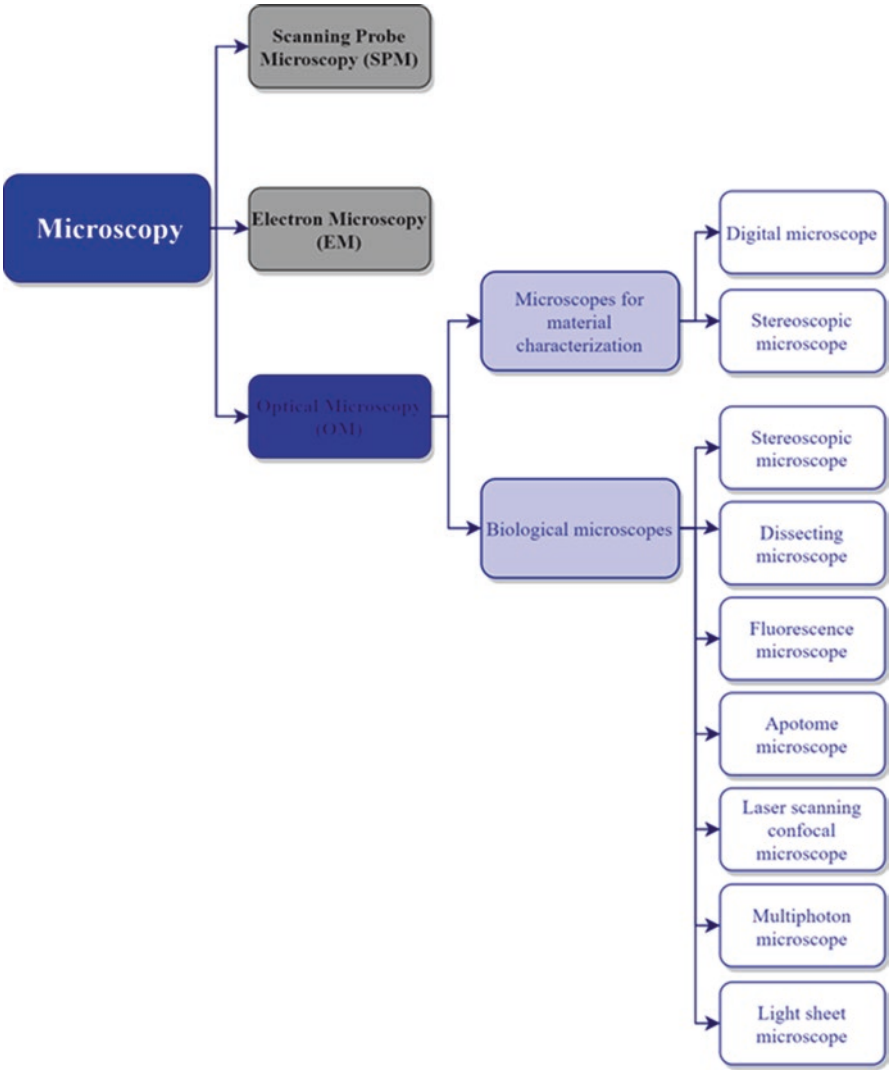

Fig. 2.13 Classification of the several types of microscopy. Light microscopy shows two main subclassifications based on the application, for material characterization and biological samples

References

1. Davidson M (2018) Introduction to lenses and geometrical optics. https://micro.magnet.fsu.edu/primer/lightandcolor/lensesintro.html. Accessed 24 Feb 2021
2. Jacobson K (2010) Fluorescence microscopy. In: Encyclopedia of life sciences (ELS). John Wiley & Sons Ltd, Chichester. https://doi.org/10.1002/9780470015902.a0002637.pub2
3. González H, Nuñez M, Arce H (1997) Visión y lentes delgadas, 1st edn. Las Prensas de Ciencias-UNAM, Mexico City
4. Hecht E (2002) Optics. Addison-Wesley, San Francisco
5. Ruzin SE (1999) Plant microtechnique and microscopy. Oxford University Press, New York
6. Zhang Y, Gross H (2019) Systematic design of microscope objectives. Part I: system review and analysis. Adv Opt Technol 8:313–347. https://doi.org/10.1515/aot-2019-0002
7. Sandoval E (2005) Técnicas aplicadas al estudio de la anatomía vegetal. Instituto de Biología-UNAM, Mexico City
8. Hunger K (ed) (2003) Industrial dyes: chemistry, properties, applications. Wiley-VCH, Weinheim. https://doi.org/10.1002/3527602011
9. Kasten FH (1989) The origins of modern fluorescence microscopy and fluorescent probes. In: Kohen E, Hirschberg JG (eds) Cell structure and function by microspectrofluorometry. Academic Press, San Diego. https://doi.org/10.1016/B978-0-12-417760-4.50008-2
10. Masters BR (2010) The development of fluorescence microscopy. In: Encyclopedia of life sciences (ELS). John Wiley & Sons Ltd, Chichester. https://doi.org/10.1002/9780470015902.a0022093
11. Hewitt PG (2002) Conceptual physics, 9th edn. Addison Wesley, San Francisco
12. Zissis G, Damelincourt JJ (2002) Electrical discharge light sources: a challenge for the future. J High Temp Mater Process 6:521–537. https://doi.org/10.1615/HighTempMatProc.v15.i3.20
13. Olympus (2021). Light sources in fluorescence microscopy. https://www.olympus-lifescience.com/en/microscope-resource/primer/techniques/fluorescence/fluorosources/.htm. Accessed 24 Feb 2021
14. Coling D, Kachar B (1998) Principles and application of fluorescence microscopy. Curr Protoc Mol Biol 44:14–10. https://doi.org/10.1002/0471142727.mb1410s44
15. Reichman J (2017) Handbook of optical filters for fluorescence microscopy. Chroma Technology Corporation, Lane Bellows Falls
16. Zeier J, Ruel K, Ryser U et al (1999) Chemical analysis and immunolocalisation of lignin and suberin in endodermal and hypodermal/rhizodermal cell walls of developing maize (*Zea mays* L.) primary roots. Planta 209:1–12. https://doi.org/10.1007/s004250050601
17. Boerjan W, Ralph J, Baucher M (2003) Lignin biosynthesis. Annu Rev Plant Biol 54:519–546. https://doi.org/10.1146/annurev.arplant.54.031902.134938

Confocal and Multiphoton Microscopy

3

Ramón Carriles, Laura E. Zavala-García,
and Lino Sánchez-Segura

Abstract

Confocal and multiphoton microscopy are considered advanced instruments in the field of light microscopy due to the complexity of the optical and electronic components employed to build the instruments; however, the physical concepts involved in both instruments are comparable to those of basic fluorescence microscopy. The efficacy of laser scanning confocal microscopy (LSCM) lies in decreasing the out-of-focus collection of light leading to a reduction of the blurriness of the acquired images. A combination of transverse resolution and noninvasive optical sectioning results in very high-quality 3D images of biological specimens. This chapter explains the basic concepts in confocal microscopy that lead to the improved contrast and generation of three-dimensional images of biological and material samples. On the other hand, multiphoton microscopy (MM) is based on using nonlinear optical phenomena to provide the contrast mechanism for image acquisition implemented in a laser scanning microscope. In a nonlinear phenomenon, two or more photons are combined to generate the signal from the sample; some examples of these phenomena that have been used in MM are Two-Photon Excited Fluorescence (TPEF), Second Harmonic Generation (SHG), Third Harmonic Generation (THG), and Coherent Anti-Stokes Raman Scattering (CARS). A multiphoton microscopy is able to produce high-resolution 3D images and hyperspectral imaging.

Ramón Carriles
División de Fotónica, Centro de Investigaciones en Óptica, A.C., León, Guanajuato, Mexico
ramon@cio.mx

Laura E. Zavala-García
Centro de Desarrollo de Productos Bióticos, Instituto Politécnico Nacional, Yautepec, Morelos, Mexico
elizavala1993@gmail.com

Lino Sánchez-Segura
Departamento Ingeniería Genética, Centro de Investigación y de Estudios Avanzados del Instituto Politécnico Nacional, Carretera Irapuato-León, Guanajuato, Mexico
lino.sanchez@cinvestav.mx

S.-K. Kamaraj et al. (eds.), *Microscopic Techniques for the Non-Expert*,
https://doi.org/10.1007/978-3-030-99542-3_3

Keywords

Multiphoton microscopy · Confocal microscopy · Photobleaching · Laser · 3D images

3.1 Introduction

A typical challenge confronting the microscopist using fluorescence imaging is related to the thickness and the texture of the tissue. Variations of size and morphology of cells within tissue produce artifacts that prevent form properly focusing the sample and degrade the resolution of the imaged structures. These phenomena produce blurry images, out-of-focus points in panoramic micrographs, and overlapping structures (Fig. 3.1) [1–3].

To appreciate the great advance that the confocal microscope represented, we must understand the main deficiency in the fluorescence microscope, the blur. An ideal fluorescence microscopy image should be restricted in the depth of focus, i.e., the signal should be limited to being generated at the focal plane. If this condition is not met, fluorescence light from different parts of the sample will be captured by the detector as corresponding to the same plane and the image will look blurry or "out of focus"; this is the result of trying to have a limited two-dimensional view of the three-dimensional object that is the cell [4]. In the fluorescence microscope, the illumination is projected uniformly onto the sample, resulting in signal being

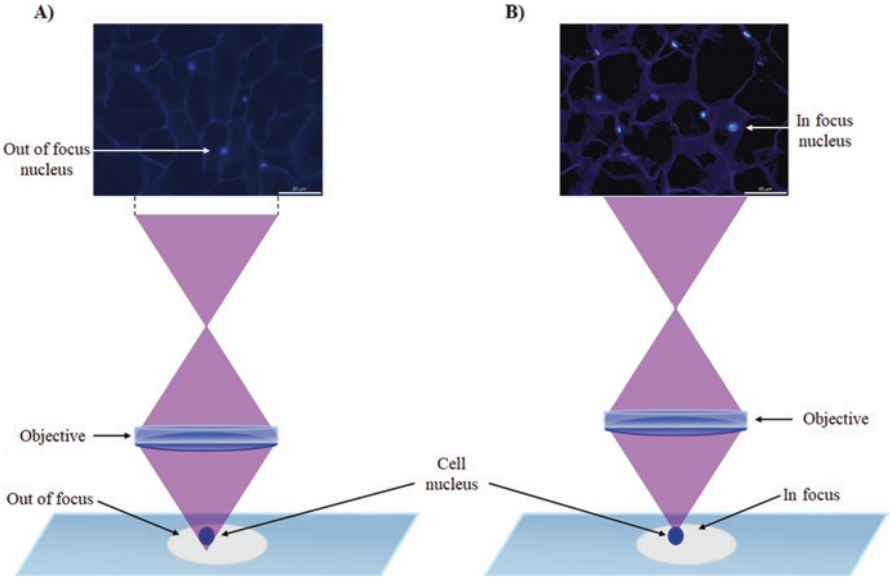

Fig. 3.1 Plant tissue visualized by fluorescence microscopy. (**a**) Image from a thick sample illustrating out-of-focus contributions and blurriness. (**b**) A thin sample produces a focused image

generated in a much larger volume than the focal plane of the objective (Fig. 3.1a). The signal photons can also be scattered within the sample and produce contributions from points outside of the focal plane, producing lower contrast and resolution in the image (out-of-focus) [5].

This situation was analyzed by Marvin Minsky in 1955 and conceptualized in the following idea: "An ideal microscope would examine each point of the specimen and measure the amount of light scattered or absorbed by that point" [1, 6]. This idea was implemented by placing two pinholes, one in the illumination path and the other in the detection line. The excitation light is focused by an auxiliary lens onto the first pinhole that is placed strategically so that the objective lens will form an image of this small aperture inside the sample, exactly at the point where one wants to induce fluorescence. Note that signal photons generated by scattered excitation light anywhere else in the sample will not pass through the selected point. Prof. Minsky put a second objective and pinhole on the transmitted side of the specimen. This collection objective will image the focal volume of the excitation objective onto the second pinhole; therefore, only the signal photons generated at the focus of the first objective will be collected and all other photons generated anywhere else in the sample will be blocked from reaching the detector by the second pinhole (Fig. 3.2a). "We end up with an elegant, symmetrical geometry: a pinhole and an objective lens on each side of the specimen" [5]. This arrangement significantly reduces the blurriness due to scattered excitation and signal photons. The price we have to pay is that now we have to build the image point by point through raster scanning the focal volume of the excitation objective. The name confocal microscopy is derived from the fact that, in geometrical optics, the planes where the pinholes are located are said to be confocal to one another. It is also possible, and common, to use only one objective to excite and collect the signal; the illumination and fluorescence can be separated because they are of different colors.

The introduction of the pinholes for confocal microscopy (CM) allows acquisition of the fluorescence signal only from the focal plane of the microscope objective (Fig. 3.2b). The pinhole is central to the confocal microscope, it is easier to visualize it as an aperture similar to the diaphragm of antique photographic cameras. The first pinhole of CM's were static round holes in an opaque material situated between light detector and sample [7]; modern instruments are capable of adapting the pinhole size to obtain better images. Fluorescent light is emitted without any specific preferred direction and it also can be scattered in the sample in several directions (360°); the pinhole blocks most of this unwanted light (Fig. 3.2b). On the other hand, the function of the pinhole displays more complexity, in comparison to a barrier-filter, because it is also an important component for determining both the axial and the transverse resolutions of the microscope. A smaller pinhole has theoretically better resolution, but transmits less light to the sample, so the signal-to-noise ratio decreases [8]. The pinhole diameter shows higher efficiency to eliminate out-of-focus light between 50 and 200 μm without significant loss of detectable focal plane light [7]. However, the diameter of the pinhole is not arbitrary, it is adjusted according to the diameter of the Airy disc produced by the objective in order to increase the resolution and decrease the thickness of the optical plane [7].

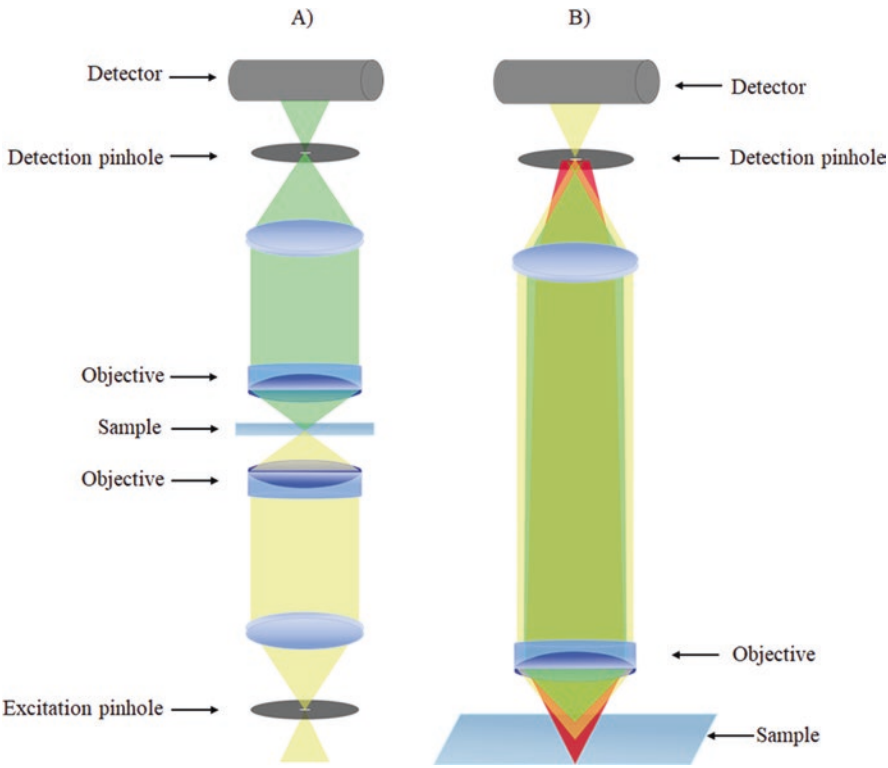

Fig. 3.2 The confocal microscope. (**a**) Scheme of a confocal microscope in transmission; the excitation pinhole is imaged at the focal point in the sample before being imaged by the detection objective through the detection pinhole. (**b**) The pinhole produces exact illumination and recovery of fluorescence only in the focal plane; as illustrated, the orange and green beams, produced outside of the focal plane, will be blocked by the detection pinhole

What is the Airy disc? To respond to this question, we first should ask, what is diffraction? diffraction is an optical effect present in all propagating waves by which their propagation is perturbed and distorted by the presence of an obstacle in their path; for example, when an opaque screen with a small hole in the center is illuminated by a lamp, the shadow projected on the opposite side produces a diffracted pattern. The sharp division that typically is present between an illuminated zone and the shadow zone disappears, producing transitional steps composed of regions with lower light intensity [9]. Diffraction is more visible when the aperture hole is of similar size as the wavelength of the illuminating light; this is the cause for us not to see diffraction easily in everyday life, the wavelength of light is approximately 500 nm. There are two limit cases for diffraction: *Fraunhofer diffraction* and *Fresnel diffraction*, also called far field and near field diffraction, respectively. The near field case is not relevant for our discussion, so we will focus only on *Fraunhofer diffraction*. When light is projected onto a screen containing a small circular aperture and then we look at the illumination pattern in a distant screen, we will see the

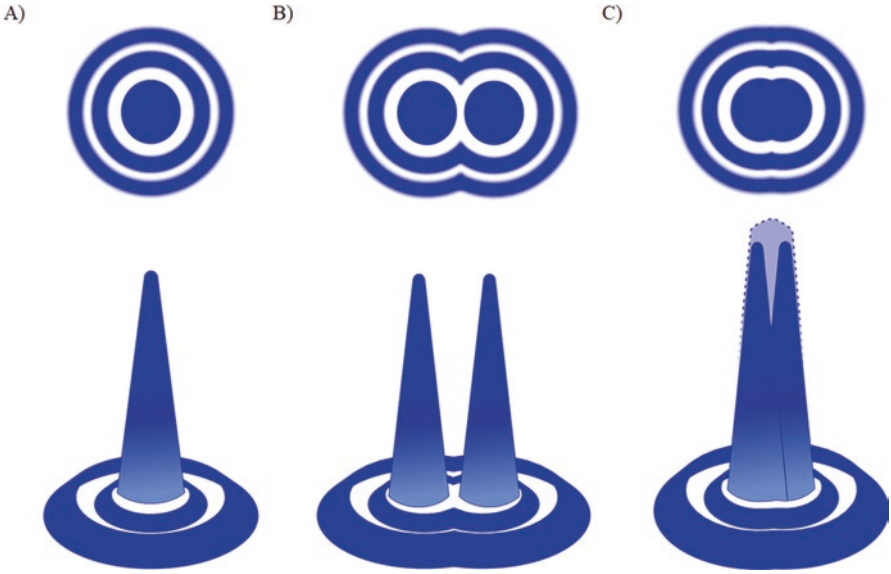

Fig. 3.3 Diffraction intensity patterns forming an Airy disc. (**a**) Airy disc due to a circular aperture. (**b**) Two emitting fluorescent molecules are resolved if they are separated by more than the distance between the central peak maximum of the Airy disc and the minimum of the first dark disc. (**c**) Intensity distribution pattern of two unresolved fluorescent molecules

diffraction pattern. The pattern will consist of a central bright spot, surrounded by a dark disc and subsequent bright and dark alternating discs (Fig. 3.3a). This intensity distribution of diffracted light by a circular aperture is called the Airy disc and was described by Sir George Biddell Airy (1801–1892), Astronomer Royal of England, he found the central disc is surrounded by a dark ring that corresponds to the first zero of a Bessel function [7, 10].

In an optical system, such as a microscope objective, the Airy disc size is determined by factors such as the numeral aperture of the optical components and the wavelength of light. In optical microscopes, including confocal, the Airy disc determines the focal spot size and the maximum resolution of the instrument, meaning the smallest discernable feature. There are several ways to define the resolving power or *Resolution* of an optical system; in microscopy, the most accepted criterion is due to Rayleigh and it establishes that two signal sources of equal intensities should be considered just resolved when the principal intensity maximum of one coincides with the first intensity minimum of the other (Fig. 3.3b) [7, 10, 11]. The *Point Spread Function* (PSF) of an optical instrument or element is the 3D light distribution formed by the system when imaging a point source; in the axial dimension it has an elliptical shape that is affected by the mounting medium, and the imaged specimen itself, among others [11]. When two features are not resolved (Fig. 3.3c) the image is visualized as if there were only one feature with distorted form.

If a structured object is visualized, its image will be formed by several individual diffraction patterns convolved from a series of single-point sources forming the object [4]. The isolated patterns of the Airy disc can be recovered and separated in the original signal by Fourier transforms (deconvolution) because the lens system previously performed a Fourier transform on the spatial distribution of light rays in the object space to form a frequency distribution of interference patterns in the image space [7]. The PSF is very important because it provides a measure of the microscope performance. In the case of confocal microscopes, the PSF distribution gives a transverse resolution (resolution along the focal plane) of approximately 180–200 nm that, depending on the biological sample, could correspond to the size of an organelle like a mitochondrion [4].

3.2 Sources of Light in Confocal Microscopy

The sources of light in optical microscopy include several types of tungsten lamps that produce intense white light, UV lamps for fluorescence microscopy and lasers. The most important difference between sources is their intensity and the emitted range of wavelengths, which can expand from the ultraviolet (250 nm) to the near infrared (2 μm). An important difference between lamps and lasers is that lamps emit incoherent light [2]. The most common source of coherent light is the laser. A laser (an acronym for *light amplification by stimulated emission of radiation*) is a dispositive that produces and amplifies an intense beam of highly coherent, highly directional light. The first laser was made in 1960 by Maiman using a flash-pumped rod of ruby with polished ends (ruby laser) [9, 12]. The concept of coherence in optics is intimately related to the relative phase between two sources of light or between one part of a beam and another part; we will not try to explain it since it is beyond the scope of this book, a cartoonish illustration is presented in Fig. 3.4a, b. The main consequences in microscopy related to the coherence of lasers are that coherent sources can emit more intense beams and that the emitted light is propagated in specific directions (in contrast with incoherent sources that typically emit

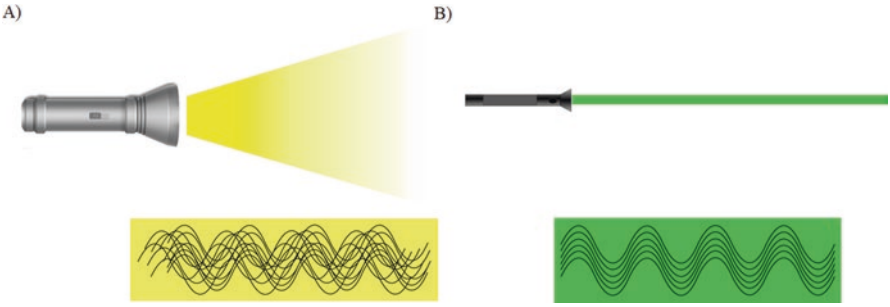

Fig. 3.4 (**a**) Incoherent source, propagation of light rays from a lamp. (**b**) Coherent source, propagation of laser light. In both panels, the wavy lines represent the individual light waves that make up the beams

in all directions). If we could isolate a single light wave from an incoherent source, we would see that the wave changes its phase after a short time, and loses intensity because it diverges [9].

A laser consists of three main components: first a gain medium that amplifies light by means of the basic process of stimulated emission, second a pump source which creates a population inversion in the gain medium, and third two mirrors (one of them with slight losses to allow the beam to exit, called the output coupler) that form a resonator or optical cavity in which light is trapped, traveling back and forth between the mirrors [10].

The confocal microscope incorporates one or more lasers as light sources for illuminating the samples; this is preferred than lamps because lasers have high radiance and produce monochromatic light. However, the coherent illumination causes trouble in microscopy because unwanted interference effects degrade the images [2]. The configuration of the laser in confocal microscopy is versatile, it can be from the opposite side of the observer, or it may be epitaxial. The epitaxial illumination is used for viewing opaque and fluorescent objects. Sometimes the configuration of confocal microscope for biological sciences is opposite to the observer; however, in recent years more microscopists use the epitaxial configuration due to its versatility to observe biological samples and opaque biomaterials, this type of material has to be seen by light scattered and reflected from its surface [2].

For Laser Scanning Confocal Microscopy (LSCM) operators it is important to know the characteristics of their laser. Two broad groups of lasers exist, continuous wave (CW) or quasi–CW, and pulsed laser. A CW laser exhibits a steady flow of coherent energy and its output power undergoes little or no change with time [12]. Many gas lasers, such as Ar-ion lasers and HeNe, operate on CW mode. Both of these lasers are widely used in LSCM because they can emit in different spectral lines; for example, the Ar-ion laser emits in the blue range (458, 488, and 514 nm), while the HeNe in the red range (543, 594, 612, and 632 nm). Pulsed lasers have an output beam that changes with time, they produce short optical pulses, usually in a repetitive way and with pulse duration usually ranging from nanoseconds (1 ns = 10^{-9} s) to femtoseconds (1 fs = 10^{-15} s). Typical examples of pulsed lasers are many solid-state and liquid lasers, such as Nd:YAG, Ti:Al_2O_3, and dye lasers. This type of laser is used mainly in multiphoton microscopes.

3.3 Signal Detector

The acquisition of the images in LSCM is different compared to the fluorescent microscope in which a digital camera is used. In confocal, the light emission captured by the objective can be recorded by several classes of photosensitive detectors, such as photomultipliers, photodiodes, and solid-state charge-coupled devices (CCDs). The most widely used detectors in modern confocal microscopes are photomultiplier tube (PMT). In the PMT, when a signal photon reaches the photocathode it releases an electron through the photoelectric effect; this electron is accelerated by a high voltage toward a sequence of electron multiplier stages, placed along the

tube and called dynodes, where this one electron liberates many more electrons, by secondary emission, that eventually reach the anode and leave in the form of a current (Fig. 3.5a, b). The dynodes are connected along a series of resistors that divide up the high voltage applied between the photocathode and the anode. To increase the gain of the signal from the sample, the kinetic energy of electrons between adjacent dynodes could be increased in the order of 200 eV, this would involve that one initial electron is able to release between 4 and 8 secondary electrons in each dynode, and each one of these electrons will release other 4 to 8 in the next dynode in a cascade effect. The total amplification factor in the dynode chain is typically between 10^6 and 10^8, thus a single signal photon incident on the PMT can produce a measurable current of around 1 pA. In order to estimate the efficiency of the PMT, the number of photoelectrons emitted from the photocathode divided by the number of incident photons is calculated, this parameter is called quantum efficiency (η), and is expressed as a percentage. The efficiency parameter is affected by the transfer of energy of incident photons to valence band of photocathode, in this step not all electrons are emitted as photoelectrons. The photocathode is made of alkali metals or semiconductors, usually in combination [13]. In a basic configuration of a LSCM, a multialkali photomultiplier (composed of SB-Na-K-Cs) is generally used due to its high sensitivity over a wide spectral response range from the ultraviolet to near-infrared region. While in advanced, more sensitive configurations a gallium arsenide phosphide (GaAsP) photomultiplier is preferred, due to its higher sensitivity and quantum efficiency in the visible region, although it shows poor performance in the ultraviolet region. The main differences between PMTs are the chemical composition of the electron multipliers, internal array, and electron trajectory, according to these characteristics PMTs are classified into two types: normal discrete dynodes consisting of multiple stages and continuous dynodes such as microchannel plates (MCP-PMT). Figure 3.5a, b show a cross section of a linear focused dynode (MCP-PMT) and box-and-grid structure of PMT, respectively. The MCP-PMT is more used in applications for image intensifiers for low-light-level imaging, fast time response as ultrafast photometry, and photon-counting imaging tubes for ultra-low light level imaging.

3.4 Formation of the Digital Image in LSCM

The representation of a real physical object or scene in LSCM is through a digital image visualized in 2D or 3D, from which we can obtain an accurate spatial (geometric) and/or spectral (for the case of hyperspectral imaging, where a spectrum of the signal light is collected at each pixel) representation with sufficient detail (resolution) for processing, compression, storage, and display.

Raster images are electronic files that consist of discrete picture elements, called pixels (short for picture elements). Digital images recorded from the LSCM are composed of pixels. Associated with each pixel is a number that is the average radiance (or brightness) of a relatively small area within a scene, representing the color or scale of grays at a single point in the image [14]. The sample area recorded by a

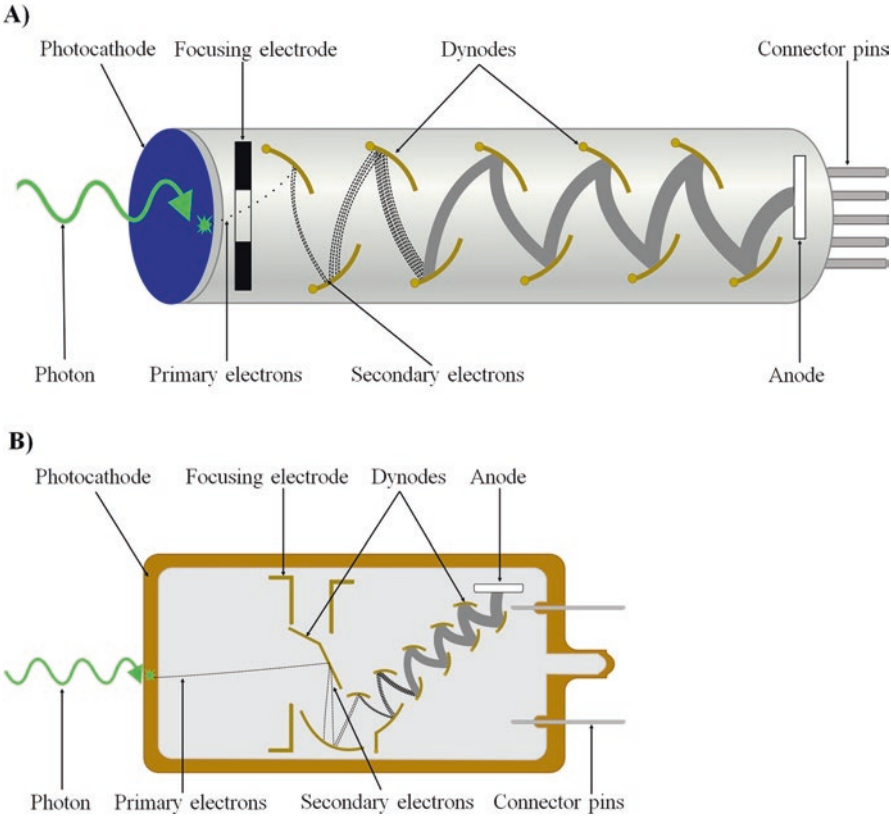

Fig. 3.5 Schematic configuration of a photomultiplier tube commonly used in a confocal microscope. (**a**) Linear-focused type photomultiplier tube (MCP-PMT). (**b**) Box-and-grid type photomultiplier

single pixel is related to the distance between two adjacent detection units in the detector and the amplification provided by the objective when projected into the focal plane [4]. Typically, a unit pixel can represent a sample size from a few microns to hundreds of nanometers, depending on the magnification used during acquisition.

An important practical point is that the resolution of the image is not controlled by the magnification of the microscope objective, but by the numerical aperture. The resolution is the minimum resolvable feature on the sample. The magnification only enlarges the image but it does not increase the detail already present in it determined by the NA. To acquire an image one has to balance different factors such as NA, magnification, pixels per line, pixel acquisition time, and laser power. The correct choice depends on the answer to questions such as, what is important to see or enhance in the final image? What will the image be used for? How large of an area do I need to image? What are the capabilities of my microscope? How high or low is the optical power damage threshold of the sample?

3.5 Scanning System for Processing Signal of the Sample

Modern LSCM are complex equipment that integrate improved optical components with multiple laser illumination devices and an efficient signal collection system with efficient photomultipliers. The signal from the detectors is processed by electronic interfaces to convert it into digital information (pixels) for storage and display in monitors and possible manipulation by software. An often overlooked step in this complex chain of events is the scanning mechanism; it is an important component of the confocal microscope that has an impact on the final image characteristics.

The simplest way to achieve confocal imaging is to leave the optics fixed and move the sample. There are two major advantages to moving the object: all the lenses work on axis, and the field of view is not constrained by optics. Lenses can easily be diffraction-limited for the single on-axis focus [2]. On-axis optics make it easier to correct for spherical and chromatic aberrations as well as coma. This design idea was applied to early versions of confocal microscopes designed by Minsky [6]. However, the greatest problem with this design is the inertia of the sample holder system, relatively low translation speeds and possible vibrations; these problems are especially acute at points where there are changes in the scanning direction.

To improve the quality of scanning, it is preferred to steer the laser beam instead of the sample stage. In modern confocal microscopes, the beam scanners are most typically small mirrors mounted on galvanometers (often called "galvos"). The galvanometer is a small electromechanical dispositive that gyrates in response to an applied current; ideally, its angular displacement is proportional to the applied current (Fig. 3.6). Typically, a galvo can be driven at different frequencies of oscillation, but they suffer from possible adverse inertia effects. Another relatively common

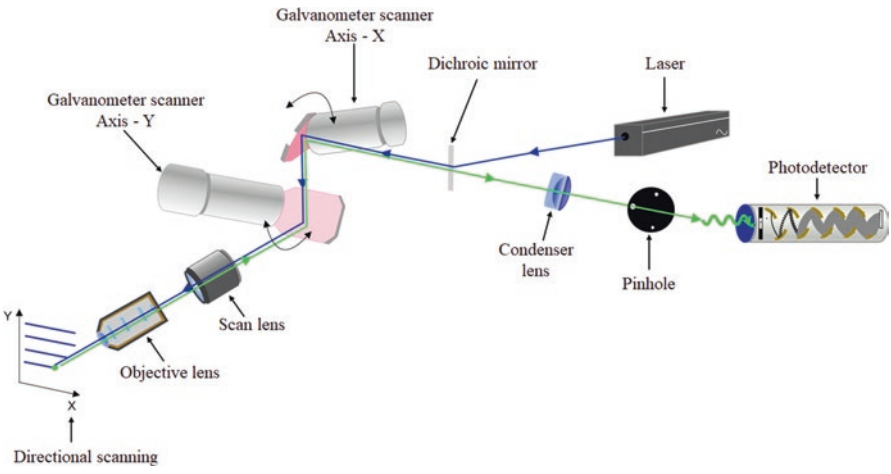

Fig. 3.6 The scan head of LSCM. The galvanometer mounted mirrors (*X*-*Y*) are responsible for changing the trajectory of the laser beam incident on the sample

scheme for scanning is through resonant scanners, they are mostly used in applications where high scanning rates are needed; in this case, the scanners are driven at a specific frequency at which they are resonant, therefore increasing their scanning speed but losing the possibility of adjusting the scan rate. There are other less common scanning technologies such as polygonal mirrors, acousto-optic scanners, and microelectromechanical devices.

Two galvo mirrors are mounted in perpendicular scanning directions inside of what is known as the scan head of the microscope; this arrangement allows for scanning the laser beam in a raster pattern like that of a television screen. One movement of the scanners, typically the one corresponding to the horizontal or *X*-axis, is scanned 100 to 1000 times faster than the other (*Y*-axis or vertical). There exist two modalities of scanning: in the first mode the scanning begins on one side of the field of view (generally left side) and when it reaches the end of the line (right side) the laser returns to the initial side of the field of view and continues scanning the second line; in the second mode, called Z-shape or Z-scanning, after reaching the end of line the laser beam scans the second line in the opposite direction until it reaches the initial side of the field. Many efforts in LSCM go into trying to improve the acquisition velocity by increasing the rates of scanning and developing faster communication buses, electronics, and computer systems capable of processing the enormous amount of data generated per image.

To acquire 3D images, an extra scan in the *z*-axis is needed, this is typically implemented with a moving stage. The three-dimensional reconstruction of samples requires a logical sequence. It all starts with the illumination of a point of the sample followed by recording the signal through the pinhole (pixel collection, that for 3D imaging is sometimes referred to as voxel collection, from volume pixel). Subsequently, the scan is repeated in order to form a grid of points in the plane (image formation). The stative moves the focal plane in the sample along the optical axis and the previous steps are repeated. This process allows for a stack collection. The image of every slice is collected and merged by the software. However, the LSCM shows some limitations in the *z*-direction due to the shape of the PSF of the microscope, which is not isotropic [4]. The resolving power in depth is inferior to the resolving power in the *xy*-plane. Also, the so-called registration problem can become a major challenge; this refers to the fact that there could be small lateral displacements of the sample that will lead to one plane image not being vertically aligned with the one immediately under it, creating a distortion in the final 3D image.

3.6 Fluorochromes for Confocal Microscopy

Confocal microscopy renders higher quality images than simple fluorescence microscopy; also, generally, it is more sensitive and specific. In many instances, the traditional fluorochromes used in fluorescence microscopy are also used, with excellent performance, in LSCM. The main difficulty in transferring stain protocols from fluorescence microscopy to LSCM is related to adjusting the dye concentration and finding the excitation and emission spectra of the fluorochromes with the lasers available in the confocal microscope.

The most widespread dyes used in LSCM microscopy are derivatives of fluorescein and rhodamine as *N*,*N*-dimethylamino (Janelia Fluor) [15]. The chemical modification of these molecules leads to a great diversity of molecules with several target affinities. For example, the isothiocyanates, succinimidyl esters, and pentafluorophenyl esters coupled with amino groups of target molecules show affinity for sulfhydryl groups. In recent years, a large family of fluorochromes for LSCM has been developed with a higher capacity to be conjugated with a great variety of antibodies, peptides, proteins, tracers, and amplification substrates for cellular labeling and detection.

The cyanine dyes (tetramethylindo(di)-carbocyanines) composed of Cy2, Cy3, Cy3.5, Cy5, Cy5.5, Cy7, and Cy7.5 are based on the partially saturated indole nitrogen heterocyclic nucleus with two aromatic units being connected via a polyalkene bridge of varying carbon number. These dyes show fluorescence excitation and emission profiles that are similar to many of the traditional dyes, such as fluorescein and tetramethylrhodamine, but with improved water solubility, photostability, and higher quantum yields. On the other hand, the Alexa Fluor family (350, 346, 405, 433, 488, 496, 532, 546, 555, 561, 568, 594, 647, 660, 680, 700, 750, and 784) is derived from tris(triethylammonium)-8-hydroxypyrene-1,3,6-trisulfonate; it contains a triethylammonium ion and basic molecules of 8-[2-[4-(2,5-dioxopyrrolidin-1-yl)oxycarbonylpiperidin-1-yl]-2-oxoethoxy]pyrene-1,3,6-trisulfonate; triethylazanium molecule. It derives from the hydride of a pyrene. Alexa Fluor dye molecules can be attached to proteins without significant self-quenching, leading to brighter conjugates. Besides, Alexa Fluor dyes show improved performance at longer wavelengths, toward the red end of the spectrum (>600 nm); this is advantageous because typically there is less background fluorescence at longer wavelengths. Other commercial fluorochromes families for LSCM brands include boratedipyrromethene (BODIPY) and Supe Bright, among others.

The newest class of special fluorochromes applied in confocal microscopy are the reactive dyes used in textile and paper industry; these are ideal for applications on cellulosic fibers, and many other fibers and molecules associated with the cell wall of several microorganisms such as fungi, bacteria, and plant cells. These novel molecules have a chemical group capable of bonding with the reactive dye, e.g., wool or polyamide fibers. An example is the Direct Yellow 96, also known as diphenyl Brilliant Flavine 7GFF, direct Yellow 7GFF, Solophenyl Flavine 7GFE, or Solophenyl Flavine 7GFE 500, depending on the application in the industry. This dye yields fluorescent signals generally in the blue to green wavelengths and provides an alternative to the more commonly used fluorophore in fluorescence microscopy. Direct Yellow 96 showed an excellent performance in LSCM but has poor brightness in fluorescence microscopy. The greater advantage of these novel fluorochromes is the flexibility and compatibility when used with other dyes and also have higher water solubility, photostability, and quantum yields. For example, in the stained root of *Zea mays*, Direct Yellow 96 and propidium iodide do not show overlap between stained structures, the cell wall and nucleus of cells, respectively (Fig. 3.7).

Fig. 3.7 *Zea mays* root dyed with Direct Yellow 96 and propidium iodide show higher performance and photostability in LSCM with respect to traditional fluorochromes used in fluorescence microscopy. Direct Yellow 96 stains the cell wall of the cells and propidium iodide attaches to cell nucleus

The most recent labeling application development is based on quantum dot (QD) nanocrystals. QDs consist of nanometrical structures (from 1 to 10 nm) with spherical shape and are formed with semiconductor materials, such as cadmium selenide (CdSe), surrounded by a zinc sulfide (ZnS) shell. The QD nanoparticles can be synthetized with broad spectral ranges of fluorescence, from 350 to 750 nm, the fluorescence emission range depends on the diameter of the semiconductor particle. The QDs are used for a wide range of applications including light-emitting diodes (LEDs), photovoltaic, single-electron transistors, and fluorescent biomarkers for biological and biomedical research. They show greatest advantages for biological applications since they are biocompatible with proteins and antibodies, have a photostable emission during prolonged times of visualization and high fluorescence performance. To reach higher compatibility and affinity to biomolecules diluted in water or buffers, QDs must be functionalized by "cap exchange" or "ligand exchange." Both processes involve the substitution of native hydrophobic ligands such as TOP (trioctylphosphine), TOPO (trioctylphosphine oxide), HDA (hexadecylamine) on the surface of quantum dots with hydrophilic ligands through mass action. Each of these substituting ligands is composed of bifunctional groups such as thiols (–SH) to bind to the ZnS shell on the QD surface and carboxyls (–COOH), amines ($–NH_2$), or hydroxyls (OH) to improve solubility and linking with biomolecules [16].

Novel technologies of molecular labeling have been developed in recent years such as HaloTag and SNAP-tag. The molecular mechanism of HaloTag includes modified proteins as haloalkane dehalogenase which can be designed to covalently bind to synthetic ligands (HaloTag ligands) [17]. While SNAP-tag is based in the system of proteins for DNA repair as O^6-alkylguanine-DNA alkyltransferase

(hAGT) which can react with several fluorescent substrates. This technique has been more applied in the analysis and quantification of protein expression cytometric and microscopy [18]. Finally, some classic stains as Basic Fuchsin reclassified as fluorogenic dye have been used to measure lignification as a rapid and informative method for determining the spatial abundance of lignin in grass cell walls when visualized in LSCM [19].

3.7 Photobleaching and Loss of Fluorescence

In fluorescence, electrons of the fluorophore molecule show a transitory change of energy to higher orbitals when stimulated with light, the decay of these excited electrons produce a photon typically in the visible spectrum. However, during the observations in fluorescence microscopy, some samples show loss of fluorescence or fading. This phenomenon is called photobleaching or photolysis damage and is characterized by broken and irreversible modification of the fluorescent molecule, resulting in the loss of its ability to emit light [7, 20].

Stabilization of fluorescent samples against photobleaching is a great technical defiance during the processing of biological samples. To improve the performance of fluorochromes it is necessary to understand the photo-destruction process. This phenomenon is poorly understood, and little information is available on the bleaching process even of the most common fluorophores. Several theories have been proposed to explain photobleaching. Some studies propose possible photodynamic interactions between excited fluorophores and molecular oxygen dissolved in the mounting medium as the cause for degradation. This interaction can affect the relative quantum yield of the fluorochrome during intersystem crossing, from excited state S* to the long-lived triplet excited state T*. Probably some types of oxygen free radicals appear in the excited molecule and damage the active sites of the fluorochromes; however, this chemical reaction depends on the cell physiology in the case of live cells and the compartmentalization of some metabolites and enzymes on fixed cells.

Not all fluorochromes have the same resistance to the photobleaching process; for example, the amphiphilic styryl fluorochrome FM4–64 of Synaptored C2, used to visualize organelle morphology such as endocytic vesicles in mammal cells and vacuoles in plant cells, exhibits short-lived fluorescence under confocal microscopy. On the other hand, DAPI, the most used fluorochrome to stain the cell nucleus, fluoresce for a long time in any type of cell and microscopy (fluorescence microscopy or LSCM).

A common strategy to increase photobleaching resistance of fluorochromes is to stabilize the cells by use of several antifade mounting media diluted in buffers that inhibit the reactivity of some enzymes and formation of free radicals in the cells; however, these mounting media frequently produce some type of artifacts such as bubbles and fluorescence background. Another approach is to reduce the excitation light power as much as possible, this obviously has a limit set by the emission efficiency of the sample.

3.8 Multiphoton Microscopy

As mentioned in a previous chapter, a major challenge in microscopy is how to create contrast within a sample made mainly of water. As described in connection with fluorescence microscopy, one common approach is to use external dying agents to provide the contrast. Fluorescent proteins are another possible solution used by researchers. A completely different scheme is to create photons of new frequencies inside the sample by combining two or more photons from the excitation beam; this approach takes advantage of the so-called nonlinear optical phenomena. These phenomena require very high excitation intensities, which are possible using ultrashort pulsed lasers, as will be discussed. Although not every material will produce a detectable signal, when nonlinear phenomena can be used as contrast agents they offer advantages such as being endogenous and the possibility of optical sectioning, which will be explained later.

Nonlinear optics is a well-established field of study, the variety of effects it encompasses is extraordinarily rich [21]. One oversimplified way to think about nonlinear optical phenomena is to say that they occur when light can interact with light within a medium without altering the medium itself. Note that in our everyday experience, i.e., in linear optics, a beam of light cannot "see or feel" another beam of light, unless one of them induces changes in a material; also, light of a given wavelength will not change its color. Some examples of nonlinear phenomena that have been used as contrast mechanisms in microscopy are Two-Photon Excited Fluorescence (TPEF), Second Harmonic Generation (SHG), Third Harmonic Generation (THG), Coherent Anti-Stokes Raman Scattering (CARS), among others. According to Erickson-Bhatt and Boppart, the term multiphoton microscopy (MM) refers to a laser scanning microscopy technique in which two or more photons combine to generate high resolution, 3D images of microscopic samples [22, 23]. The combining photons can come from more than one source and are focused simultaneously into the sample where they combine through a nonlinear interaction producing a signal photon at a different wavelength which is detected and used to assemble the final image pixel by pixel.

To understand the basic physical ideas behind nonlinear optics we will employ a classical picture of an electron in an atom. All matter is made of atoms consisting of a very heavy nucleus with positive charge surrounded by shells of negative electrons. Light is an electromagnetic wave, meaning that it is made of oscillating electric and magnetic fields that propagate in space and time. Since the farther an electron is from the nucleus, the weaker its binding force, valence electrons are the easiest to perturb and are responsible for the optical properties of the system. An unperturbed valence electron will feel a potential similar to the one illustrated by the blue line in Fig.3.8 and will occupy the state of least energy, namely, at the bottom of the potential. Note that close to the equilibrium position of the electron, the potential can be approximated by a parabolic potential (red line in the inset of Fig. 3.8), and the force felt by the electron will be linear (analogous to the force applied by a spring, Hooke's law). When a light wave is incident on the atom, the valence electron feels a second force given by the product of the electric field and

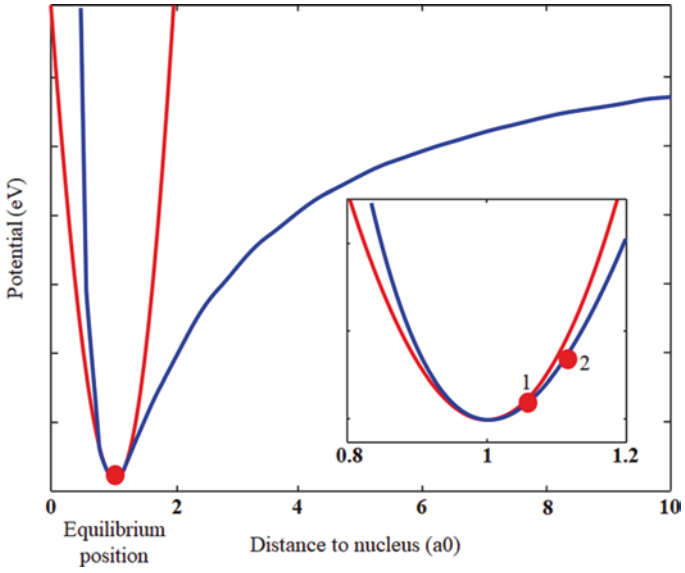

Fig. 3.8 Representation of the electron potential as a function of distance to the nucleus. The inset shows a magnified view of the equilibrium position. The red dot represents an electron

its charge. If the electric field is relatively weak, the force on the electron will also be weak and it will result in a small perturbation around the equilibrium position. This small perturbation will "push" the electron to "climb" (gain energy, position 1 in the inset of Fig. 3.8) inside its potential and at the same time it feels a restoring linear force due to the potential well that tries to pull it back to its equilibrium position; the resulting motion will be that of a harmonic oscillator. This model can be used to understand many linear optical phenomena [24].

If the amplitude of the exciting wave increases, i.e., the power of the incident light increases, and becomes large enough as to displace the electron beyond the parabolic approximation (position 2 in the inset of Fig. 3.8), the response of the system is no longer approximated by a harmonic oscillator. In this case, we need to approximate the atomic potential using terms with an order higher than two, i.e., a parabolic plus a cubic potential; we get an anharmonic oscillator. This is the realm of nonlinear optics. From the material point of view, when the light field has a high intensity the interaction between the material and the field is no longer linear; we need to introduce nonlinear terms to describe the sample response. These new terms lead to effects that have no parallel in linear optics. For example, as aforementioned in linear optics if you have a green laser, it will remain green no matter what you do; however, there are multiple nonlinear optical effects that can change the color of the incident light, among them SHG and THG.

The most common MM technique is TPEF [25]. Two photon absorption was first proposed theoretically by Maria Goeppert Mayer in her doctoral dissertation in 1931, but it had to wait 30 years before the first experimental observation of the

effect by Kaiser; coincidentally, in the same year of 1961 the first report on experimental SHG was published by Franken. Goeppert Mayer's contribution has been acknowledged, at least partially, by naming the unit to measure two-photon absorption cross section in her honor, the Goeppert Mayer is defined as $1GM = 10^{-50}$ cm^4 s photon^{-1}. In the mid-1970s of last century, Sheppard and co-workers recognized the viability to use nonlinear phenomena in microscopy; in particular they suggested that the high intensities needed to efficiently excite optical nonlinearities in a sample can be reached only in the focal volume; this idea is what we know now as optical sectioning capability of MM. The first two-photon laser scanning fluorescence microscope was invented by Denk, Strickler, and Webb in 1990 [26]; since its first inception, MM has evolved into a well-stablished technique with enormous potential applications, especially in the visualization of deep tissues.

The description of nonlinear optical phenomena is more conveniently represented in terms of quantum mechanical energy levels; as an example, we will review the linear fluorescence process already described in a previous chapter. In contrast to the classical picture, where the energy of an electron can take any value, in a quantized description the energy of the electron can only have well-defined values called energy levels (represented by thick lines in Fig. 3.9). In particular, the lowest level is known as the ground state. Due to possible vibrations or rotations of molecules, there are also energy sublevels (illustrated by the thin lines in Fig. 3.9). When light is incident on a sample (Fig. 3.9a), it can be absorbed and the energy carried by the photon promotes an electron from the ground state to an excited state (Fig. 3.9b), this excitation occurs in a timescale of a few femtoseconds. In this process, the energy of the incident photon, given by $h\nu_{exc}$, where h is Plank's constant and ν_{exc} is the frequency of the exciting light, is equal to the energy difference between the excited and the ground states (Δ_{exc}). If the photon energy is not large

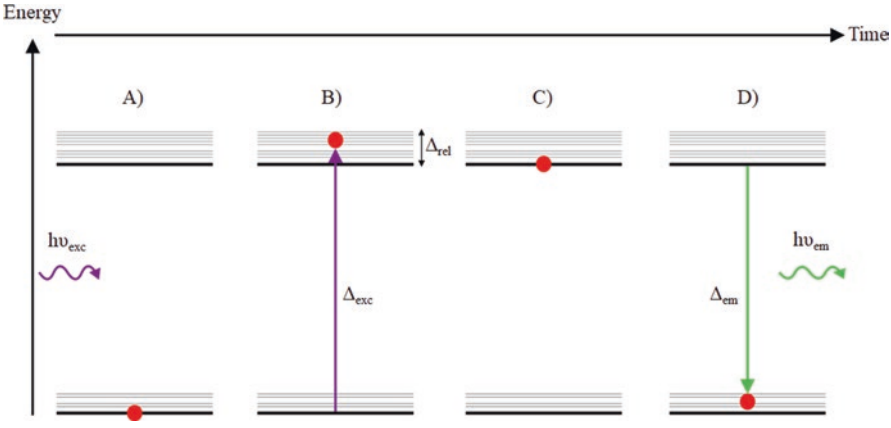

Fig. 3.9 Succession of events during linear fluorescence. (**a**) Electron in ground state and incoming exciting photon. (**b**) Electron excited to roto-vibrational state after absorption of an exciting photon. (**c**) Electron relaxes to lowest roto-vibrational state of the excited manifold. (**d**) Electron relaxes to ground state by emission of fluorescence photon of frequency υ_{em}

enough to provide the energy difference between the excited and ground states then, there can be no absorption. After a few picoseconds, the excited electron cedes some of its energy to the roto-vibrational levels and relaxes to the lowest energy sublevel of the excited state without emitting any light (non-radiative relaxation, Fig. 3.9c) and, after some time (fluorescence lifetime, typically from picoseconds to several nanoseconds depending on the system), it further relaxes from this state back to the ground state by emission of a photon (Fig. 3.9d). The emitted photon has an energy $h\nu_{em}$ which has to be equal to the energy difference between the lowest excited state and the ground state, Δ_{em}.

Now, we give a description of the nonlinear processes that are most relevant for microscopy, TPEF and SHG, the first one being the most important. TPEF is the emission of fluorescence after the *simultaneous* absorption of two photons (in a timescale of sub-femtoseconds); however, we will begin with SHG since it more straightforwardly illustrates some important points. The schematic of SHG emission is shown in the left panel of Fig. 3.10. Notice that all the action happens in one panel, representing that the whole process we will describe happens instantaneously (it actually takes a few femtoseconds). Again we start with a valence electron in its ground state and, in this case, two identical incident photons of relatively long wavelength (say 800 nm). The system will annihilate both photons *simultaneously* and promote the electron to an excited *virtual* state (dashed line in left panel of Fig. 3.10) from which it goes back to the ground state emitting a photon with exactly twice the energy of one of the incident photons (in this case 400 nm, blue photon leaving SHG panel of Fig. 3.10). A virtual state is not an energy level of the atom or molecule but rather a quantum mechanical superposition of an atomic state and the

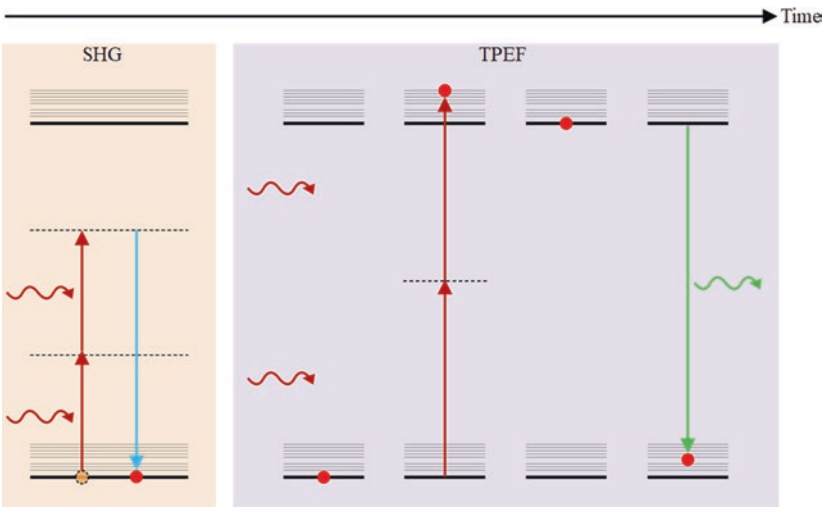

Fig. 3.10 Succession of events during SHG and TPEF. First panel: SHG is emitted after electron excitation to virtual state by the energy provided by two incoming photons; note that $\upsilon_{em} = 2\ \upsilon_{exc}$. Second panel: TPEF emission; note that the sequence is the same as for linear fluorescence but there are two photons being absorbed simultaneously

photon state. The reason the whole process is almost instantaneous is because, according to Heisenberg's uncertainty principle $\Delta E \Delta t = \hbar/2$ (ΔE is the energy difference between ground and virtual states, Δt is the lifetime of the virtual state and $\hbar$ is Plank's constant), the virtual state can only live for an extremely short time if the energy difference of the states is significant. So, in short, SHG takes two photons of the same frequency ν, and "transforms" them into one photon of frequency 2ν, hence its name. Note that there is no absorption of photons, since the system never goes into one of its excited states, and that the atom or molecule begins and ends in exactly the same state; these types of phenomena are called parametric. Some other important characteristics of SHG are that, due to symmetry, it is forbidden in centrosymmetric materials (materials with a center of inversion); and that the intensity of the phenomenon depends strongly on crystallographic orientation with respect to the photon propagation direction, this is called the phase-matching condition [21, 27], and results in the emission of coherent radiation in a specific direction. In microscopy, this emission is typically in the forward direction, i.e., in the same direction as the excitation beam; this facilitates the collection of the signal. For some samples, mainly due to scattering, there might be also a backward detected signal but it is typically weaker.

The physics of TPEF is similar to linear fluorescence; the difference is that in the initial absorption process instead of one photon, two photons of the same frequency are absorbed simultaneously, in a sub-femtosecond timescale similar to SHG (compare the first two panels of Fig. 3.9 with the corresponding panels of Fig. 3.10). The absorption is instantaneous because a virtual state (indicated by a dashed line in Fig. 3.10) as the one in SHG, not a real energy state of the system, is involved as the intermediate state for absorption; although, in contrast to SHG, the electron final excited state is an actual energy state of the system (second panel of TPEF in Fig. 3.10). This explains why the phenomenon is neither parametric nor instantaneous, the electron relaxes to the lowest excited state energy by ceding energy to roto-vibrational states (in picoseconds) and stays there for some time (typically hundreds of picoseconds and up to a few microseconds, depending on the molecule), just as in linear fluorescence. So, while the whole excitation-emission process in SHG are instantaneous, for linear fluorescence and TPEF it is not, only the excitation part of these processes is. Eventually, the electron relaxes back to its ground state by releasing its excess energy in the form of a photon. The energy of the emitted photon is less than the sum of the energies of the two absorbed photons because of the energy transferred to the roto-vibrational states. In contrast to the well-directed emission of SHG, TPEF is emitted in all directions, i.e., in a solid angle of 4π steradians.

As was mentioned before, nonlinear phenomena are seldom observed in everyday life because they need very intense fields to be excited. These intensities can only be achieved by focusing laser beams. Intensity, measured in Watts per unit area, is a measure of spatial and temporal energy density; this is because 1 W = 1 J/s, so the unit of intensity can also be written as energy per unit area per unit time. We can also think of intensity as the number of photons, each one with energy given by $E = h\upsilon$, that are incident per unit area per unit time. Notice that a high power is not

necessarily sufficient to have a large intensity, because it could be that we also have a large area over which the energy is distributed and/or a long time. Although most lasers emit a continuous beam of light, there are also pulsed lasers that emit a given number of pulses per second. In this last case, the intensity can be calculated by dividing the power of the laser by the number of pulses per second to get the energy per pulse, and then dividing this number by the area and the pulse duration. From the previous discussion it is clear that there are 3 main ways to obtain high intensities: using high powers, focusing the laser to a small spot, or using pulses with short durations. If we use a high-power laser, there is a large amount of energy incident onto the sample and therefore it is likely we will damage it. The spot size that we can obtain with a given lens, or system of lenses, has a minimum spot size limited by diffraction theory and we cannot overcome this barrier. Fortunately, one amazing feature of pulsed lasers is that their pulses can be extremely short in duration; one of the most common lasers of this type, the Titanium: Sapphire (Ti: Sapp) laser, emits 80,000,000 pulses per second with each pulse having a duration of around 100 fs (1 femtosecond is 10^{-15} s). If we have a 1 mW CW laser emitting at 800 nm focused down by a 0.5 NA microscope objective, giving an estimated diameter at the focal spot of approximately 1 μm, the intensity will be around 6.4×10^5 W/cm^2. On the other hand, if we were to have 1 mW of the previously described Ti:Sapp laser under the same focusing conditions it will have an intensity of approximately 7.96×10^9 W/cm^2; 10,000 times more intense than the CW case, even though in both cases we have the same amount of energy involved.

The laser described above is one of the main light sources used in MM. Ti:Sapp lasers can be tuned between 650 and 1080 nm, and offer fixed pulse durations between 10 and 200 fs; typically they have a maximum output power between 1 and 3 W when tuned at 800 nm, because at that wavelength we have the maximum laser emission. It is worth noting that very short pulses, below ~80 fs, are very difficult to handle because they are made by a superposition of many different frequencies and the index of refraction of all optical elements varies with frequency; this problem is known as "dispersion compensation" in MM; also, lasers with pulses of around 50 fs or less are typically not very tunable. Other common light sources for MM are optical parametric oscillators (OPOs) and optical parametric amplifiers (OPAs). These devices are not considered lasers because their principle of operation is not stimulated emission but a nonlinear interaction, a technical point that is beyond this discussion. OPAs and OPOs are highly tunable and able to reach spectral regions well beyond the Ti:Sapp capabilities. Both instruments offer the possibility of being tuned from 300 to 20,000 nm; however, this broad tunability is not necessary for MM where the requirement is typically visible and near-infrared wavelengths; they require a Ti:Sapp laser as "seed" of the pulses that they convert to another wavelength regime, and possibly amplify. Actually, the main hindrance to higher accessibility to MM is the very high cost of the instruments, of which approximately 30–50% can be just the ultrafast light source.

Optical sectioning is a central feature of MM, in particular to its extraordinary capability to produce 3D images. As mentioned, when using a nonlinear effect as contrast mechanism, there is a restricted volume where the effect can be excited; the

focal volume is determined by the objective lateral and axial resolutions and is typically of a few femtoliters. In contrast, when linear fluorescence is used to visualize the sample, the signal can be generated almost from any illuminated point in the sample where a fluorophore exists due to the very high excitation efficiency of the phenomenon; typically the whole trajectory of the beam of exciting light within the sample will induce fluorescence. When the signal light from the sample is collected, either in a camera or in a single element detector, a linear fluorescence image will appear blurry because the collected light does not come from a single point but from the whole path of the light, so the collected light can only be assigned as coming from a specific position of the scanners, not the sample. In the MM case the signal generation is well localized to a specific point, thanks to optical sectioning, and the light collected at that particular pixel (or in 3D, voxel), can be assigned to a particular physical point in the sample. This allows for three-dimensional imaging and even for 3D optical histology where a slice of a large sample is imaged in 3D and then the intensity incident on the sample is increased well beyond the value for sample ablation, thus physically removing the already imaged section of the sample and repeating the process for a full 3D reconstruction [28].

Another factor that contributes to improving the 3D capabilities enabled by optical sectioning is the utilization of near-infrared (NIR) light sources for excitation in MM because this is the spectral region where ultrashort pulse lasers typically emit. Tissue has reduced absorption at NIR wavelengths, the 700 to 1000 nm spectral range is known as the "optical window" due to the relative transparency of biological tissue; on a side note, this is why if you put your finger on an intense white light source what you see is that your tissue looks red. Another important characteristic is that scattering depends strongly on the wavelength of light, it is significantly reduced at long wavelengths. When NIR light is used for excitation, for example, of TPEF or SHG, there is a reduction of the scattering of up to an order of magnitude as compared with excitation in the visible or UV. These reduced absorption and scattering lead to an increased penetration depth of the excitation, thus allowing the imaging of deep tissue; there are reports in the literature of neurons imaged up to 1 mm in depth, compare this with the few tens of microns of penetration offered by other techniques. So, even without optical histology, it is possible to obtain 3D images of tissue structure up to hundreds of microns in depth, or in very favorable conditions up to 1 mm.

Using NIR illumination also solves the problem of phototoxicity in tissue and cells induced by UV radiation. The adverse reaction of organisms or tissue to UV light is a major challenge in fluorescence microscopy, where it is necessary its use to induce fluorescence. Since the wavelengths mostly used in MM are closer to the IR than to the UV, samples can be observed without damage for longer periods of time and also one does not have to worry as much for the possible physiological changes induced by the exciting radiation. In TPEF, photobleaching is reduced as compared to linear fluorescence techniques, including confocal microscopy. This is due to the use of longer excitation wavelengths, which have lower energy per photon, and to the fact that the effects are only excited in a small volume not in the whole beam trajectory. The fluorophores outside of the focal volume do not get

excited because of the low energy density and bleach less. Again, this allows for longer observation times without sample damage.

Since confocal microscopy is widely known and available in modern biology, it is important to highlight some of the main advantages of MM in comparison to confocal; these include reduced photobleaching, longer observation times, less phototoxicity, deeper penetration into tissue, less background noise (due to optical sectioning and reduced scattering), and less signal loss (in confocal some of the signal photons are scattered and then blocked by the pinhole). On the other hand, probably the main disadvantage of MM, although not the only one, is the high cost and complexity of the ultrafast excitation source. Although we have focused on TPEF, there are other techniques in MM that have been successfully demonstrated, among them SHG is perhaps the one most used after TPEF [29]. This type of microscopy is well suited for probing ordered structures, either biological or crystalline materials; this is a result of the symmetry conditions under which SHG is present, only on noncentrosymmetric materials. Another interesting characteristic of SHG microscopy is that it is endogenous, in other words, there is no need for external chromophores, the signal comes directly from the nonlinear optical properties of the media. In biology, it has been extensively used to image collagen and, more recently microtubules (see Figs. 3.11 and 3.12).

Since both, confocal and multiphoton microscopes, are based on laser scanning, the architecture of both instruments is very similar; the main difference being the excitation source, typically diode lasers in confocal versus ultrafast lasers or OPOs in MM. The other obvious difference is the lack of excitation and detection pinholes in MM, this somewhat simplifies the design and alignment of the instrument. It should be mentioned that the point spread function (think of it as the smallest discernable volume) of a confocal microscope is smaller than that of a TPEF

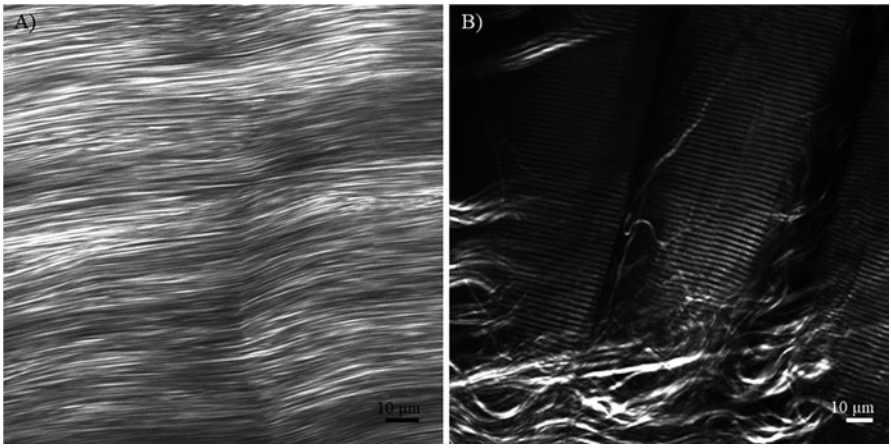

Fig. 3.11 SHG imaging from collagen and myosin. (**a**) Image from the tendon. (**b**) From the muscle–tendon junction of the gastrocnemius muscle of rat. *Images courtesy of V. Piazza and M. Alata-Tejedo*

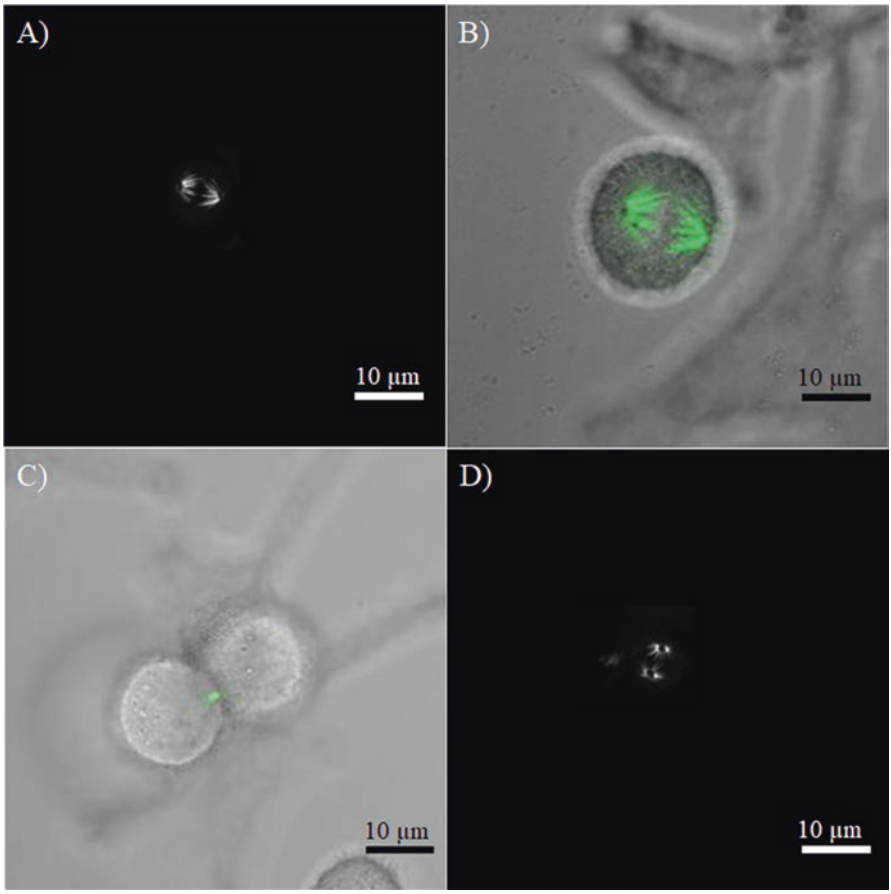

Fig. 3.12 Visualization of tubulin during cell division. (**a**) SHG signal from the microtubules of the mitotic spindle of dividing HeLa cells. (**b**) Superposition of bright field image in gray and SHG signal in green. (**c**) SHG signal, in green, from the microtubules of the intercellular bridge of two cells that have just divided. (**d**) SHG signal from a mitotic spindle in a different position. *Images courtesy of V. Piazza and M. Alata-Tejedo*

microscope, under equivalent conditions of operation. Other possible differences between the instruments are the filters used for signal detection, the anti-reflection coatings used in the optical elements (lenses, filters, dichroics, etc.) need to adjust to the different excitation wavelengths in both schemes, the objectives for MM need to be optimized for NIR performance in order to achieve the highest possible resolution, the mirror coatings used in confocal and sometimes optimized for UV and visible light need to be replaced for coatings tailored for NIR. The use of ultrashort laser pulses for MM introduces the problem of how to keep the pulses short when they arrive at the sample (we want the highest possible intensity at the sample, not somewhere else): as mentioned before an ultrashort pulse will be made of many different frequencies, when the pulse travels through any material different

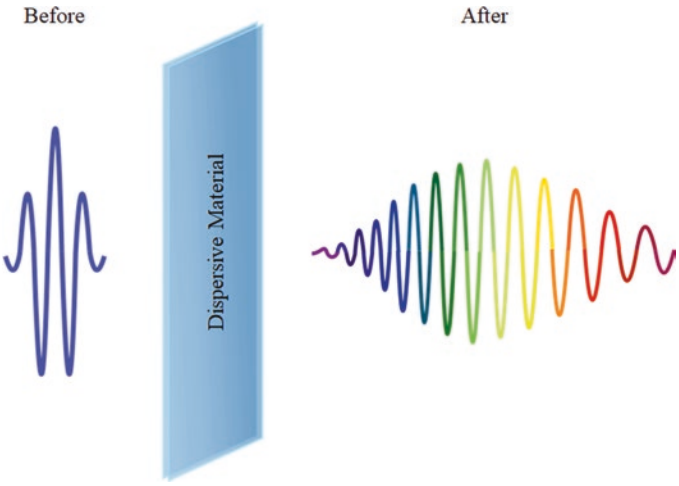

Fig. 3.13 Schematic representation of pulse stretching due to material dispersion. The incident pulse is made of many frequencies traveling together, inside the material low frequencies will travel faster than high frequencies, after the pulse leaves the materials it would have stretched in time and different frequencies will occur at different times within the pulse

frequencies will see different indices of refraction and therefore will travel at different speeds (the lower frequencies will have higher speeds than the higher frequencies); this effect distorts the pulse, stretching it on time since some frequencies will get ahead of others (see Fig. 3.13). This adverse effect can be mitigated by a device called compressor in which lower frequencies will be required to travel longer distances than the higher frequencies, thus compensating for the dispersive effects of the materials in the laser optics. Discussion of some of these specialized topics is beyond our scope and the interested reader is referred to the literature [30]. A detailed description of how to build a MM can be found in reference [31].

3.9 Spectroscopy by Multiphoton Microscopy

In biological and material sciences, there are increased demands for research tools that allow to describe endogenous molecules compartmentalized in cell organelles or synthetic molecules encapsulated into a biopolymer matrix, i.e., nano or microparticles. High-performance liquid chromatography (HPLC) is a widely used indirect method to identify and quantify molecules; however, this technique is composed of complicated processing steps in which a small error in the measurement can result in a large error [32]. Spectroscopy by two-photon microscopy is a rapid, nondegrading, and noninvasive method to identify molecules by spectral fingerprint (SF). SF has been used for the comparison and classification of biological molecules for a wide variety of plant products, including grains, fruits, vegetables, wines, honey, teas, and herbal medicines [33].

Some specimens contain a great diversity of pigments that produce autofluorescence; for example, in plants and green algae the chlorophylls are the dominant pigment in photosynthetic tissues, while in human skin and hair, the color is composed of two pigments (brown), eumelanin, and pheomelanin (yellow to red). In all cases, the spectral fingerprint of the pigments does not change in the specimen; however, the relative ratio of the different pigments can change during the growth, physiological stages, and environmental adaptations. For this reason, it is used as a reference in some studies such as diseases, ecological interactions, and metabolomic. In-plant tissues, several compounds with autofluorescence are interacting in the same cell, each one shows a different adsorption spectra and quantum yield (QY); these characteristics can produce overlapping emission peaks. One strategy to separate the overlapping spectra is to change the wavelength of excitation and unmixing techniques; however, the spectrum of every pigment can vary when it is illuminated with a laser at a different wavelength. The near-infrared (NIR) excitation for two-photon fluorescence shows several advantages with respect to linear fluorescence, one of them is related to the Ti:Sapp laser capacity to be tuned at different wavelengths with a resolution of 1 nm, the spectrum can change and reveal other spectral features that were overlapping. Besides, two-photon excitation produces lower scattering, has excellent three-dimensional spatial resolution and reduces photodamage. It is important to note that the fingerprint fluorescence spectra generated by single-photon excitation are different than those produced by two-photon excitation [34].

In modern multiphoton microscopy equipment, hyperspectral imaging is usually called *Lambda mode* and, when it is used, the internal configuration of the microscope changes. After the collection pinhole, the signal is sent to a prism that disperses it into its different constituent colors. Following the prism, there is a motorized slit mounted on a translation stage; the slit aperture determines the spectral bandwidth that will be transmitted, while the stage is used to center the slit on the wavelength of interest. Finally, once the desired bandwidth and central wavelength are selected, the signal goes to a multichannel PMT, typically consisting of 32 elements. This setup is in effect a spectrometer, it can record the signal in steps of 1, 5, and 10 nm of bandwidth in the visible region (350 to 750 nm). Another possible scheme is to use a multichannel detector directly after the prism. Choosing the right parameters allows us to separate the fluorescence produced by a sample with several fluorophores, assuming that the spectral emission of each one is different from the others. With the spectral information of the different fluorophores is built from unmixing the spectral channels; This spectroscopic analysis of the signal does not limit the acquisition of images, in modern microscopes, it is possible to obtain a multispectral channel image. One example of the utility of this analysis is the description of samples from aquatic freshwater ecosystem conditioned by photosynthesis activity, the algae communities live in intimal relation with bacteria (Fig. 3.14a, d, fluorescence image), the green algae show a predominant chlorophyll spectrum from 613 to 713 nm (Fig. 3.14b, spectral curve), while the bacteria community show spectra in the blue region from 413 to 433 nm (Fig. 3.14e, fluorescence image). The raw image of unmixing channels showed the areas of the pixels extracted to build the spectral graph (Fig. 3.14c, f).

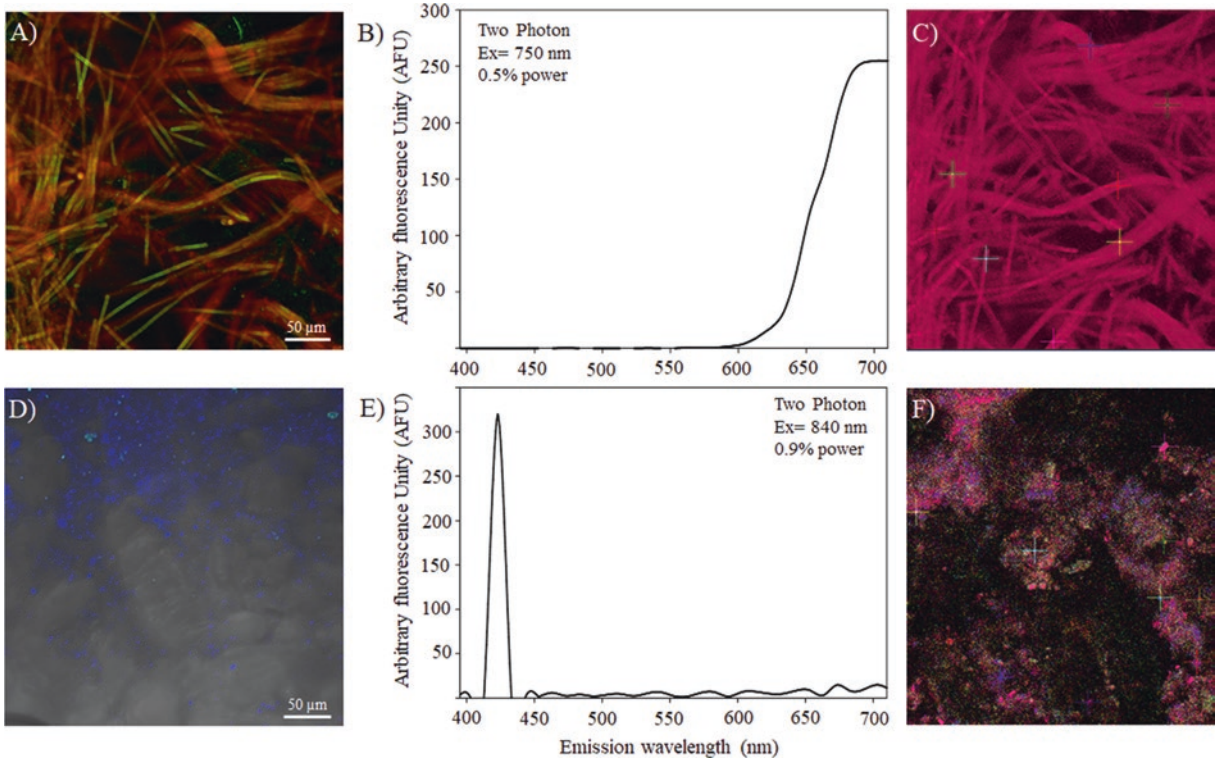

Fig. 3.14 The lambda mode analysis of the multiphoton microscopy. (**a**) Fluorescence image from the algae community. (**b**) Spectral curve corresponding to chlorophyll pigment. (**c**) Raw image after unmixing channels showing the recovered image. (**d**) In contrast, a bacteria community showed fluorescence in the blue region. (**e**) The spectral graph shows an emission located in the blue region of the visible spectrum. (**f**) Raw image of unmixed channels showing the recovered data. Image courtesy of *Gabriela Olmedo-Álvarez* and *Valeria Souza-Saldivar*

Another application of hyperspectral imaging is in the characterization of the native spectrum of fluorescent dyes and their interactions with biological molecules (Fig. 3.15a). The emission spectra of fluorochromes can sometimes be heavily influenced by the medium in which they are diluted; the cell is very complex and therefore there can be significant spectral changes even with the same fluorophore. The native spectral curves of rhodamine B and eosin Y, excited with two photons, show a spectrum that is conserved when they are exposed to different environmental conditions. These fluorescent dyes are used in nanotechnology to mark nanoparticles that are subsequently administrated to plants and animals. The trackability of the

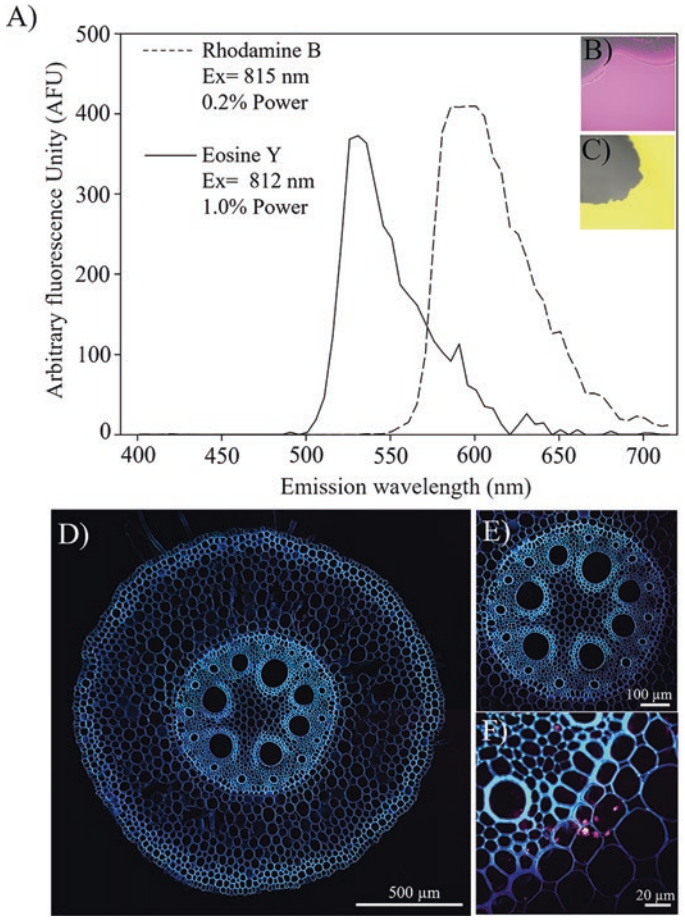

Fig. 3.15 Characterization of the spectrum of several dyes by lambda mode in multiphoton microscopy. (**a**) Spectral curve of rhodamine B and eosine Y. (**b**) Image stained with rhodamine B. (**c**) Image stained with eosine Y. (**d**) Image of seedlings of *Zea mays* labeled with nanoparticles stained with rhodamine B. (**e**) Close up of vascular cylinder of panel. (**f**) Showing the Stele of the root, the nanoparticles are not visible, the nanoparticles are confined between casparian strip and endodermis

nanoparticles in the cells is possible when the nanoparticles show a higher quantum efficiency of fluorescence. For example, nanoparticles labeled with rhodamine B and administrated to the seedling of *Zea mays* allow tracking the dynamics of internalization from the water medium to the pith of the root. Multiphoton microscopy allows finding the accumulation of the nanoparticles deep into the tissues of the organism.

References

1. Paddock SW (2000) Principles and practices of laser scanning confocal microscopy. Mol Biotechnol 16:127–149. https://doi.org/10.1385/MB:16:2:127
2. Webb RH (1996) Confocal optical microscopy. Rep Prog Phys 59:427–471. https://doi.org/10.1088/0034-4885/59/3/003
3. Müller M (2006) Introduction to confocal fluorescence microscopy, 2nd edn. SPIE Press, Washington. https://doi.org/10.1117/3.639736
4. Diaspro A, Faretta M, Sapuppo P (2008) Confocal microscopy. Leica Microsystems CMS GmbH, Mannheim
5. Singh A, Gopinathan KP (1998) Confocal microscopy: A powerful technique for biological research. Curr Sci 74:841–851. https://www.jstor.org/stable/24101088
6. Minsky M (1988) Memoir on inventing the confocal scanning microscope. Scanning 10:128–138. https://doi.org/10.1002/sca.4950100403
7. Ruzin SE (1999) Plant microtechnique and microscopy. Oxford University Press, New York
8. Kino GS, Corle TR (1996) Confocal scanning optical microscopy and related imaging systems, 1st edn. Academic Press, San Diego. https://doi.org/10.1016/B978-0-12-408750-7.X5008-3
9. Hewitt PG (2002) Conceptual physics, 9th edn. Addison Wesley, San Francisco
10. Hecht E (2002) Optics. Addison-Wesley, San Francisco
11. Dunst S, Tomancak P (2019) Imaging flies by fluorescence microscopy: principles, technologies, and applications. Genetics 211:15–34. https://doi.org/10.1534/genetics.118.300227
12. Träger F (2012) Springer handbook of lasers and optics. Springer Science & Business Media Berlin-Heidelberg. https://doi.org/10.1007/978-3-642-19409-2
13. Hamamatsu Photonics KK (2007) Photomultiplier tubes – Basics and Applications, 3rd edn, Hamamatsu Photonics K.K
14. Mendoza F, Lu R (2015) Basics of image analysis. In: Park B, Lu R (eds) Hyperspectral imaging technology in food and agriculture. Springer Science+Business Media, New York. https://doi.org/10.1007/978-1-4939-2836-1
15. Grimm JB, Muthusamy AK et al (2017) A general method to fine-tune fluorophores for live-cell and in vivo imaging. Nat Methods 14:987–994. https://doi.org/10.1038/nmeth.4403
16. Karakoti AS, Shukla R et al (2015) Surface functionalization of quantum dots for biological applications. Adv Colloid Interf Sci 215:28–45. https://doi.org/10.1016/j.cis.2014.11.004
17. Los GV, Encell LP et al (2008) HaloTag: a novel protein labeling technology for cell imaging and protein analysis. ACS Chem Biol 3:373–382. https://doi.org/10.1021/cb800025k
18. Lukinavičius G, Reymond L, Johnsson K (2015) Fluorescent labeling of SNAP-tagged proteins in cells. In: Gautier A, Hinner MJ (eds) Site-specific protein labeling: methods and protocols, 1st edn. Springer Science+Business Media, New York. https://doi.org/10.1007/978-1-4939-2272-7
19. Kapp N, Barnes WJ et al (2015) Imaging with the fluorogenic dye Basic Fuchsin reveals subcellular patterning and ecotype variation of lignification in *Brachypodium distachyon*. J Exp Bot 66:4295–4304. https://doi.org/10.1093/jxb/erv158
20. Diaspro A, Chirico G et al (2006) Photobleaching. In: Pawley JB (ed) Handbook of biological confocal microscopy, 3rd edn. Springer Science+Business Media, New York. https://doi.org/10.1007/978-0-387-45524-2

21. Boyd WR (2007) Nonlinear optics. Academic Press, San Diego. https://doi.org/10.1016/B978-0-12-121682-5.X5000-7
22. Erickson-Bhatt SJ, Boppart SA (2015) Biophotonics for assessing breast cancer. In: Meglinski I (ed) Biophotonics for medical applications. Elsevier Ltd, Cambridge. https://doi.org/10.1016/C2013-0-16335-0
23. Rubart M (2004) Two-photon microscopy of cells and tissue. Cir Res 95:1154–1166. https://doi.org/10.1161/01.RES.0000150593.30324.42
24. Fowles GR (1989) Introduction to modern optics, 2nd edn. Dover Publications, New York
25. So PTS, Dong CY et al (2000) Two-photon excitation fluorescence microscopy. Annu Rev Biomed Eng 2:399–429. https://doi.org/10.1146/annurev.bioeng.2.1.399
26. Denk W, Strickler JH, Webb WW (1990) Two-photon laser scanning fluorescence microscopy. Science 248:73–76. https://doi.org/10.1126/science.2321027
27. New G (2011) Introduction to nonlinear optics. University Press, Cambridge. https://doi.org/10.1017/CBO9780511975851
28. Tsai PS, Friedman B et al (2003) All-optical histology using ultrashort laser pulses. Neuron 39:27–41. https://doi.org/10.1016/s0896-6273(03)00370-2
29. Pavone FS, Campagnola PJ (2014) Second harmonic generation imaging. CRC Press, Taylor and Francis Group, Boca Raton. https://doi.org/10.1201/b15039
30. Diels JC, Rudolph W (2006) Ultrashort laser pulse phenomena, 2nd edn. Academic Press, Massachusetts. https://doi.org/10.1016/B978-0-12-215493-5.X5000-9
31. Young MD, Field JJ et al (2015) A pragmatic guide to multiphoton microscope design. Adv Opt Photonics 7:276–378. https://doi.org/10.1364/AOP.7.000276
32. Krasieva TB, Stringari C, Liu F, Sun CH, Kong Y, Balu M, Meyskens LF, Gratton E, Tromberg BJ (2012) Two-photon excited fluorescence lifetime imaging and spectroscopy of melanins in vitro and in vivo. J Biomed Opt 18:031107. https://doi.org/10.1117/1.JBO.18.3.031107
33. Luthria DL, Mukhopadhyay S, Robbins RJ, Finley JW, Banuelos GS, Harnly JM (2008) UV spectral fingerprinting and analysis of variance-principal component analysis: a useful tool for characterizing sources of variance in plant materials. J Agric Food Chem 56:5457–5462. https://doi.org/10.1021/jf0734572
34. Cheng PC (2006) Interaction of light with botanical specimen. In: Pawley JB (ed) Handbook of biological confocal microscopy, 3rd edn. Springer Science+Business Media, New York. https://doi.org/10.1007/978-0-387-45524-2

Scanning Probe Microscopy: Tipping the Path Toward Atomic Visions

4

F. Ruiz-Perez, R.V. Tolentino-Hernandez, J.A. Barón-Miranda, and F. Caballero-Briones

Abstract

The Scanning Probe Microscopy (SPMs) are a set of techniques to obtain information about composition, structure, electric and magnetic properties, between other, of the surface of different samples, from scale to atomic scale, which also have the ability even to modify its surfaces. SPMs include Scanning Tunneling Microscopy (STM), Atomic Force Microscopy (AFM), and Scanning Electrochemical Microscopy (SECM). In this chapter, the fundamentals of SPMs, basic devices, and the signal response used to generate the sample surface image are reviewed. With emphasis on the AFM technique, its operation modes are described, further describes the purpose of the measurements, as well as artifacts that may affect the results and recommendations for solving them. Recommendations for successful imaging and processing tips, as well as good experimental practices are provided. Different applications examples and the results obtained are shown. This chapter aims to provide to non-specialized readers in SPMs an overview of surface characterization techniques, their advantages, and limitations.

Keywords

Scanning probe microscopy · Resolution · Lithography · Forces · Contact/non-contact mode

F. Ruiz-Perez ·R. V. Tolentino-Hernandez · J. A. Barón-Miranda · F. Caballero-Briones (✉)
Instituto Politécnico Nacional, Materiales y Tecnologías para Energía, Salud y Medio Ambiente (GESMAT), CICATA, Altamira, Mexico
email: fcaballero@ipn.mx

S.-K. Kamaraj et al. (eds.), *Microscopic Techniques for the Non-Expert*,
https://doi.org/10.1007/978-3-030-99542-3_4

4.1 Introduction

Scanning Probe Microscopy are a family of techniques that have as a common feature, the use of a physical device that is usually a tip, that sweeps onto the sample, either in direct contact or just above the surface to be interrogated, acquiring, or generating a signal that can provide morphological, structural, chemical, electrical, magnetic information between other, from micro to atomic scale. The scan in the x–y axes leads to a map of the studied properties and the response in the z-axis allows to obtain tridimensional information. The need of accurate position control of the probe over the sample requires a feedback signal, i.e., a closed loop that follows an input value (setpoint) that can be a voltage or a current to keep the probe at the same conditions for the sample surface by using a control such as a PID (proportional-integral-differential). The spatial information is generated when the probe interacts with the surface, sensing the variation of properties such as the valleys and peaks (topography), the surface conductivity, the magnetization, and the electrochemical potential. The sensing mechanisms can be an optomechanical transducer, a current or voltage, or an electrochemical potential. The feedback loop responds to the variation of the surface properties during the scan to keep the setpoint value, making the probe move in the z-axis, then generating a tridimensional map. The variety in aspect ratios of the probes allow interactions with the sample from some microns to a few nanometers, and it is even possible to achieve atomic resolution, i.e., atoms can be observed! An additional feature of SPMs is that the probe can also modify the sample surface, for example, making an indentation to get mechanical properties or to create lines, moving atoms to "write" something, or oxidizing/reducing local points to create a pattern.

The general principle of scanning probe microscopy is illustrated in Fig. 4.1.

In this chapter, an excursion through different scanning probe techniques with an emphasis on Atomic Force Microscopy (AFM) will be done. Some of the experimental parameters to be considered, some tricks to achieve good images, and the

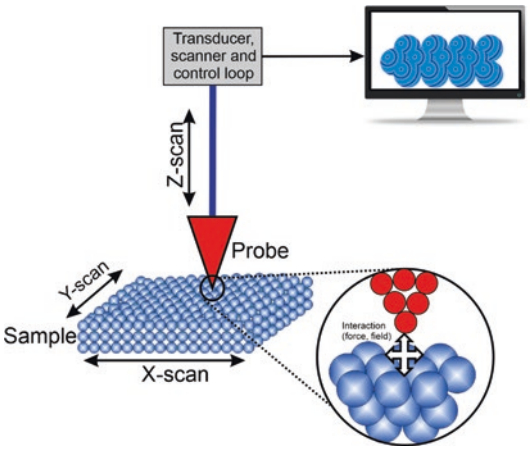

Fig. 4.1 The general principle of the scanning probe microscopy

operation and different modes of commercial AFM will be revised. Finally, some applications of AFM will be depicted as detailed as possible to introduce nonspecialized readers to the technique and its capabilities, so they can visualize both routine and novel experiments to be done. The references will provide further reading to the curious user.

4.2 Types of Scanning Probe Microscopy

As mentioned in the introduction, the common feature of SPMs is the use of a sensing mechanism based on a tip that interrogates the sample surface, together with a closed-loop that controls the tip-sample distance while interacting with the surface properties. Depending on the properties that are sensed as well as the detection mechanism, several microscopies can be defined. Some of these methods are described in the following sections.

4.2.1 Scanning Tunneling Microscopy

Nowadays, the use of scanning probe microscopes has big relevance for the development of nanoscience. The scanning tunneling microscope (STM) was the first microscope of this category, developed by Binning and Rohrer in 1981 [1]. The principal elements of this technique are a probe tip attached to a piezoelectric transducers which provide movement on the 3 axes (*X*, *Y*, *Z*), a conductive sample, control feedback loop, and processing, and display equipment. STM operating mode is described below [2, 3]:

1. A voltage is applied between the tip and the sample.
2. The movement system brings the tip closer to the sample until a current (the tunneling current) flow between both, this happens before the tip and sample are in direct contact, approximately 0.5–1 nm of distance.
3. A specific tunneling current value corresponds to a specific tip-sample distance, the current value increases as separation decreases; measuring the tunneling current quantity can be used to control the separation between the tip and sample.
4. Meanwhile, the tip is moving over the surface of the sample in the *X* and *Y* axes, if the distance between tip and sample increases or decreases due to a ridge or a well on the sample surface, the tunneling current would change, then the control loop will drive the *Z*-axis by raising or lowering to keep the tunnel current constant.

For maximum STM resolution, a sharp tip is required. The tips are fabricated from metal cutting with a wire cutter or by electrochemical polishing sharpening a wire of some metal like tungsten (W). The main goal is to produce an atomically sharp tip [4]. A tip, which is not thin enough, can limit the resolution of the final image.

When a bias voltage is applied to the system, the tip-sample gap is brought close to contact in the order interatomic distance (i.e., 0.2–10 Å), a tunnel current flow is measured between tip and sample, where the electrons of the occupied density of states of the tip can tunnel through the empty density of states surface states and vice versa. The common set up for tunnel current (I_t) measurement is 1 nA at a bias voltage of surface (V_s) of 50 mV for metallic surfaces and $I_t = 1$ nA at $V_s = 1.5$ V for semiconductor surfaces. The amount of tunnel current represents "the magnitude of energetic and spatial overlap between of the STM tip and that of the sample surface electron states" and filling of electron energy levels (local Fermi level). The tunnel effect is a phenomenon in which an electron with a certain energy crosses a barrier with higher energy. During STM operation, the electron is initially in the STM tip or in the sample, depending on the polarity of the measurement, and the energy of the electron is smaller than the vacuum level because the work function between the tip and surface of the sample [5, 6]. In Fig. 4.2(a) a scheme of set up, (b) energy diagram for tip–sample relationship in an STM measurement, and (c) an STM image of clean Au (100) are presented.

STM can be performed in air, vacuum, and electrochemical media. The latest requires the use of an external power source, a bipotentiostat, which simultaneously controls the potentials of the sample and the tip. Tunnel current depends on the spatial and energetic overlaps of the local density of states (LDOS) from tip and sample surfaces, as well as the charge distribution in these electronic states. Experimentally, the distance between the tip and the sample surface, local corrugation and LDOS distribution on the sample surface, and effective bias voltage, which is primarily determined by the local Fermi level, all play a role. This allows the

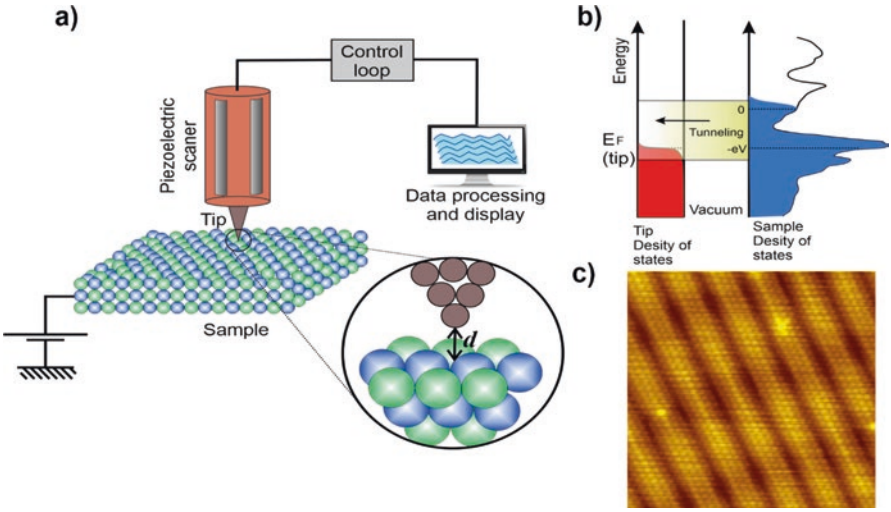

Fig. 4.2 Scheme of (**a**) scanning tunneling microscope set up, (**b**) energy diagram in a STM measurement, and (**c**) clean Au (100) surface (Image credit: Erwinrossen: File: Atomic_resolution_Au100.JPG, see upload log, Public Domain) [7]

STM system to detect all surface properties of the sample at subangstrom spatial resolution. In STM for imaging, also spectroscopy can be performed with an STM instrument. This measure is called scanning tunneling spectroscopy (STS). Spectroscopic data can be obtained as the normalized (dI/dV)/(I/V) since STS measures the differential conductivity (dI/dV) and the information is a convolution between the sample and the tip LDOS adjusted by the tunneling coefficient (T) that depends on bias voltage, then, for finite applied voltages, the application of a normalization method to reduce the T effects in needed. With STS, not only filled or empty states can be studied such as in conventional spectroscopic techniques, instead, both filled and empty states near the Fermi level can be analyzed by STS. The STS technology allows the examination of various phenomena that occurs on conductive surfaces, such as thin-film growth, molecular adsorption, chemical reaction, and charge density wave [8, 9].

4.2.2 Atomic Force Microscopy

Gerd Binning and Heinrich Rohrer, in 1986, received the Nobel Prize in physics for their design of the scanning tunneling microscope [10]. However, one problem of STM is that it can be only used in conductive samples to generate the tunneling current. To solve this limitation, in the same year, Binnig, Quate, and Gerber proposed a new microscopy. The Atomic Force Microscope (AFM) was proposed as a new technique to map and determine the morphology of insulating, conductive, biological materials, polymers, ceramics glasses, in a liquid phase, and other samples alike [11].

The atomic force microscopes have the following essential components [12]:

1. A sharp tip is mounted on a cantilever spring, which can be soft or hard.
2. A method to sense the cantilever deflection (laser and photodetector).
3. A feedback system to control the deflection.
4. A piezoelectric system to move the sample and the tip.
5. A display system to convert the data into an image.

The principle of AFM operation is based on the mechanical contact between the tip and the surface of the sample to be analyzed by sensing the sharp tip–sample surface interaction forces while raster-scanning the tip across the surface, if we are able to detect a tip attached to a cantilever acting as a spring and sense the deflection force, all types of forces can be measured. In base to Hooke's law, the force and the deflection are proportional and depend on the spring constant of the cantilever. The AFM is a scanning technique; therefore, the tip (which is supported in the cantilever) will scan the surface of the sample moving on the X–Y axes in the process the cantilever will flex up or down, this operation principle is like a turntable in which the needle passes through the grooves engraved on the vinyl, during the scan the feedback control system moves the tip to maintain constant contact. During the scan, the cantilever deflection will be detected by a laser that impacts the photodetector which

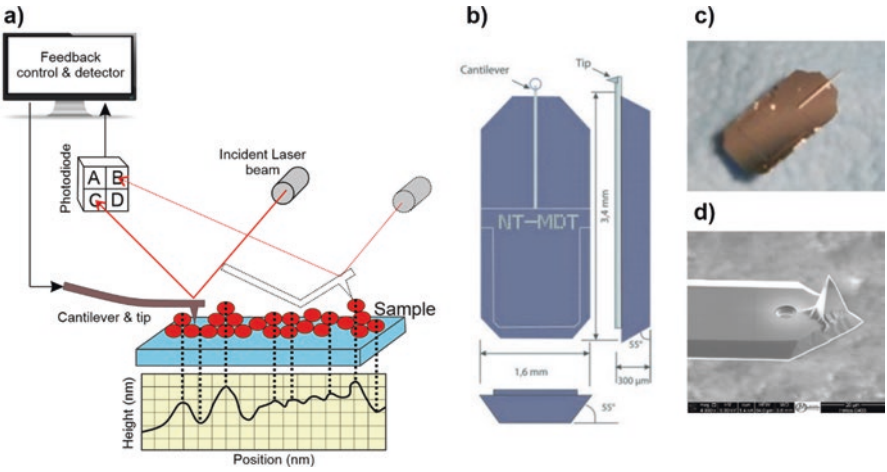

Fig. 4.3 (**a**) Schematic representation of AFM; (**b**) silicon chip, cantilever, and tip scheme; (**c**) photograph of cantilever; and (**d**) SEM image of a typical AFM tip

records the sampling evolution, then a software interprets the data generating an image of the surface of the sample [13, 14].

Figure 4.1 shows a schematic representation of the forces acting in the sharp tip–surface interaction; in the ideal case of a single atom, repulsion occurs in the contact area of the tip end due to the overlapping electronic shells of the tip and sample atom. A trace of the topography of the sample surface with atomic resolution can be obtained because the interatomic repulsive forces are short-range forces and are confined to a very tiny area (they are "atomic forces"!). In addition, long-range forces (e.g., electrical forces, magnetic forces, and van der Waals forces) that are not suited for atomic resolution imaging may occur during the tip–sample interaction and can be detected and processed in different ways described in the following sections, to extract more information of the sample [15]. The detection of these long-range forces provides the different modes that can be implemented in an AFM such as magnetic force microscopy (MFM) and Scanning Surface Potential Microscopy (SSPM), for example. In Fig. 4.3, a schematic representation of a typical AFM setup and details of the silicon chip, cantilever, and tip probe are presented.

4.2.3 Scanning Electrochemical Microscopy

Scanning electrochemical microscopy (SECM) is based on the movement of an ultramicroelectrode (UME) into a solution, which measures the current between the UME-substrate (metal, polymer, glass) when are nearby [16]. The SECM system (Fig. 4.4) has four main elements: an ultramicroelectrode (UME), a bipotentiostat, the UME positioning system (X, Y, Z axes), and the computer to control the devices and save the measured data. The measured current is the result of the redox process

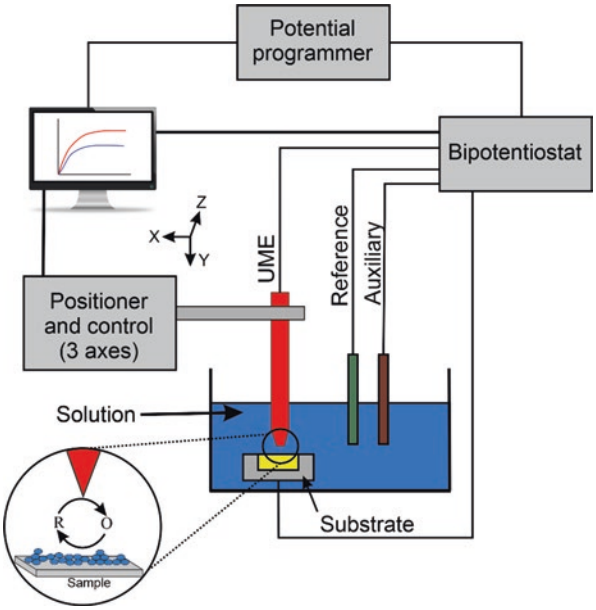

Fig. 4.4 Schematic representation of the SECM system

between the tip and sample and is controlled by the electron transfer at the interfaces. The current is inversely proportional to the gap spacing (s). This dependency is used for non-contact surface profiling in electrolytic solutions. A plot that current as a function of the potential supplied to the UME is called a voltammogram [17]. SECM can be used for imaging-patterned sensor surfaces, studying local corrosion, forensic sciences, investigating very fast electrochemical reactions, and surface modification.

Nonconductive samples can be probed in SECM providing a feasible method for analyzing cell membranes and other biophysical systems. The redox processes in an individual cell can be probed by SECM. Figure 4.5a shows an SECM image of a human breast cell and Fig. 4.5b an optical micrograph of the same cell (SECM area is delimited by the white square). SECM has a resolution in the range of several tenths or hundreds of microns, but it is very useful when studying biological systems, corrosion, circuits, and other systems where the local electrochemical response is of interest.

4.3 AFM Operation Modes

Typically, AFM systems are operated in three open-loop modes: contact mode, non-contact mode, and intermittent contact mode. The contact mode acquires sample information by monitoring interaction forces while the cantilever tip remains in contact with the target sample [19]. The non-contact mode is used to explore atomic,

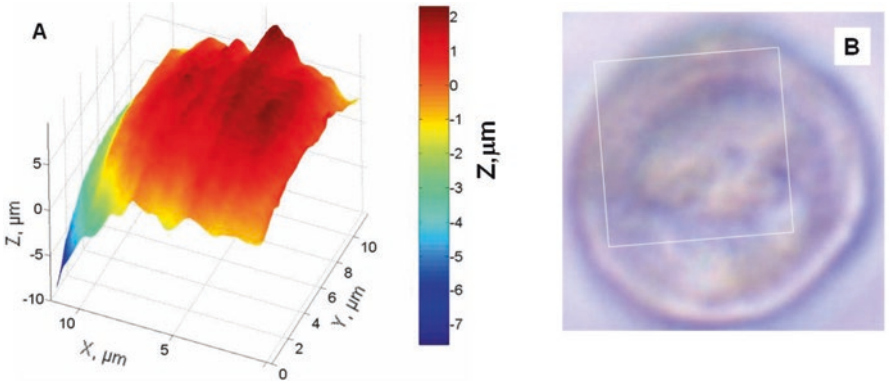

Fig. 4.5 Substrate imaging (constant current mode). (**a**) SECM image of a portion (10 × 10 µm) of a human breast cell using a 120-nm radius tip. (**b**) Optical micrograph of the same cell showing the SECM image area delimited by a white square [18]

electric, or magnetic forces in a sample by moving the cantilever slightly away from the sample surface and oscillating it near its natural resonance frequency. The topographical information of the sample may be retrieved by placing the cantilever on a piezoelectric device (PZT) and monitoring the change from its natural resonance frequency owing to sample attractive interactions [20]. Intermittent contact mode of operation, on the other hand, combines the benefits of both contact and non-contact modes by gathering sample data and oscillating the cantilever tip at or near its natural resonance frequency while allowing the cantilever tip to impact the surface sample for a brief period of time [21].

In Fig. 4.6, a scheme of the AFM operation in its three main modes as well as the surface topography that would be generated in each mode are presented. The intermittent contact mode provides information about the surface topography in a larger area in comparison to the contact mode. Due to the lateral drag forces exerted by the probe tip during the operation of AFM in contact mode, the sample surface can be damaged. A brief description and operational characteristics of each mode are given next.

4.3.1 Contact AFM

In this mode, the surface of the sample is scanned from the interaction of the tip and the sample that are in close contact as shown in Fig. 4.6a. The tip–sample interaction forces are mainly repulsive. The slope of the curve in the contact regime is quite steep, according to a van der Waals curve (Fig. 4.7) calculated for various interatomic distances. This is because the electron clouds between the atoms of the tip and the sample reject each other electrostatically at such small distances (and this is the reason behind the name "atomic force"). As a result, the repulsive van der Waals force dominates any other attractive force that may tend to act.

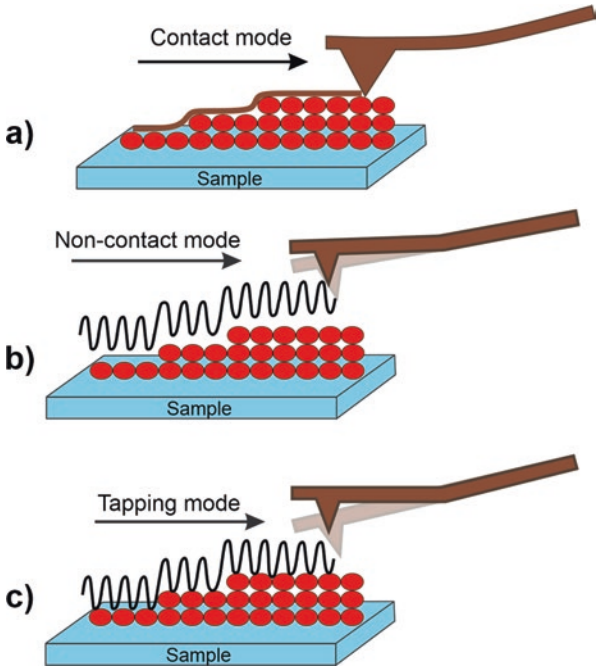

Fig. 4.6 Contact mode (top), non-contact mode (middle), and intermittent contact (tapping) mode (bottom)

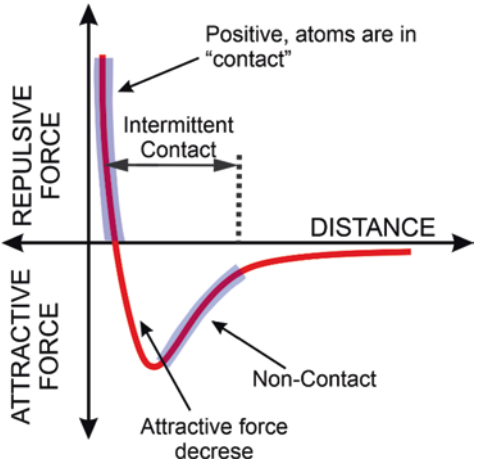

Fig. 4.7 Interatomic force (van der Waals curve) variation versus distance between AFM tip and sample

Besides these repulsive forces, another two forces generally can act during contact mode operation: capillary force which is caused by a contaminant layer (usually moisture) over the sample's surface, as well as the force applied by the cantilever. When the contamination layer is homogeneous over the sample surface, the

capillary force will be attractive and constant. However, cantilever's deflection and spring constant define the magnitude and direction of the cantilever forces acting on the sample [22].

In the contact mode, surface profile analysis can be performed in different ways: constant height mode or constant force mode. In the first mode, the PZT scanner holding the AFM tip laterally scans the surface of the sample without moving in the z-direction. The surface topography may be estimated using the cantilever deflection caused by the tip–sample interaction. The existence of steps on the sample's surface, which may damage the tip when it is pressed against the surface imperfections during the scanning process, is a disadvantage of this technology. Other approaches for imaging in the attractive regime, such as AC modulation techniques, are already in use, including the force modulation technique, which has been shown to attain real atomic resolution on surfaces [23, 24].

In the constant force mode, a control loop keeps a constant normal force applied between the tip and the surface of the sample. The tip is positioned and the required force on the sample is applied using a PZT element. The tip is initially set in contact with the sample at a specific position until the required cantilever deflection is achieved. The cantilever deflection is measured using a photodiode device while the tip is scanned laterally across the sample. A set value in a DC feedback amplifier is used as a reference to compare the measured deflection value and the resulting error signal is used to trigger the PZT positioning element by manipulating the applying voltage. As a result, the cantilever raises or lowers to reestablish the appropriate deflection and keep the force sample surface constant. The voltage applied by the feedback amplifier to the PZT element is a measure of the surface topography and is expressed as a function of the lateral position of the sample, which is used to obtain the surface topography image [25]. The main issue in the contact-mode AFM measurement is that the shear forces resulting from the lateral scanning of the tip generally tend to damage soft samples and distort output image's features. As a result, this mode is unsuitable for evaluating delicate biological and polymer surfaces since it degrades the samples significantly.

4.3.2 Non-Contact AFM

In the Non-Contact AFM (NC-AFM) mode (Fig. 4.6b), the cantilever tip hovers about 10 nm above the sample surface to sense the attractive van der Waals forces acting between the tip and the sample, which induce a frequency shift in the stiff cantilever's resonant frequency and topographic images are constructed by scanning the tip above the surface by maintaining constant frequency shift during scanning. In NC-AFM, the attraction forces between the sample and tip are weaker than the forces used in the contact mode, so it is necessary to apply small oscillations to measure the frequency, amplitude, or phase changes of the cantilever during the measurement, and not sense the sample–tip interaction forces. Usually, this is performed by the control loop monitoring the amplitude of the fixed frequency and

feeding set value, exactly as for the DC modes. The main disadvantage of this mode is that it cannot be used in a liquid environment, only on dry samples. This is because the moisture contaminant layer is frequently thicker than the range of the van der Waals force gradient, significantly lowering the resolution of the topographical images. In the practice NC-AFM mode is more used to determine a set point where tip touches surface of sample for control feedback loop [26].

4.3.3 Intermittent Contact AFM

Widely known as tapping AFM mode (T-AFM) (Fig. 4.6c) from a brand owned by Bruker Analytics, the intermittent contact mode, also known as vibrating mode, was a great advance in AFM technology. This measurement mode allows high-resolution imaging of soft samples that are difficult to examine using C-AFM mode. Friction and adhesion issues commonly found in conventional AFM imaging systems are overcome. In this mode, when the cantilever is not yet in contact with the surface, it is forced to oscillate near its natural resonant frequency using a PZT element which applies a force on the cantilever base and makes the cantilever tip vibrate at amplitudes that are typically in the range 20–100 nm when is not yet in contact with the surface. The vibrating tip is now brought closer to the surface of the samples which is softly "tapped." The tip hits the surface and lifts off alternately at high frequencies (some 100–300 kHz commonly) during the measurement. The amplitude of vibration varies according to the topography of the sample's surface owing to energy losses induced by intermittent touching of the tip with the surface. T-AFM mode has a number of features that make it a preferred operation mode. The vertical and lateral resolutions are excellent, there is less sample contact than in contact AFM mode, and measurements in a liquid environment are possible [27, 28].

4.3.4 Phase Imaging Mode

Phase imaging mode refers to recording the phase shift signal in T-AFM mode that allows mapping variations in local surface physical properties of the sample due to the difference in terms of adhesion, friction, and viscoelasticity forces that are not revealed in C-AFM and NC-AFM modes. Phase imaging enables surface properties to be observed beyond pure topography and establishes AFM technology as key in nanoscale characterization in materials science [29, 30]. For example, when measuring a material with zones with different mechanical properties, such as a polymer blend, or with different wetting characteristics (hydrophilic–hydrophobic) or with different molecular ordering, the contrast in the phase image can reveal this contrast. In Fig. 4.8, topography and phase images of ZnO thin film are presented, the brighter spots are related to Zn element present in the film and dark for oxygen, delta of brightness in phase image is not related to height.

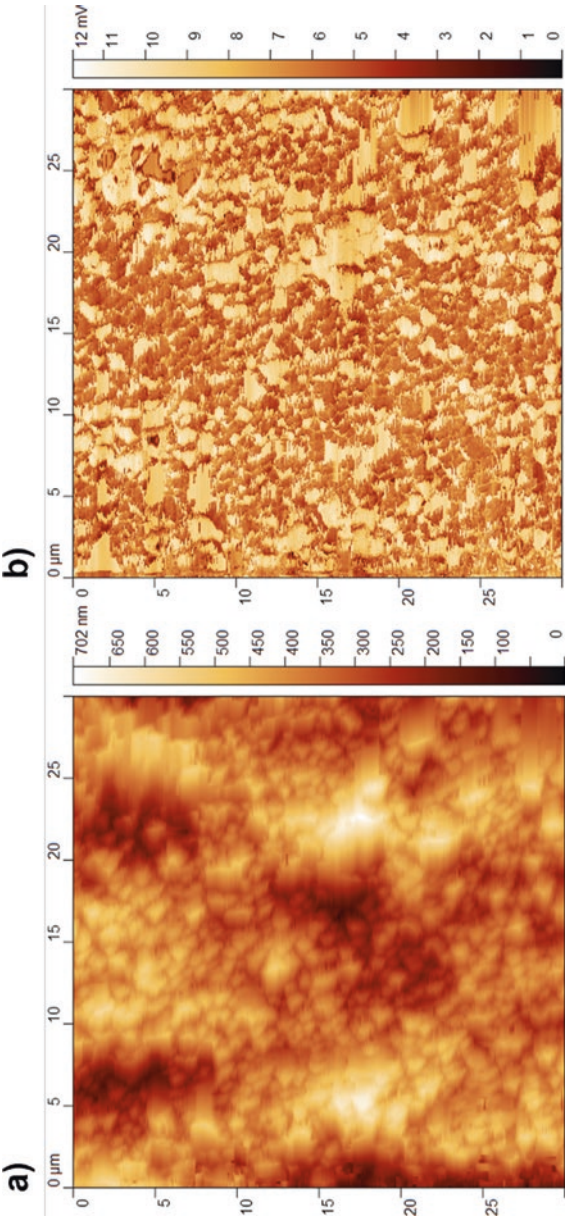

Fig. 4.8 (**a**) Topography and (**b**) phase image of ZnO thin film (Image credit: R. V. Tolentino-Hernandez)

4.3.5 Conductive AFM

Conductive AFM (CAFM) is an additional SPM method supported in AFM technology that has gained popularity in the fields of the dielectric characterization of materials. Besides a simultaneous topography and 2D tunneling current mapping by charges on the tip and by applying DC or AC voltage between tip and sample it can detect thickness variations in the sub-Å regime and which can image surface potentials and contact potential differences. With this technique some features of the surface sample like the morphological as well electrical such as local conductivity, voltage defects, electron transport and emission, localized charges, electroluminescence, photocurrent, etc. [31].

4.3.6 Magnetic AFM

In Magnetic AFM (M-AFM), magnetic forces are measured by the interaction of magnetic domains of the surface sample with a magnetized tip. The operation mode is like the described for the NC-AFM, because magnetic fields decay rapidly with distance, the probe must be close enough to the surface to measure the magnetic domains for sample local properties, scanning the tip some tenths or hundreds of nanometers above the surface, enough to avoid topography and magnetic image convolution. The main motivation for using AFM to measure magnetic properties was for applications in magnetic storage device manufacturing [32].

4.3.7 Electrochemical AFM

Electrochemical AFM (E-AFM) is a straightforward technique to study a surface as a function of applied potential. Electrochemical reactions cause changes in the surface topography as a function of applied voltage; hence, this technique is called electrochemical force microscopy. The measurement usually consists of an in situ imaging of such processes in an electrochemical cell adapted with the addition of electrodes to bias the sample and a potentiostat coupled with the AFM system. It is possible to examine the changes in the sample topography by the modification of the applied potential during the scanning to induce local oxidation or reduction processes [33].

4.3.8 AFM-Lithography

The tight control of the motion of the probe across the surface makes even a conventional AFM a flexible instrument for the manipulation of surfaces at the nanometric scale. Because AFM-Lithography (AFM-L) can be done in a typical environmental room and can be used to change any type of material, either conductive or

insulating, hard or soft, it is less restricted than STM. In addition, conductive tips may be used in the AFM-L to give STM-like characteristics such as low-energy resist exposure, induced oxidation, aided etching, and induced deposition rate. The fundamental distinction between STM and AFM-L is that STM is generally used in an air or vacuum environment, whereas AFM-L is used in an air environment in a constant voltage mode [34].

4.4 Some Common Features in AFM Measurement (AFM Artifacts)

Artifacts in AFM images result from various factors (e.g., contaminated sample, broken tip, sample, and tip size ratio, to mention some). The resultant image can display several artifacts and mask the real topography of the sample surface, so it is important for the user to be able to identify these artifacts. Some artifacts are described below and summarized in Fig. 4.9.

4.4.1 Aspect Ratio

The most common artifact is based on the shape and geometry of the tip. This occurs when the sides of the tip approach the particle to be measured before its apex (Fig. 4.9a). As a result, the apparent size of the particle increases. The most important question to consider is that the observed "particle size" is a result of the tip convolution with the particle's real size and geometry. The question became crucial when the particles are in the same order of magnitude as the tip radius; in this case, a large overestimation of the particle size can occur. One way to solve this is to use a tip with a reduced tip radius; however, this would imply an increase in the applied pressure damaging the sample and wearing the tip. Other solutions include the use of tip deconvolution software's after a scanning microscopy image of the tip; the tip shape is introduced into the software and a deconvolution function leads to the "real" topography. However, it is often enough to measure with a tip radius below the expected particle size.

4.4.2 Convolution

To solve this, artifact is necessary to use a sharper tip to reduce the dead zones and scan as much as possible. Sometimes the tip radius increases without notice because of tip wearing upon repeated use. AFM instruments often provide calibration grids that have features with defined x, y, z sizes, which are useful to test the available tips.

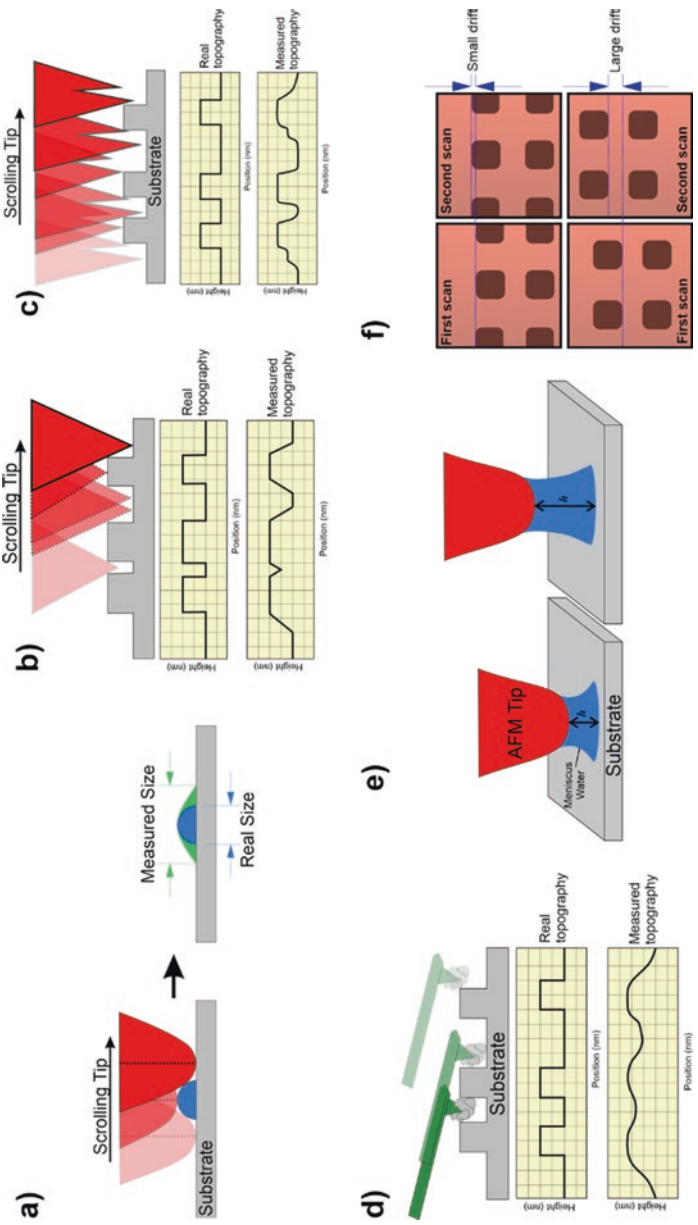

Fig. 4.9 Schematic representation of (**a**) aspect ratio, (**b**) convolution, (**c**) broken tip, (**d**) dirty tip, (**e**) meniscus, and (**f**) sample drift AFM artifacts

4.4.3 Broken and Dirty Tip

If the tip is damaged, broken, or contaminated with remnants of other samples, both artifacts produce similar results (Fig. 4.9c, d). Contamination of AFM tip is very common when scanning, for example, biological or other soft samples. A broken tip is a result of applying too much pressure or accidentally touching the sample. When a sample is analyzed with a broken or dirty tip, the resulting images have unexpected shapes. A very common feature is a repeated triangle pattern imprinted all over the surface. This indicates that the tip is chirped. To corroborate, a scan must be done in different scanning directions, for example, at 0° and 90° with respect to the cantilever axis. If the patter rotates with the scanning direction, it is an artifact possibly due to a broken tip. In the case of dirty tips, two approaches are usual, one is to apply a higher pressure, that would let the dirt away; the other is to raise the tip and try to image in another sector. Based on the experience and what is known about the sample any repeated patterns or scratches in the surface that should not be there can be attributed to a broken or dirty tip. To avoid damaging the tip a slow rate of sampling onto the unknown surface can be used and maintain a greater distance between the tip and the surface during the first scan and then adjust it gently. In the case of broken tips, they must be replaced immediately, and images discarded.

4.4.4 Meniscus

AFM can be deployed in almost any environment (vacuum, gas, or liquid) although it is typically carried out in ambient conditions. A common problem of AFM in ambient conditions is the formation of a layer of water over the sample and/or at the tip. The thickness of this layer depends on relative environmental humidity and can be less than 1 nm to several nanometers. When the tip and sample get close enough to the water layer, a meniscus forms, however, as the tip-sample gap increases the meniscus breaks at a bigger distance than it formed (Fig. 4.9e). This results in an attractive force between the tip and the sample called capillary force, when separating the tip and the sample, the surface area of the meniscus increases, this corresponds to a greater attraction force. The capillary force can modify the oscillation of the cantilever. Additionally, the meniscus could modify the sample surface, as a mini-electrochemical cell could form, leading to sample oxidation, dissolution, and redeposition. The best way to get rid of the water layer is to reduce the environmental relative humidity with the use of a mechanical desiccator, or dehumidifier materials such as silica gel in the AFM chamber.

4.4.5 Sample Drift

This artifact involves the uncontrolled movement of the sample while it is being scanned. Sample drift is an important problem in high-resolution microscopy which causes significant inconvenience when characterizing samples with “small” features

(Fig. 4.9f). Drift can be identified as a distortion of the image, which can be solved by changing the slow scan direction. The best way to avoid this artifact is to keep a constant temperature during the measurement, and to await a few moments after sample mounting, to allow the system to reach thermal equilibrium. If the drift continues can be due to mechanical instabilities in the instrument; in that case, the best way to reduce drift effects is to do faster scans, with the consequent loss of resolution.

4.5 Some Tips About Image Processing

After the measurement, data processing of the generated images is usually required for a successful evaluation of the obtained data. Many instruments including processing software, and open software are available on the Internet. In this case, the compatibility of the instrument format with the processing software must be ensured. As a general rule, the processed images must be saved in an image format to be printed/pasted in reports and papers or with the same instrument format with another name and always keep the original instrument data.

After processing, statistical analysis for evaluating the surface parameters like roughness and heights profiles can be done, but also the simulation of typical surfaces and instrumental defects, like noise or artifacts named above, for the improvement of our images and data. Even though, the data treatment truly helps in the obtention of reliable information, many times the excess of treatment of the data gave us untrustworthy information, like the modification of the existing surfaces generating purely artificial surfaces (false images). In Fig. 4.10, examples of treated images are given, in Fig. 4.10a) a usual treatment called flatten for obtaining a leveled surface. The original images usually have an unparallel surface, sometimes due to the contribution of the mounting tapes or adhesives in the sample bottom or another mechanical issue; the algorithm can propose a straight line to level the sides of the image, or the user can set a plane in the image that the user knows is flat, or a polynomial if the PZT has a contribution; this is very common with cylindrical PZTs. After flattening, the z-scale must be set back to zero. In Fig. 4.10b), the image presents scratches that could be due to dirt. The line correction feature (deleting rows) deals with this type of discrepancy using several different correction algorithms, and as observed, a better view of the grains on the sample surface is obtained. Other processing tools are the Fourier filters and smoothing. The former can be used if periodical feature shows up, for example, due to electric noise; the latter, only in case of mechanical instabilities; however, as shown in Fig. 4.10c) the abuse of processing leads to an unrealistic surface that must not be reported.

4.5.1 2D or 3D?

The processing software of AFM instruments has the option to prepare a 3D map that can be very nice for presentation. However, many publications only show 2D images. Why? Because as shown in Fig. 4.11, in the 3D images some features can

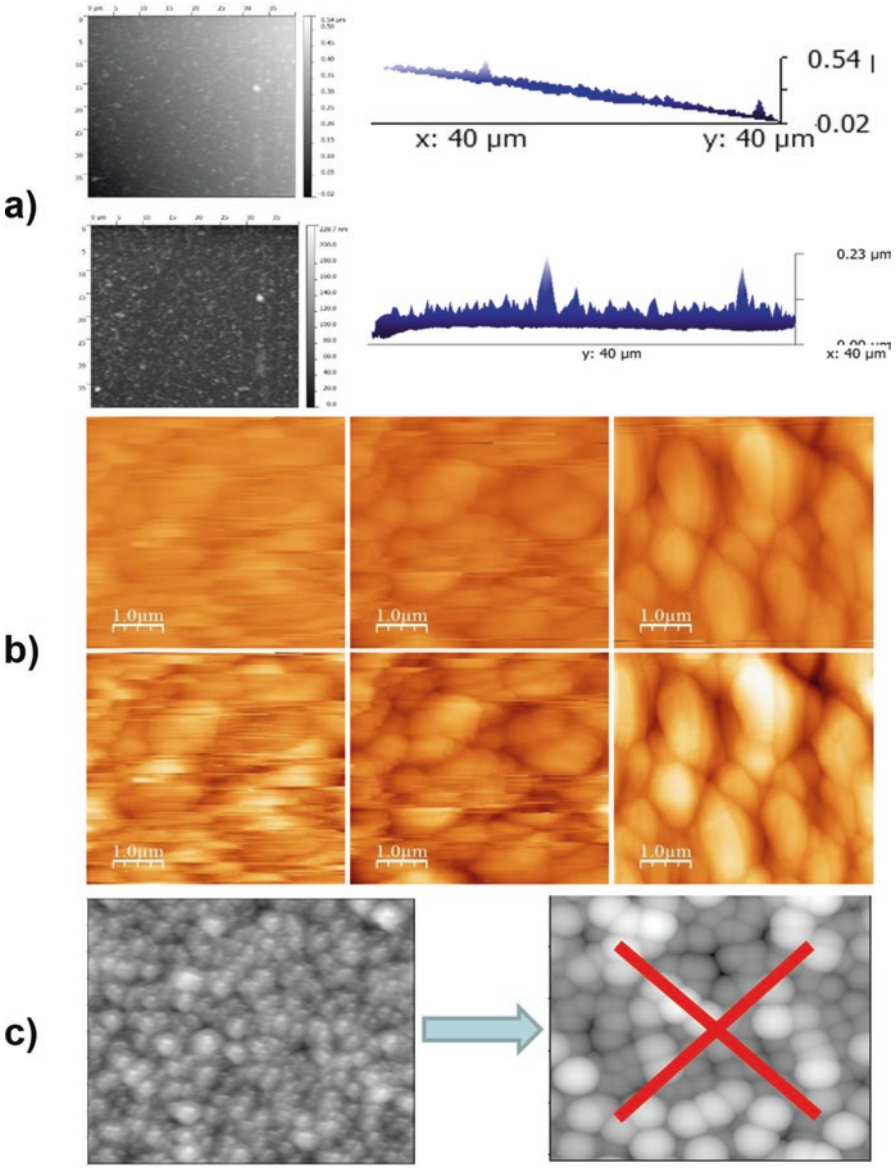

Fig. 4.10 AFM images with different treatments (**a**) flatten, (**b**) line removal, and (**c**) image smoothing

be hidden or enhanced, depending on how the image is displayed. The image at the left side shows very enhanced peaks, it could be described as a very rough topography; on the other hand, the image at the right can be described as very flat. Then to avoid misleading interpretations, it is more convenient to show only 2D images for the publications.

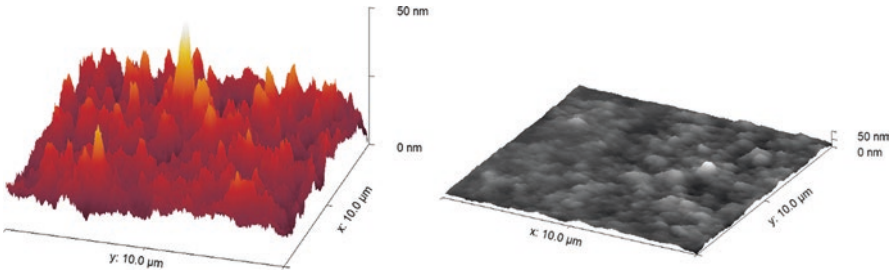

Fig. 4.11 3D AFM 10 × 10 µm^2 images of the same rGO/glass films with different display characteristics

4.6 Examples of Application

In this section, some applications of AFM in their different modes will be described, pointing out some of the experimental challenges and achievements, to allow the readers to propose novel experiments related to their interests [35–42].

Topography is the most common application of AFM. Identification of the morphological features, grain sizes, and roughness are among the most requested analysis to be done by external users.

In the first example, blood cells were imaged in the intermittent contact mode, as an example of observing a soft, loosely adhered material. The image (Fig. 4.12) was acquired as follows: first, a smear was done onto a 1 × 1 in^2 glass slide from a drop of blood and let dry. The sample was measured in the intermittent contact mode, in a TT-AFM Workshop microscope using a Si tip with a force constant of 0.4 N and resonance frequency of 200 kHz. The intermittent contact mode was chosen to avoid scratching the cells from the glass slide. The red cells are observed after carefully tuning the PID control gains and the amplitude of the oscillating tip.

A question that every user who has a deposited or growth film onto a substrate is: can we determine the film thickness using AFM? The answer is yes, but some adjustments must be done. People usually try to do a step in the film border using tape or a piece of material that avoids the film growth. This is a good idea for "line of the sight" deposition techniques such as sputtering or ion beam, where the impinging atoms come from the same direction and few surface diffusion occurs, thus a mechanical mask is often enough to have a defined step where the AFM can differentiate the height difference, i.e., the film thickness. However, when dealing with wet deposition techniques such as electrodeposition, spray pyrolysis, chemical bath deposition to name a few, making a step is often a hard issue. Using a mask does not impede the diffusion of the liquid within the mask, thus a long hill instead of a step is formed; the same happens at the air–liquid interface of the film, due to capillarity. The problem is illustrated in Fig. 4.13.

In the next example, AFM was used to determine the thickness of films, after evaporating part of the film using a Nd:YAG ablation laser operating at 1064 nm. The laser was focused onto the sample surface and a shot was done; the operation

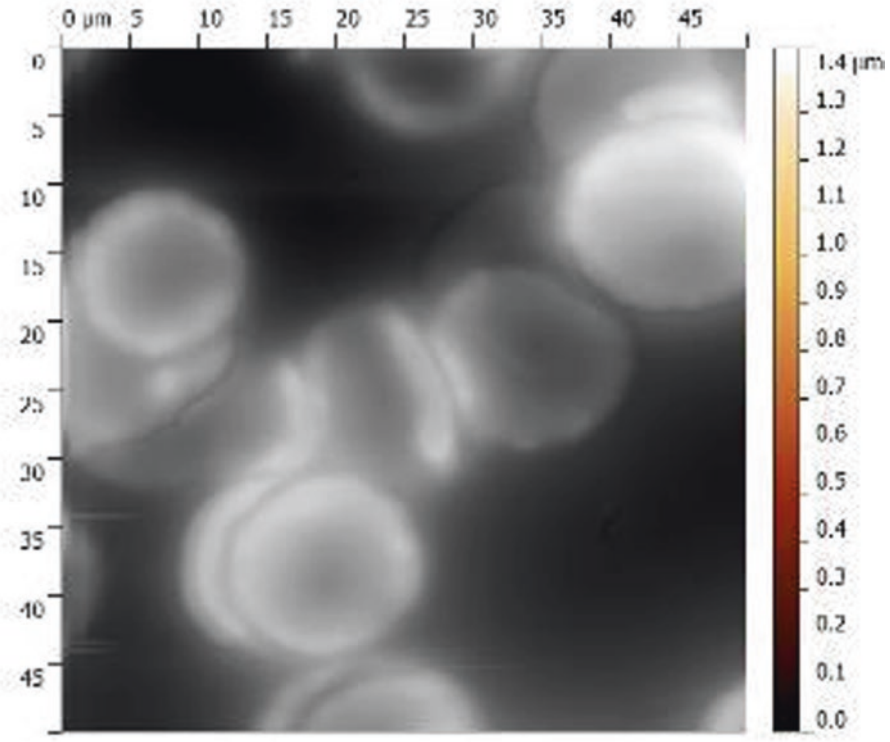

Fig. 4.12 50 × 50 µm^2 AFM image of red blood cells, obtained in the intermittent contact mode (Image credits J. A. Baron-Miranda)

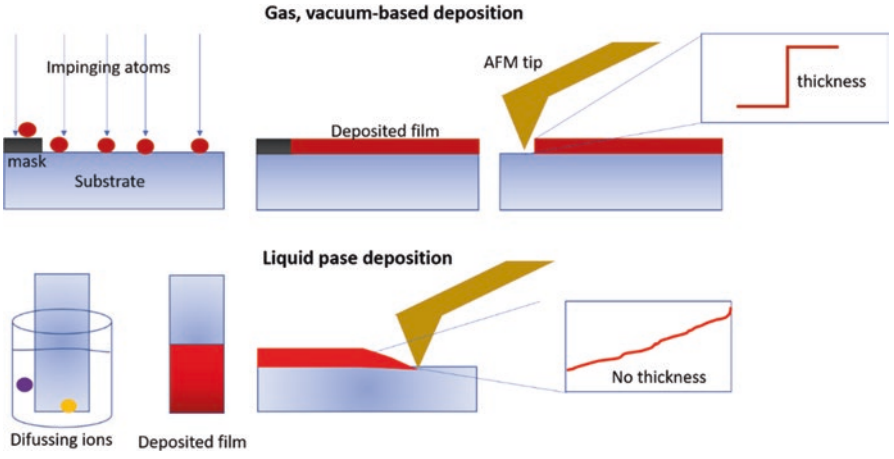

Fig. 4.13 Comparison between gas- and liquid-based deposition of thin films and the problem of thickness determination by AFM

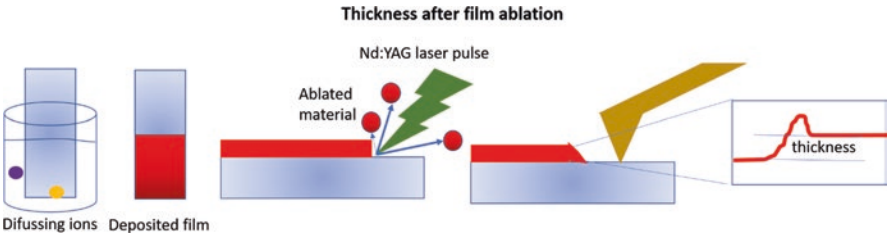

Fig. 4.14 Scheme of the thickness determination on a sample prepared by chemical bath deposition after being ablated with a Nd:YAG laser, using the AFM

was repeated until no film was observed in a portion. Then, the thickness was measured by doing a scan in the contact mode using the AFM, until a defined profile corresponding to the substrate–film interface is found as shown in Fig. 4.14.

Figure 4.15a) shows a 10× optical microscope image where the chip and cantilever can be appreciated over the ablated region of the film. The AFM image was acquired in the contact mode using a regular Si tip, and flattened using a plane function, indicating three points on the surface corresponding to the substrate. This operation displaces the zero to the substrate, then the height difference corresponds to the film thickness. In some cases, a mound of ejected material was observed just at the interface, then, the thickness is determined as indicated in the scheme in Fig. 4.15b, by taking parallel lines along the substrate and the flatter part of the film. Several profiles can be taken across the interface to obtain an average.

The magnetic force microscopy (MFM) mode takes advantage of the long-range interaction of magnetism, so a magnetized tip can respond to the magnetic states in the sample surface, bending the cantilever and then producing an image of the surface magnetization that is represented in Fig. 4.16a. In Fig. 4.16b, the scheme of the MFM experiment is presented: before the measurement, a Cr/Co covered Si tip is approached to a permanent magnet, this operation aligns the magnetic dominion in the tip along the magnetic field direction provided by the permanent magnet. Afterward, a topographic scan is done to image the surface morphology, then, the tip is lifted using the corresponding tool in the software (usually MFM is a separated module in some microscope brands) until an image with no correlation with the surface is obtained. Typically, the lift is some hundreds of nanometers above the surface, enough to avoid the tip "touch" the surface but enough to let the sample feel the magnetic force. In the left of Fig. 4.16b), images of the topography of a magnetic recording tape and a Cu_2O film growth onto a Cu substrate are presented. Then, the tip is lifted at 600 nm and the scanner performs the same sweep above the surface. The images observed in center of Fig. 4.16b) are obtained in the phase channel of the instrument. In the case of the magnetic tape, the lines where the recording head has "printed" information are clearly observed. In the corresponding MFM images of the Cu_2O film, strips corresponding to magnetic dominion are also observed. Right images of Fig. 4.16b) correspond to a second MFM scanning in the same region, but acquired in a 90° direction, i.e., the scanner sweeps the surface 90° with respect to the cantilever axis. The MFM image of the recording tape is exactly

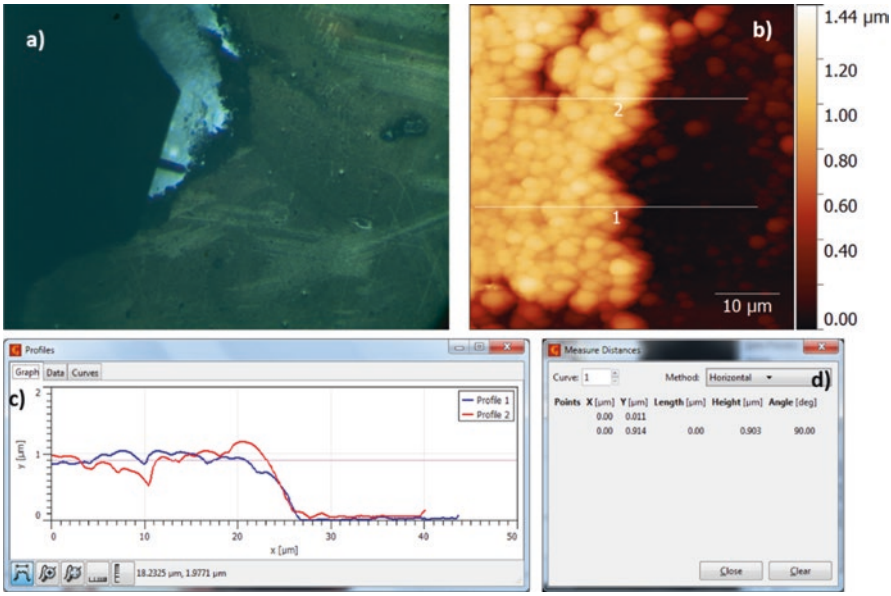

Fig. 4.15 (**a**) Optical micrograph showing the AFM tip onto the film–substrate interface of a CdS/glass film prepared by chemical bath deposition; (**b**) 40 × 40 µm^2 AFM image at the film–substrate interface with two profiles indicated along with the interface; (**c**) vertical profiles of the 1 and 2 lines shown in (**b**) where the height difference can be observed; (**d**) calculated thickness, 903 nm (Image credit: Y. Peñaloza-Mendoza)

the same, indicating that the magnetic dominion is not affected by the direction of the scanning as the material is stronger magnetized than the tip. On the other hand, the rotated MFM image of Cu_2O is also rotated and different than the 0° one. This indicates that magnetic states at the surface are affected by the tip magnetization as tip scans in one or another direction as if the tip were "recording" information onto the material as it passed. This is a typical behavior of a paramagnetic material.

Current sensing mode allows the study of electrical properties at the micro-nano level. Current images, as well as local IV curves, can be performed providing information of local defects such as metal inclusions, short circuits, and conduction mechanisms among others. As in any other measurement, it is useful to have a reference from which the system can be calibrated. In this case, calibration means that the tip deflection shall be kept in value where the tip is deflected enough to do a good electrical—ohmic—contact. A larger deflection, i.e., forces onto the surface such as the electrostatic or Van der Waals interactions, would lead to tip or sample wearing and a smaller force will lead to increased resistances due to the meniscus or irregular contact area, for example. These situations are shown in Fig. 4.17.

After the optimal force (tip deflection) is found, a current image must be obtained at a tip-voltage difference that ensures a clean visualization of the features. Here, a correlation between topography and current is usually expected. In the present case, an indium tin oxide (ITO)-coated glass with a known sheet resistance, was chosen

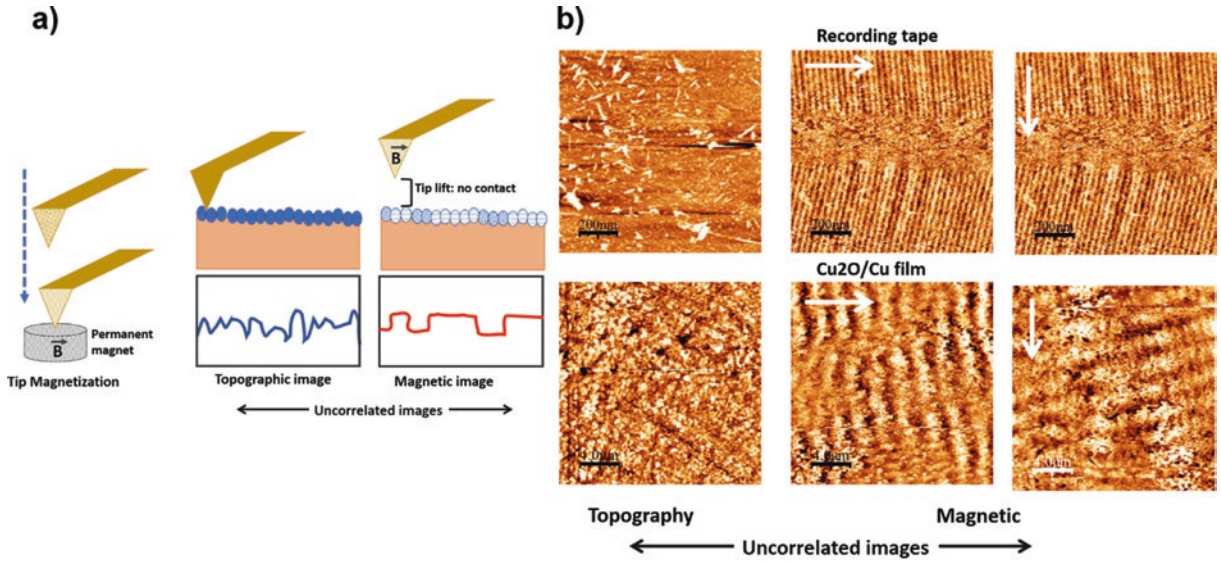

Fig. 4.16 (**a**) Scheme of the MFM experiment and (**b**) 2D 20 × 20 μm^2 AFM/MFM images of a recording tape (top) and of a Cu_2O/Cu film (bottom). Magnetic images were obtained using a Cr/Co-coated Si tip at a 600 nm lift above the film surface. Arrows in the magnetic images indicate the direction of the image acquisition

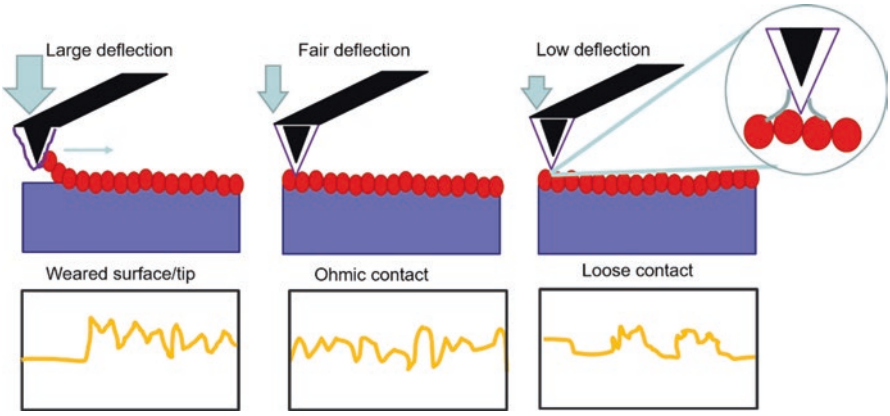

Fig. 4.17 From left to right, scheme of the effects of decreasing deflection of the cantilever onto the sample surface, on the electrical images. The scheme presents the case of conducting Pt-coated tips that wear under strong tip–sample contact

Fig. 4.18 Photography of a CuInSe2 film deposited onto a Cu/fiberglass substrate

as standard. As ITO is deposited onto insulating glass, a way to measure the electrical properties of a conductive or semi-conductive sample deposited over an insulating substrate is to fix the sample with carbon tape on both sides and afterward paint the sample, to establish electrical contact, with silver ink as shown in Fig. 4.18.

The sample was mounted for CAFM glued to the sample holder with contact adhesive, then painted from the holder to the Cu surface using conductive silver ink.

In Fig. 4.19a, the sample-tip circuit is shown. The tip is grounded and the voltage is applied to the sample. A maximum DC voltage difference of ±12 V can be applied; however, the usual recommendation is, to begin with, some hundreds of mV to avoid tip fusion or sample damage and increase voltage in the limits of sample stability. The current signal is amplified, depending on the instrument capabilities: hundreds of pA up to a few mA are possible to record depending on the nature

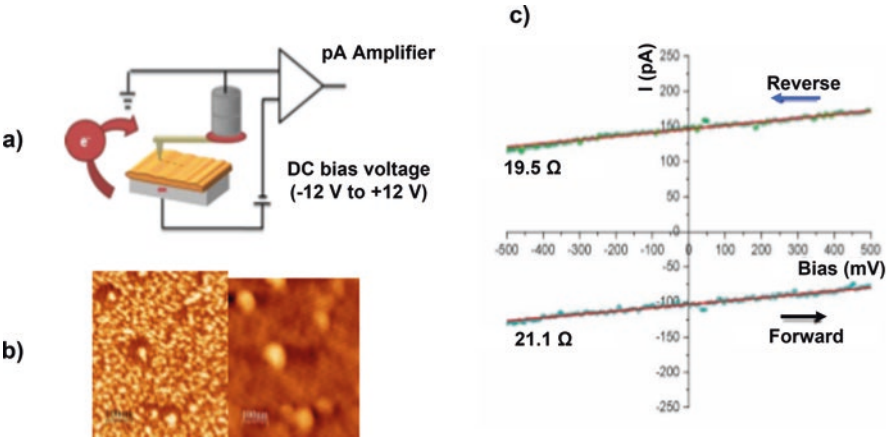

Fig. 4.19 (**a**) Circuit of the CAFM setup; (**b**) current and topography image of tin-doped indium oxide (ITO, In_2O_3:Sn) coated slide, previously degreased with ethanol, rinsed with deionized water, and dried with a N_2 flux. Topographic and current images were acquired in a Dimension 3000 microscope using Pt tips, in the contact mode. The current image was acquired using a potential between the tip and the sample of +500 mV (tip is grounded as shown in the scheme). And (**c**) a voltage scan was done from −500 mV to +500 mV (forward scan) and then in the reverse direction as observed on the right side

of the surface sample, applied voltage, and tip characteristics. In Fig. 4.19b, a topography image and the corresponding current image of the ITO substrate are shown; it is possible to observe a correlation between two images: the highest topography spots (right) correspond to higher current features (left). After the topography and current image are acquired at a low voltage, an IV curve is obtained (Fig. 4.19c), sweeping the voltage forward and backward. If the contact is ohmic, a linear relation of the current and voltage will be observed for a metallic conducting sample; from the slope, the resistance can be obtained. In the example, the calculated resistance was ca. 20 ohm, which corresponds to the sheet resistance of the tested ITO. A displacement in the *y*-axis of the IV curves is observed. This corresponds to a capacitive contribution given by adsorbed water.

Once the measuring conditions for CAFM are established, samples can be measured at different tip-sample voltages. In Fig. 4.20, Cu_2O is a p-type semiconductor, thus the substrate–film–tip system can be modeled as a Schottky diode. Setting the tip-sample voltage in a negative value will cause electrons to flow from the sample to the tip; concurrently, when a positive bias is applied, holes will flow from the sample to the tip (or electrons from the tip to the sample). Therefore, the current image can inform about the conduction mechanism in forward and in reverse bias. Figure 4.20 presents the mentioned bias conditions and two images of the Cu_2O/Cu system at −1000 mV and + 1000 mV, where the current images were overimposed to the topography image. At negative bias, the current seems to flow from the grain borders, while at a positive bias, the whole grains are “illuminated” with the current flow, evidencing the different conduction mechanisms.

In Fig. 4.21a, a sequence of current images of Cu_2O/Cu films at different positive and negative biases is presented. With increasing bias in each direction, the current increases also, displaying brighter features. It is noteworthy to observe that the conducting features depend on the bias. The graph in Fig. 4.21b) presents the IV curve of the system obtained by sweeping the voltage from negative to positive voltages. The typical Schottky diode response is observed, with the exponential increase of the current in the first quadrant corresponding to the diode in the forward direction and in the third quadrant to the diode breakdown in the backward direction.

Another experiment to be explained is the photocurrent imaging in an n-type CdS/glass film. Here, the sample was alternatively illuminated with white light, in the vicinity of the AFM tip, through an optical fiber attached to the microscope, as depicted in the scheme of Fig. 4.22a. When illuminated, local photocurrent response can be observed in the current image, as observed in Fig. 4.22b with this experiment, the effects of doping, defects, and surface passivation can be observed.

The last example to be described is the case of a graphene oxide film deposited onto a glass substrate by dip coating. The film was reduced with a chemical treatment. The interest was to develop transparent electrodes. The film was measured by CAFM applying a tip–sample current of +500 mV. The topography image (Fig. 4.23) shows an uneven surface with a mean height of around 20 nm. Notice that this is not necessarily the film thickness. On the other hand, the electrical current image and the corresponding current profile show electrical conduction all over the sample surface, indicating that rGO is deposited onto the entire measured region, although some voids in the electrical image indicate possible defects in the film.

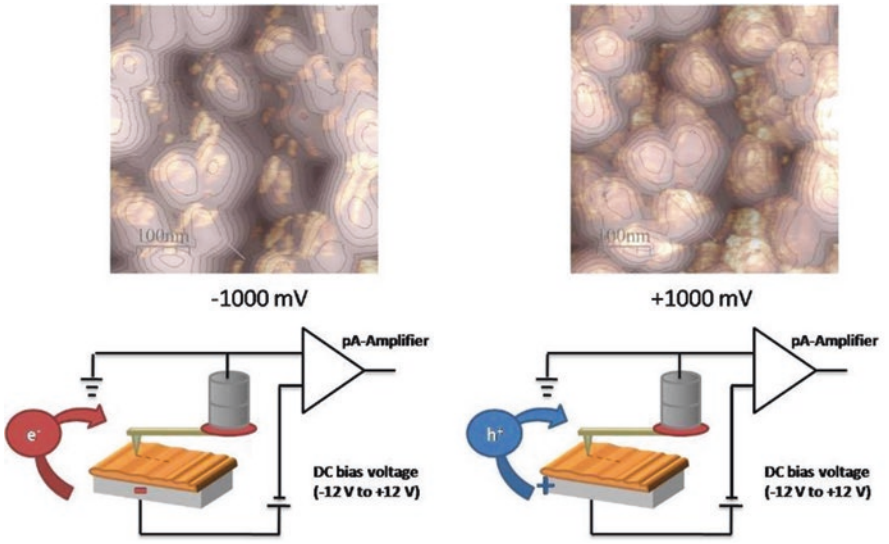

Fig. 4.20 Top: overimposed 2D current + topography 500 × 500 nm^2 images of a Cu_2O/Cu film; bottom: circuit of the CAFM measurement at negative and positive bias, indicating the flow of electrons and holes from the sample to tip, respectively

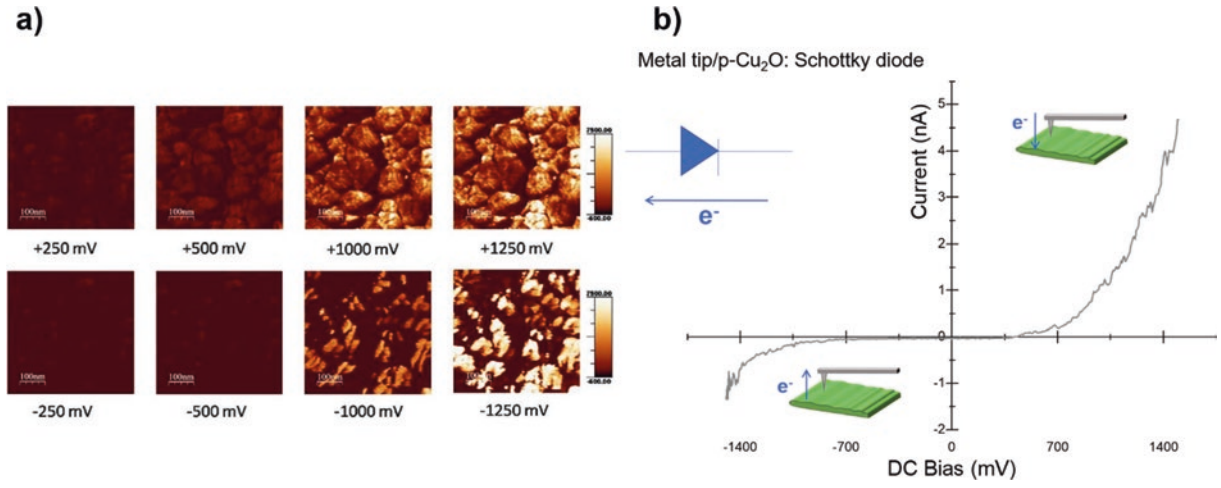

Fig. 4.21 (**a**) Series of current images of a Cu_2O/Cu film measured at increasing positive and increasing negative tip-sample voltages. (**b**) IV curve of the system

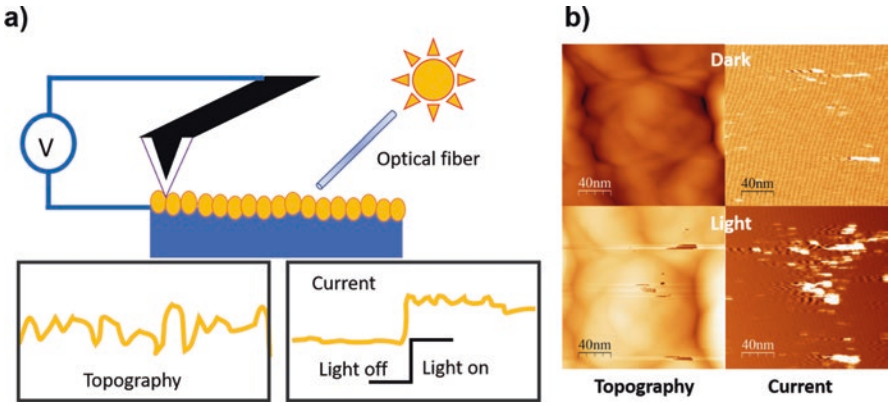

Fig. 4.22 (**a**) Scheme of the local photocurrent measurement using the CAFM setup and an optical fiber that brought a spot of white light in the vicinity of the tip and (**b**) 100 × 100 nm^2 topography and current images of a CdS/glass film. Top images correspond to the non-illuminated film while bottom ones to the illuminated film. The contact between the film and the sample holder was done with silver ink. In the case of IV curves, the film–Ag and film–tip contacts must be considered for a quantitative interpretation

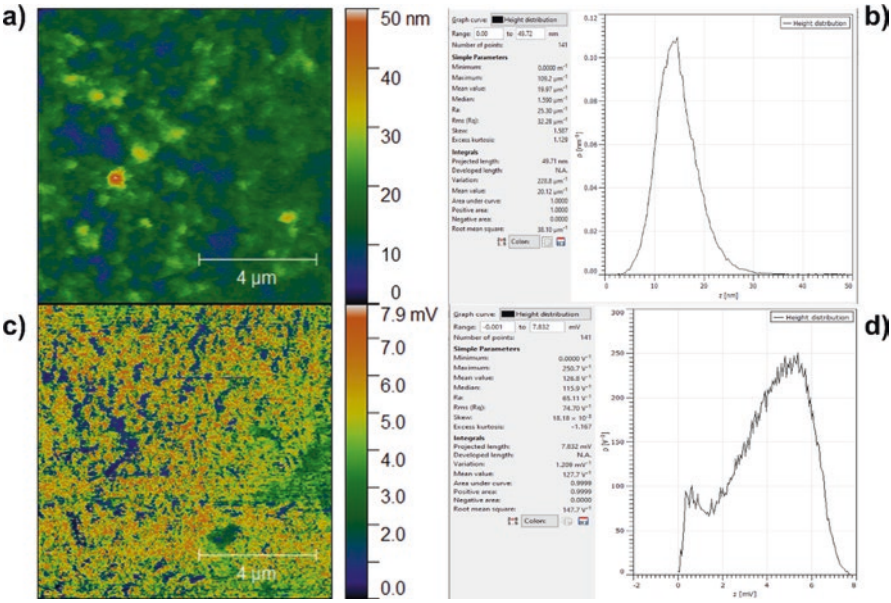

Fig. 4.23 (**a**, **b**) Topography 10 × 10 µm^2 image of rGO/glass film and corresponding profile and statistics; (**c**, **d**) Current 10 × 10 µm^2 image and corresponding current profile and statistics

4.7 Concluding Remarks

Through the present chapter, the fundamentals of Scanning Probe Microscopy have been revised, with emphasis on Atomic Force Microscopy and its measuring modes. Some good experimental practices for having successful AFM images are described as well as tips for image processing. Some examples of the application of the AFM modes are presented, explaining the purpose of the measurement, with the scope of giving the nonspecialized reader a panorama of what can be done with AFM and encouraging them to try their experiments.

Acknowledgments This work was financed by CONACYT-Mexico under 40798 Grant and by SIP-IPN under 2021-1513. FRP is financed by CONACYT and BEIFI-IPN grants.

References

1. Binnig G, Rohrer H (1983) Scanning tunneling microscopy. Surf Sci 126(1–3):236–244. https://doi.org/10.1016/0039-6028(83)90716-1
2. Feenstra RM (1994) Scanning tunneling spectroscopy. Surf Sci 299–300:965–979. https://doi.org/10.1016/0039-6028(94)90710-2
3. Voigtländer B (2015) Scanning probe microscopy – atomic force microscopy and scanning tunneling microscopy. Springer. https://doi.org/10.1007/978-3-662-45240-0
4. Ibe JP et al (1990) On the electrochemical etching of tips for scanning tunneling microscopy. J Vac Sci Technol A Vacuum Surfaces Film 8(4):3570–3575. https://doi.org/10.1116/1.576509
5. Binnig G, Rohrer H, Gerber C, Weibel E (1982) Tunneling through a controllable vacuum gap. Appl Phys Lett 40:178–180. https://doi.org/10.1063/1.92999
6. Binnig G, Rohrer H, Gerber C, Weibel E (1982) Surface studies by scanning tunneling microscopy. Phys Rev Lett 49(1–5):57–61. https://doi.org/10.1103/PhysRevLett.49.57
7. Erwinrossen (2007) File: atomic resolution Au100.JPG – Wikimedia Commons. [online] Commonswikimedia.org Available at: (https://commons.wikimedia.org/wiki/File:Atomic_resolution_Au100.JPG)
8. Vázquez de Parga AL, Miranda R (2012) Scanning tunneling spectroscopy. In: Bhushan B (ed) Encyclopedia of nanotechnology. Springer, Dordrecht. https://doi.org/10.1007/978-90-481-9751-4_111
9. Julian Chen C (1988) Theory of scanning tunneling spectroscopy. J Vac Sci Technol A 6:319–322. https://doi.org/10.1116/1.575444
10. NobelPrize.org. The Nobel Prize in Physics 1986. [online] Available at: (https://www.nobelprize.org/prizes/physics/1986/summary/). Accessed 5 Mar 2021
11. Binning G, Quate CF (1986) Atomic force microscope. Phys Rev Lett 56(9):930–933. https://doi.org/10.1103/PhysRevLett.56.930
12. Rugar D, Hansma P (1990) Atomic force microscopy. Phys Today 43(10):23–30. https://doi.org/10.1063/1.881238
13. Meyer E (1992) Atomic force microscopy. Prog Surf Sci 31(1):3–49. https://doi.org/10.1016/0079-6816(92)90009-7
14. Johnson D, Hilal N, Bowen WR (2009) Basic principles of atomic force microscopy. In: Atomic force microscopy in process engineering. Butterworth-Heinemann, pp 1–30. https://doi.org/10.1016/B978-1-85617-517-3.00001-8
15. Zhang H, Huang J, Wang Y, Liu R, Huai X, Jiang J, Anfuso C (2018) Atomic force microscopy for two-dimensional materials: a tutorial review. Opt Commun 406:3–17. https://doi.org/10.1016/j.optcom.2017.05.015

16. Slim C, Griveau S, Bedioui F (2019) Scanning electrochemical microscopy. In: Encyclopedia of analytical science, 3rd edn. Academic Press, pp 79–88. https://doi.org/10.1016/B978-0-12-409547-2.13947-2
17. Bard AJ, Mirkin MV (2012) Scanning electrochemical microscopy, 2nd edn. CRC Press Taylor & Francis, pp 1–15. https://doi.org/10.1201/b11850
18. LaForge F (2011) File: Fig6 SECM.jpg – Wikimedia Commons. [online] Commons.wikimedia.org. Available at: (https://commons.wikimedia.org/w/index.php?curid=17338959)
19. Fung R, Huang S (2001) Dynamic modeling and vibration analysis of the atomic force microscope. ASME J Vib Acoust 123(4):502–509. https://doi.org/10.1115/1.1389084
20. Basso M, Giarre L, Dahleh M, Mezic I Numerical analysis of complex dynamics in atomic force microscopes. In: Proceedings of the 1998 IEEE international conference on control applications (Cat. No. 98CH36104), IEEE. 2, (1998), 1026–1030. https://doi.org/10.1109/CCA.1998.721613
21. Sebastian A, Salapaka M, Chen D, Cleveland J Harmonic analysis based modeling of tapping-mode AFM. In: Proceedings of the 1999 American Control Conference (Cat. No. 99CH36251), IEEE 1, (1999), 232–236. https://doi.org/10.1109/ACC.1999.782775
22. Jalili N, Laxminarayana K (2004) A review of atomic force microscopy imaging systems: application to molecular metrology and biological sciences. Mechatronics 14(8):907–945. https://doi.org/10.1016/j.mechatronics.2004.04.005
23. Carpick RW, Salmeron M (1997) Scratching the surface: fundamental investigations of tribology with atomic force microscopy. Chem Rev 97(4):1163–1194. https://doi.org/10.1021/cr960068q
24. Giessibl FJ (1995) Atomic resolution of the silicon (111)-(7x7) surface by atomic force microscopy. Science 267(5194):68–71. https://doi.org/10.1126/science.267.5194.68
25. Overney RM, Meyer E, Frommer J, Brodbeck D, Lüthi R, Howald L, Giintherodt H-J, Fujihira M, Takano H, Gotoh Y (1992) Friction measurements on phase-separated thin films with a modified atomic force microscope. Nature 359:133–135. https://doi.org/10.1038/359133a0
26. García R, San Paulo A Amplitude curves and operating regimes in dynamic atomic force microscopy, Ultramicroscopy, 82, 1–4, (2000), 79–83. https://doi.org/10.1016/S0304-3991(99)00132-1
27. Magonov SN, Elings V, Whangbo M-H (1997) Phase imaging and stiffness in tapping-mode atomic force microscopy. Surf Sci 375(3–2):L385–L391. https://doi.org/10.1016/S0039-6028(96)01591-9
28. Xiang W, Tian Y, Liu X (2020) Dynamic analysis of tapping mode atomic force microscope (AFM) for critical dimension measurement. Precis Eng 64:269–279. https://doi.org/10.1016/j.precisioneng.2020.03.023
29. Nguyen-Tri P, Ghassemi P, Carriere P, Nanda S, Assadi AA, Nguyen DD (2020) Recent applications of advanced atomic force microscopy in polymer science: a review. Polymers 12(5):1142. https://doi.org/10.3390/polym12051142
30. Garcia R (2020) Nanomechanical mapping of soft materials with the atomic force microscope: methods, theory and applications. Chem Soc Rev 49:5850–5884. https://doi.org/10.1039/D0CS00318B
31. Benstetter G, Biberger R, Liu D (2009) A review of advanced scanning probe microscope analysis of functional films and semiconductor devices. Thin Solid Films 517(17):5100–5105. https://doi.org/10.1016/j.tsf.2009.03.176
32. Hartmann U (1999) Magnetic force microscopy. Annu Rev Mater Sci 29(1):53–87. https://doi.org/10.1146/annurev.matsci.29.1.53
33. Macpherson JV, Unwin PR (2000) Combined scanning electrochemical-atomic force microscopy. Anal Chem 72(2):276–285. https://doi.org/10.1021/ac990921w
34. Tseng AA, Notargiacomo A, Chen TP (2005) Nanofabrication by scanning probe microscope lithography: A review. J Vac Sci Technol B 23:877–894. https://doi.org/10.1116/1.1926293
35. Caballero-Briones F, Palacios-Padrós A, Calzadilla O, Sanz F (2010) Evidence and analysis of parallel growth mechanisms in Cu2O films prepared by Cu anodization. Electrochim Acta 55(14):4353–4358. https://doi.org/10.1016/j.electacta.2009.10.031

36. Iwan A, Caballero-Briones F, Bogdanowicz KA, Barceinas-Sánchez JDO, Przybyl W, Januszko AM, Baron-Miranda JA, Espinosa-Ramirez AP (2018) Jesus Guerrero-Contreras, Optical and electrical properties of graphene oxide and reduced graphene oxide films deposited onto glass and Ecoflex® substrates towards organic solar cells. Adv Mater Lett 9:58–65. https://doi.org/10.5185/amlett.2018.1870
37. Barón-Miranda A, Calzadilla O, Arvizu-Rodríguez LE, Fernández-Muñoz JL, Guarneros-Aguilar C, Chale-Lara FF, Páramo-García U, Caballero-Briones F (2016) Local electrical response in alkaline-doped electrodeposited CuInSe2/Cu films. Coatings 6(4):71. https://doi.org/10.3390/coatings6040071
38. Caballero-Briones F, Palacios-Padrós A, Sanz F (2011) CuInSe2 films prepared by three step pulsed electrodeposition. Deposition mechanisms, optical and photoelectrochemical studies. Electrochim Acta 56(26):9556–9567. https://doi.org/10.1016/j.electacta.2011.06.024
39. Peñaloza-Mendoza Y, Alvira FC, Caballero-Briones F, Guarneros-Aguilar C, Ponce L (2018) Influence of laser pulse regime on the structure and optical properties of TiO2 nanolayers. Mater Res Express 5:125022. https://doi.org/10.1088/2053-1591/aae2e5
40. Barón-Miranda JA, Calzadilla O, San-Juan-Hernández S, Diez-Pérez I, Díaz J, Sanz F, Chále-Lara FF, Espinosa-Faller FJ, Caballero-Briones F (2018) Influence of texture on the electrical properties of Al-doped ZnO films prepared by ultrasonic spray pyrolysis. J Mater Sci Mater Electron 29:2016–2025. https://doi.org/10.1007/s10854-017-8113-x
41. Caballero-Briones F, Calzadilla O, Chalé-Lara F, Rejón V, Peña JL (2015) Mg-doped CdS films prepared by chemical bath deposition, optical and electrical properties. Chalcogenide Lett 12(4):137–145
42. Caballero-Briones F, Santana G, Flores T, Ponce L (2016) Photoluminescence response in carbon films deposited by pulsed laser deposition onto GaAs substrates at low vacuum. J Nanotechnol 2016:1–6. https://doi.org/10.1155/2016/5349697

Atomic Force Microscopy: An Advanced Imaging Technique—From Molecules to Morphologies

5

Jeevan Kumar Reddy Modigunta, Selvamani Vadivel, G. Murali, Insik In, and Montree Sawangphruk

Abstract

Atomic force microscopy (AFM) is an extensively used advanced characterization technique for a nanoscale range of materials. This chapter clearly describes the importance and advantages of AFM, its working principles, modes of measurement, and its applications in interdisciplinary fields such as chemistry, materials science, and biology.

Keywords

Atomic force microscopy · Surface morphology · Sheet thickness · Materials science · Contact mode

The authors Jeevan Kumar Reddy Modigunta and Selvamani Vadivel both contribute equally.

Jeevan Kumar Reddy Modigunta · G. Murali · Insik In (✉)
Department of Polymer Science and Engineering, Department of IT-Energy Convergence (BK21 FOUR), Chemical Industry Institute, Korea National University of Transportation, Chungju, South Korea
in1@ut.ac.kr

Selvamani Vadivel · Montree Sawangphruk
Department of Chemical and Biomolecular Engineering, School of Energy Science and Engineering, Centre of Excellence for Energy Storage Technology, Vidyasirimedhi Institute of Science and Technology, Rayong, Thailand
montree.s@vistec.ac.th

S.-K. Kamaraj et al. (eds.), *Microscopic Techniques for the Non-Expert*,
https://doi.org/10.1007/978-3-030-99542-3_5

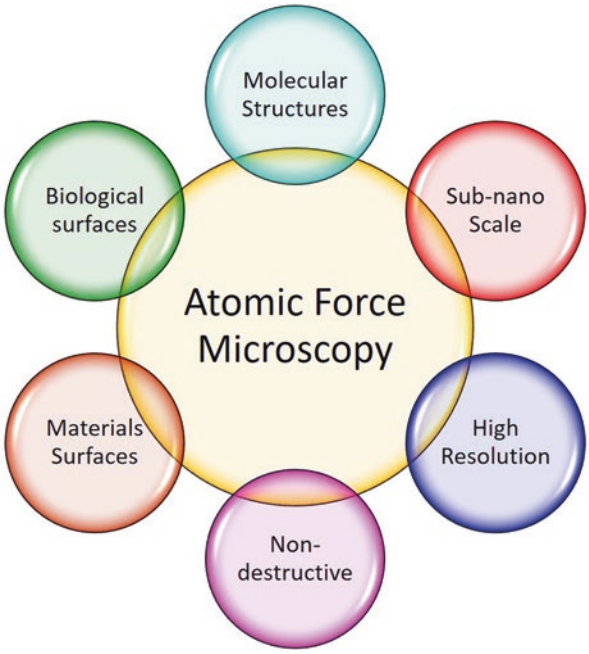

Fig. 5.1 The advantages of atomic force microscopy measurements

5.1 Introduction

The advancement of atomic force microscopy began in 1981 from IBM's researchers on developing scanning tunneling microscopy (STM), as inspired by Russell Young's stylus profiler [1, 2]. Atomic Force Microscopy (AFM) was invented four decades ago by Binnig et al. [3]. In 1987, Wickramsinghe et al. further developed a new AFM setup using a vibrating cantilever technique containing a light-lever mechanism [4]. AFM has become an essential instrument in nanoscience and technology with peculiar abilities to provide three-dimensional imaging at sub-nanometer levels without vacuum or contrast imaging agents [5]. AFM measurement has a broad scope and is more helpful for understanding science and technology in the present era. AFM has been used for the detection of microstructures and surface properties of materials. AFM is used to study various samples such as plastic, metals, glasses, semiconductors, and biological samples (i.e., cells and bacteria walls). It does not require any conductive coatings on the samples' surface as used in STM or scanning electron microscopy. Some of the advantages of AFM are shown in Fig. 5.1.

In comparison to AFM, the optical and electron microscopes can quickly generate 2D (x- and y-directions) images of sample surfaces with a higher magnification of ~ ×1000 (optical microscope) and ~ ×100,000 (electron microscope), respectively. However, these microscopes fail to measure the sample surface on the third dimension (z-direction) by their height (e.g., particles and sheets) or depth (e.g.,

pores). The appropriate AFM probe can scan the surface topology to an extreme magnification of ~ ×1,000,000, which is better than the existing electronic microscopes. Interestingly, the resolution and magnification measured at *z*-direction are usually higher than the *x* and *y* directions.

The rapid advancements of AFM analysis have made notable developments in nanomaterials' characterization in science and engineering. In recent years, there have been many nanomaterials invented and characterized, including graphene. In the past few decades, AFM has been developed majorly in the following aspects:

1. Identifying and revealing more information about the materials at the nanometer level, such as electrical properties, mechanical properties, magnetic properties, surface functionalization, and thermal properties.
2. Easy to combine or integrate with other advanced measurements like optical techniques (infrared, Raman, and fluorescence spectroscopies), molecular characterization techniques (like nuclear magnetic resonance), and so on.
3. Fitting into the life sciences and materials research at different controlled physical parameters (temperature, wet chemical environment, solutions at different pH, illuminating with varying sources of light, and so on).

Based on these advancements in AFM measurements, the application of AFM has further been exploited in interdisciplinary fields for the analyses beyond the topography of materials (semiconductor, polymer, and biological) such as the interfacial interactions, phase transformations at different physical and biological conditions, current vs. voltage characteristics, and defects at the nano-domains of semiconductors.

Depending on the area of interest, different mode of operations is possible in the AFM measurements. Combining AFM with other analyzing techniques like infrared and Raman spectroscopy will achieve a nanometer-scale resolution for the sample analysis. The combination of AFM with other techniques which includes atomic force microscopy-infrared spectroscopy (AFM-IR) [6], atomic force microscopy nuclear-magnetic resonance (AFM-NMR) [7], atomic force microscopy-nuclear rheometer (AFM-Nano-rheology) [8], and atomic force microscope and light-sheet microscope (AFM-LS) [9] were recently developed. Based on the application, the mode of AFM analyses changes such as Bio-AFM for fluid cell enabled contact mode in aqueous solution; dynamic mode AFM (DM-AFM), which oscillates the AFM tip to reduce the friction; and force–distance curve-based AFM (FD-AFM) helps to record pixel-by-pixel measurements at atomic scale for the biological surfaces. Among the various modifications, molecular recognition AFM (MR-AFM) is employed for mapping the specific interactions, especially for biological samples. Multi-parametric AFM (MP-AFM) is used for the mapping of multiple physical or chemical properties. Multi-frequency AFM (MF-AFM) is used for detecting samples while oscillating the cantilever tip at various frequencies to find numerous material properties. Correlation of advanced optical microscope with AFM (Opto-AFM) has been employed for imaging the complex biological systems and a high-speed AFM (HS-AFM) for rapid acquisition of images by a factor of ~1000 to

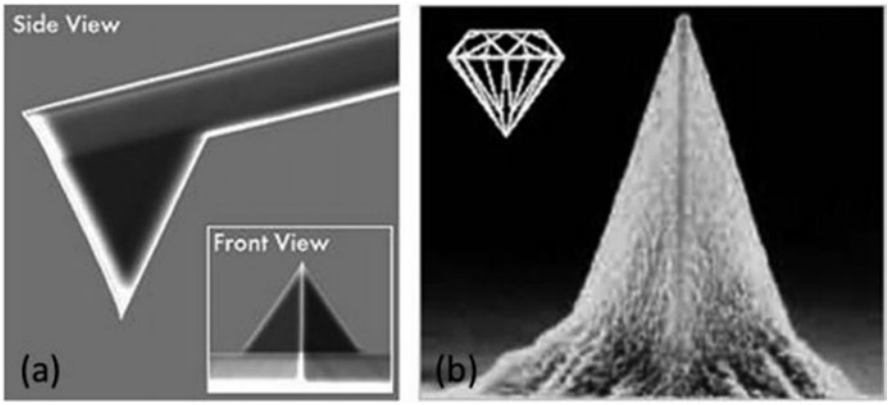

Fig. 5.2 (**a**) The cantilever with silicon nitride (Si_3N_4) tip and (**b**) diamond-coated AFM tip (reprinted with permission from reference [5])

provide access to the dynamic processes in the biological sciences [10]. In this chapter, the authors introduce AFM principles, modes of analysis, different kinds of materials used in the AFM instrument, working methodology, and their applications in detail.

5.2 Principle

AFM works on the combined principles of the Scanning Tunneling Microscope (STM) and the stylus profilometer. In particular, a sharp tip of silicon or carbon mounted on a cantilever spring (Fig. 5.2a) is dragged across the surface of samples with simultaneous feedback system adjustments between the model and tip of the probe. The sharp probe tip runs a raster scan across the sample surface with accurate positioning to the sub-nanometer range. The close feedback loop controls the probe movement to maintain a constant distance between the sample and the tip. The close feedback loop controls the probe movement to sustain a constant distance and a typical forces applied between tip and sample may change from 10^{-11} to 10^{-18} Å. The minimal force required to mobilize the cantilever through a minimum distance can be as small as 10^{-4} N, so the space is discernible, as small as 10^{-4} Å [11]. Therefore, nondestructive imaging of topography is possible without or with minimal damage to the surface of the sample. The surface outline is recorded by monitoring the feedback loop from the photodiode response, which generates the samples' surface topography based on the cantilever deflections.

The commonly used AFM probes consist of a sharp tip and a microcantilever, as shown in Fig. 5.2a. Template-assisted etching methods are usually employed for the fabrication of commercial cantilevers. A silicon wafer was pit etched by masking with desired measurements such as depth of the cavity, width of the recess in a pyramidal shape, or sharp needle type, followed by silicon nitride (Si_3N_4) coating.

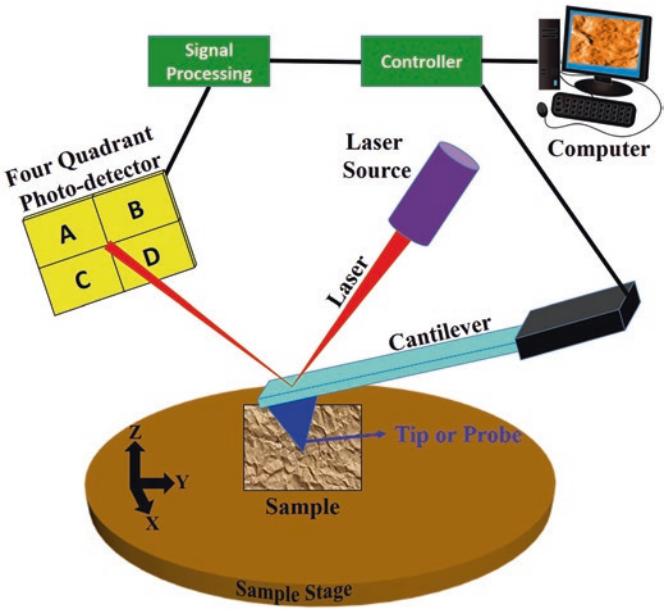

Fig. 5.3 Schematic for the working principle of AFM analysis

Finally, the base silicon substrate was selectively etched to get the desired configuration of the morphology. Several kinds of cantilevers are available based on the application, required sensitivity, and mode of operation. Cantilevers are available in different types such as V-shaped, gold-coated, sharpened needle type, super tip type, and ultra-clever type tips. The diamond-coated tip of the cantilever is shown in Fig. 5.2b. Based on the fabrication process the cantilever tips curvature radius is in the range of a few nm to 30 nm. Most of the microcantilevers are in the range 30–40 μm in width, 125–450 μm in length, and the thickness in the micrometer range to a few micrometers. During the AFM measurement, the laser source used for recording deflections from the cantilever should be highly dense to get an excellent spatial resolution and have very high sensitivity toward the photodiode detector to get a high-quality measurement.

The laser beam directly hits on the surface of the cantilever and reflects towards the mirror. The mirror directly receives the deflected laser beam by the highly sensitive photodetector. The photodiode, a highly-sensitive detector generally used to measure all dimensions as four quadrants (A, B, C, and D) (Fig. 5.3). The A + B detects the UP motion in the four quadrants, and C + D detects the cantilever's DOWN motion. Similarly, A + C sees the LEFT, and B + D detects the RIGHT side motions. Likewise, the deformation or twist in the cantilever will cause a change in the laser beam's position partially on the photodetector. The exact position of the laser beam is determined by using the following process:

The vertical position of the laser is proportional to ((A + B)-(C + D))/(A + B + C + D). Whereas ((A + C)-(B + D))/(A + B + C + D) is proportional to

lateral position. The normalization to the sum signal of (A + B + C + D) is used to eliminate cantilever reflectivity. The optical lever measures the angle of cantilever deflection but not the displacement. Hence, short cantilever probes are more sensitive to detect deflection changes than longer probes. Depending on the cantilever's movement, the photodetector receives the laser beam in different places, and further, they are converted into signals in the processor. The signal processor and cantilever are connected to the control unit, which further joined with the computer to convert signals into images and data. The detailed schematic, working principle of the AFM analysis is shown in Fig. 5.3.

The AFM scanners have horizontal and vertical movements in *XY* and *Z* dimensions. The sample stage in AFM has a piezoelectric scanner that determines the sample's position by nanometer scale, where the high voltage drives the *XYZ* directional movements in multiples of hundreds. The distorted AFM images are recorded during the piezo scanner's nonlinear motion while applying the steady voltage, whereas the piezoelectric materials do not respond to the applied voltages. The modern AFM instruments are equipped with *XYZ* position monitoring sensors, and the nonlinearity of the voltage is rectified by using a closed feedback loop. For more accuracy in the measurements, the voltages are tuned until the scanner reaches the desired position and it is called as closed-loop method [12].

The other procedure is an open-loop method, in which the nonlinearity is first adjusted then followed by the nonlinear voltage to drive the scanner to get the linear movement. A standard grid image was taken for calibration using different scan rates, scan sizes, and scan angles in this procedure. Finally, after finishing the scans and parameter corrections, the scanner movement against the applied voltage and scan conditions is obtained by fitting the data. This open-loop method is more beneficial to get a good high-resolution image. But this process is vulnerable to the position sensors and noise of the instrument. The sensors research development has helped to develop different sensors for different positions in AFM instruments such as optical sensors, capacitive sensors, strain gauge, and inductive sensors to overcome the sensitivity issues and get more accurate measurement. Therefore, in all the AFM measurements, by utilizing the combined effort from the sensor technology, high-resolution imaging is carried out using the closed-loop method instead of the open-loop method.

The deflection sensitivity of the cantilever is determined by its length and the sensitivity of the photodetector. For better reproducibility and precise measurements, the incident point and the approach/retract turning point are usually excluded from the calculation. The cantilever's short length is more preferred for obtaining high sensitivity during measurement of displacement in the pm range. The cantilever's effective length and laser position realignments will determine the deflection sensitivity due to laser spot position change. In general, the deflection sensitivity must be measured for every single AFM measurement due to the laser beam's realignment. The deflection sensitivity is calibrated by calculating the change in deflection of the cantilever from the voltage deflection. For a cantilever with a rectangular cross-section, the spring constant (k) can be expressed as:

$$k = \frac{Et^3 w}{4L^3}$$

Here, E is Young's modulus of the cantilever material (silicon or silicon nitride), t, w, and L are the thickness, width, and length of the cantilever, respectively. The k value is different for each cantilever as there may be a slight change in the cantilever's manufacturing process through microfabrication techniques. The thickness of the cantilever can be controlled by careful fabrication, but a minimum of 10% thickness error can cause an error in the spring constant three times. But in usual practice, the value given by the manufacturer is used for further calculations. The cantilevers must be calibrated before recording to get an accurate force value. The easy method to measure the spring constant (k) value is by using the following formula.

$$k = bf^3$$

Where resonance frequency (f) of a probe and b is the probe factor from the references. The direct measurement of the resonance frequency is by "auto-tune" in tapping mode analysis of AFM. But this method has poor accuracy due to the slight changes in the cantilever's dimension than as shown in reference value. The other way for calculating the resonance frequency of the cantilever is using the formula:

$$f = \frac{1}{2\pi}\left[\frac{k}{m_0}\right]^{0.5}$$

where k is the spring constant, m_0 is the effective mass of the lever. The toughness of the leveler is also an essential aspect in the calculation of resonance frequency. The leveler's softness is inversely proportional to the spring constant and directly proportional to the sensing of the deflection on the samples' surface [13]. But the cantilever must be smaller to keep the frequency higher for the detection of vibrations during the analysis. After several modifications and considering the different variables, finally, in the modern methods of AFM instrumentation, the cantilever's thermal noise has been used to calculate the spring constant and considered reliable [14]. The spring constant formula is as follows:

$$k = k_B T / z^2$$

where k_B and T are Boltzman constant = 1.3805×10^{-23} Joule/Kelvin and absolute temperature in Kelvin, respectively. Almost all AFM instruments with automatic software use this method, whose frequency ranges are from a few kHz to 2 MHz.

5.3 Working

In AFM, the cantilever/tip assembly plays a vital role and is often referred as a probe, which governs data interaction and quality. The tip's substrate is typically made of silicon/silicon nitride which is different from the cantilever material. Each material has its advantages; for instance, silicon-based materials are used to

fabricate sharp tips. The tip shape and size or radius at the apex are more critical, which defines the quality and range of operations. The corrugated AFM nail limits an image's resolution substantially on the lateral side of view due to the large surface area.

The AFM probes fabrication is a tedious method in the earlier days and made with a diamond shard by gluing to the thin metallic foil or wire (as a cantilever made up of Fe, W, or Ni). The first commercial AFM probe consists of Si_3N_4 thin film coated on the glass substrate as a cantilever and the square pyramidal-shaped tip with an apex of the radius of curvature about 20 nm. Such pyramidal AFM tips offer an opening apex angle of 60–70°. The AFM probe tips are customizable, and the generation has evolved into several types depending on the applications. For ambient and vacuum analysis, the monolith types of probes are more appropriate, especially monolithic silicon, fabricated from the Si wafer through etching. A diamond tip glued cantilever is also commercially available for high wear resistive, stable shape imaging, and more reliable electrical measurements. In addition to the sharp-edged tip, the round-headed apex with a large surface of 50–100 nm was also deployed for nano-mechanical measurements and low wear imaging. Off-late, owing to the high flexibility of AFM tip, the surface modification or coating has been introduced, especially for the study of chemical and biological applications. For example, the gold-coated tip provides better imaging for biological samples through gold–thiol interactions. Similarly, the cobalt or platinum-coated tips offer a good platform for electric or magnetic property measurements.

5.4 Sample Preparation and Handling

The experiment of AFM starts with sample preparation, probe selection, and microscope settings. More attention needs to pay while imaging the artifacts, which appear as substantial contrast change or identical structures as islands. Several factors influence such artifacts including, sample surface contamination, AFM tip condition, and shape. Therefore, it is highly advisable to store the samples under controlled conditions before the analysis. The AFM tip apex is vulnerable to damage on interaction with bulk samples, and hence additional care should be taken.

The AFM imaging requires:

1. Solid and rigid adherence of samples to the substrate to avoid their displacement by the probe.
2. Good dispersion.
3. The surface roughness should be lower than the sample particle size.

The substrate choice is not limited; however, the glass slide, freshly cleaved mica, or HOPG surface are commonly used. The polymeric adhesives are often required to affix the nano-sized samples to the substrate, facilitating strong particle-to-substrate affinity than the tip-to-substance interactions. The most common binders are poly-D-lysin, poly-L-lysin, poly-ethyleneimide (PEI), and

aminopropyltriethoxy-silane (APTES) improve adhesive property thru chemical bonding [15]. For fine powders (<150 nm), the uniform distribution is achieved via the dusting method followed by flipping and gentle tapping to remove the agglomerated particles. Similarly, the drop-casting process also provides good images. The sample is prepared by dispersing in alcohol/toluene/water (0.1 mg/ml) and deposited over the glued substrate or freshly peeled mica substrate [16]. Before scanning, the sample should be dried at ambient or accelerated heating under dust-free conditions. In the case of larger granular particles (>500 nm), a polished metal substrate with thermal wax glue offers a better platform for scanning. The sample preparation and imaging also be a big challenge, especially for biological samples owing to the low elastic modulus is in the range of kPa, for cells. However, some of the macromolecules and bone-type materials display significantly higher elastic modulus in GPa. Although special conditions are required for those samples due to wetness and softness, the AFM probe extends its application to study the variation of local surface charge, hydrophobicity, and nano-mechanical properties. Extreme care should pay in case of bio-sample to meet the essential requirement of substrate flatness and chemical compatibility through mechanical trapping and non-covalent physisorption. Not only powders but also biological cell samples are prepared by dispersion-evaporation, spray drying, and dip coating methods over the freshly cleaved mica substrate. Further, to improve the strong binding, chemical functionalization (i.e., Salinization) is applied to those samples.

5.5 Modes of AFM Analysis

The mode of AFM operations are broadly classified into two types such as contact or static and dynamic mode. The latter has further been subdivided into intermittent contact or tapping (standard or soft) and noncontact modes (as shown in Fig. 5.4).

In detail, the contact AFM mode is also known as a repulsive or static mode of operations, where the tip of the cantilever is in perpetual contact with the sample surface. The cantilever's spring constant must be lower than the effective spring

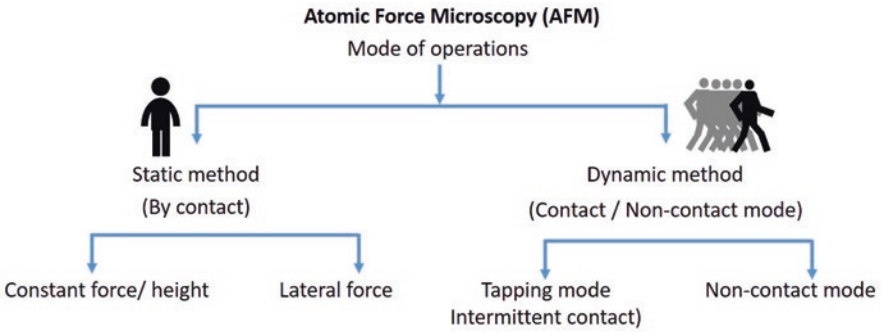

Fig. 5.4 The classification of fundamental modes of operations in atomic force microscopy

constant of atom–atom interactions in solids. This method is mainly used to image the hard surfaces to get a molecular or atomic level resolution of crystalline substrates. During the operation, the tip gently scans across the surface. The interaction or contact force between the sample and AFM tip is calculated from the cantilever's force constant and its deviation. Generally, a constant force or deflection feedback mode is used to measure such repulsive interactions, which vary from sub-nano to a few micro newtons in range. The AFM feedback systems are more sensitive to detecting such deflection. A piezo-actuator is usually employed to minimize the cantilever deflection by retracting the AFM probe (by vertical *x*-*y* movement) and maintaining a constant deflection, which further helps to retain the force between the tip and sample remains the same. The repulsion force F experienced by the AFM-tip is directly related to the cantilever deflection value *x* and calculated from Hook's law:

$$F = -kx$$

where *k* is spring constant. At ambient conditions, on this side, the initial large force typically from ten to a hundred nano-Newtons between the tip and sample damage or deform the surface of soft materials.

On the other side, the sample's rigid texture destroys the tip apex's sharpness during operations' contact mode. The probe with soft cantilevers <1 N/m is preferable to achieve high deflection sensitivity while keeping the interaction force is significantly low. The cantilever's length also plays a vital role, which varies from a few tens of micrometers to several hundreds, usually 400–500 μm; however, the shorter length offers higher sensitivity, while the materials have the same force constant.

A constant height mode of scanning can also be performed under static conditions to get atomic resolution by maintaining the probe at a fixed height. In such cases, no feedback force has been applied to the probe. Such high-resolution imaging can only be achieved for smooth samples. This method's significant advantage is high-speed scanning; however, it is limited to the cantilever's resonant frequency. Besides, it also has some drawbacks while scanning the soft materials, for instance, soft polymers, bio-samples, etc., which destroy the sample by scratching due to the proximity of tip and sample. In this contact AFM method, the soft cantilever's tip is susceptible to distort the image features by lateral or shear forces and the surface contaminants, especially in the ambient air atmosphere. The initial high pressure and the lateral shear force tend to suppress the spatial resolution and damage the soft sample by scrapping. The detailed cantilever deflection and modes of operation are shown in Fig. 5.5.

In contact mode of operation, lateral force imaging is also performed, where the cantilever deflection is in a horizontal direction, which is controversial to the conventional vertical movement. The characteristic of the change in samples' surface friction can be gauged using this method by measuring the interaction between the tip and sample, resulting in lateral bending or twisting of the cantilever. The lateral deflection arises by the change in frictional coefficient of a sample via the applied force to the cantilever during the lateral scanning.

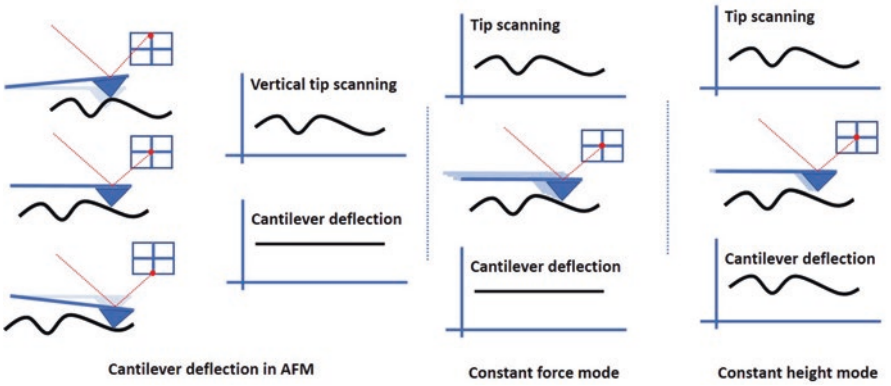

Fig. 5.5 Cantilever deflection and types of static mode of operations in AFM

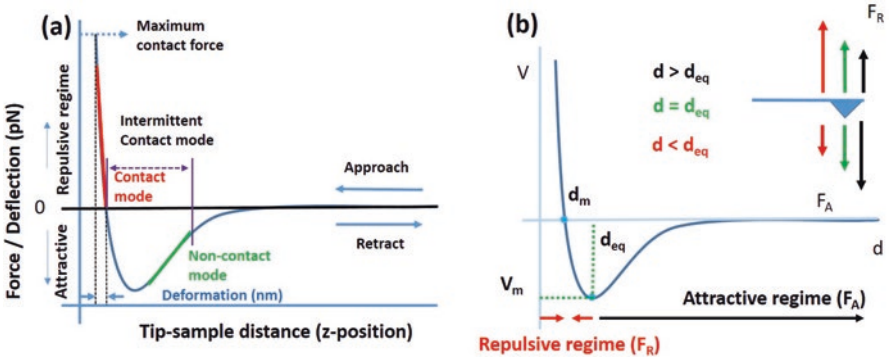

Fig. 5.6 (**a**) Force–distance curve and (**b**) Lennard–Jones potential plot of nonbonding interactions at different circumstances

It is challenging to choose the mode of imaging for individual samples in advance; however, the deflection vs. distance, i.e., force curve measurements between the models to tip, guides to select the appropriate test condition and the probe (as shown in Fig. 5.6a). The elastic and inelastic deformation force between the AFM tip-sample capillary or adhesion can easily be distinguished using the force curve. In specific, if the tip-sample distance is well pronounced, then the resultant force is Van der Waals attractive. On the other hand, the close-enough space leads to strong repulsion (Pauli's) due to orbital overlapping. The approximate force can be calculated using the Lennard-Jones potential graph (Fig. 5.6b), which describes the interaction between nonbonding atoms as a function of distance:

$$V(d) = 4V_m \left[\left(\frac{d_m}{d} \right)^{12} - \left(\frac{d_m}{d} \right)^{6} \right]$$

$V(d)$ is intermolecular potential. V_m is well-depth, and a measure of attraction between the particles, d-particle separation from the center, and d_m distance at $V = 0$, i.e., how close the two nonbonding particles and referred to as van der Waals radius. As the separation distance is equal to the equilibrium distance ($d = d_{eq}$), the resultant force is zero on the tip until the external force is applied. Suppose the tip-sample space is below the equilibrium distance ($d < d_{eq}$) the consequent potential energy increases due to the atomic orbitals overlapping (repulsive force, $F_{R,}$ is dominant). On the contrary, the significant separation between the tip and sample, $d > d_{eq,}$ displays high negative potential and tends to reach equilibrium, indicating the existence of robust, attractive force [17].

The feedback acquisition should be high under an optimized scanning rate to record a stable AFM image, which could be achieved by setting a low deflection set point to minimize the tip-sample force. The selection of soft AFM cantilevers could also overcome excessive force. Similarly, other interference forces such as capillary or meniscus and other attractive forces that arise from the monolayer adsorption of water vapor/gas molecules could be neutralized by the complete immersion in liquids.

In the noncontact mode of imaging, the AFM tip is hungover (~50–150 Å) to scan the topographic image by a smaller amplitude of the cantilever's oscillation (<10 nm). Typically, the interaction between tip and sample is attractive van der Waals force, which is substantially weaker than that of the force used in the contact mode of operations. This method's main advantage is to achieve high-resolution images due to poor possible interaction with the sample surface, which retains the tip's sharpness, especially in extreme hydrophobic samples. However, it is not that easy to preserve the AFM tip in the van der Waals regime. The slow-scan imaging, the poor lateral resolutions, and the attractive gradient force due to the thick fluid contaminants hampered such a noncontact mode of operation. Such limitation has been suppressed by employing a high-performance feedback controller, ultra-high vacuum chamber, etc.

In the dynamic mode, the Tapping method is a widely employed and more effective method to scan the sample while comparing it to the noncontact AFM imaging. It overcomes some of the problems and limitations associated with other modes of AFM operations, including destructive frictional force, electrostatic interference, capillary interaction, and adhesion. Herein, the probe is associated with a piezoelectric transducer to oscillate the cantilever near the resonance frequency (10 – a few 100 kHz) to sense long-distance van der Waals forces (both attractive and repulsive force regimes). During the operation, the lower end of the AFM tip is close to the sample and record the damping oscillation amplitude, which is typically in the range greater than 20 nm. Upon scanning, the AFM tip experiences intermittent contact with the models by vertical oscillation, and the frequency range is 50–500 k cycles per second. In this mode, either the cantilever's oscillation amplitude or phase change is used in a feedback loop to maintain a constant probe-sample distance by z-axis movement, which is the direct measurement of sample height (Fig. 5.7).

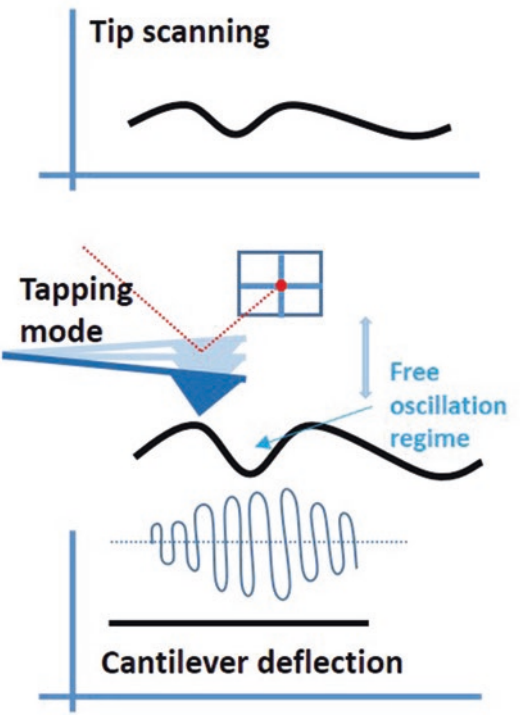

Fig. 5.7 Dynamic tapping mode of AFM operation

On the sample surface, the oscillation amplitude decreases, whereas, at the depression point, it reaches maximum owing to more space for probe the swinging. The tapping mode of scanning is less destructive and preferable, where the high frequency of oscillation significantly reduces the adhesion force between the tip and samples due to viscoelastic stiffness. The significant difference between the non-contact and tapping mode of dynamic operation is the AFM tip placement during the probe oscillation; in the former case, the tip stays only at the attractive Van der Waals regime, whereas such control extends into the repulsive force region in the tapping mode. In practice, the probe's lower force constant minimizes the immense tip-sample attraction to oscillate freely, typically in the range of a few tens of N/m. Besides, this technique offers high lateral resolution images (1–5 nm) with significantly less or no damage to soft samples. However, the speed of scanning is slower compared to the contact mode of imaging. Not surprisingly, the soft Si probe is widely applied for tapping mode of operation at ambient air conditions, also providing a good image in fluid media. Generally, wide-ranging resonance frequencies are more desirable to acquire complete scanning faster; however, the standard probe used in the dynamic mode of AFM operation is limited and requires distinctive geometries.

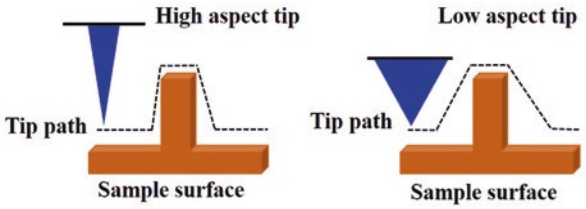

Fig. 5.8 The probe or tip with a high aspect ratio will provide a high resolution. The probe with high radius curvature results in a low aspect ratio due to tip convolution. In both cases, the height of the sample is not affected, but the resolution of the image drastically varies

5.6 Factors Affecting AFM Imaging

The quality of the AFM image depends on several factors; however, the tip shape and the apex's radius of curvature play a significant role. In contrast to the sharp apex, the broad and dull tip edge fails to scan the sample's more minor features. For example, a larger tip size will result in a more prominent feature size than its original or the actual size, and it cannot differentiate between two or more adjacent features of the samples. Therefore, a sharp tip cantilever is required. The debris accumulated over the edge also distorts the image quality. Imaging small features and scanning small areas at high resolution requires ultra-sharp tips. However, the commercial probes with very high aspect ratios are widely available, made with materials such as carbon nanotubes or tungsten spikes. These kinds of costly probes are still an unresolved issue for everyday usage of AFM analysis. To achieve a high atomic resolution, using an appropriate ideally sharp probe is needed. The probe-to-sample interaction at the surface must be improved by modifying the surface morphology and/or functional groups, and dimensions of the probe (Fig. 5.8).

5.7 Applications

AFM, a powerful imaging tool to study nano and sub-nano level scale surface morphologies in the broad discipline of materials, including semiconductor technology, surface chemistry of thin-film, polymer coatings, molecular as well as cell biology, piezoelectric, and ferroelectric properties. Among all these studies, let us consider the molecules and morphologies for easy understanding.

5.7.1 Molecules

Biomolecule structure imaging is not accessible due to their poor sensitivity that deviates from the average molecular structures. The bimolecular designs can be determined using the soft-touch AFM in combination with the image analysis method. By this method, many molecules and highly complex and basic structures can also be studied. Figure 5.9 describes the AFM images of double-helical

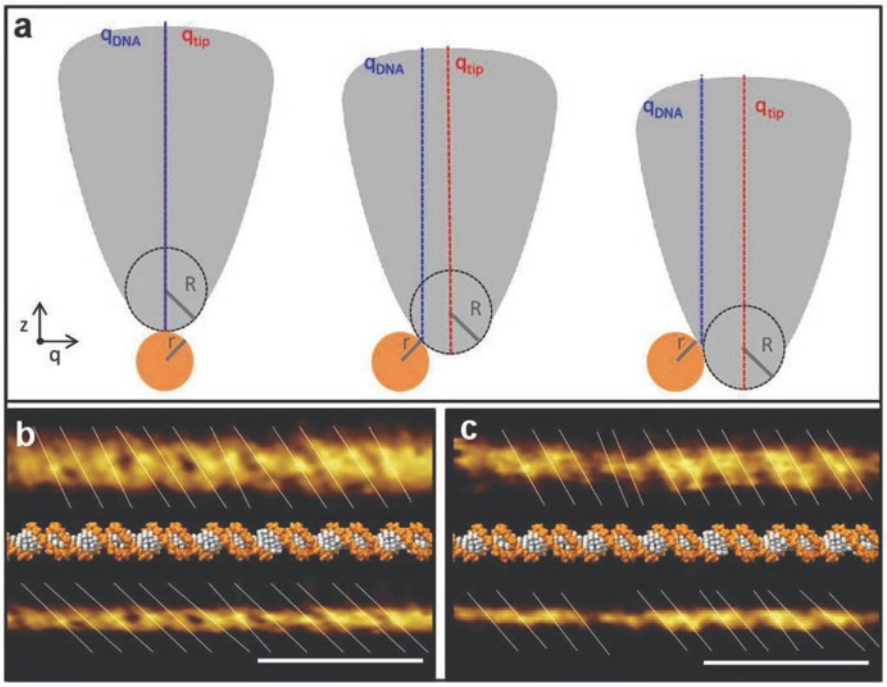

Fig. 5.9 The chiral angle measurement of the double helix of DNA using AFM. (**a**) Schematic for the AFM tip with radius *R* at different positions on the surface of DNA sample with radius *r* (cross-sectional view for easy understanding). (**b**, **c**) The AFM topography of digitally straightened parts of DNA before (top) and after (bottom) correcting with a definite tip size in comparison with the B-DNA crystal structures. (**b**) $r = 1.1 \pm 0.1$ nm, $R = 1.3 \pm 0.2$ nm, and (**c**) $r = 0.9 \pm 0.1$ nm, $R = 1.7 \pm 0.2$ nm. Scale bars: 10 nm; reprinted with permission from reference Pyne et al. [18]

DNA. This combination of AFM with image analysis technique is more helpful in understanding the biological complex molecules [18, 19].

The asphaltene's complex structure has been imaged using AFM with functionalized tip, as shown in Fig. 5.10. Coal-derived asphaltene (CA) sample preparation for the analysis is shown in Fig. 5.10a, and CA molecular structure is characterized using AFM at different distances. Currents are shown in Fig. 5.10b–g. The asphaltene's molecular structure is visible at the sample to tip distance of −0.9 Å using AFM analysis, as shown in Fig. 5.10c. The STM analysis of the CA sample at different currents is shown in Fig. 5.10e, f. From this analysis, AFM measurement has resulted as a replica of CA's chemical structure is seen compared to STM analysis.

An indispensable metrology technique of AFM is used in the semiconductor field to characterize the trenches and holes present in the high-performance microelectronic circuits. The integrated circuit matrix's topography and electric properties have been studied by combining the Kelvin force probe and scanning capacitance probe with conductive AFM. Besides, such nanoprobe technique helps to

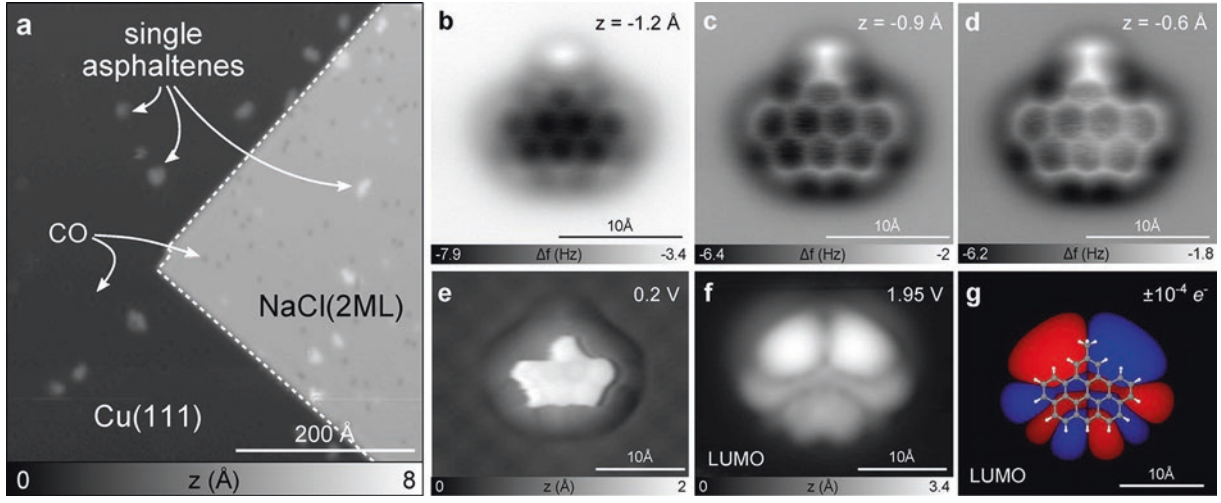

Fig. 5.10 (**a**) Coal-derived asphaltene (CA) sample preparation and analysis. Scanning tunneling microscopic overview image of the CA sample on NaCl(2 ML)/Cu(111) substrate prepared using a flash evaporation process. (**b–d**) AFM images of CA on NaCl(2 ML)/Cu(111) at different set-points z from (I = 1.4 pA, V = 0.2 V). (**e**) STM image of CA (I = 10 pA, V = 0.2 V). (**f**) STM image at the NIR (I = 1.4 pA, V = 1.95 V). (**g**) LUMO orbital of CA with the molecular structure overlaid as a guide to the eye. CO-functionalized tips have been used for all AFM and STM measurements shown (reprinted with permission from reference Schuler et al. [20])

investigate the localized failure, mainly invisible soft failure in memory chips due to complex layout.

In material chemistry, especially energy storing lithium-ion batteries, the localized lithium concentration has been studied during cycling by integrating with a Raman spectrometer. AFM helps to understand the evolution and degradation of solid electrolyte interfacial layer formation over the electrode, especially anode by operando and in situ measurements [21]. The localized electrical, mechanical properties, aging effects, and other limiting factors of the cathode include inactive localized area, surface contaminants (either physisorbed or chemisorbed), reaction products, etc. Mechanical properties of thick electrodes used in high-energy batteries are crucial, especially to retain the integrity of stiffness and elastic modulus; hence contact-resonance, frequency, or amplitude modulation AFM methods is employed for investigation. The contact-resonance AFM (CR-AFM) is a static contact mode of operation and susceptible to tip damage. In contrast, frequency or amplitude modulation is a dynamic nondestructive tapping mode of scanning and offers high-resolution images. The bulk electrode's surface conductivity has been investigated with a conductive probe AFM, where the Kelvin probe provides to measure the surface potential at micro to the nanoscale level.

The AFM also provides high-resolution real-time 3D images (both vertical and lateral imaging) for biological samples, although it is probe selective. This technique helps to study the micromechanical properties of biosamples such as surface properties, viscoelastic nature, Young's modulus, adhesion, mechanical, and friction forces. In contact mode, soft probes are preferable for macro-biomolecules, where the stiffness is $\leq$0.1 N/m, for instance, soft silicon probe, etc. Besides, biologic samples offer reduced interference under the liquid immersed condition, especially in buffered media. Off-late, the AFM analysis extends its application to perform the nondestructive imaging of living cell's membrane, especially membrane protein, lipids, and their interactions. The amplitude modulation or frequency modulation method of AFM offers high-resolution bio-images both in ambient and vacuum conditions.

5.7.2 Morphologies

The surface morphologies of the biological and inorganic materials can be easily studied using AFM analysis. The dimensions of the samples were also understood using AFM analysis. In the biological system, the major components of the human blood collected from a healthy donor i.e., platelets and erythrocytes were analyzed in air. Figure 5.11a, c are height images, whereas (b) and (d) are error signal images.

The surface profiling of the inorganic MXene ($Ti_3C_2T_x$) sheets using AFM analysis provides a clear understanding of the prepared MXene sheets' thickness and size [23]. The AFM image of MXene nanosheets is shown in Fig. 5.12. The height profile describes the synthesized MXene as multilayer in structure with an average thickness of ~200 nm.

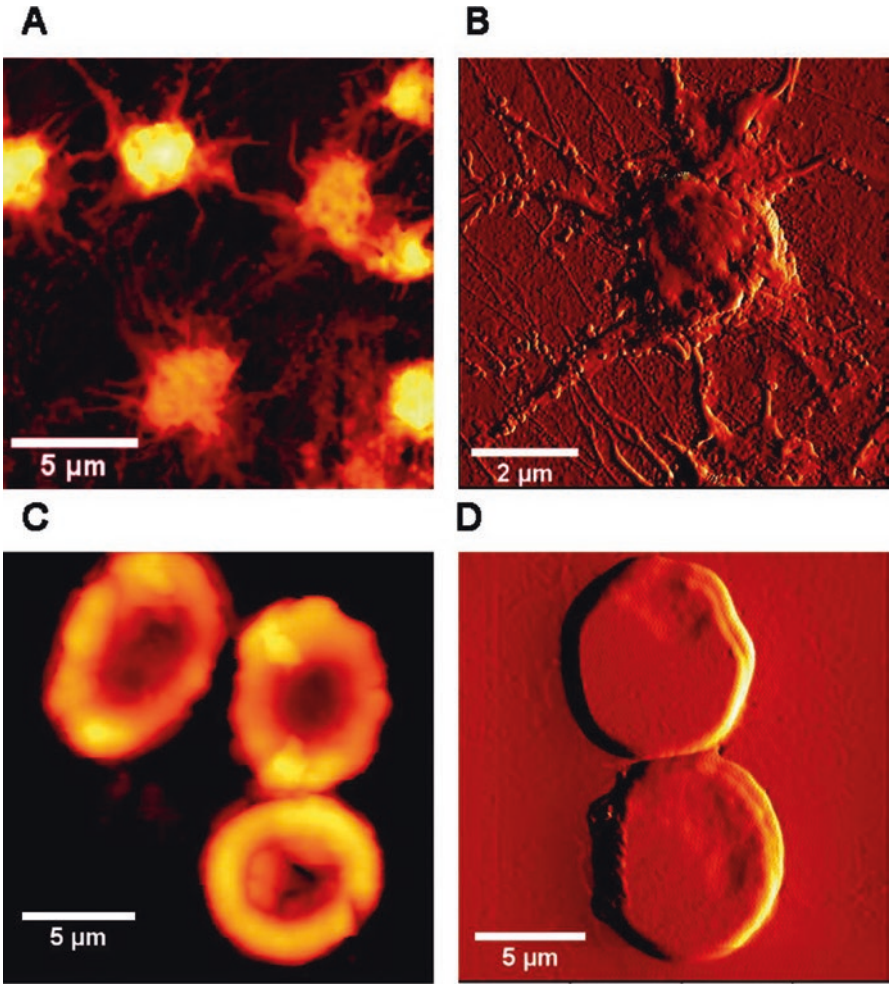

Fig. 5.11 AFM imaging in air of human platelets (**a**, **b**) and erythrocytes (**c**, **d**) from healthy donors. (**a**) and (**c**) are height images, whereas (**b**) and (**d**) are error signal images (reprinted with permission from reference Carvalho et al. [22])

The surface depth profile and pore size were analyzed for the honeycomb patterned porous polymer films fabricated using the breath-figure method [24]. The porous structures were differentiated in AFM analysis depending on the morphology of the polymer films. Single-layer pores and multilayers pores were distinguished, as shown in Fig. 5.13.

In summary, AFM is one of the advanced techniques used for the recording and analysis of the topology of the materials, and the molecular structures of the materials. There is no other technique having the capability of direct molecular structure imaging. Combining AFM with other procedures like IR, NMR, and other optical instruments is an added advantage for characterizing the rare phenomenons

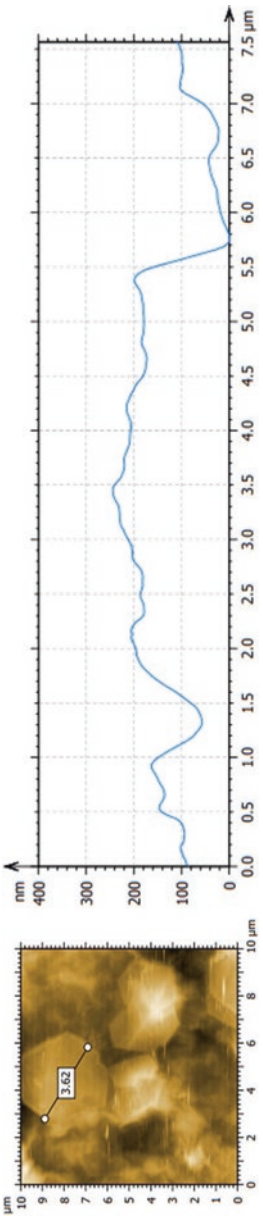

Fig. 5.12 AFM analysis of MXene flakes by contact mode with sheet thickness of ~200 nm and 3.62 µm size

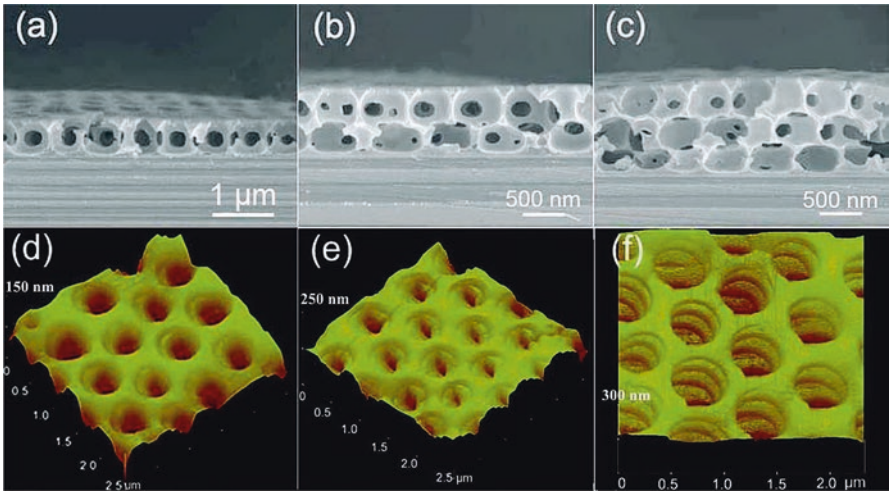

Fig. 5.13 Honeycomb patterned porous polymer films fabricated using breath figure method by dissolving polymer material in carbon disulfide solvent and cast on a silicon substrate. (**a–c**) Cross-sectional SEM images of the single, double, and multilayer porous structures. (**d–f**) Three-dimensional AFM images with depth profile (reprinted with permission from reference Dong et al. [24])

in science and engineering. The biological samples are easily studied without any damage using the AFM method. AFM is one of the best nondestructive techniques without using any conductive additive on the samples' surface for the analysis. AFM is the best tool to understand the polymer systems' interfacial phenomenons, a biological system's bioimaging with high-resolution capability ~100,000 times that of other techniques. Further modification of probes used like change in the cantilever's size and shapes, surface modification of the probe tips using gold or diamond coatings helps get the samples' better resolution and accuracy using AFM analysis. Further improvements and changes by addressing the present issues in AFM can become a powerful tool for understanding many unknown phenomenons in science and technology.

Acknowledgments This research was supported by the Radiation Technology R&D program (NRF-2017M2A2A6A01019289), funded by the Ministry of Science, ICT and Future Planning. This research was supported by the Basic Science Research Program through the National Research Foundation of Korea (NRF), funded by the Ministry of Education (2018R1A6A 1A03023788 and 2021R1I1A1A01055790). Additionally, this work was supported by the Korea Institute for Advancement of Technology (KIAT) grant funded by the Korean Government (MOTIE) (P00008500, The Competency Development Program for Industry Specialist). This work was supported by the Material Components Global Investment Linkage Technology Development Project (Global Open Technology Development Project) (20013593) of the KEIT, MOTIE (KOREA).

References

1. Binning G, Rohrer H, Gerber C, Weibel E (1993) Surface studies by scanning tunneling microscopy. In: Neddermeyer H (ed) Scanning tunneling microscopy. Springer, Dordrecht, pp 31–35. https://doi.org/10.1007/978-94-011-1812-5_1
2. Young R, Ward J, Scire F (1972) The Topografiner: an instrument for measuring surface microtopography. Rev Sci Instrum 43(7):999–1011. https://doi.org/10.1063/1.1685846
3. Binnig G, Quate CF, Gerber C (1986) Atomic force microscope. Phys Rev Lett 56(9):930–933. https://doi.org/10.1103/PhysRevLett.56.930
4. Martin Y, Williams CC, Wickramasinghe HK (1987) Atomic force microscope–force mapping and profiling on a sub 100-Å scale. J Appl Phys 61(10):4723–4729. https://doi.org/10.1063/1.338807
5. Nguyen-Tri P, Ghassemi P, Carriere P, Nanda S, Assadi AA, Nguyen DD (2020) Recent applications of advanced atomic force microscopy in polymer science: a review. Polymers 12(5). https://doi.org/10.3390/polym12051142
6. Dazzi A, Prater CB (2017) AFM-IR: technology and applications in nanoscale infrared spectroscopy and chemical imaging. Chem Rev 117(7):5146–5173. https://doi.org/10.1021/acs.chemrev.6b00448
7. Mousoulis C, Maleki T, Ziaie B, Neu CP (2013) Atomic force microscopy-coupled microcoils for cellular-scale nuclear magnetic resonance spectroscopy. Appl Phys Lett 102(14):143702–143702. https://doi.org/10.1063/1.4801318
8. Lherbette M, dos Santos Á, Hari-Gupta Y, Fili N, Toseland CP, Schaap IAT (2017) Atomic force microscopy micro-rheology reveals large structural inhomogeneities in single cell-nuclei. Sci Rep 7(1):8116. https://doi.org/10.1038/s41598-017-08517-6
9. Hobson CM, Kern M, O'Brien ET, Stephens AD, Falvo MR, Superfine R (2020) Correlating nuclear morphology and external force with combined atomic force microscopy and light sheet imaging separates roles of chromatin and lamin A/C in nuclear mechanics. bioRxiv:2020.2002.2010.942581. https://doi.org/10.1101/2020.02.10.942581
10. Dufrêne YF, Ando T, Garcia R, Alsteens D, Martinez-Martin D, Engel A, Gerber C, Müller DJ (2017) Imaging modes of atomic force microscopy for application in molecular and cell biology. Nat Nanotechnol 12(4):295–307. https://doi.org/10.1038/nnano.2017.45
11. Maghsoudy-Louyeh S, Kropf M, Tittmann BR (2018) Review of progress in atomic force microscopy. Open Neuroimaging J 12:86–104. https://doi.org/10.2174/1874440001812010086
12. Kenkel S, Mittal S, Bhargava R (2020) Closed-loop atomic force microscopy-infrared spectroscopic imaging for nanoscale molecular characterization. Nat Commun 11(1):3225. https://doi.org/10.1038/s41467-020-17043-5
13. Shao Z, Mou J, Czajkowsky DM, Yang J, Yuan J-Y (1996) Biological atomic force microscopy: what is achieved and what is needed. Adv Phys 45(1):1–86. https://doi.org/10.1080/00018739600101467
14. Horcas I, Fernández R, Gómez-Rodríguez JM, Colchero J, Gómez-Herrero J, Baro AM (2007) WSXM: a software for scanning probe microscopy and a tool for nanotechnology. Rev Sci Instrum 78(1):013705. https://doi.org/10.1063/1.2432410
15. Engel A, Müller DJ (2000) Observing single biomolecules at work with the atomic force microscope. Nat Struct Biol 7(9):715–718. https://doi.org/10.1038/78929
16. Vesenka J, Manne S, Giberson R, Marsh T, Henderson E (1993) Colloidal gold particles as an incompressible atomic force microscope imaging standard for assessing the compressibility of biomolecules. Biophys J 65(3):992–997. https://doi.org/10.1016/S0006-3495(93)81171-8
17. Stylianou A, Kontomaris S-V, Grant C, Alexandratou E (2019) Atomic force microscopy on biological materials related to pathological conditions. Scanning 2019:8452851. https://doi.org/10.1155/2019/8452851
18. Pyne A, Thompson R, Leung C, Roy D, Hoogenboom BW (2014) Single-molecule reconstruction of oligonucleotide secondary structure by atomic force microscopy. Small 10(16):3257–3261. https://doi.org/10.1002/smll.201400265

19. Gross L, Mohn F, Moll N, Liljeroth P, Meyer G (2009) The chemical structure of a molecule resolved by atomic force microscopy. Science 325(5944):1110. https://doi.org/10.1126/science.1176210
20. Schuler B, Meyer G, Peña D, Mullins OC, Gross L (2015) Unraveling the molecular structures of asphaltenes by atomic force microscopy. J Am Chem Soc 137(31):9870–9876. https://doi.org/10.1021/jacs.5b04056
21. Lang S-Y, Shi Y, Hu X-C, Yan H-J, Wen R, Wan L-J (2019) Recent progress in the application of in situ atomic force microscopy for rechargeable batteries. Curr Opin Electrochem 17:134–142. https://doi.org/10.1016/j.coelec.2019.05.004
22. Carvalho FA, Connell S, Miltenberger-Miltenyi G, Pereira SV, Tavares A, Ariëns RAS, Santos NC (2010) Atomic force microscopy-based molecular recognition of a fibrinogen receptor on human erythrocytes. ACS Nano 4(8):4609–4620. https://doi.org/10.1021/nn1009648
23. Murali G, Rawal J, Modigunta JKR, Park YH, Lee J-H, Lee S-Y, Park S-J, In I (2021) A review on MXenes: new-generation 2D materials for supercapacitors. Sustainab Energy Fuels 5(22):5672–5693. https://doi.org/10.1039/D1SE00918D
24. Dong R, Yan J, Ma H, Fang Y, Hao J (2011) Dimensional architecture of ferrocenyl-based oligomer honeycomb-patterned films: from monolayer to multilayer. Langmuir 27(14):9052–9056. https://doi.org/10.1021/la201264u

Exploring the Microcosm at Atomic Precision Using Atomic Force Microscopy

6

Lakshmipathy Muthukrishnan

Abstract

Atomic force microscopy (AFM) unlike electron microscopy and X-ray crystallography is one of the most sought-after mechanobiological approach to study bio/non-biocomplexes. Taking inputs from scanning tunnelling microscopy, AFM was found capable of probing the topographical details at the atomic scale by measuring a small force existing between the surface and the tip. Alongside semiconductor science and technological applications, AFM has been employed to image the morphology of biomolecules, cellular components, tissues, and cells. Besides electron microscopy, AFM has been recruited to study the biological materials in a liquid medium with minimal sample preparation; one of the hallmarks in characterizing the topography at resolutions unachievable by conventional optical microscopy. There are several factors (support for sample preparation, adhesion force, elasticity of the cell, Young's modulus, cell stiffness, etc.) involved in improving the bioimaging efficiency of AFM. This chapter attempts to bring out the connotation of AFM to understand and image selected biological entities (virus, bacteria, and cancer cells) and their application in disease diagnosis. Furthermore, it offers a basic understanding of AFM, their evolution, working principle, and a deeper insight into the performance characteristics of imaging bio/non-biocomplexes.

Keywords

Atomic force microscope · Adhesion force · Young's modulus · Elasticity · Topography · Mechanobiology

L. Muthukrishnan (✉)
Department of Conservative Dentistry and Endodontics, Saveetha Dental College and Hospitals, Saveetha Institute of Medical and Technical Sciences, Chennai, Tamil Nadu, India
e-mail: wilgince.apollon@uanl.edu.mx

S.-K. Kamaraj et al. (eds.), *Microscopic Techniques for the Non-Expert*,
https://doi.org/10.1007/978-3-030-99542-3_6

6.1 Introduction

Atomic force microscope (AFM) constitutes one of a kind scanning probe microscope beheld with a demonstrated imaging resolution of the order of nanometer, a thousand times better than the optical diffraction limit. It analyses by just feeling or touching the surface of the material using a mechanical probe. It is one of the tools used for measuring, probing, and capturing the manipulated matter at the nanoscale. By hiring some principles of a scanning tunnelling microscope, the AFM was developed during the early 1980s with the first commercial AFM introduced in 1989.

Indeed, AFM has drawn great attention with its widespread application toward solid-state physics, semiconductor technology, biomolecular engineering, polymer science, and surface chemistry engineering. Its application has been further extended to molecular, cellular biology, and medicine adopting mechanobiological principles. This attributes to understanding the mechanism involved in the signalling response from the biological entities (proteins, cells, tissues, etc.) based on the physical forces and the mechanical properties. It is this mechanical cue that measures the forces virtually from any scale ranging from cells, tissues, viruses, and extracellular/intracellular architecture [1, 2].

A highly sensitive tool that has evolved for measuring microstructural properties and the intermolecular forces at nanolevel with an atomic precision has profound implications in the field of electronics, semiconductors, polymers, and biomaterials. A microlevel cantilever system working on a feedback mechanism operates on three different open-loop modes such as non-contact, contact, and tapping modes. The non-contact mode provides the topographical information about the sample by targeting electric, magnetic, and atomic forces; while contact mode retrieves data pertaining to the interaction forces on the sample [3].

On the other hand, tapping and/or intermittent contact mode provides the combined characteristic features of both non-contact and contact modes of operation. It has been a widely practised technique finding its application in biological sciences to define the cell-to-cell or cell-to-protein or drug-to-protein interactions, biomolecular assemblies, interactions in biological pathways, and cell movements [4–6]. Moreover, the topographical features and their quantification have relatively added much more advantage to probe single molecules [7, 8] as illustrated in Fig. 6.1.

AFM has several advantages and disadvantages over conventional microscopes for bio-imaging. Although the staining technique has been the most sought-after approach in studying the cellular details, a minimal pre-treatment procedure is essential to image the biological structures. On the other hand while using AFM, the biomolecules can be imaged under real-time physiological conditions at nanoscale. There exist some limitations while using an electron microscope which could be surpassed by AFM technique in exploring the functional properties of the biomolecules. With the advent of AFM, the time taken for capturing bio-images was too long which was soon overcome by commercially available fast-scanning AFMs. One of the disadvantages that the conventional AFM faced was capturing the inside of the sample unlike optical and electron microscopes which can have deeper insights. Secondly, the limited scanning range roughly 100×100 μM pertaining to

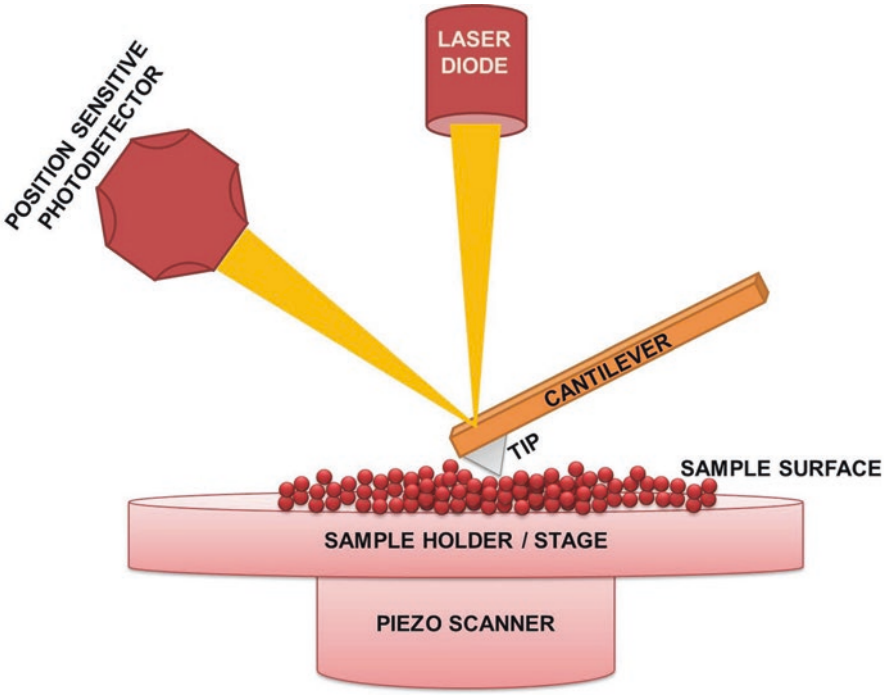

Fig. 6.1 Typical AFM imaging procedure in which a pyramidal tip attached to a flexible cantilever scans over the sample surface. When a beam of light is focused at the back of the tip, there is a significant deflection and as a result, the tip moves and this movement helps generate a detailed image of the sample

X and Y with respect to 2D is restricted to around 10 μm in height attributing for *Z* axis. Some of the characteristic features of the optical techniques (starting from light microscopy to atomic force microscopy) have been enlisted in Table 6.1 [9].

6.2 Evolution of Atomic Force Microscopy

The discovery of scanning probe microscopy (with characteristic atomic precision and resolution) had sown the seed for the development of AFM for a more precise resolution. It was Russell D. Young from the National Bureau of Standards who first explored the detection strategy. He initially combined the detection of tunnelling current using a scanning device to retrieve surface information of metals without direct interaction. This setup came into existence as Topografiner in which a constant voltage when applied could maintain the constant flow of tunnelling current and by keeping the tip scanning over the surface. The working mechanism encountered in scanning tunnelling microscope was to facilitate sturdy positioning of the tip above the surface of the sample by increasing the vibration. Such improvisation was brought about by physicists Gerd Binnig and Heinrich Rohrer in IBM research

Table 6.1 Comparative analysis of various optical techniques used for imaging

Microscopy	Resolution limit	Characteristic features
Light microscopy	~0.2 μm	Samples could be imaged in liquid or air and the resolution is limited by the wavelength of visible light
Fluorescence microscopy	~0.2 μm	Samples could be imaged in liquid or air. Fluorescence stains could localize molecular components. Confocal laser scanning microscopy enables 3D view of the biological samples. Although resolution is limited by the wavelength of light, it could be surpassed by super resolution techniques
Scanning electron microscopy (SEM)	nm level	Sample placed in vacuum. Sputter coating for electron conductivity. Electron beam probes the surface of the metal labelled sample
Transmission electron microscopy (TEM)	nm level	Contrasting images owing to impeding electrons and operates under vacuum. Requires heavy metal staining and image contrast through staining
Atomic Force Microscopy (AFM)	nm level	Imaging is achieved by the cantilever's position on the sample surface. It provides three-dimensional view and measures nanomechanical properties of the sample. Samples can be imaged in liquid or air at nanometre scale

Table 6.2 Timelines in the development of Scanning Tunnelling Microscope (STM)

Year	Progress made	References
1972	The precursor for STM i.e. Topografiner was developed by Russell D. Young.	[10]
1981	The first STM was constructed by Binnig, Rohrer, Weibel and Gerber	[11]
1982	The first image of Si(111) – (7 × 7) was captured by Binnig, Rohrer, Weibel and Gerber	[11]
1985	Atomic Force Microscope (AFM) was first invented by Binnig, Quate and Gerber	[12]
1986	Binnig and Rohrer were awarded with Nobel prize in Physics	[12]
1987	Feenstra had imaged the sensitive element of GaAs (Gallium arsenide)	[13]
1990	Meyer and Amer introduced Optical beam deflection method	[14]
	Eigler had demonstrated the first positioning of single atoms on the surface using a low temperature STM	[15]
1993	Zhong, Inniss, Kjoller and Elings have introduced Tapping mode in AFM	[16]
1995	Giessibl had demonstrated the first atomic resolution using an AFM	[17]
1998	Stipe and Ho have introduced the first vibrational spectroscopy with the STM	[18, 19]

laboratory, Zurich. They made a simple alteration in mechanical design while developing STM with an enhanced atomic resolution. Their contribution had fetched them the Nobel Prize for Physics in 1986. The highlights in the evolution of AFM have been enlisted in Table 6.2.

6.3 Bio-imaging Using AFM

The stereotype about AFM and its application to study the surface chemistry of metals and solids was broken when a live plant cell in water was imaged in the early 1990s. Concerns pertaining to cell damages incurred by the exertion of mechanical forces used to operate the cantilever tip upon imaging were defeated prior to successful imaging of variety of mammalian cells. Priority was given to mammalian cells as they adhere well to the surface and could not be removed using mechanical shears driven by the cantilever tip. On the other hand, smaller cells like bacteria, yeasts, and viruses need to be immobilized onto surfaces before subjecting them to AFM imaging. Entrapment using membrane filters and tethering by surface functionalization have been employed to achieve immobilization for effective imaging. For instance, porcine-derived gelatin combined with freshly cleaved mica was used to coat the bacteria and immobilize. The underlying principle relies on the electrostatic interaction that occurs between the bacterium with negative charge and gelatin with positive charge respectively [20, 21] (Fig. 6.2).

The mechanical force applied to the cantilever has an influence over the resolution of the cells subjected to imaging. The vertical forces in the contact mode are in the order of 10–30 nN. This criterion typically does not cause any damage to cells but they are sufficient enough to explore the underlying structures with utmost visibility. The optimum scanning force required for imaging cell membranes and rigid

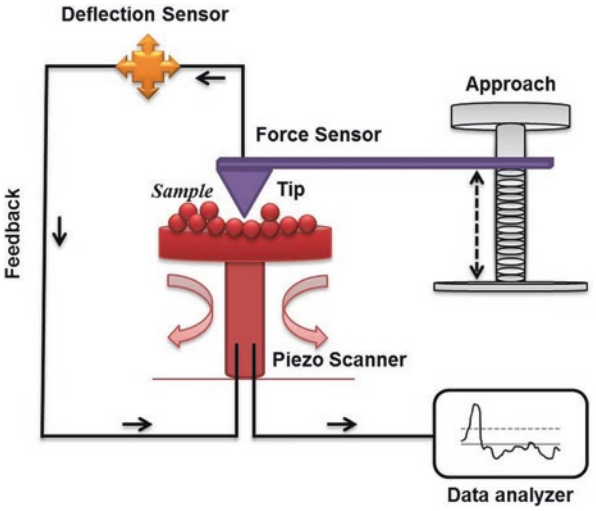

Fig. 6.2 Cantilever/tip assembly and its interaction with a sample. AFM probe interacts by raster scanning motion while scanning the surface of the sample. The up-to-down and side-to-side motion of AFM tip is sensed through a laser beam, reflected from the cantilever. This deflected beam is further tracked down by position-sensitive photo-detector (PSPD) picking up the vertical and lateral motion of the probe. Deflection sensitivity of such detectors is calibrated based on motion corresponding to a unit voltage. The information gathered would be analyzed by Data analyzer and reproduced as image

cytoskeleton was found to be in the range of 2–20 nN. On the other hand, when a force of 100 nN was exerted, a hole is formed by the punching of the tip without any apparent damage to the cell [22]. Secondly, the force responsible for creating a depression was shown to image the nuclei and cellular actin networks. For instance, when Madin–Darby Canine Kidney (MDCK) cells were subjected to AFM analysis, there was an increase in force which further increased the image resolution of the nucleus without rupturing the cell [23].

6.3.1 Bracing and Propping up of Specimen

Biological samples are physically adsorbed and/or covalently bound to a solid support. Such braces play a critical role in retrieving optimal information via AFM imaging. Conversely, samples prepared below par entice vibrational oscillations leading to the formation of poor resolution images. Initially, muscovite mica disks sized 5 mm were integrated with 10 mm Teflon disks by using Araldite glue. Here, the hydrophobic surface of Teflon repels the droplet positioning it onto the surface of mica, thereby preventing the contact with the buffer solution. In order to minimize the vibrational oscillations, key factors such as clean surfaces (for enhancing the gluing of the mica to Teflon disks) and completely sealed surfaces (with no bubbles) under the glued surface were given prime importance during the preparation of samples. Apart from mica, hydrophobic highly oriented pyrolitic graphite (HOPG) or glass with hydrophobic properties has also been used for adsorption.

There are several instances where the biological samples could pose a challenge while adhering to specimen supports—HOPG and glass. For instance, the nuclear envelope of the oocyte of native Xenopus could not be immobilized successfully on mica but could be achieved using 400-mesh carbon-coated copper grids coated with parlodion. By affixing the carbon-coated copper grids to 12 cm diameter plastic Petri dishes using Araldite glue, the nuclear envelope was made open based on charge difference that preferentially eased the adherence toward the grid, with the nuclear envelope facing toward the support. Besides, non-covalent attachment was also performed employing lipid layers. This concept was applied for adhering actin filaments with lipid bilayers attached to mica using Langmuir-Blodgett technique [24].

In the case of bacteria, there are several methods of surface immobilization so as to enable surface scanning, data generation, and evaluation of biophysical properties (Fig. 6.3). To list a few, powered entrapment of bacteria, filter membranes, physical adsorption of bacteria to support based on charge difference and chemical fixation using glutaraldehyde [25] have been successfully demonstrated using *Klebsiella terrigena*. Among them, the most common method employed to fasten bacterial cells to the surface is by imparting positive charge through the surface by the deposition of poly-L-lysine [26]. Furthermore, biofilm forming bacteria produces adhesive exopolymeric substances (exopolysaccharides) capable of adhering to glass coverslips under ambient physiological conditions. There are special appendages present in the bacteria viz. pili or fimbria that augments generation of

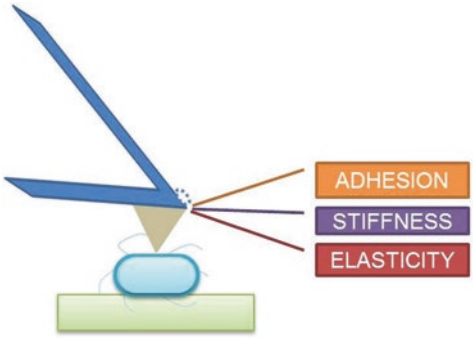

Fig. 6.3 Cell adhesion, stiffness, and elasticity describe the biophysical outcomes of various cellular processes. By exerting force on the cantilever, AFM measures the adhesion, stiffness, and elastic properties of a cell under externally induced deformation

adhesion forces for effective adsorption resulting in high-resolution bio-imaging [27–29].

Moreover, there are some studies that have reported on the exploitation of synthetic fixatives and agar pads to augment adhesion of yeast cells onto the substrate. A common method of immobilization was adopted to entrap yeast cells on a polycarbonate porous membrane or polydimethylsiloxane (PDMS) stamp [30]. Some of them are expensive and also demand physiologically relevant settings for growing and attaching the cells, there is a great possibility of detachment and lateral cell drift that interferes with the AFM imaging. Interestingly, there have been some reverse experiments where the bacterial cells instead of attaching to the substrate, are directly attached to the cantilever relative to their small size. For performing such experiments, the tip is substituted by a spherical probe or detached completely prior to calibration of cantilever. Furthermore, the cells would be attached to the surface and/or cantilever tip to study the eell-to-cell interactions [31].

6.3.2 Adhesion Force

Adhesion of cells to the surface constitutes an important physiological process involving highly regulated interactions for effective imaging. This could be very well demonstrated in mammalian cells where the adhesion is fostered by innumerous cellular processes such as differentiation, tissue development, and inflammation. Besides cell stiffness and elasticity, adhesion remains to be an important parameter computed from the values of the retraction curve. This could be done simply by pulling down and raising the tip from the surface of the cell until probing action is accomplished. In real time, the tip is calibrated on a hard surface in order to determine the spring constant ($k_{\text{cantilever}}$) of the cantilever. It is where the adhesion property culminates in obtaining standard AFM images and force experiments so as to explore the cell-to-cell and cell-to-small molecule interaction. Hence, the adhesive force that exists between the cantilever tip and the cell shows a single inverted peak for a single event and upon scanning might subsequently produce multiple inverted peaks over multiple events. It is this change in force that attributes the strength of the adhesion relative to the interspace existing between the cantilever tip and the surface of the sample [32] (Table 6.3).

Table 6.3 Summary of the adhesion forces between a microbial cell and cantilever

Bacterial culture	Point of attachment	Nature of adhesion	References
Escherichia coli	Surface and cantilever	Variable adhesion force with reported values in the range of <0.1 nN to >9 nN	[27, 33, 34]
Bacillus subtilis	Surface	Mean adhesion force (MAF) of 1 ± 0.6 nN at the interface of bacterial cell and silicon nitride tip	[34]
Pseudomonas aeruginosa	Surface and cantilever	MAF was found in the range of 0.2 nN (pili) and 1 nN (whole cell)	[35]
Pseudomonas fluorescens	Surface	MAF of ~0.5 nN with slight variation between wild type and mutants	[36]
Staphylococcus aureus	Surface and cantilever	MAF at the cell and von Willebrand factor corresponds to ~2 nN irrespective of the position of the cell and cantilever	[37, 38]
Staphylococcus epidermidis	Surface and cantilever	MAF corresponds to ~2 nN between the cell and fibrinogen irrespective of the position of cell and cantilever	[39]
Pseudomonas putida	Surface	MAF of 0.7 ± 0.3 nN at the cell and cantilever interface	[27]
Micrococcus luteus	Surface	MAF of 1 ± 0.6 nN existing between the cell and cantilever	[27]
Listeria monocytogenes	Surface	MAF in the range of 0.10–0.22 nN	[40]
Sulfobacillus thermosulfidoxidans	Surface	For planktonic cells and biofilm, the adhesion force corresponds to ~0.15 nN and ~0.5 nN respectively	[41]

It is clearly evident from Table 6.3 that AFM has been casted to demonstrate the differences in adhesion force amid clinical and wild-type strains in which wild-type strain showcased greater adhesion toward the tip with different behavior. Although lipopolysaccharides (LPS) and EPS have been found associated with bacterial (*P. aeruginosa*) adhesion, those belonging to wild type showed increased adhesion toward the surface, whereas their relatively mutant counterpart (with an altered LPS structure and charge) showed diminished adhesion. It is concluded that even though strains presented similar adhesion forces, their adhesion events differed significantly. However, the adhesion events ensued over short interspaces in the mutant strain, whereas, the same pattern was observed at long interspaces in the wild-type strains. This provided direct evidence to the involvement of an adhesin *LapA* protein, located on the surface of the cell [36].

Similarly, the molecular mechanisms involved in the adhesion of bacterial cells were studied using a Gram-positive strain, *Streptococcus mutans* (*S. mutans*). It is a caries causing bacterium responsible for increasing the risk of endocarditis once it enters the bloodstream (bacteremia). Bacterial adhesion is facilitated by a surface protein, P1 which under refined conditions showed weak adhesion toward salivary agglutinin, the key binding partner. But when the same was attached to the

cantilever tip, a strong adhesion could be observed which may be due to the cumulative binding effect of several P1 proteins. It was inferred that diverse parts of P1 protein tethered to cantilever tip did not form ordered domains, but formed high order P1-derived polypeptides interacting with other P1 cell surface proteins [42].

Besides interpreting data from retraction curves, the interaction among definite molecules within the microbial surface was studied by affixing the desired molecule to the tip. For instance, lectin and concanavalin A obtained from *P. aeruginosa* were fastened to the tip to dictate the conformation, distribution, and adhesion patterns of individual polysaccharides present on the cell surface of *Lactobacillus rhamnosus* GG (a probiotic) using force-distance mapping. This approach enabled to clearly differentiate the polysaccharide complement present on the wild type from the adhesion-deficient mutant [43]. Interestingly, by knowing the surface components of a bacterium, Strauss et al. have functionalized the tip using the antimicrobial peptide cecropin P1 (CP1) to explore the binding pattern. From earlier studies, it was deciphered that the length of the LPS had some influence over the robustness in the binding pattern. Longer the LPS, stronger was the adhesion efficiency and vice versa. Secondly, they also showed that the bactericidal action of the AMP (CP1) was not due to the binding strength but entirely relied upon the degree of attachment toward the substrate [44].

The functionalized cantilevers of AFM have been recruited to explore the cell surface properties of yeasts. By analyzing the surface hydrophobicity and macromolecular interactions, fluctuations if any may attribute to the thickness of the membrane. In a similar fashion, tips functionalized using concanavalin A lectins were employed to study and gauge the positional and adhesion properties of mannan oligosaccharides present on the surface of two Saccharomyces strains, namely, *S. cerevisiae* and *S. carlsbergensis*. The extension and elastic properties of the surface mannoproteins of *S. cerevisiae* were found to be comparatively better than that of *S. carlsbergensis* albeit their similar cell wall compositions [45].

6.3.3 Elasticity

Elasticity remains one of the factors that determine the mechanical properties of the cell in understanding the surface properties of microorganisms using AFM. It is not only used to image the topography of the cell at high resolution but also to measure the elastic properties using nano-indentation technique. The force curves obtained were recorded and converted into force versus indentation curves using appropriate methods. Further, these curves were analyzed with various theoretical models (Hertz model—to calculate Young's modulus; Alexander and de Gennes (AdG) model—to define the polymeric surface behavior) to provide quantitative information on the elasticity (Young's modulus).

The nano-indentation method facilitates computation of mechanical properties of mammalian cells that include glial cells, platelets, cardiomyocytes, epithelial cells, endothelial cells, and osteoblasts [46]. For instance, AFM has been employed to measure the elasticity of sheaths of the archeon *Methonospirillum hungatei* GP1

using depression technique (complementary to the indentation method). In accordance, the elastic modulus of 20–40 GPa withstanding an internal pressure of 400 atm have been reported. Similarly, the elastic modulus for the isolated murein sacculi of Gram-negative strain was found to be 25 MPa that typically correlated with the elasticity of the peptidoglycan layer. Furthermore, the nano-indentation method was applied to determine the wall compressibility of *Magnetospirillum gryphiswaldense* whole cell as 42 mN m^{-1} and turgor pressure in the range 85–150 kPa [46].

Force experiments were conducted to determine the elasticity and stiffness of the cell from the approach or extension curve. When the AFM tip makes an initial contact with the cell surface, some long-range interaction forces occur between the cantilever tip and live cell. This forms a flat line attributing the first regime of the extension curve. But, even before the tip makes any contact with the surface of the cell, forces such as electrostatic and van der Waals, combine with forces associated with the physical interaction generating a non-linear change (nonlinear compression) attributing the second regime of the extension curve. This regime projects the switch in force relative to variation in distance thereby reflecting the elastic property of the cell wall [27, 47].

Supposing the microbes are aired to extrinsic environmental conditions, pertinent changes associated with the cell wall (either damage or loss in cell wall structure) elasticity are very well deciphered using AFM. For instance, Volle et al. [27] have evidenced the changes associated with cell wall elasticity, while *Bdellovibrio bacteriovorus* preyed on *E. coli* biofilm. Typical cell wall architecture of a biofilm-forming bacterium is that its cell wall consists of an outer membrane, a thin peptidoglycan layer, and an inner plasma membrane. When *Bdellovibrio* sp. predates *E. coli* by secreting various enzymes, there is a considerable modification and destabilization of the cell wall. Furthermore, there had been a significant increase in both the force and the distance of the non-linear regime that measures the biochemistry and biophysical changes associated with the prey cell. On the other hand, treatment with nanoparticles of size <5 nm could bring about modifications and thus destabilize the cell wallowing to their small size; whereas nanoparticles of size ≤100 nm did not show any deleterious effect on the cell wall [48] as evident from AFM analysis. Some of the Young's Modulus measurements of Gram-positive and -negative bacteria (E_{cell}) have been enlisted in Table 6.4.

Furthermore, Young's modulus measurement for different types of mammalian cells has also been reported based on the elastic property. Imaging has been done by AFM probing of appropriate objects, i.e., erythrocytes either in free form or in buffer under physiological conditions. The pre-imaging procedures viz. drying, freezing, and fixing up of the cells using chemical agents were also found to improve the AFM images and indentation results. But the possibility of bringing about changes in cell structure, viability, and elasticity during fixation may interfere with the resolution of the images probed by AFM. For instance, Young's modulus of erythrocytes treated with 5% formalin increased (119.5 ± 15 kPa) by 10-folds on a par with the untreated ones (16.05 ± 2.3 kPa) [59]. Some of the Young's Modulus measurements of mammalian cells have been tabulated (Table 6.5).

Table 6.4 Young's Modulus measurement of Gram positive and Gram negative strains using AFM

Bacteria	Strain	Conditions	*E* (MPa)	References
Shewanella putrefaciens	CN32	pH 4; force spec mode	0.21	[49]
		pH 10; force spec mode	0.04	
		Force vol mode	69–98	[50]
Escherichia coli	NCTC 9001	Whole cells	221	[51]
E. coli	ATCC 9637	Whole cells	2.6	[52]
Staphylococcus aureus	ATCC 25923	Whole cells	0.57	[52]
Bacillus casei	–	Whole cells	769	[53]
E. coli	BE100	Whole cells	32	[54]
B. subtilis	–	Whole cells	50	[54]
Streptococcus agalactiae		Whole cells	7.9	[55]
Rhodococcus wratislaviensis	–	Whole cells	20±3–105±5	[56]
Pseudomonas aeruginosa	–	Whole cells	0.05–0.025	[57]
S. aureus	–	Whole cells	0.05	[58]

Table 6.5 clearly elucidates the measurement of Young's modulus for a wide variety of mammalian cells (normal cells, neurons, and cardiac cells) that range from few kPa to a few hundred kPa. This difference in Young's modulus has been due to the influence of cytoskeletal constituents such as F-actin, microtubules, and binding proteins capable of forming cellular cortex and is also believed to contribute the most of the Young's modulus of cells. The differences observed within the cortex among different cell types determine the Young's modulus pertaining to the mechanical properties of actin networks [70].

AFM applications have been extended to determine the viscoelastic property of mammalian cancer cells. In accordance, while comparing the mechanical properties of metastatic cells PC3 with non-tumoral WPMY-1 prostate cells, the viscoelastic property and stiffness of PC3 were found to decrease augmenting for higher deformation capacities on a par with the WPMY-1 cells [71]. Interestingly, AFM has also been used to evaluate the changes associated with cellular elasticity, morphometric alterations, and metastasization process which were quantified by Young' modulus parameter. The inhibitory effect of Rho-associated coiled-coil containing protein kinase (ROCK, Y-27632) on breast cancer epithelial cells was also evaluated using AFM where the inhibitor significantly increased the cell rigidity thereby preventing the metastasis and migration of cell [72].

6.3.4 Stiffness

Stiffness of the cell and its measurement elaborate the total health status of the cell. For instance, a healthy microbial cell exhibits typical cell stiffness by maintaining a constant turgor pressure. This constitutes the third regimen in the approach curve, where, two springs push each other. By measuring the slope, the spring constant

Table 6.5 A summary on Young's modulus measurement of mammalian cells using AFM

Mammalian cells	*E* (kPa)	Indentation (nm)	Model	References
Rat liver endothelial cell	2	–	Hertz model	[60]
Cardiac cells	90–110	80	Sneddon model	[61]
Endothelial cells (HUVEC)	10–11	–	Hertz model	[62]
Erythrocytes	19–33	–	Hertz model	[63]
Human mesenchymal stem cells (hMSCs)/chondriocytes/osteoblasts	33/39/52	–	Hertz model	[64]
Ovarian cancer cell line (high/low)	0.494/0.884	1000	Hertz model	[65]
Human melanoma cell line	0.421	500–1000	Hertz model	[66]
Human colon cancer cell line	0.479	1400	Sneddon model	[67]
Benign/aggressive prostate tumors	3.03/1.72	500	Sneddon model	[68]
Human cervix cell line End1/E6E7	5.5	<150	Sneddon model	[69]
HeLa cells	2.48	<150	Sneddon model	[69]

pertaining to cell stiffness could be determined. Alongside, the spring constant also reflects the turgor pressure of the cell which in turn depends on the imaging buffer and its ionic strength. Obviously, any change in the environmental pH also affects the cellular stiffness which ultimately alters the turgor pressure [73]. This interaction is modelled as compression of two springs and given in the form of equation [74]:

$$\frac{1}{k_{\text{effective}}} = \frac{1}{k_{\text{cell}}} + \frac{1}{k_{\text{cantilever}}} \tag{6.1}$$

where k_{cell} and $k_{\text{cantilever}}$ represent the spring constant of the cell and cantilever, respectively; $k_{\text{effective}}$ represents the slope of the linear compression which is calculated from the spring constants, k_{cell} and $k_{\text{cantilever}}$.

On the other hand, when the microbes are exposed to any hazardous chemicals or inhibitory substances like antibiotics, cell membranes would be the prime target where there would be a drastic change in the turgor pressure thus making the cells deficient to regulate osmosis. For instance, when bacteria are exposed to the antimicrobial peptide magainin (MAG2), there would be a rapid permeability of AMP across the membrane to form pores leading to the paralysis of the cell. This was demonstrated using *E. coli*, which when treated with MAG2, the cell suffered time-sensitive reduction in cell stiffness. Alongside, with the formation and stabilization

of pores on the outer surface of cell membranes, the turgor pressure could no longer be maintained and tended to collapse attributing to decline in cell rigidity by 50%.

More interestingly, the effects of single-walled carbon nanotubes (SWCNTs) forming networks across the membrane in bringing about a steady decrease in cell stiffness have also been reported [47, 75]. It was proposed that the SWCNTs executed cell penetration, membrane disruption, and leakage of cell contents. In order to mimic SWCNT piercing single cell, a sharpened AFM tip was used. Prior to cell penetration, there was no significant decrease in single-cell stiffness but allowed them to conclude that the network formation has contributed to an overall decrease in turgor pressure. There is yet another case where the changes/decrease in cell stiffness could also be a positive factor. This was evidenced in a cyanobacterium, *Anabaenopsis circularis* whose characteristic gliding movement changes frequently due to the gliding speed in turn changing the cell stiffness (mimicking ill health of a cell) attributing for a positive health sign.

Nanoparticles have been found to play a pivotal role in influencing the turgor pressure of a bacterial cell upon interaction. For instance, a bacterium (*E. coli*) exposed to hematite nanoparticles showed a 20-times increase in spring constant over untreated ones. But it is still unclear whether the alterations in cell stiffness were associated with fluctuations in turgor pressure or by the interaction of the nanoparticles surrounding the cell [76]. Furthermore, antibiotic treatment could bring about a steady increase in turgor pressure and tend to decrease over a period of time with values similar to that of the untreated ones. This could be one of the strategies adopted by the bacterium to surpass the antibiotic action by increasing the turgor pressure which in turn increases the stiffness of the cell [77, 78].

Stiffness of the mammalian cells has been determined by following various procedures and parameters [75, 79]. But the differences in settings, application of theoretical models and the selection of cantilevers influence the Young's modulus leading to diversity in Young's modulus of the same cells characterized under different environmental conditions. There are several models proposed based on settings, cantilevers, and detection procedures. Theoretical models such as Hertz model, the Chen model, and Tu model have been used to determine the Young's modulus under similar settings.

Among various models, Hertz model constitutes one of the popular models applicable to samples with diversified properties such as homogenous, isotropic, linear elastic material properties, infinite thickness, and smooth surface. This model helps to conquer the inherent features of the cell meticulously at its center under controlled experimental procedures. On the other hand for characterizing or imaging thin samples such as lamellipodia area, Chen and Tu models are used. Additionally, they are employed to probe well- and non-adhered regions that constitute the peripheral regions of a cell [80, 81].

Cell stiffness constitutes one of the important parameters and biomarkers in optimizing the strategies for the personalized treatment of cancer. Xu et al. [65] have conducted various studies on epithelial cancer cells from which they interpreted that ovarian cancer cells exhibit softer and lower intrinsic variability in cell stiffness rather than the non-ovarian cancerous cells. Furthermore, the ovarian cancer cells

(HEY A8) typically demonstrated deformation owing to the loss of cell stiffness serving as a biomarker for progressing metastatic cancer, which the parental cells (HEY) failed to convey. This approach could perhaps help detect the biomarkers associated with cell stiffness and to evaluate the relative metastatic potential of other cancer cell types.

6.4 Applications of AFM

6.4.1 Virus Imaging

Virus is defined as a submicroscopic infectious agent that resides and replicates inside the living host cells (intracellular parasite) for its survival. They are capable of infecting all life forms from plants, animals, and human beings. It is indeed quintessential to understand the molecular mechanisms involved in the viral infection to devise methods and therapeutic strategies to encounter emerging viral infections. In order to realize the pathophysiology of viral infection, a deeper knowledge of viruses is the need of the hour for which direct visualization of virus particles is required. As for the size of the virus particles, their visualization using electron microscopy is much preferred. Using AFM, the morphology of tobacco mosaic virus (TMV), other large plant viruses, Moloney murine leukemia virus and HIV virus on the cell surface have been imaged in their crystalline form [82, 83]. Similarly, single virions of herpes, vaccinia, and mimivirus have also been captured using AFM probing [84, 85].

One of the characteristic features of AFM in imaging virus is to bring out the overall architecture differentiating them from one another allowing for rapid identification and classification. It is therefore a useful tool in deducing a type of virus present in a population with general level of contamination such as cellular material, degraded virions, and macromolecular impurities. Secondly, the quantitative properties of a virus could be well furnished using AFM imaging. For instance, AFM could provide measures of viruses present in hydrated and dried states; ultimate details about the degree of shrinkage. But there exist some limitations in measuring the linear variations—the finite tip size and tip-to-tip variation in the radius of curvature. However, AFM height measurements are much simpler and safer while imaging non-crystalline or paracrystalline array of viruses with varied morphological features viz. helical, rod-shaped, and spherical viruses. For viruses with spherical and cylindrical symmetry, the height measurements of AFM would be accurate pertaining to their diameters whereas their individual measurements would usually be accompanied by modest error of the order of 5% or less. It is by repeating the AFM measurements in a particular field and at different scan directions, good statistics could be obtained facilitating compilation of histograms of various size distributions (to a precision of angstroms).

For instance, if the distribution belongs to Gaussian distribution, it is presumed that for the particles bestowed with general morphology or icosahedra having only one triangulation number, this approach would be applied to differentiate variation

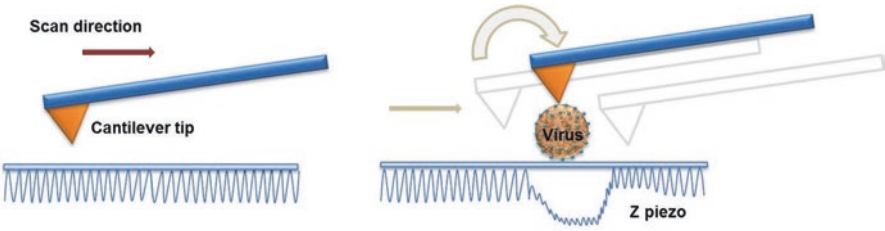

Fig. 6.4 Typical architecture of a virion probed using Atomic Force Microscope. The schematics represent the jumping mode imaging and z-piezo actuation along the scan line

in their diameters to some degree about the mean owing to the physiological state or degree of maturation. Furthermore, this approach has been successfully applied to Moloney murine leukemia virus (MuLV). On the other hand, if there exists a more complex distribution with multiple peaks and shoulders, it could be inferred that particles of different classes might be present with triangulation numbers 3, 4, and 7 [86–88] (Fig. 6.4).

AFM has also been used to study the underlying mechanisms involved in interactions between viral capsid and genome, morphological changes associated with virion maturation, capsid stabilization, and uncoating. It is by the nano-indentation method, the mechanical properties of individual molecules and particles at nanoscale level had been investigated. Furthermore, virus particles are studied by recording an image using AFM cantilever while scanning over the viral surface. Secondly, the cantilever is destined toward the virus core. Thirdly, an indentation is made by the cantilever on a single virus particle and the response is recorded as force–distance curve [89, 90]. This force–indentation curve curtails approximate linearity facilitating easy quantification of stiffness vide spring constant based on Young's modulus (Elastic theory):

$$k = \alpha \left(Eh^2 / R \right) \tag{6.2}$$

where k represents the spring constant of the virus particle; R, the radius and h, shell thickness; α attributes for proportionality factor and E, Young's modulus. The value of k would be derived from force–indentation curve and mean value of R and h would be realized from the virus PDB structure. The constant α which has an approximate value of 1 could be omitted [91].

As for the homogeneity of surface properties with constant radius and cell thickness, it can be approximated to an ideal capsid. On the other hand, heterogeneity of viral shell showcases the realistic description and challenge in deciphering the actual structure. This involves the use of more elaborate approaches such as computational methods, molecular dynamic simulation studies along with analyzing normal mode, elastic network, and finite element modelling. Yet another important parameter that characterizes the material properties of a virus is its breaking force (the maximum force the virus resists before its deformation), which allows real-time quantification of the virus resistance to mechanical forces [92, 93]. The mechanical properties in the AFM probing over capsid maturation have also been

documented. The maturation of capsid is a process associated with sequence of conformational changes formed over the viral capsid during virion formation while infecting the host cell. The maturation mechanism has been demonstrated using the Bacteriophage HK97 model which is capable of self-assembling into immature prohead I structure in which the gp5 capsid protein includes the Δ-domain. This Δ-domain unlike other viruses would be cleaved off by the protease activity leading to the formation of strong threefold interactions among the hexamers. During AFM nano-indentation, a major transition from prohead II to a more rigid particle is accompanied by an increase in the spring constant value from 0.018 Nm^{-1} to 0.12 Nm^{-1}. Furthermore, expansion and covalent cross-linking have been well demonstrated using AFM during the formation of Head II particle in three different ways such as increase in the Young's modulus to 1 GPa from 0.3 GPa, increase in the breaking force to 0.9 nN from 0.56 nN and resistance [94, 95].

In another AFM nano-indentation experiment, the mechanical changes of λ phage associated with self-assembly and genome packaging were investigated. The study revealed the occurrence of major capsid reinforcement when gpD was added, with stiffness increased from 0.12 Nm^{-1} for the procapsid to 0.2 Nm^{-1} for the gpD decorated capsids with breaking force significantly increased to 0.88 nN from 0.48 nN [96].

6.4.2 Imaging Bacteria

To image bacteria, there is a new approach in AFM viz. peak-force-tapping (PFT) mode capable of providing topographical information and mapping nanomechanical properties such as elasticity, adhesion, modulus, and deformations. This approach on par with the conventional AFM imaging, works with a very low force thus reducing lateral force and mechanical damage to the sensitive biological samples. By this technique, a chemical-specific hydrophobic CH_3 modified AFM probe has been designed to test hydrophilic domains of SiO_2 surrounded by hydrophobic layer of dimethylmethylsilane. Such modifications have captured the images with better resolution (512 × 512 pixels) and at a faster scanning (8 min) rate. This has been applied to scan the spores of *Aspergillus fumigatus* immobilized onto a polycarbonate membrane. The results obtained showed a strong adhesion force of 4723 ± 586 pN for the hydrophobic patches with 0–1000 pN for the neighboring hydrophilic areas [97].

Furthermore, nano-indentation studies were conducted to establish a correlation between the nanomechanical properties and bacterial aggregation. Such nanomechanical-based indentation studies have helped to understand the effect of various antimicrobials (ticarcillin and tobramycin) or novel antibiotics and antimycobacterial (ethambutol and isoniazid) drugs on *Pseudomonas aeruginosa*, *Acinetobacter baumannii*, and their respective biofilms [98–100]. Leradi et al. [101] have demonstrated a different approach in detecting the bacteria resistant to antibiotics in a short span of time. The morphological alterations evidenced in an antibiotic-sensitive *Klebsiella pneumoniae* exposed to different antibiotics have

been reported. But no significant morphological disturbances were seen in antibiotic-resistant strains. Similarly, the antibacterial action of Sushi peptides on Gram-negative bacteria such as *Pseudomonas aeruginosa* and their mechanisms of action have been imaged using AFM. Three different stages of their action viz. damage to the outer membrane, permeabilization through the inner membrane and disintegration of both membranes via "carpet-model" have been well documented at the nanometer scale [102].

In a similar fashion, Mularski et al. [103] have revealed time-resolved AFM images of antimicrobial peptide caerin 1.1 interacting with *K. pneumoniae* cells. From the experiment, they could decipher the localized defects caused by the AMP leading to the formation of pores on the cell membrane. This mechanism was compared by visualizing them using a scanning electron microscope which corroborated with the AFM images. When the concentration of AMP was increased threefold, pores appeared apparently on the outer membrane when visualized from AFM images.

Besides antibiotic treatment, the deleterious effect induced by silver nanoparticles (AgNPs) to the antibiotic-resistant strains has been imaged using AFM. A comparative study on the antibacterial mechanism induced by AgNPs on Gram-positive *S. aureus* and Gram-negative *K. pneumoniae* has been demonstrated by the morphological and topographical differences. Control cells showed typical spheroid and rod shape morphology whereas those treated with AgNPs showed depressions or grooves in the form of "pits" accompanied by increased surface roughness and cell shrinkage (28% and 41%) have been well elucidated [104] (Fig. 6.5).

AFM is now gaining importance in the field of medical diagnostics for the rapid detection of antibiotic-resistant bacteria by recruiting nanomechanical sensors [105], one of the alternatives to conventional microbiological techniques. It is based on the cantilever fluctuations induced by the viable and dead strains of *S. aureus* and *E. coli*, the sensitivity is determined. There was a rapid reduction in fluctuations to antibiotic-treated (antibiotic resistant) strains of *E. coli* wherein the fluctuations were relatively large in the living population. Interestingly, the antibacterial effect induced by fosfomycin on methicillin-resistant *Staphylococcus pseudintermedius* was clearly explained from the height images of AFM associated with cellular dimensions. The increased surface roughness with substantial topographical changes such as shrinkage and cell membrane damage emphasized the antibacterial mechanism on a par with smooth surfaced control cells at nanoscale dimension [106].

6.4.3 Cancer Diagnosis

One of the major criticalities faced by the modern world associated with lack of cellular adaptation is cancer and whose early diagnosis poses a challenge for successful treatment. It is only at a later stage that cancerous cells are detected owing to their difficulty in visualizing very small tumors of size <1 mm^3 and identifying biomarkers with utmost specificity and sensitivity [107, 108]. It was reported from

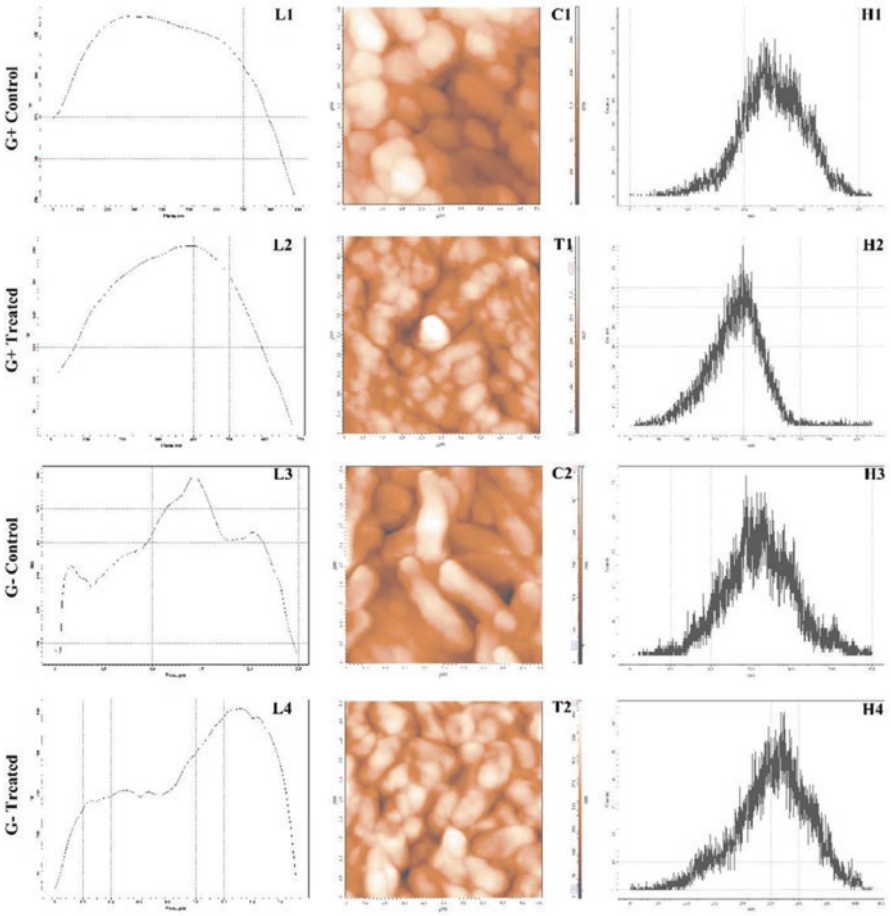

Fig. 6.5 The morphological and topographical difference between the control and AgNPs treated cells at nanoscale has been clearly demonstrated using AFM. (C1) Gram-positive bacteria control (T1) Gram-positive bacteria with morphological disturbances exposed to AgNPs (C2) Gram-negative control bacteria and (T2) Gram-negative bacteria treated with AgNPs. Treated cells exhibited increased surface roughness and cell shrinkage owing to membrane damage induced by AgNPs resulting in *pit* formation. Respective line profiles (L1 – L4) and histogram analyses (H1 – H4) have been illustrated. Modified figure from [104]

various studies that the cancer cells exhibit less stiffness than normal cells (Fig. 6.6). In this scenario, Cross et al. [109] have proposed a nanomechanical approach to detect cancerous cells. With the development of AFM, detection of cancer at single-cell level by exploring the mechanical properties in combination with routine morphological and histopathological analysis could typically differentiate them from normal cells with utmost certainty. In order to determine the cell population for obtaining statistically meaningful data, stiffness variations in a single cell and in a population should be taken into account. Further, applying the same to the

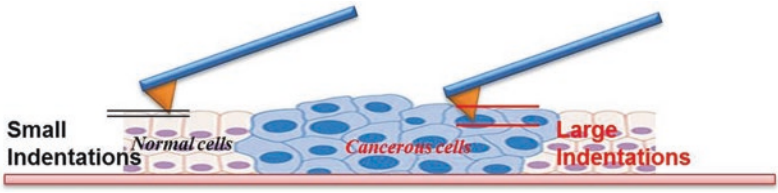

Fig. 6.6 AFM imaging of the cancerous cells and normal cells and their corresponding indentations experienced by the cantilever tips

heterogeneous population with multiple indentations at different locations on each cell would be appropriate to calculate Young's modulus [110].

Moreover, consecutive probing of the cantilever tip over the cell surface during the measurements could influence the elastic properties with respect to time and this aspect demands further investigation. In this line, AFM measurements under static conditions might not be as sensitive a method as interference method in the detection of rapid and dynamic changes occurring in the cytoskeleton of the cell. But cytoskeleton remodelling might have a significant influence for which it needs to be probed to the next location. This is accomplished by continuous monitoring of changes in the Young's modulus during measurements with respect to time [111]. There are studies that showed the possibility of differentiating normal cells from cancer cells, original cancer cells from metastatic cancer cells based on the hardness and mechanical properties (Young's modulus, stiffness, and adhesion) using AFM. However, the relationship between invasion and metastasis of tumor cells within the microenvironment was well explored using AFM. By monitoring the extracellular matrix (ECM) microenvironment, leads pertaining to disease-induced tissue stiffness alterations were also reported [112]. For instance, when a regular liver tissue is challenged microscopically with liver fibrosis tissue and cirrhosis tissue using AFM, significant differences in their hardness could be evidenced. Upon comparison, liver cirrhosis tissues showed not much difference in hardness with hepatocellular carcinoma tissue suggesting an increase in hardness which might be due to the progression of cancer prior to cirrhosis. This was found contrary to some of the reports disproving the fact that cancerous cells need not be softer than the normal cells and can be more rigid than the normal cells during the process of carcinogenesis [113, 114].

6.5 AFM in Combination with Other Technologies

Cancer poses a great challenge for any technology to differentiate primary tumor cells from metastatic tumor cells with enhanced criticality in the diagnosis and treatment. Indeed, primary and metastatic cancer cells exhibit diverse genetic maps providing a major cue in the clinical diagnosis. It is well known that Raman spectroscopy could successfully differentiate cancer cells from healthy cells, metastatic cancer cells from primitive cells, and cancerous tissues from healthy ones [115,

116]. One of the prominent characteristics of Raman spectroscopy is that it gives a clear picture about chemical composition of a material but impossible for AFM. When AFM is combined with Raman spectroscopy, the substance present on the cell surface along with the chemical constituents that make up the substance could also be deciphered [117].

Confocal laser scanning microscopy involves high-resolution optical imaging with in-depth selectivity pertaining to optical sectioning and construction of 3D structures from the obtained images. AFM when merged with a confocal laser scanning microscope (CLSM), the mechanobiological properties of individual cancer cells would be deciphered. Furthermore, their combination correlates to notch points that ease subsequent imaging of subcellular components. This would help monitor the disease progression as the cancer development at an early stage showcases an appreciable change in the mechanical properties and morphology. This change in elasticity as detected from AFM would be correlated with the cancer in its early transformation process. For instance, a multifunctional protein α-enolase (ENO1) is not only involved in the glycolysis pathway but also serves as a receptor for fibrinogen in cancer progression. The combined use of AFM and CLSM had exposed the gene silencing of ENO1 followed by transformation of pancreatic cancer cells into coarser ones. This causes damage to the adhesion force existing between cancerous cells and stroma, leading to invasion and metastasis in pancreas [118, 119].

Furthermore, the joint use of AFM and Data mining techniques helped to categorize brain tumors at 94.74% efficiency and accuracy in classification. This combinatorial approach could differentiate type II from types III and IV tumors. Alongside patients with stage II tumors could also be diagnosed at an early stage thereby preventing the risk of cancer metastasis [120]. In addition, AFM imaging combined with mechanical measurement has been on rise in the biomedical field to determine the cell structure and functional aspects at single-cell level. Eventually, this approach might help differentiate the cancer cell from the normal cell providing lead for visual drug research. This developing trend might help surpass the shortcomings of either technique used in combination showcasing the expanding applications of AFM.

6.6 Conclusion and Future Prospects

AFM remains one of the successful imaging techniques since its development having a significant role in imaging biological materials and in understanding the mechanical properties of a wide array of cells. Their progress from initial imaging modes (contact, non-contact, and tapping) and force-driven mechanical computation modes to rapid and multispectral mechanical quantification modes (peak force mode) qualify AFM as an extremely important tool in exploring the physicochemical and mechanobiological properties of the cell. Conversely, the HS-AFM (High-speed atomic force microscopy) allows visualization of the conformational changes of proteins in real time. For instance, the mechanism of proton pumps, protein–DNA interactions, protein–ligand interactions, diffusion, and assembly of the

membrane and scaffold. Interestingly, the flexibility of biomolecules in attaining the best shape for improved binding to the target (antibody interaction with the antigen) could very well be appreciated. Moreover, the ultrashort HS-AFM cantilevers enable exploration of fast protein dynamics, theoretical predictions, and molecular dynamics simulation studies within microseconds with the help of high-speed force spectroscopy (HS-FS). Although, the development and application of HS-AFM are at their infancy, its contribution to the physical phenomena occurring in the biological systems is yet to be unravelled.

Besides hunting for impaired tissues, AFM has been realized to study the mechanistic aspect of cells as novel and a potential diagnostic biomarker for detection of infectious diseases and to understand the disease progression. There are several challenges that need to be addressed before AFM technology could be realized for a wide variety of biological applications.

The first and foremost challenge in AFM measurement of cells is its manual operation, where, the probes are manually controlled to target cells by setting the parameters to acquire cell force curves and to process the data. Going manually in turn reduces the experimental efficacy taking several minutes to image/to obtain measurement of the cell. However, to retrieve prognostic information, more cells need to be probed/enumerated making the operation laborious and cumbersome thereby limiting the application of AFM at a single-cell level. This demands an improvement in the level of operation from manual to automation that facilitates AFM probing at maximum efficiency.

Secondly, variation in the response time of a cell to the external environment and AFM's mechanical mapping time. The response time was determined to be ~1 ms, significantly less than the mechanical mapping of ~10 min. Due to the variation in time, the mechanical properties of the cell in real time and their monitoring are made difficult. With the advent of HS-AFM, this time gap has been significantly reduced with imaging times less than 100 ms and is applicable to image rigid, flat, and small-sized samples for obtaining real-time images of cells. Further, they are also used to image mammalian cells with approximately 5 s in response to external stimuli.

One of the most important factors that determine the efficiency of AFM measurements is the standardization. For instance, the mechanical properties of the cell is determined by Young's modulus which ultimately depends on several parameters such as experimental conditions, instrumental parameters, cell state, and data analysis. Furthermore, the results obtained can only be compared under similar experimental conditions. On the other hand for biomedical applications, multiple clinical cases are required to authenticate the reliability while gauging the mechanical property. So, the need for sample preparation and standardization of AFM with relative values pertaining to cancer and normal cells remains a mandate. There are several reports highlighting direct measurement of mechanical properties of a localized cancer tissue encompassing cancerous cells, normal cells, blood vessels, etc. but the criticality relies on the detection of individual cancer cells and their mechanical properties. So, the tumor tissues present at different locations may exhibit different mechanical properties, which need to be extracted for comparative evaluation. More

interestingly, AFM in combination with other complementary techniques shows a ray of hope in countenancing AFM to resolve unanswered queries in life sciences in near future.

Acknowledgments The author would like to thank the contributors and their articles which served as a base for preparing this manuscript. The timely support rendered by the Saveetha Institute of Medical and Technical Sciences is greatly acknowledged.

References

1. Hoffman BD, Grashoff C, Schwartz MA (2011) Dynamic molecular processes mediate cellular mechanotransduction. Nature 475(7356):316–323. https://doi.org/10.1038/nature10316
2. Howard J, Grill SW, Bois JS (2011) Turing's next steps: the mechanochemical basis of morphogenesis. Nat Rev Mol Cell Biol 12:392–398. https://doi.org/10.1038/nrm3120
3. Morita S, Giessibl FJ, Meyer E, Wiesendanger R (eds) (2015) Non-contact atomic force microscopy: volume 3. Springer
4. Leckband D (2000) Measuring the forces that control protein interactions. Annu Rev Biophys Biomolecular Struct 29:126. https://doi.org/10.1146/annurev.biophys.29.1.1
5. Lee GU, Chrisey LA, Colton RJ (1994) Direct measurement of the forces between complementary strands of DNA. Science 266:771–773. https://doi.org/10.1126/science.7973628
6. Luckham PF, Smith K (1999) Direct measurement of recognition forces between proteins and membrane receptors. Faraday Discuss 111:307–320. https://doi.org/10.1039/a807048b
7. Muller DJ, Engel A (1997) The height of biomolecules measured with the atomic force microscope depends on electrostatic interactions. Biophys J 73:1633–1644. https://doi.org/10.1016/S0006-3495(97)78195-5
8. Shih HJ, Shih PJ (2015) Tip effect of the tapping mode of atomic force microscope in viscous fluid environments. Sensors (Basel) 15(8):18381–18401. https://doi.org/10.3390/s150818381
9. Piontek MC, Roos WH (2018) Atomic force microscopy: an introduction. In: Peterman E (ed) Single molecule analysis. Methods in molecular biology. Humana Press, New York, 1665. https://doi.org/10.1007/978-1-4939-7271-5_13
10. Young R, Ward J, Scire F (1972) The Topografiner: an instrument for measuring surface microtopography. Rev Sci Instrum 43(7):999. https://doi.org/10.1063/1.1685846
11. Binnig G, Rohrer H, Gerber C, Weibel E (1982) Tunnelling through a controllable vacuum gap. Appl Phys Lett 40(2):178. https://doi.org/10.1063/1.92999
12. Binnig G, Quate CF, Gerber C (1986) Atomic force microscope. Phys Rev Lett 56:930. https://doi.org/10.1103/PhysRevLett.56.930
13. Feenstra RM, Stroscio JA, Tersoff J, Fein AP (1987) Atom-selective imaging of the GaAs(110) surface. Phys Rev Lett 58:1192. https://doi.org/10.1103/PhysRevLett.58.1192
14. Meyer G, Amer NM (1988) Novel optical approach to atomic force microscopy. Appl Phys Lett 53:2400. https://doi.org/10.1063/1.100425
15. Eigler D, Schweizer E (1990) Positioning single atoms with a scanning tunnelling microscope. Nature 344:524–526. https://doi.org/10.1038/344524a0
16. Zhong Q, Inniss D, Kjoller K, Elings VB (1993) Fractured polymer / silica fiber surface studied by tapping mode atomic force microscopy. Surf Sci Lett 290(1):L688–L692. https://doi.org/10.1016/0167-2584(93)90906-Y
17. Giessibl FJ (1995) Atomic resolution of the silicon (111)-(7×7) surface by atomic force microscopy. Science 267(5194):68–71. https://doi.org/10.1126/science.267.5194.68
18. Stipe BC, Rezaei MA, Ho W (1998) Single-molecule vibrational spectroscopy and microscopy. Science 280(5370):1732–1735. https://doi.org/10.1126/science.280.5370.1732

19. Stipe BC, Rezaei MA, Ho W (1999) A variable-temperature scanning tunnelling microscope capable of single-molecule vibrational spectroscopy. Rev Sci Instrum 70(137). https://doi.org/10.1063/1.1149555
20. Allison DP, Sullivan CJ, Mortensen NP, Retterer ST, Doktycz M (2011) Bacterial immobilization for imaging by atomic force microscopy. J Vis Exp 54:2880. https://doi.org/10.3791/2880
21. Vahabi S, Nazemi Salman B, Javanmard A (2013) Atomic force microscopy application in biological research: a review study. Iranian J Med Sci 38(2):76–83
22. Aliofkhazraei M, Ali N (2014) 7.09 - AFM applications in micro/nanostructured coatings. In: Hashmi S, Ferreira Batalha G, Van Tyne CJ, Yilbas B (eds) Comprehensive materials processing, pp 191–241. https://doi.org/10.1016/B978-0-08-096532-1.00712-3
23. Allison DP, Mortensen NP, Sullivan CJ, Doktycz MJ (2010) Atomic force microscopy of biological samples. WIREs Nanomed Nanobiotechnol 2:618–634. https://doi.org/10.1002/wnan.104
24. Goldsbury CS, Scheuring S, Kreplak L (2009) Introduction to atomic force microscopy (AFM) in biology. Curr Protoc Protein Sci. https://doi.org/10.1002/0471140864.ps1707s58
25. Vadillo-Rodríguez V, Busscher HJ, Norde W, de Vries J, Dijkstra RJB, Stokroos I, van der Mei HC (2004) Comparison of atomic force microscopy interaction forces between bacteria and silicon nitride substrata for three commonly used immobilization methods. Appl Environ Microbiol 70(9):5441–5446. https://doi.org/10.1128/AEM.70.9.5441-5446.2004
26. Liu Y, Camesano TA, Camesano TA, Mello CM (2008) Immobilizing bacteria for atomic force microscopy imaging or force measurements in liquids. Microbial Surfaces 984:163–188. https://doi.org/10.1021/bk-2008-0984.ch010
27. Volle CB, Ferguson MA, Aidala KE, Spain EM, Núñez ME (2008) Spring constants and adhesive properties of native bacterial biofilm cells measured by atomic force microscopy. Colloids Surf B: Biointerfaces 67(1):32–40. https://doi.org/10.1016/j.colsurfb.2008.07.021
28. Flemming HC, Wingender J (2010) The biofilm matrix. Nat Rev Microbiol 8(9):623–633. https://doi.org/10.1038/nrmicro2415
29. Váchová L, Palková Z (2018) How structured yeast multicellular communities live, age and die? FEMS Yeast Res 18(4). https://doi.org/10.1093/femsyr/foy033
30. De T, Chettoor AM, Agarwal P, Salapaka MV, Nettikadan S (2010) Immobilization method of yeast cells for intermittent contact mode imaging using the atomic force microscope. Ultramicroscopy 110(3):254–258. https://doi.org/10.1016/j.ultramic.2009.12.003
31. Mathelie-Guinlet M, Viela F, Vijloen A, Dehullu J, Dufrene YF (2019) Single-molecule atomic force microscopy studies of microbial pathogens. Curr Opin Biomed Eng 12:1–7. https://doi.org/10.1016/j.cobme.2019.08.001
32. Potthoff E, Guillaume-Gentil O, Ossola D, Polesel-Maris J, LeibundGut-Landmann S, Zambelli T, Vorholt JA (2012) Rapid and serial quantification of adhesion forces of yeast and mammalian cells. PLoS One 7(12):e52712. https://doi.org/10.1371/journal.pone.0052712
33. Liu Y, Black MA, Caron L, Camesano TA (2006) Role of cranberry juice on molecular-scale surface characteristics and adhesion behavior of *Escherichia coli*. Biotechnol Bioeng 93:297–305. https://doi.org/10.1002/bit.20675
34. Laskowski DJ, Strzelecki J, Pawlak Kj Dahm H, Balter A (2018) Effect of ampicillin on adhesive properties of bacteria examined by atomic force microscopy. Micron 112:84–90. https://doi.org/10.1016/j.micron.2018.05.005
35. Beaussart A, Baker AE, Kuchma SL, El-Kirat-Chatel S, O'Toole GA, Dufrêne YF (2014) Nanoscale adhesion forces of *Pseudomonas aeruginosa* type IV pili. ACS Nano 8(10):10723–10733. https://doi.org/10.1021/nn5044383
36. Ivanov IE, Boyd CD, Newell PD, Schwartz ME, Turnbull L, Johnson MS, Whitchurch CB, O'Toole GA, Camesano TA (2012) Atomic force and super-resolution microscopy support a role for LapA as a cell-surface biofilm adhesin of *Pseudomonas fluorescens*. Res Microbiol 163(9–10):685–691. https://doi.org/10.1016/j.resmic.2012.10.001
37. Viela F, Prystopiuk V, Leprince A, Mahillon J, Speziale P, Pietrocola G, Dufrêne YF (2019) Binding of *Staphylococcus aureus* protein a to von Willebrand factor is regulated by mechanical force. MBio 10(2):e00555–e00519. https://doi.org/10.1128/mBio.00555-19

38. Kwiecinski JM, Crosby HA, Valotteau C, Hippensteel JA, Nayak MK, Chauhan AK, Schmidt EP, Dufrêne YF, Horswill AR (2019) *Staphylococcus aureus* adhesion in endovascular infections is controlled by the ArlRS-MgrA signaling cascade. PLoS Pathog 15(5):e1007800. https://doi.org/10.1371/journal.ppat.1007800
39. Herman P, El-Kirat-Chatel S, Beaussart A, Geoghegan JA, Foster TJ, Dufrêne YF (2014) The binding force of the staphylococcal adhesin SdrG is remarkably strong. Mol Microbiol 93(2):356–368. https://doi.org/10.1111/mmi.12663
40. Eskhan AO, Abu-Lail NI (2013) Cellular and molecular investigations of the adhesion and mechanics of *Listeria monocytogenes* lineages' I and II environmental and epidemic strains. J Colloid Interface Sci 394:554–563. https://doi.org/10.1016/j.jcis.2012.11.038
41. Li Q, Becker T, Zhang R, Xiao T, Sand W (2019) Investigation on adhesion of *Sulfobacillus thermosulfidooxidans* via atomic force microscopy equipped with mineral probes. Colloids Surf B: Biointerfaces 173:639–646. https://doi.org/10.1016/j.colsurfb.2018.10.046
42. Heim KP, Sullan RM, Crowley PJ, El-Kirat-Chatel S, Beaussart A, Tang W, Besingi R, Dufrene YF, Brady LJ (2015) Identification of a supramolecular functional architecture of *Streptococcus mutans* adhesin P1 on the bacterial cell surface. J Biol Chem 290(14):9002–9019. https://doi.org/10.1074/jbc.M114.626663
43. Francius G, Lebeer S, Alsteens D, Wildling L, Gruber HJ, Hols P, De Keersmaecker S, Vanderleyden J, Dufrêne YF (2008) Detection, localization and conformational analysis of single polysaccharide molecules on live bacteria. ACS Nano 2(9):1921–1929. https://doi.org/10.1021/nn800341b
44. Strauss J, Kadilak A, Cronin C, Mello CM, Camesano TA (2010) Binding, inactivation and adhesion forces between antimicrobial peptide cecropin P1 and pathogenic *E. coli*. Colloids Surf B: Biointerfaces 75(1):156–164. https://doi.org/10.1016/j.colsurfb.2009.08.026
45. Alsteens D, Dupres V, Mc Evoy K, Wildling L, Gruber HJ, Dufrêne YF (2008) Structure, cell wall elasticity and polysaccharide properties of living yeast cells as probed by AFM. Nanotechnology 19(38):384005. https://doi.org/10.1088/0957-4484/19/38/384005
46. Touhami A, Nysten B, Dufrene YF (2003) Nanoscale mapping of the elasticity of microbial cells by atomic force microscopy. Langmuir 19:4539–4543. https://doi.org/10.1021/la034136x
47. Volle C, Overton K, Greer H, Ferguson M, Spain E, Elmore D, Núñez M (2018) Measuring the effect of antimicrobial peptides on the biophysical properties of bacteria using atomic force microscopy. Biophys J 114(3):354a. https://doi.org/10.1016/j.bpj.2017.11.1969
48. Mathelié-Guinlet M, Grauby-Heywang C, Martin A, Février H, Moroté F, Vilquin A, Béven L, Delville M-H, Cohen-Bouhacina T (2018) Detrimental impact of silica nanoparticles on the nanomechanical properties of *Escherichia coli* studied by AFM. J Colloid Interface Sci 529:53–64. https://doi.org/10.1016/j.jcis.2018.05.098
49. Gaboriaud F, Bailet S, Dague E, Jorand F (2005) Surface structure and nanomechanical properties of Shewanella putrefaciens bacteria at two pH values (4 and 10) determined by atomic force microscopy. J Bacteriol 187(11):3864–3868. https://doi.org/10.1128/JB.187.11.3864-3868.2005
50. Gaboriaud F, Parcha BS, Gee ML, Holden JA, Strugnell RA (2008) Spatially resolved force spectroscopy of bacterial surfaces using force-volume imaging. Colloid Surfaces B: Biointerfaces 62:206–213. https://doi.org/10.1016/j.colsurfb.2007.10.004
51. Eaton P, Fernandes JC, Pereira E, Pintado ME, Xavier MF (2008) Atomic force microscopy study of the antibacterial effects of chitosans on *Escherichia coli* and *Staphylococcus aureus*. Ultramicroscopy 108(10):1128–1134. https://doi.org/10.1016/j.ultramic.2008.04.015
52. Perry CC, Weatherly M, Beale T, Randriamahefa A (2009) Atomic force microscopy study of the antimicrobial activity of aqueous garlic versus ampicillin against *Escherichia coli* and *Staphylococcus aureus*. J Sci Food Agric 89:958–964. https://doi.org/10.1002/jsfa.3538
53. Kumar U, Vivekanand K, Poddar P (2009) Real-time nanomechanical and topographical mapping on live bacterial cells - *Brevibacterium casei* under stress due to their exposure to Co^{2+} ions during microbial synthesis of Co_3O_4 nanoparticles. J Phys Chem B 113(22):7927–7933. https://doi.org/10.1021/jp902698n

54. Deng Y, Sun M, Shaevitz JW (2011) Direct measurement of cell wall stress stiffening and turgor pressure in live bacterial cells. Phys Rev Lett 107(15):158101. https://doi.org/10.1103/PhysRevLett.107.158101
55. Saar-Dover R, Bitler A, Nezer R, Shmuel-Galia L, Firon A, Shimoni E, Trieu-Cuot P, Shai Y (2012) D-alanylation of lipoteichoic acids confers resistance to cationic peptides in group B streptococcus by increasing the cell wall density. PLoS Pathog 8:e1002891. https://doi.org/10.1371/journal.ppat.1002891
56. Dhahri S, Ramonda M, Marlière C (2013) In-situ determination of the mechanical properties of gliding or non-motile bacteria by atomic force microscopy under physiological conditions without immobilization. PLoS One 8(4):e61663. https://doi.org/10.1371/journal.pone.0061663
57. Aguayo S, Bozec L (2016) Mechanics of bacterial cells and initial surface colonisation. In: Leake M (eds) Biophysics of infection. Advances in experimental medicine and biology. Springer, Cham, 915. https://doi.org/10.1007/978-3-319-32189-9_15
58. Aguayo S, Strange A, Gadegaard N, Dalby MJ, Bozec L (2016) Influence of biomaterial nanotopography on the adhesive and elastic properties of *Staphylococcus aureus*. RSC Adv 6:89347–89355. https://doi.org/10.1039/C6RA12504B
59. Mozhanova AA, Nurgazizov NI, Bukharaev AA (2003) Local elastic properties of biological materials studied by SFM. SPM-2003. In: Proceedings Nizhni Novgorod, March 2–5, pp 266–267
60. Braet F, Rotsch C, Wisse E, Radmacher M (1998) Comparison of fixed and living liver endothelial cells by atomic force microscopy. Appl Phys A 66:S575–S578. https://doi.org/10.1007/s003390051204
61. Mathur AB, Collinsworth AM, Reichert WM, Kraus WE, Truskey GA (2001) Endothelial, cardiac muscle and skeletal muscle exhibit different viscous and elastic properties as determined by atomic force microscopy. J Biomech 34(12):1545–1553. https://doi.org/10.1016/s0021-9290(01)00149-x
62. Sato H, Kataoka N, Kajiya F, Katano M, Takigawa T, Masuda T (2004) Kinetic study on the elastic change of vascular endothelial cells on collagen matrices by atomic force microscopy. Colloids Surf B: Biointerfaces 34(2):141–146. https://doi.org/10.1016/j.colsurfb.2003.12.013
63. Dulińska I, Targosz M, Strojny W, Lekka M, Czuba P, Balwierz W, Szymoński M (2006) Stiffness of normal and pathological erythrocytes studied by means of atomic force microscopy. J Biochem Biophys Methods 66:1–11. https://doi.org/10.1016/j.jbbm.2005.11.003
64. Yourek G, Hussain MA, Mao JJ (2007) Cytoskeletal changes of mesenchymal stem cells during differentiation. ASAIO J 53(2):219–228. https://doi.org/10.1097/MAT.0b013e31802deb2d
65. Xu W, Mezencev R, Kim B, Wang L, McDonald J, Sulchek T (2012) Cell stiffness is a biomarker of the metastatic potential of ovarian cancer cells. PLoS One 7(10):e46609. https://doi.org/10.1371/journal.pone.0046609
66. Weder G, Hendriks-Balk MC, Smajda R, Rimoldi D, Liley M, Heinzelmann H, Meister A, Mariotti A (2014) Increased plasticity of the stiffness of melanoma cells correlates with their acquisition of metastatic properties. Nanomedicine 10(1):141–148. https://doi.org/10.1016/j.nano.2013.07.007
67. Tang X, Kuhlenschmidt TB, Li Q, Ali S, Lezmi S, Chen H, Pires-Alves M, Laegreid WW, Saif TA, Kuhlenschmidt MS (2014) A mechanically-induced colon cancer cell population shows increased metastatic potential. Mol Cancer 13:131. https://doi.org/10.1186/1476-4598-13-131
68. Wang X, Wang J, Liu Y, Zong H, Che X, Zheng W, Chen F, Zhu Z, Yang D, Song X (2014) Alterations in mechanical properties are associated with prostate cancer progression. Med Oncol 31(3):876. https://doi.org/10.1007/s12032-014-0876-9
69. Hayashi K, Iwata M (2015) Stiffness of cancer cells measured with an AFM indentation method. J Mech Behav Biomed Mater 49:105–111. https://doi.org/10.1016/j.jmbbm.2015.04.030
70. Pegoraro AF, Janmey P, Weitz DA (2017) Mechanical properties of the cytoskeleton and cells. Cold Spring Harb Perspect Biol 9(11):a022038. https://doi.org/10.1101/cshperspect.a022038

71. Zouaoui J, Trunfio-Sfarghiu AM, Brizuela L, Piednoir A, Maniti O, Munteanu B, Mebarek S, Girard-Egrot A, Landoulsi A, Granjon T (2017) Multi-scale mechanical characterization of prostate cancer cell lines: relevant biological markers to evaluate the cell metastatic potential. Biochim Biophys Acta Gen Subj 1861(12):3109–3119. https://doi.org/10.1016/j.bbagen.2017.09.003
72. Cascione M, De Matteis V, Toma CC, Pellegrino P, Leporatti S, Rinaldi R (2017) Morphomechanical and structural changes induced by ROCK inhibitor in breast cancer cells. Exp Cell Res 360(2):303–309. https://doi.org/10.1016/j.yexcr.2017.09.020
73. Arfsten J, Leupold S, Bradtmöller C, Kampen I, Kwade A (2010) Atomic force microscopy studies on the nanomechanical properties of *Saccharomyces cerevisiae*. Colloids Surf B: Biointerfaces 79(1):284–290. https://doi.org/10.1016/j.colsurfb.2010.04.011
74. Goss JW, Volle CB (2020) Using atomic force microscopy to illuminate the biophysical properties of microbes. ACS Applied Bio Mater 3(1):143–155. https://doi.org/10.1021/acsabm.9b00973
75. Liu S, Ng AK, Xu R, Wei J, Tan CM, Yang Y, Chen Y (2010) Antibacterial action of dispersed single-walled carbon nanotubes on *Escherichia coli* and *Bacillus subtilis* investigated by atomic force microscopy. Nanoscale 2(12):2744–2750. https://doi.org/10.1039/c0nr00441c
76. Zhang W, Hughes J, Chen Y (2012) Impacts of hematite nanoparticle exposure on biomechanical, adhesive and surface electrical properties of *Escherichia coli* cells. Appl Environ Microbiol 78(11):3905–3915. https://doi.org/10.1128/AEM.00193-12
77. Mularski A, Wilksch JJ, Wang H, Hossain MA, Wade JD, Separovic F, Strugnell RA, Gee ML (2015) Atomic force microscopy reveals the mechanobiology of lytic peptide action on bacteria. Langmuir 31(22):6164–6171. https://doi.org/10.1021/acs.langmuir.5b01011
78. Pogoda K, Piktel E, Deptuła P, Savage PB, Lekka M, Bucki R (2017) Stiffening of bacteria cells as a first manifestation of bactericidal attack. Micron 101:95–102. https://doi.org/10.1016/j.micron.2017.06.011
79. Thomas G, Burnham N, Camesano TA, Wen Q (2013) Measuring the mechanical properties of living cells using atomic force microscopy. J Vis Exp 76:50497. https://doi.org/10.3791/50497
80. Spedden E, Staii C (2013) Neuron biomechanics probed by atomic force microscopy. Int J Mol Sci 14(8):16124–16140. https://doi.org/10.3390/ijms140816124
81. Darling EM, Zauscher S, a Block J, Guilak F. (2007) A thin-layer model for viscoelastic, stress-relaxation testing of cells using atomic force microscopy: do cell properties reflect metastatic potential? Biophys J 92:1784–1791
82. Malkin AJ, Plomp M, McPherson A (2002) Application of atomic force microscopy to studies of surface processes in virus crystallization and structural biology. Acta Crystallogr Sect D Biol Crystallogr 58(10):1617–1621. https://doi.org/10.1107/S090744490201274X
83. Kuznetsov Y, Low A, Fan H, McPherson A (2004) Atomic force microscopy investigation of wild-type Moloney murine leukemia virus particles and virus particles lacking the envelope protein. Virology 323(2):189–196. https://doi.org/10.1016/j.virol.2004.02.023
84. Kuznetsov Y, Gershon PD, McPherson A (2008) Atomic force microscopy investigation of vaccinia virus structure. J Virol 82(15):7551–7566. https://doi.org/10.1128/JVI.00016-08
85. Kuznetsov YG, Xiao C, Sun S, Raoult D, Rossmann M, McPherson A (2010) Atomic force microscopy investigation of the giant mimivirus. Virology 404(1):127–137. https://doi.org/10.1016/j.virol.2010.05.007
86. Kuznetsov YG, Daijogo S, Zhou J, Semler BL, McPherson A (2005) Atomic force microscopy analysis of icosahedral virus RNA. J Mol Biol 347(1):41–52. https://doi.org/10.1016/j.jmb.2005.01.006
87. Kuznetsov YG, Zhang M, Menees TM, McPherson A, Sandmeyer S (2005) Investigation by atomic force microscopy of the structure of Ty3 retrotransposon particles. J Virol 79(13):8032–8045. https://doi.org/10.1128/JVI.79.13.8032-8045.2005
88. Kuznetsov YG, McPherson A (2011) Atomic force microscopy in imaging of viruses and virus-infected cells. Microbiol Mol Biol Rev 75(2):268–285. https://doi.org/10.1128/MMBR.00041-10

89. Gibbons MM, Klug WS (2008) Influence of non-uniform geometry on nanoindentation of viral capsids. Biophys J 95(8):3640–3649. https://doi.org/10.1529/biophysj.108.136176
90. de Pablo PJ (2013) Atomic force microscopy of viruses. Subcell Biochem 68:247–271. https://doi.org/10.1007/978-94-007-6552-8_8
91. Michel JP, Ivanovska IL, Gibbons MM, Klug WS, Knobler CM, Wuite GJL, Schmidt CF (2006) Nanoindentation studies of full and empty viral capsids and the effects of capsid protein mutations on elasticity and strength. Proc Natl Acad Sci 103(16):6184–6189. https://doi.org/10.1073/pnas.0601744103
92. Cieplak M, Robbins MO (2013) Nanoindentation of 35 virus capsids in a molecular model: relating mechanical properties to structure. PLoS One 8(6):e63640. https://doi.org/10.1371/journal.pone.0063640
93. Kononova O, Snijder J, Kholodov Y, Marx KA, Wuite GJL, Roos WH, Barsegov V (2016) Fluctuating nonlinear spring model of mechanical deformation of biological particles. PLoS Comput Biol 12(1):e1004729. https://doi.org/10.1371/journal.pcbi.1004729
94. Veesler D, Johnson JE (2012) Virus maturation. Annu Rev Biophys 41:473–496. https://doi.org/10.1146/annurev-biophys-042910-155407
95. Hendrix RW, Johnson JE (2012) Bacteriophage HK97 capsid assembly and maturation. Adv Exp Med Biol 726:351–363. https://doi.org/10.1007/978-1-4614-0980-9_15
96. Hernando-Pérez M, Lambert S, Nakatani-Webster E, Catalano CE, de Pablo PJ (2014) Cementing proteins provide extra mechanical stabilization to viral cages. Nat Commun 5:4520. https://doi.org/10.1038/ncomms5520
97. Alsteens D, Dupres V, Yunus S, Latgé JP, Heinisch JJ, Dufrêne YF (2012) High-resolution imaging of chemical and biological sites on living cells using peak force tapping atomic force microscopy. Langmuir 28:16738–16744. https://doi.org/10.1021/la303891j
98. Formosa C, Grare M, Duval RE, Dague E (2012) Nanoscale effects of antibiotics on *P. aeruginosa*. Nanomedicine 8(1):12–16. https://doi.org/10.1016/j.nano.2011.09.009
99. Powell LC, Sowedan A, Khan S, Wright CJ, Hawkins K, Onsøyen E, Myrvold R, Hill KE, Thomas DW (2013) The effect of alginate oligosaccharides on the mechanical properties of Gram-negative biofilms. Biofouling 29(4):413–421. https://doi.org/10.1080/08927014.2013.777954
100. Wu Y, Zhou A (2009) In situ, real-time tracking of cell wall topography and nanomechanics of antimycobacterial drugs treated mycobacterium JLS using atomic force microscopy. Chem Commun J 7021–7023. https://doi.org/10.1039/b914605a
101. Ierardi V, Domenichini P, Reali S, Chiappara GM, Devoto G, Valbusa U (2017) *Klebsiella pneumoniae* antibiotic resistance identified by atomic force microscopy. J Biosci 42:623–636. https://doi.org/10.1007/s12038-017-9713-6
102. Li A, Lee PY, Ho B, Ding JL, Lim CT (2007) Atomic force microscopy study of the antimicrobial action of Sushi peptides on Gram negative bacteria. Biochimica et Biophysica Acta (BBA) – Biomembranes 1768(3):411–418. https://doi.org/10.1016/j.bbamem.2006.12.010
103. Mularski A, Wilksch JJ, Hanssen E, Strugnell RA, Separovic F (2016) Atomic force microscopy of bacteria reveals the mechanobiology of pore forming peptide action. Biochimica et Biophysica Acta (BBA) - Biomembranes 1858(6):1091–1098. https://doi.org/10.1016/j.bbamem.2016.03.002
104. Muthukrishnan L, Chellappa M, Nanda A (2019) Bio-engineering and cellular imaging of silver nanoparticles as weaponry against multidrug resistant human pathogens. J Photochem Photobiol B Biol 194:119–127. https://doi.org/10.1016/j.jphotobiol.2019.03.021
105. Longo G, Alonso-Sarduy L, Rio LM, Bizzini A, Trampuz A, Notz J, Dietler G, Kasas S (2013) Rapid detection of bacterial resistance to antibiotics using AFM cantilevers as nanomechanical sensors. Nat Nanotechnol 8(7):522–526. https://doi.org/10.1038/nnano.2013.120
106. Neethirajan S, DiCicco M (2014) Atomic force microscopy study of the antibacterial effect of fosfomycin on methicillin-resistant *Staphylococcus pseudintermedius*. Appl Nanosci 4(6):703–709. https://doi.org/10.1007/s13204-013-0256-3

107. Mitchell MJ, Jain RK, Langer R (2017) Engineering and physical sciences in oncology: challenges and opportunities. Nat Rev Cancer 17(11):659–675. https://doi.org/10.1038/nrc.2017.83
108. Cohen JD, Li L, Wang Y, Thoburn C, Afsari B, Danilova L, Douville C, Javed AA, Wong F, Mattox A, Hruban RH, Wolfgang CL, Goggins MG, Dal Molin M, Wang TL, Roden R, Klein AP, Ptak J, Dobbyn L, Schaefer J, Silliman N, Popoli M, Vogelstein JT, Browne JD, Schoen RE, Brand RE, Tie J, Gibbs P, Wong HL, Mansfield AS, Jen J, Hanash SM, Falconi M, Allen PJ, Zhou S, Bettegowda C, Diaz LA Jr, Tomasetti C, Kinzler KW, Vogelstein B, Lennon AM, Papadopoulos N (2018) Detection and localization of surgically resectable cancers with a multi-analyte blood test. Science 359(6378):926–930. https://doi.org/10.1126/science.aar3247
109. Cross S, Jin YS, Rao J, Gimzewski JK (2007) Nanomechanical analysis of cells from cancer patients. Nat Nanotechnol 2:780–783. https://doi.org/10.1038/nnano.2007.388
110. Lekka M, Fornal M, Pyka-Fościak G, Lebed K, Wizner B, Grodzicki T, Styczeń J (2005) Erythrocyte stiffness probed using atomic force microscope. Biorheology 42(4):307–317
111. Reed J, Troke JJ, Schmit J, Han S, Teitell MA, Gimzewski JK (2008) Live cell inferometry reveals cellular dynamism during force propagation. ACS Nano 2(5):841–846. https://doi.org/10.1021/nn700303f
112. Jorba I, Uriarte JJ, Campillo N, Farre R, Navajas D (2017) Probing micromechanical properties of the extracellular matrix of soft tissues by atomic force microscopy. J Cell Physiol 232:19–26. https://doi.org/10.1002/jcp.25420
113. Gang Z, Qi Q, Jing C, Wang C (2009) Measuring microenvironment mechanical stress of rat liver during diethylnitrosamine induced hepatocarcinogenesis by atomic force microscope. Microsc Res Tech 72(9):672–678. https://doi.org/10.1002/jemt.20716
114. Deng X, Xiong F, Li X, Xiang B, Li Z, Wu X, Guo C, Li X, Li Y, Li G, Xiong W, Zeng Z (2018) Application of atomic force microscopy in cancer research. J Nanobiotechnol 16(1):102. https://doi.org/10.1186/s12951-018-0428-0
115. Kendall C, Isabelle M, Bazant-Hegemark F, Hutchings J, Orr L, Babrah J, Baker R, Stone N (2009) Vibrational spectroscopy: a clinical tool for cancer diagnostics. Analyst 134(6):1029–1045. https://doi.org/10.1039/b822130h
116. Zhao J, Zeng H, Kalia S, Lui H (2017) Using Raman spectroscopy to detect and diagnose skin cancer in vivo. Dermatol Clin 35(4):495–504. https://doi.org/10.1016/j.det.2017.06.010
117. Zhang H, Xiao L, Li Q, Qi X, Zhou A (2018) Microfluidic chip for non-invasive analysis of tumor cells interaction with anti-cancer drug doxorubicin by AFM and Raman spectroscopy. Biomicrofluidics 12(2):024119. https://doi.org/10.1063/1.5024359
118. Fu QF, Liu Y, Fan Y, Hua SN, Qu HY, Dong SW, Li RL, Zhao MY, Zhen Y, Yu XL, Chen YY, Luo RC, Li R, Li LB, Deng XJ, Fang WY, Liu Z, Song X (2015) Alpha-enolase promotes cell glycolysis, growth, migration and invasion in non-small cell lung cancer through FAK-mediated PI3K/AKT pathway. J Hematol Oncol 8:22. https://doi.org/10.1186/s13045-015-0117-5
119. Principe M, Borgoni S, Cascione M, Chattaragada MS, Ferri-Borgogno S, Capello M, Bulfamante S, Chapelle J, Di Modugno F, Defilippi P, Nisticò P, Cappello P, Riganti C, Leporatti S, Novelli F (2017) Alpha-enolase (ENO1) controls alpha v/beta 3 integrin expression and regulates pancreatic cancer adhesion, invasion and metastasis. J Hematol Oncol 10(1):16. https://doi.org/10.1186/s13045-016-0385-8
120. Louis DN, Perry A, Reifenberger G, von Deimling A, Figarella-Branger D, Cavenee WK, Ohgaki H, Wiestler OD, Kleihues P, Ellison DW (2016) The 2016 World Health Organization classification of tumors of the central nervous system: a summary. Acta Neuropathol 131:803–820. https://doi.org/10.1007/s00401-016-1545-1

7 Scanning Electron Microscopy (SEM): Learning to Generate and Interpret the Topographical Aspects of Materials

Sachin Jaidka, Ruchika Sharma, Shobhneek Kaur, and Dwijendra P. Singh

Abstract

Scanning Electron Microscope (SEM) is a technique used to visualize a specimen's surface topography, composition, crystallographic, and microstructural information. Resolution achieved by SEM is up to nanometers range (~10 nm). SEM generally includes scanning X-ray beams across specimens (metal, plastics, ceramics, silicon crystals, or chips) to record energy dispersive spectra (EDS). At the same time, electrons are used to record the topographical images in SEM. Generally, the instrument works in a high vacuum system (~10^{-4} torr), and image formation (in raster scan pattern) occurs due to electron–matter interaction. The pattern obtained in SEM is 3-dimensional with an extensive magnification range. Sample preparation plays a vital role in revealing the properties of materials. SEM can quickly analyze fractured surfaces and also evaluate corrosion in specimens. It is also used in the elemental recognition of base matrix, segregated phases, and identifying air pores in samples. Nowadays, SEM has a broad scope, such as vaccination testing, gas sensing, and forensic investigations.

Keywords

SEM · Materials science · Crystallography · Topography · Microstructure

S. Jaidka · R. Sharma (✉) · D. P. Singh
Energy Materials Lab, School of Physics and Materials Science,
Thapar Institute of Engineering and Technology, Patiala, Punjab, India

S. Kaur
Department of Physics
GSSDGS Khalsa College
PatialaPunjabIndia

S.-K. Kamaraj et al. (eds.), *Microscopic Techniques for the Non-Expert*,
https://doi.org/10.1007/978-3-030-99542-3_7

7.1 Introduction

The Scanning Electron Microscope (SEM) is mainly used to identify materials on a microscopic scale (~0.5 nm). The instrument generally uses a highly accelerated beam of electrons to identify materials. An average human eye can observe two dots with a difference of 0.2 mm. If the dots have a distance of less than 0.2 mm, it will be a single dot for a normal human eye. In order to view things at a much smaller level, one must need a microscope. Before proceeding to the instrument's working, let us first recall the brief history. The first microscope was invented in the sixteenth century by two Dutch opticians. The microscope thus designed was the compound microscope that involved more than one lens in a sequence. A few decades later, Giovanni Faber coined the term microscope (in Greek, micro stands for small and scope stands to aim). The invention of the microscope grew up in the mid-seventeenth century by Italians and Dutch, as no one knows the exact timing and inventor of this invention. In the seventeenth century, optical microscopes were considered for biological purposes, as Robert Hooke designed a two-lens microscope, and after a few years, Leeuwenhoek (Fig. 7.1) designed a single-lens microscope. In the history of microscopes, Leeuwenhoek made a remarkable discovery of ~500 microscopes. Nine still exist out of these 500 microscopes, whereas some are still a mystery [1].

In the nineteenth century, achromatic objectives came into attention leading to advancement in microscopes technology. Later on, in 1857, a more modern microscope was invented by Zeiss (the first mass producer of the high-quality microscope) (Fig. 7.2), having a resolution of around 0.2 μm. Germany became the primary hub to gain maximum knowledge about sciences and, most notably, microscopes. Within a few years, along with modern civilization, modernization of microscope was also achieved, with tremendous professional applications [1, 2].

Fig. 7.1 Anton von Leeuwenhoek

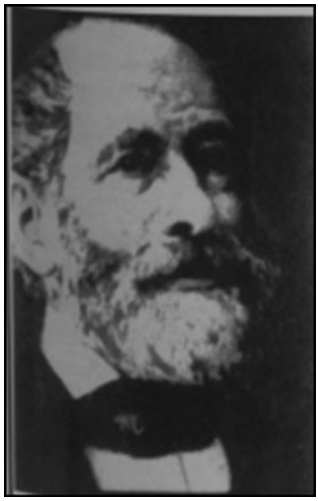

Fig. 7.2 Carl Zeiss

Fig. 7.3 Ernst Ruska and Max Knoll

In 1931, Ernst Ruska and Max Knoll discovered the first electron microscope (later won Noble Prize for the same) (Fig. 7.3). The microscope's resolution was 100 nm and later on updated to 0.05 nm. Year after year, more modulations were performed by different scientists [2]. In 1938, the first commercial electron microscope was discovered by Siemens. Electron microscopes (having various lens combinations) were developed to overcome the limitations of light microscopes (400–700 nm wavelength). The magnification of the light microscope is about 1000×, and at the same time, electron microscopes have much higher magnification (~30,000×). A comparison between electron and light microscope is given in Table 7.1.

Initially, the electron microscope was divided into three categories:

(i) *SEM*

Scanning Electron Microscope is used to analyze the sample's surface by scanning it using a focused beam of electrons. The images produced are used to identify the surface topography and sample composition. A modern-day SEM setup is shown in Fig. 7.4 to understand the system in a better way.

(ii) *TEM*

Table 7.1 Difference between light and electron microscope [3]

Sr. No.	Characteristics	Light microscope	Electron microscope
1	EM spectrum	400–700 nm	4 nm
2	Resolving power	~200 nm	0.5 nm
3	Magnification	×1000 to ×1500	×500,000
4	Lens used	Glass	Electromagnetic lens
5	Radiation source	Tungsten or quartz lamp	High voltage tungsten lamp, LaB_6
6	Internal environment	Air	Vacuum
7	Sample support	Glass slide	Copper grid
8	Focusing screen	Human eye	Fluorescent screen
9	Staining	Water soluble dyes	Heavy metals

Fig. 7.4 Modern-day SEM setup

TEM stands for Transmission Electron Microscopy, and when a beam of electrons is transmitted from a sample, making an image on a fluorescent screen. This transmitted electron beam sometimes damages the samples/specimen, which is the drawback of this microscopy. However, the resolution of TEM is much higher than that of SEM.

(iii) *REM*

Reflection Electron Microscope is somewhat similar to TEM. The difference arises when the elastically scattered electrons are used in REM instead of the transmitted electron beam. A year-wise development summary of SEM is given in Table 7.2.

The main focus here is on Scanning Electron Microscopy. SEM reveals the surface topography, morphology (shape, size, etc.), and compounds composition. The high spatial resolution of SEM makes it a powerful tool to characterize a wide range of samples from several nanometers to micrometer ranges.

SEM means scanning a sample/specimen using an electron beam. As soon as the electron beam falls on the sample, atoms of the sample eject out electrons. Due to inelastic scattering, the atoms move to an excited state and then return to their

Table 7.2 The evolution of SEM over time [3]

Sr. No.	Year	Development
1	1935	Concept of SEM by Max Knoll
2	1938	Idea and development of STEM by Ardenne
3	1942	SEM with 50 nm resolution by Zworykin
4	1956	Signal processing, image quality improved [4]
5	1957	Observation of voltage contrast
6	1960	Scintillating secondary electron detector with improved signal-to-noise ratio [5]
7	1960	Stereographic 3D images [6]
8	1963	Development of E-T detector [7]
9	1965	First commercial SEM "stereoscan" invented [7, 8]
10	1970	EDS coupled with SEM
11	1970–1990	LaB_6 cathode gun, field emission gun, electron backscattered diffraction, cathodoluminescence in SEM, large specimen stage developed up to 23 cm, autofocus and auto stigmator functions, low-temperature cryo stage, variable pressure SEM
12	Since 1990	Automations and analysis were improved with the invention of computers
13	2000–present	The resolution of microscopes has been improving

ground state by releasing energy. The production of X-rays balances this difference in energy. These X-rays are produced when the electron from an atom's outer shell in an excited state replaces the inner shell electron. The X-rays give information about the composition of the specimen. At the same time, different electrons provide different types of information, such as Auger electrons telling us about surface-sensitive compositional information; primary backscattered electrons give information on atomic number and topography. In order to get this information, one must know about SEM from its initial stage, as described further.

A modern-day SEM has a magnification of around one million times, and due to this reason, it becomes a powerful tool for scientists to work at such a micro-level. As seen in Fig. 7.4, the SEM instrument has many parts. The monitor screen is used to view and save images of the sample placed in the instrument. The detailing of this instrument is discussed in Sect. 7.2.

7.2 Instrumentation

The principle of any device itself tells about how it will work and what component one has to choose.

Principle In the presence of positive electric potential, electrons are bombarded over the specimen with the help of an electron gun. To align the electron beam, metallic apertures and magnetic lenses are used. As soon as the electrons strike the

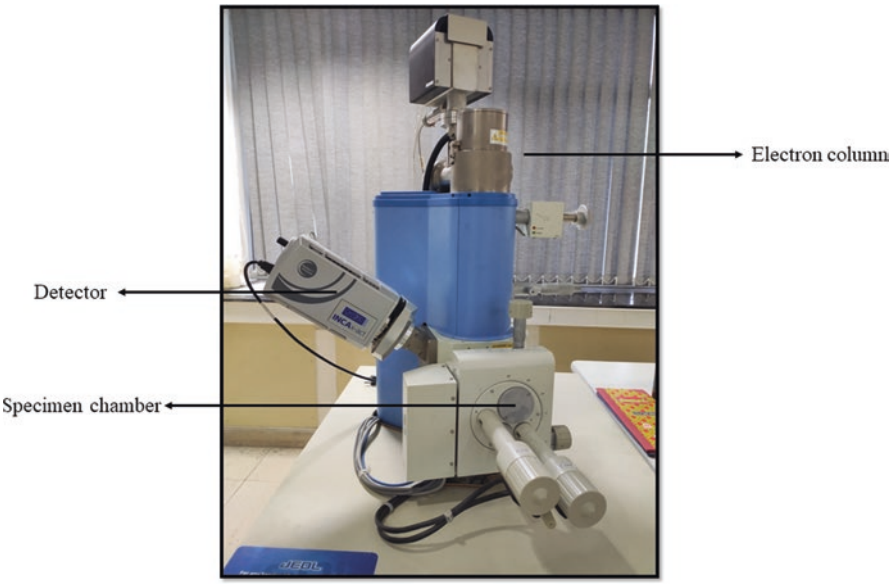

Fig. 7.5 Photograph showing electron column and electron chamber

specimen, it produces signals containing information about surface topography and other properties as well which are displayed on the screen.

Components There are two critical components involved in SEM, which are:

(a) *Electronic Console*:
This component controls the adjustments of the instrument via knobs and switches. CRT that produces images is also a part of the electronic console. This electronic console manages and controls filament current, accelerating voltage, magnification, brightness, etc. A computer system controls the instrument's functioning to remove the bulky and excessive knobs. The image of the specimen can be viewed on the computer screen and can be saved at our convenience.

(b) *Electron column*:
It is a place where the origination of an electron beam takes place inside a vacuum. The originated electron beam is concentrated over a particular area with a specific diameter, and then the surface of the specimen is scanned. The stage control of the sample is placed just opposite the specimen chamber. It can be rotated in 360° and can be inclined up to 90°. The components involved in the electron column are electron source to produce electron probe, specimen chamber, secondary electron detector, sample stage (controlled by goniometer), an image display unit (Fig. 7.5).

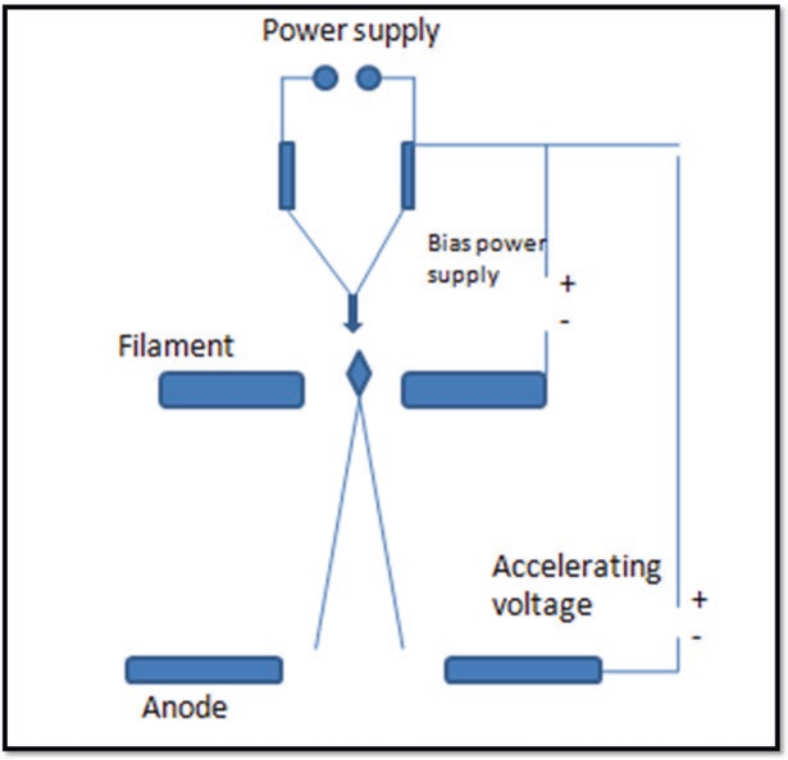

Fig. 7.6 Schematic of an electron chamber

7.2.1 The Illumination System

This portion contains an electron gun, condenser lenses, objective lens, scanning coil to scan electron probe, etc., and this whole optical system must be kept in a vacuum [9] (Fig. 7.6).

7.2.1.1 Electron Gun

An electron gun is situated in the upper part of the electron column. The free electrons can be produced by thermionic emission or cold field emission where the electron source can be of various types, such as tungsten, LaB_6, cold field emission, and Schottky. Thermionic emission contains tungsten filament heated at 2700 K using an electric current because of its high melting point and low cost. Thus, the electrons leave the filament. The electrons escape with low acceleration, and therefore a high voltage is applied between the filament and metal plates. The filament here acts as a cathode, and the metal plate acts as an anode. To adjust the current of the electron beam, the Wehnelt electrode must be placed between cathode and anode with negative voltage.

Table 7.3 Features of different emission guns [10–12]

	Tungsten	LaB_6	Field emission gun	Schottky emission gun
Heating temperature	2800 K	1900 K	300 K	1800 K
Lifetime	50 h	500 h	Some years	1–2 year
Energy	3–4 eV	2–3 eV	0.3 eV	0.7–1 eV
Electron source size	~17 μm	~10 μm	~5–10 nm	~15–20 nm
Vacuum	High	Very high	Super high	Ultrahigh

Next, there is no need to heat the filament in cold field emission. The electrons can easily escape at room temperature. The cold field emission generally has a high electron yield and produces an image at atomic resolution. However, the drawback of this instrument is that it is very costly, and a very high vacuum has to be maintained for it. Different electron guns with their varying features are stated in Table 7.3.

7.2.2 Lens: The Different Types of Lenses Used in Electron Microscope Are as Follows

7.2.2.1 Electromagnetic Lens

This lens is action generated due to the flow of direct current, and a magnetic field is produced in a winding of insulated copper wire. The density of the magnetic line decides the magnetic behavior of this lens. The path followed by an electron in the system is circular (1) due to deviation offered by the magnetic field and (2) perpendicular plane of magnetic field and velocity vector. This circular path results in the rotation and magnification of the image. Whenever the current through the coil varies, it directly changes its strength which an optical lens cannot achieve. The focal width of the lens is proportional to the power of the magnetic field.

7.2.2.2 Condenser Lens

It is the first lens system in a microscope. The electron beam from the anode now has to pass through the focal point. The electron beam is converged by two condenser lenses placed between the focal point and anode. Here, the condenser lens can identify the intensity of the electrons and the beam's brightness. The absolute character of the condenser lens is that any increase or decrease in the excitation of the condenser lens decides the broadening and sharpness of the beam, which in turn decreases or increases the number of electrons approaching the objective lens, respectively.

7.2.2.3 Projective Lens

This lens helps to obtain the final image of the specimen. The final image is obtained with the help of two lenses on a fluorescent screen or photosensitive film. The magnetic lens is responsible for aberrations like chromatic aberration (rays pass through

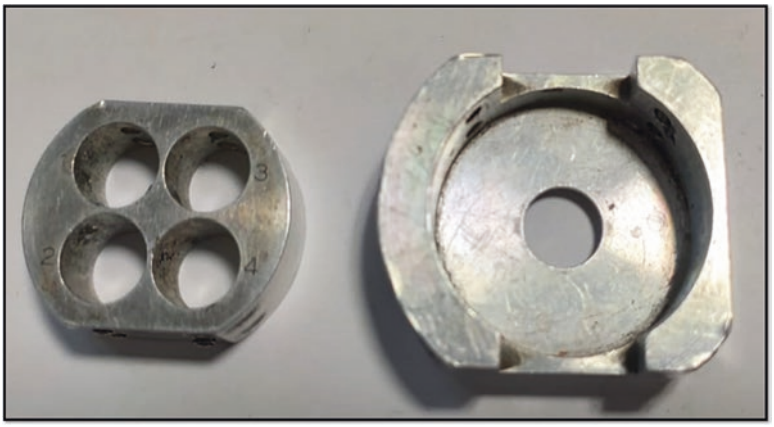

Fig. 7.7 Specimen holder

lens focus at different points due to variation of refractive index with wavelength), spherical aberration (an intrinsic defect that takes the shape of a sphere), distortion, and astigmatism (due to contamination of lenses). The role of the objective lens is to observe the diameter of the electron probe.

7.2.2.4 Apertures

The electron column contains many apertures to remove the irrelevant electrons from lenses. The lens aperture also discovers the spot size of the beam. This spot, later on, is used to find out the resolution by reducing the brightness of the beam.

7.2.2.5 Scanning System

The deflection coils in the objective lens are used to form images. In order to minimize the aberrations such as astigmatism in the electron beam, a magnetic field is used, or a corrector is applied.

7.2.3 Sample Holder

The specimen stage is at the bottom of the electron column. Here, the sample is placed and operated with a goniometer. On the front side of the chamber, there is a manual control system for the rotation of the specimen. The specimen can be moved into any direction (x, y, and z-direction) and rotation. X and Y-axes are for horizontal motion, Z-axis for vertical motion, T for tilting, and R for rotation. The sample is connected to an aluminum stub. The sample holder is placed in the microscope manually or by vacuum lock. An electron microscope must be mounted on air cushions to avoid electromagnetic fields and vibrations. A photograph of the sample holder is shown in Fig. 7.7.

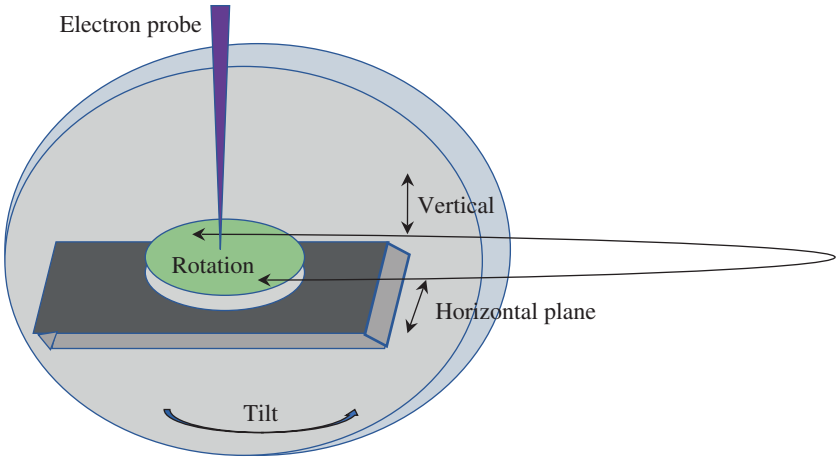

Fig. 7.8 Schematic of a sample stage

7.2.4 Vacuum System

For proper functioning of SEM, a suitable vacuum is needed because:

1. Electric current flowing through filament increases its temperature, which leads to the burning of filament in the presence of air.
2. The column operates in a dust-free environment.
3. Electron strikes with air may lead to scattering of electrons and reduce the beam's intensity. In order to increase the mean free path of an electron, a vacuum must be created.
4. Air particles must avoid combining with electrons or making any other compound and condensing on the sample. Hence, it leads to wrong observations and imaging.

Different parts of the chamber need to be vacuumed at different pressures. The vacuum maintained in the electron column must be ~10^{-4} Pa; in the specimen chamber, it should be ~10^{-3} Pa, whereas 10^{-7} Pa to 10^{-6} Pa pressure must be maintained in the field emission column. In order to maintain the vacuum at 10^{-3} Pa, an oil diffusion pump or turbomolecular pump may be used. Turbomolecular pump rotates the turbine at ~30,000 rotations per minute to vent out the gas. In case, FE gun is used, then the pump must be a sputter ion pump. The sputter ion pump creates an ultra-high vacuum for the microscope. A cold cathode gauge or Pirani gauge is used to measure the vacuum level (Fig. 7.8).

7.2.5 Detectors

The device that fetches the signals produced due to the beam's interaction and the sample is known as a detector. Several types of detectors are used in SEM. Some are

permanently fitted inside, while some are removable and can be easily removed. Depending upon the type of signals, detectors are placed and used. The primary function of an electronic detector is to convert the signal into digital images. Here we have discussed some detectors used in the signal collection and conversion of the signal to images.

7.2.5.1 Everhart-Thornley (E-T) Detector

This detector has the potential to distinguish secondary electrons (SE) and backscattered electrons (BSE). However, in SEM, this detector is used only to obtain secondary electron images, and for backscattered images, a different detector is appointed. All the electrical signals are amplified. The computer and knobs can control the brightness and contrast of images. The quantity of signal is maintained by changing the potential. At negative values, the E-T detector acts as a backscattered detector. E-T detector has amplified signals, minimum noise, more life, and is available at low cost.

7.2.5.2 Through-the-Lens (TTL) Detector

Some indirect secondary electrons and backscattered electrons devalue the SE image resolution. While working on this problem, the TTL detector comes into use. TTL detector helps to get a high-resolution image. The detector is used with a scintillator bias of 10 kV. The instrument contains a high signal-to-noise ratio. The utmost features of TTL detector are:

- It is highly efficient in collecting high-resolution SE signals without depending on emission direction.
- Instrument reduces the BSE images.

Whenever high magnification is required, low beam energy can be used. When using low beam energy, short working distances must be prioritized. This detector can also be used to identify cavities or voids.

7.2.5.3 Backscattered Electron Detector

(a) Solid-state diode (SSD) detector is a well-known BSE detector made up of p–n junction. The need for a BSE detector in SEM is that the energy of backscattered electrons is relevantly high than that of secondary electrons. In that case, the E–T detector is used for SE (having energy ~10 ev), while the BSE detector is for the backscattered electron (having energy in keV). To increase the solid angle of collection, BSE must be fixed directly below the pole piece above the specimen. The contrast in the backscattered image depends on the detector's sensitivity to the number and energy of electrons escaping the samples. Even though a solid-state BSE detector has low cost and minimum space is required, its response time is slow.

(b) Scintillator BSE detector is another BSE detector that uses a scintillator, light guide, and photomultiplier. The detector's working principle and mounting place are the same as above. This detector overcomes the limitation of the SSD-BSE detector, i.e., it has a faster response time, thus giving quick scan rates. The only restriction is that the detector is quite heavy and requires large spacing.

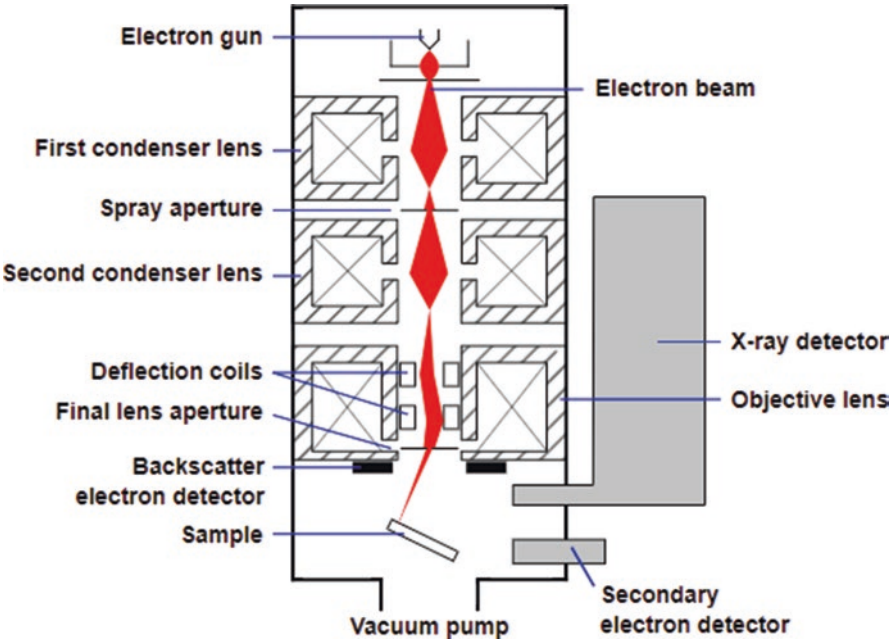

Fig. 7.9 Schematic of components of electron column and specimen chamber [1]

(c) The third type of detector is a parallel and electron multiplier named the channel plate detector. This detector is thin and can be placed between the specimen and the objective lens to resolve the limitations of both the above detectors. This detector can detect secondary electrons as well as backscattered electrons. The multiplier inside the detector is capillaries where secondary electrons fall off (Fig. 7.9).

7.2.6 Image Display

The electrons from the electron gun are focused onto the probe with the help of electromagnetic lenses. The electron beam pierces into the specimen and, as a result, generates secondary electrons, backscattered electrons, and X-rays. These output signals are gathered by detectors and produce images on the monitor screen of the display unit. Previously, the images appeared on CRT and were captured by a camera. Nowadays, the image can be recorded as a digital file on a computer.

7.3 Sample Preparation

In general, SEM can be used to analyze any material such as ceramics, biological samples, concrete, metals, and composites. So a generalized approach to preparing the sample for SEM is presented here. The following procedure can be modified

according to the nature and type of the sample that is to be analyzed. A total of six steps are presented here, which can be adjusted according to the need and category of the sample to which the specimen belongs. The generalized steps are as follows:

1. Cleaning the surface of the sample
2. Stabilizing the sample
3. Rinsing and dehydrating the sample
4. Drying the sample
5. Mounting the sample
6. Coating the sample

1. *Cleaning of sample surface*: The proper cleaning of the surface of the sample is essential because the surface may contain a variety of unwanted deposits such as dust, residue, or other contaminants, depending on the source of the material and the environment in which the sample has been prepared. Also, the experiment conducted before the preparation of the sample for SEM plays an essential role in this process.
2. *Stabilizing the sample*: Hard, dry materials such as wood, bone, feathers, dried insects, ceramic powders, composites, and metal or shells can be examined with little further treatment, but living cells, tissues, as well as whole soft-bodied organisms, usually require chemical fixation to preserve and stabilize their structure. Perfusion and microinjection, immersions, or vapors with various fixatives such as aldehydes, osmium tetroxide, tannic acid, or thiocarbohydrazides are used for fixation.
3. *Rinsing and dehydrating the sample*: After stabilization, rinsing of biological samples is done (ceramic powders, metals, and other complex samples do not need this step generally) to remove the excess fixative. Then the dehydration process of a biological sample is done very carefully. It typically uses a graded series of acetone or ethanol, which can ruin the sample if not done correctly.
4. *Drying the sample*: The scanning electron microscope operates in a vacuum. Therefore, the sample must be dry; otherwise, it will be destroyed in the microscopic chamber. Air-drying sometimes causes collapse and shrinkage of the sample, so this is commonly achieved by replacing water in the cells with organic solvents such as ethanol or acetone. Many people use a procedure called Critical Point Drying (CPD) as the gold standard for SEM specimen drying. Carbon dioxide is removed after it transitions from the liquid to the gas phase at the critical point, and the specimen is dried without any structural damage.
5. *Mounting the sample*: After the sample has been cleaned, fixed, rinsed, dehydrated, and dried using an appropriate procedure, it must be mounted on a holder that can be inserted into the scanning electron microscope. Samples are typically mounted on metallic (aluminum) stubs using double-sided conductive tape (usually carbon tape). It is essential to decide the best orientation of the sample on the mounting stub before attaching it. Reorienting the sample is difficult and can lead to significant damage to the sample.
6. *Coating the sample*: The idea of coating the specimen is to increase its conductivity in the electron microscope and to prevent the build-up of high voltage charges on a nonconducting sample. The coating prevents the charge-up phe-

nomenon of the sample by allowing the extra charge on the surface to ground through the coated conducting film. All metals are conducting in nature, so they require no coating before being used. Typically, specimens are coated with a thin layer of approximately 20–30 nm of a conductive metal (e.g., gold, gold–palladium, platinum, osmium, and tungsten).

In order to analyze solid samples, such as metals, polymers, and pellets, using SEM, the following criteria should be satisfied:

1. The surface area of the sample to be analyzed should be adequately exposed. For this, the sample is cut into a suitable size for the sample stage, and its surface is put on the top. But if we want to see the sample's internal structure, then a cross-section is taken for the proper study.
2. For solid samples such as pellets or metals, the sample is fractured to look at the cross-section of the sample. For devices such as semiconductors (which are grown or cultured on a single crystal such as that of Si or GaAs), the specimen is fractured in a specific direction due to the cleavage property of the single crystal. The obtained cross-section is a flat surface that can easily show us the properties we are looking for.
3. A cross-section can be easily made using liquid nitrogen dipping for soft samples like polymers. For this, a small cross-section of the polymer sample is cut using a razor/surgical blade, and then it is dipped in liquid nitrogen. This step instantly freezes the sample cross-section, which is then mounted on the sample stage for further study.
4. For some metal/mineral samples, mechanical polishing is required to view the sample's surface correctly, and for this, the sample is fixed in a resin and then polished. The abrasives are changed from rough to fine in this process, giving the specimen a mirror-like surface. This mirror-like surface is viewed using back-scattered electrons, providing an excellent image having different contrast (i.e., dark and bright regions) showing the presence of different phases in the sample.
5. Powder samples are analyzed by sprinkling them on conducting tape (usually double-sided carbon tape) and then coating them with a thin metal layer. Or sometimes, the powder is dispersed in an organic medium such as DI water/ethanol/acetone and then dropped on a silicon wafer/aluminum foil and dried. It is coated using a metal sputter unit and examined under SEM.

7.4 Image Acquisition and Processing

An image can be easily captured using SEM; however, specific points play an essential role in picture acquisition.

7.4.1 Beam Specimen Interaction

The electron beam can be generated through different emission guns. The beam thus passes through various components and strikes the specimen. Electrons deflect by

elastic and inelastic scattering when the electron reaches the sample. As a result of inelastic scattering, secondary electrons are generated, and due to elastic collision, backscattered electrons are produced.

(a) *Backscattered electrons*: If the scattering angle of the electron beam is more than 90°, it will produce backscattered electrons. The energy of the backscattered electron will be the same as that of the primary beam of electrons. Its resolution is 1000 nm.
(b) *Secondary electrons*: If the scattering angle of the electron beam is less than 90°, it will produce secondary electrons. They are easily bound and have energy less than 50 eV. They provide topographical information about the sample (Fig. 7.10).

Auger electrons are low-energy electrons and depict the chemical nature of the specimen. The Cathodoluminescence effect occurs when the energy of electrons is converted into light energy. The resolution of the cathodoluminescence detector and light microscope is similar after both types of X-rays, i.e., characteristic X-ray and bremsstrahlung X-rays, which are detected using an energy dispersive X-ray detector.

7.4.2 Image Disturbances

Lack of alertness and sometimes insufficient knowledge to operate SEM may lead to some failures in producing good quality images by SEM. This may also occur

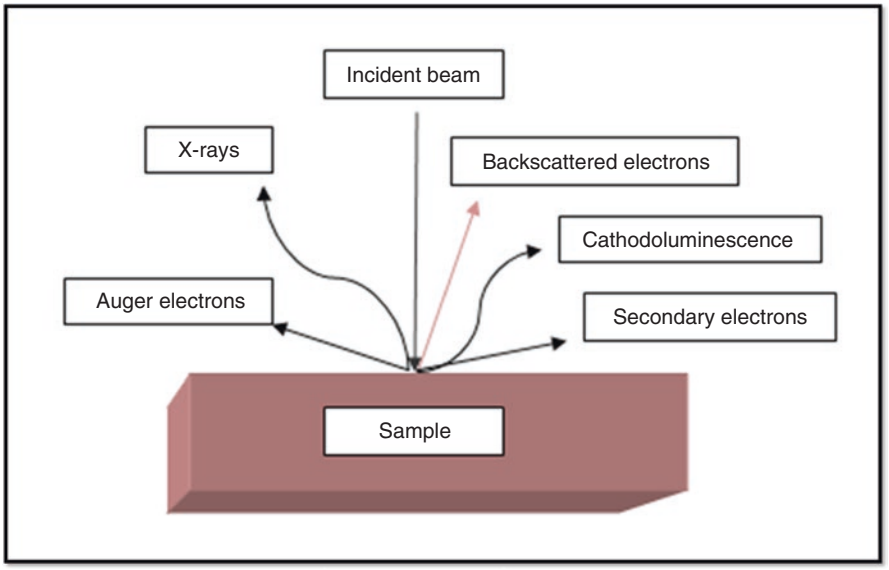

Fig. 7.10 Types of electrons produced by electron–sample interaction [9]

due to improper sample preparation. Disturbances in image acquisition can be rectified by applying suitable methods to improve them. Here, we discuss some of the measures to enhance image quality and how to get a fine surface structure [3].

(a) *Effect of accelerating voltage*: The voltage difference between anode and filament is accelerating voltage, adjusted from 200 V to 30 KV. Opting for a correct value of this voltage is necessary to resolve chromatic aberration, edge effect, etc. Thus, it is observed that in order to get a high-resolution image, the operating voltage must be high. Lower voltages are only acceptable for soft samples such as polymers [13] (Fig. 7.11).
(b) *Effect of working distance and spot size*: Working distance or spot size greatly impacts the image resolution. The working distance is inversely proportional to the image's resolution, whereas spot size is generally responsible for contrast and brightness. In order to get a minute spot size, higher brightness is needed (Fig. 7.12).

7.4.3 Analysis and Processing

Several methods for image recording and processing the data collected using SEM are discussed below [14].

7.4.3.1 Observing and Recording Using Cathode Ray Tube

SEM image is usually shown on a cathode ray tube (CRT). Most of the time, instruments have two separate tubes, i.e., one with a green-yellow emission for human eye sensitivity and a long luminescence decay time for visual observation. The other has a blue emission and a short decay time for recording micrographs with a film camera. Image time can range from 50 frames/s to 1/10th for visual observation and can be expanded to a few minutes. These long recording times are required to increase the signal-to-sound ratio. In order to resolve the rapid changes in the sample structure, image frequencies of 300 images/s were obtained. Additional

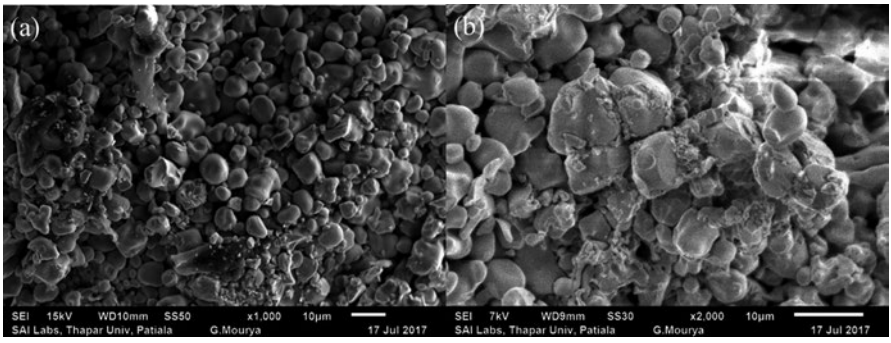

Fig. 7.11 Sample under (**a**) 15 kV accelerating voltage and (**b**) 7 kV accelerating voltage

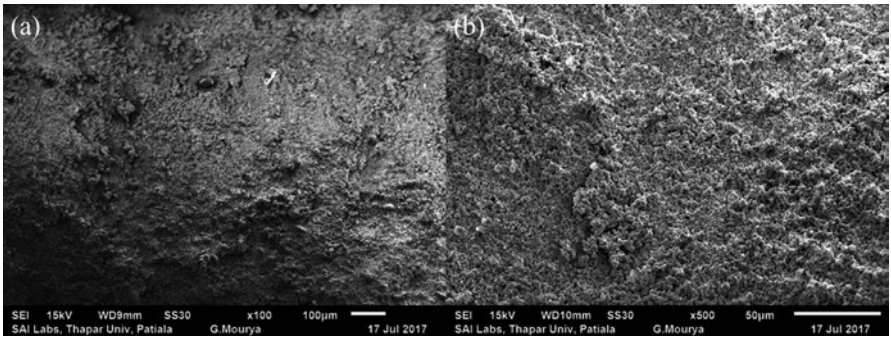

Fig. 7.12 Sample under working distance of (**a**) 9 mm and (**b**) 10 mm

nonlinearities can be introduced during the photographic recording of the CRT image and photographic processing in the darkroom. These problems can be avoided by using digital image acquisition discussed in detail later in the text.

The number of lines per frame can be increased from one line for generating a line-scan as an oscilloscope trace, up to 1000–2000 lines per frame to record an image, and it is assumed that a frame contains pixels of the order 10^5–10^6 pixels.

7.4.3.2 Digital Signal Processing Method

For any quantitative work requiring the intensity of the stored image, it will be more practical to acquire and store the picture digitally. Different image processing procedures may then be performed without repeated sample scanning, as required for analog signal processing methods. Adjusting an analog-to-digital converter (ADC) to the variable acquisition rates used to observe and record an image is not easy.

Therefore, it is much better to let the computer decide and produce signals for the x and y scan coils itself so that the speed of scanning from point to point is administered by the speed of the ADC and the data acquisition and storage rates. On the other hand, the digital image is temporarily stored in the SEM to generate a static image on the CRT and easily be transferred to the computer. Commercial slow-scan cards are available for recording 4096 × 4096 pixels at a resolution of 12–14 bits. The noise in an acquired image can be decreased quickly by using an integrated amplifier with a capacitor in the feedback loop and, on the other hand, a sample-and-hold amplifier for the period during which the capacitor is discharging between the readings of two pixels by averaging out over one sampling interval per pixel. For a CRT photograph recording, averaging many scans is not helpful because the scan can shift during the long recording time. Using a single scan with a longer sampling time per pixel is better than dividing it into shorter runs.

Digital image processing can be performed on a small microcomputer when only the most basic procedures are required, due to which they vary in cost and flexibility. After acquiring the image, a difference should be made between image enhancement, restoration, and analysis. Image enhancement procedures usually involve manipulating contrast and intensity levels and improvement of contours. It is a key

advantage of digital image processing that it no longer requires scanning the sample several times to adjust the black level and intensity to accurately record the image within the intensity range of the CRT and the photographic emulsion. The maximum signal level should be controlled only when its value exceeds 256 gray levels or more.

The first step is to examine the image's histogram, in which a curve represents the rate of occurrence of pixel strengths. Figure 7.13a, b shows the SE micrograph of a ceramic powder and a histogram of their intensities. At low intensities, when pixels are absent, we can set a cursor in the histogram to subtract this level (black/dark level). Another cursor can be positioned at the maximum intensity, expanding the intensity scale.

Image processing can also help record images with a multiple detector system to reconstruct the surface profile from the dependence of the SE or BSE signals on surface tilt and azimuthal angles or map the mean atomic number from the support of the backscattering coefficient on atomic number.

An extensive application of image analysis is stereology. For example, the ratio of the areas of four phases (features) in polished sections is equal to the ratio of their volumes, i.e.:

$$A1 : A2 : A3 : A4 = V1 : V2 : V3 : V4$$

where A1, A2, A3, and A4 are the areas, and V1, V2, V3, and V4 are the volumes of those particular phases.

Even if analog signal processing methods have been almost entirely replaced by digital image processing, many still examine analog techniques, some of which have been transformed into digital processing programs.

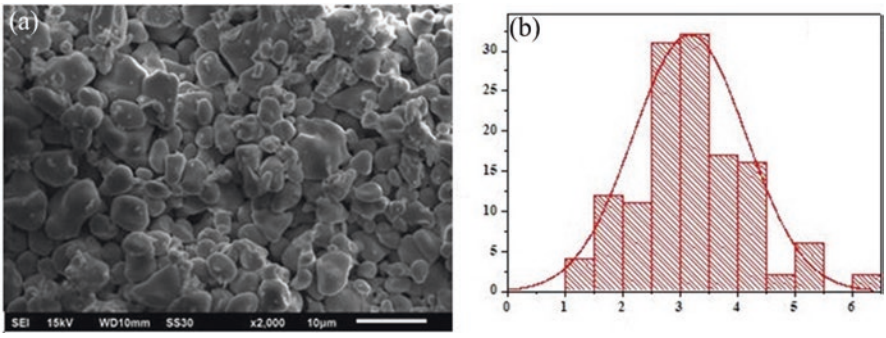

Fig. 7.13 Examples of digital image processing showing (**a**) original SE micrograph of a ceramic powder and (**b**) histogram of different intensities

7.5 Applications and Uses

The term nanoscience has gotten its speed in the last few decades. The signal analysis, which results from the interaction of specimens and electron beam SEM is being used. The specimen information is obtained in the range of nanometers (Auger electrons) and 5 μm (characteristic X-rays). With the help of SEM, one can get the following types of contrast:

- *Topography*: It depicts the texture of the specimen. The topographical feature of any material can also be related to its materialistic properties.
- *Image Morphology*: The image morphology involves the ductility, strength, reactivity, etc., of samples. The shape and size of particles can observe all these features.
- *Image Composition*: Any compound is made up of elements. Different elements have different behaviors and, when they combine, they show different properties. All the properties such as melting point, reactivity lie in this category.
- The arrangement of atoms can be easily identified by getting crystallographic information. The crystallographic information also reveals the electrical properties of metals.
- In order to map grain orientation or crystallographic orientation, SEM can be used. It also gives information like heterogeneity.

  Other than these above applications, there are some other applications of SEM:
- *Forensic Applications*: Laboratories in forensic departments use SEM to examine evidence like nails, ink, fibers, gunshot residue, paint, hair, surface fractures, and jewelry articles. In the case study, careful classification and discrimination of evidence material must be performed.
- *Nanowires for gas sensing*: The SEM technique is used to understand gas sensing behavior. Researchers are continuously improving the fabrication methods to use nanowires as gas sensors.
- *Biological Sciences*: Entomological sciences offer the study of cells and tissue at the microscopic level. In order to study at the microscopic level, SEM is being used. Various parts use SEM for vaccination testing, genetic studies, detecting the changes in species with changing weather conditions, identifying and studying new bacteria and viruses, and comparing tissue samples.
- *Soil and Rock Sampling*: Geological departments need to study the morphology of samples. The morphological study gives information about weathering process.
- The microanalysis of rocks and soil gives information on the composition of elements.
- To observe the compositional difference, BSE imaging is used.
- SEM also plays a vital role in the identification of ancient human artifacts.
- To study the toxicity in soil.

7.5.1 Advantages of SEM

1. The digital image resolution is 15 nanometers, giving microstructural information, including fracture, grain boundaries, and corrosion.
2. The instrument works with rapid speed.
3. The data produced is in digital form.
4. This analysis is easily applicable in identifying the thickness of the coating and particle size.
5. The instrument requires fewer measures for sample preparation.
6. SEM, when used with Electron Dispersive Spectroscopy (EDS), can analyze the specimen qualitatively as well as quantitatively.

7.5.2 Limitations of SEM

1. The foremost limitation of SEM is that it is expensive.
2. The SEM is quite a bulky instrument and needs ample space.
3. To operate SEM, a specially trained operator is required.
4. It carries a minute risk that the electrons that scatter will produce radiations.
5. When placed as a sample, insulators have to be coated with gold or carbon, which leads to artifacts.

Acknowledgments

1. Figures 7.3 and 7.9 lie under CC-BY-SA licensed documents, and the authors highly acknowledge Creative Commons for the same.
2. The authors are thankful to SAI labs, Thapar Institute of Engineering and Technology, Patiala for providing SEM images used in Sect. 7.4.

References

1. Kriss TC, Kriss VM (1998) History of the operating microscope: from magnifying glass to microneurosurgery. Neurosurgery 42(4):899–907
2. Oatley CW (1982) The early history of the scanning electron microscope. J Appl Phys 53(2):R1–R13. http://dx.doi.org/10.1063/1.331666
3. Ul-Hamid A (2018) A beginners' guide to scanning electron microscopy. Springer. https://doi.org/10.1007/978-3-319-98482-7
4. Smith KCA (1956) PhD Dissertation, University of Cambridge, Cambridge, UK
5. Everhart TE, Thornley RFM (1960) Wide-band detector for micro-microampere low-energy electron currents. J Sci Instr 37(7):246–248
6. Wells OC (1960) Correction of errors in stereomicroscopy. Br J Appl Phys 11:199–201
7. Pease RFW (1963) PhD Dissertation, University of Cambridge, Cambridge, UK
8. Pease RFW, Nixon WC (1965) High resolution scanning electron microscopy. J Sci Instr 42:31–35
9. Reichelt R (2007) Scanning Electron Microscopy. In: Hawkes PW, Spence JCH (eds) Science of Microscopy. Springer, New York, NY. https://doi.org/10.1007/978-0-387-49762-4_3
10. Reimer L (1985) Scanning Electron Microscopy. (Springer, Berlin)

11. Reimer L (1993) Image Formation in Low-Voltage Scanning Electron Microscopy,vol TT12. (O'Shea, D.C., ed.). (SPIE Optical Engineering Press, Bellingham & Washington)
12. DeVore W, Berger SD (1996) J Vac Sci Technol B 14:3764
13. Duncumb P, Shields PK (1966) Effect of critical excitation potential on the absorption correction. In: McKinley TD, Henrich KFJ, Wittry DB (eds) The electron microprobe. Wiley, New York, p 284
14. Goldstein J (1975) Practical Scanning Electron Microscopy: Electron and Ion Microprobe Analysis, Springer-Verlag US 1975

8 Recent Updates on Methods, Applications, and Practical Uses of Scanning Electron Microscopy in Various Life Sciences

S. Kathirvel, Selvasankar Murugesan, and Akash Marathakam

Abstract

The current abstract explores the basic concepts, fundamental principles, and advantages of SEM (Scanning Electron Microscope) over other microscopic techniques. SEM is commonly used in physical, materials, and chemical sciences. It is now widely accepted and applied in medical studies, biological science, and pharmaceutical sciences. This wide range of SEM utility in biological areas has opened up more avenues and opportunities to understand and visualise the unknown facts and concepts in biomedicine. Furthermore, advances in SEM in various life sciences have aided in the improved imaging and study of a variety of biological specimens. The progress of SEM in various life sciences is thoroughly discussed in this chapter. Apart from its life science applications, the value of SEM in nanotechnology, microchip production, and digital artwork is briefly touched upon.

Keywords

Scanning electron microscope · Electron spectroscopy · Biological · Life science

8.1 Introduction

Electron microscopes use an energetic electron beam to examine objects on a fine scale. The concept of electron microscope was developed due to the limitations of light microscopes by the physics of light. This theoretical limit had been achieved

S. Kathirvel · A. Marathakam (✉)
Department of Pharmaceutical Chemistry, National College of Pharmacy, Calicut, India

S. Murugesan
Research Department, Sidra Medicine, Doha, Qatar

S.-K. Kamaraj et al. (eds.), *Microscopic Techniques for the Non-Expert*,
https://doi.org/10.1007/978-3-030-99542-3_8

by the 1930s, and there was a scientific urge to observe the tiny details of organic cell inner structures. Using a directed beam of high-energy electrons, the scanning electron microscope (SEM) generates a variety of signals on the surface of solid specimens. Electron–sample interactions produce signals that provide information about the sample's exterior morphology (texture), chemical composition, and crystalline structure, as well as the orientation of the materials. Data is collected over a defined section of the sample's surface in most circumstances, and a 2-dimensional picture is generated to demonstrate spatial changes in these qualities. The traditional SEM approach (magnification ranging from 20× to approximately 30,000×, spatial resolution of 50–100 nm) will image areas ranging from approximately 1 cm to 5 microns in width in a scanning mode [1]. The SEM may also conduct studies of specific point locations on the sample; this method is particularly effective for qualitative or semi-quantitatively identifying chemical compositions, crystalline structure, and crystal orientations [2].

8.2 Fundamental Principles of Scanning Electron Microscopy

In Scanning Electron Microscopy (SEM), impacting electrons decelerate in the solid sample; they release kinetic energy, which is dissipated as a variety of signals induced by electron–sample interactions. Secondary electrons, backscattered electrons (BSE), diffracted backscattered electrons (EBSD), and photons are among these signals [3]. For imaging samples, secondary electrons and backscattered electrons are widely used: Backscattered electrons are ideal for illustrating compositional contrasts in multiphase samples, while secondary electrons are best for displaying sample shape and topography. Inelastic collisions of incident electrons with electrons in isolated orbitals (shells) of atoms in the sample emit X-rays. As excited electrons return to lower energy states, they produce X-rays with a specific wavelength. As a result, each element in a mineral that is 'excited' by the electron beam produces distinct X-rays. SEM analysis is called 'non-destructive'. The term 'non-destructive' refers to the fact that the X-rays produced by electron interactions do not cause the sample to lose volume, allowing for many analyses of the same materials. By focusing electron beams, SEM creates high-resolution, three-dimensional images. SEMs are employed in a wide range of industries, businesses, and academic institutions. From cutting-edge production procedures to forensic applications, the contemporary SEM has a wide range of practical uses. Topography, morphology, and composition are all demonstrated in these photographs.

8.3 Comparison Between Electron and Optical Microscopy

The difference between electron and optical microscopy can be found in the name itself, which is the type of beam applied to the sample [4]. A beam of electrons, rather than a beam of light, is used in SEMs.

Following are the three types of electron sources found in SEM:

Thermionic filament—A tungsten filament is heated within the microscope until it releases electrons. Tungsten filaments operate at a white-hot temperature, which causes them to slowly evaporate and eventually break, contaminating the electron column's upper reaches. Depending on the vacuum, a Tungsten source has an average lifespan of roughly 100 hours.

Field emission gun—Create a strong enough electric field to drive electrons away from their atoms. Because it provides high-resolution images, this is the most popular option in SEMs, but it demands a vacuum design, which can be costly.

Cerium Hexaboride Cathode—Tungsten is ten times brighter, resulting in a greater signal-to-noise ratio and resolution. A CeB6 source typically has a service life of 1500 hours or more, which is more than 15 times that of Tungsten. A CeB6 source is utilized in the desktop Phenom SEM class of instruments.

8.4 Applications of SEMS

SEMs widely used in industrial, commercial, and in many research applications. The applications are enlisted as follows.

8.4.1 Materials Science

SEMs are used in materials science for testing, quality control, and failure analysis. Nanotubes and nanofibres, high-temperature superconductors, mesoporous structures, and alloy power are all studied with SEMs in modern materials science. SEMs have revolutionised nearly every materials science business, from aerospace to chemistry to electronics and energy. In materials research, SEM pictures with high resolution and magnification are useful for checking material quality and confirming that they are fit for purpose. They can also be used to predict and prevent material failure [5]. Close observation is required for research into the design of new materials to obtain a deeper understanding of the new material and its properties. Researchers have been able to analyse cell reactions to cryopreservation using SEM, which has led to the development of cryopreservation media that reduces damage from rapid freezing. SEM has been used to investigate the impact of antibiotics on bacterial morphology and ultrastructure in order to fully understand their mechanism of action.

8.4.2 Applications of SEM Towards Nanowires for Gas Sensing and Semiconductor Inspection

Researchers are investigating novel approaches to employ nanowires as gas sensors by refining existing fabrication methods and developing new ones [6]. Recent

advances in the usage of nanowires to produce new, very sensitive gas sensors have been made. Electron microscopy is essential for defining nanowires, measuring their gas sensing behaviour, and comprehending their activity in order to improve present gas sensor manufacturing procedures. Accurate topographical information is needed for semiconductors to work reliably. SEMs generate high-resolution three-dimensional images that allow for fast and accurate semiconductor composition measurements. SEMs are one of three important quality control tools used in almost all wafer manufacturing processes. Larger monitors (19 inches) have been shown to minimise visual exhaustion for inspectors conducting regular quality control checks. As the size of new electronics devices shrinks, SEM research into the effectiveness of new production and fabrication processes in the construction of these tiny electronics has become necessary [7]. Product designers are looking for methods to make products more intuitive, cost-effective, and power-efficient as the need for electronics in our daily lives grows. The Internet of Things (interconnected computing devices having unique identifiers that can transmit information without requiring human intervention, such as smart home gadgets) is growing at a breakneck pace.

8.4.3 Microchip Assembly Applications

In semiconductor production, SEMs are frequently utilised to acquire insight into the efficacy of modern processing and fabrication processes [8]. As sizes and materials increase smaller and smaller, as well as the ability of complicated self-assembling polymers, SEMs' high-resolution and three-dimensional capacity are vital to microchip design and development. As the Internet of Things (IoT) grows more widespread in customers' and manufacturers' daily lives, SEMs will continue to play a vital role in the design of low-cost, low-power chipsets for non-traditional computers, and networked devices. Microchips are still an important part of daily life around the world, forming the foundation of every electronic subsystem. Manufacturers can achieve astonishing levels of finite detail and electronic density with new and emerging microelectronic systems, with smaller, lower-cost, and more efficient chipsets spearheading the next generation of networked devices. This presents its own set of difficulties. SEM imaging's extremely high resolution makes it ideal as a supplementary technique for microchip assembly, allowing for the three-dimensional magnifications required for advanced SEM applications on the microelectronics manufacturing line.

8.4.4 Forensic and Biological Applications

The Scanning Electron Microscope (SEM) is becoming increasingly significant in the realm of forensic investigation. Because of its capacity to study detail on a wide range of materials in an easily understandable manner, from high to low magnification with an incredible depth of focus, the SEM has become an indispensable

instrument. With the ability to evaluate the elemental composition of even the finest features on specimens, definitive identifications of the origin of some materials can be made, adding to the chain of evidence. SEMs are used to discover evidence and gain new forensic understanding in criminal and other forensic investigations.

- Analysis of gunshot residue
- Jewellery inspection
- Bullet marking comparison
- Handwriting and print analysis
- Banknote authenticity examination
- Analysis of paint particles and fibres in traffic accidents
- Analysis of filament bulbs in traffic accidents
- Identification of firearms (bullet markings comparison)
- Banknotes that have been counterfeited
- Comparison of traces
- Non-conducting materials are examined
- Surface imaging with high resolution

SEMs use in forensic sciences allows researchers to analyse a broad variety of materials at high and low magnification without losing the depth of focus, allowing them to conclude, classify material sources, and add to a body of evidence in criminal and legal cases [9]. The desktop Phenom GSR instrument was developed with automated gunshot residue analysis in mind.

SEMs can be used on everything from insects and animal tissue to bacteria and viruses in biological sciences. SEM [10] is used in many fields of biology, including cell and molecular biology for studying cell morphology, microbiology for studying bacteria and viruses and their relationships with surfaces, each other, and other cells, and genetics for studying gene expression. Among the applications are:

- Determining how ecosystems are affected by climate change.
- Discovering new bacteria and dangerous strains.
- Vaccine trials.
- The discovery of new species.
- Genetics research.
- Failure investigation.
- A comparison of materials.
- Evaluation of the process.
- Corrosion and fatigue.
- Preparing the surface.
- Detection of contamination.
- Marketing of a product or a process.
- Quality assurance.
- Defect identification and classification.

8.4.5 Medical Science Applications

SEMs are used in medical research to compare blood and tissue samples to establish the origin of disease and the efficacy of treatments on patients (while contributing to the design of new treatments). The following are some examples of popular applications:

- Detecting different types of diseases and viruses.
- Helpful in testing new vaccines and drugs.
- For comparing tissue samples between patients in a control and test group.
- Testing samples during a patient's lifetime.

Reports on the use of SEM [10–12] in diagnosis are published regularly. These studies provide estimates of the utility of SEM in specific fields (heart, kidney, and skin pathology, for example), but they are usually only valid for a limited period. Because techniques are constantly evolving, it is difficult to predict whether SEM will have positive or negative effects.

In general, SEM [13–21] has a high value in the investigation of clinical specimens related to renal diseases, tumour processes, storage disorders, and infectious agent identification.

The so-called submicroscopic pathogens, such as virus particles (tobacco virus) and bacteria, were among the artefacts observed in the early days of SEM. SEM's [22] magnification power, as well as the ability to detect virus particles and families morphologically, were key factors in its adoption in virology.

8.4.6 Application of SEM in Nanotechnology

Starting with the last decade of the past century, Nanotechnology, nanoscience, nanoparticles, nanostructures, are extremely prevalent in the specialised literature of fundamental sciences, engineering, biology, medicine etc. [23, 24]. Nanoscience and nanotechnology aim to research, develop, and deploy materials, technologies, and systems that can control matter at nanometric or even atomic scales. The science and technology's dimensional range of development is 1–100 nm having consequences in all aspects of human activity in the near future. As a subject of nanoscience and nanotechnology development, this dimensional field has upper and lower boundaries. These limits may be considered differently in nanoscience and nanotechnology, though the causes may be the same. The lower limit in nanoscience, particularly in the case of nanomaterials, is typically fixed at roughly 1 nm. This is acceptable because the measured length limit is around 0.3 nm. Quantic-type phenomena of position in determination may occur below this detectable limit. The upper limit, conventionally set at about 100 nm, is given by the fact that above this limit the special properties of these types of materials do not manifest. The modification of the properties of the nanostructured materials is principally the consequence of the following factors: The number of atoms within the limits between the

grains is much higher (40–50%) than in the classical materials with polycrystalline structure. The appearance of quantic effects that begin to manifest within this dimension range. Nanotechnology encompasses ultra-precision processing, the creation of nanometric-scale machines, molecular devices, nanorobots, supercomputers, and applications in medicine and biology. In the nanoscale domain, quantum effects, which are insignificant at the macroscopic level, have a major impact on material characteristics and the behaviour of mechanical or electrical systems.

8.4.7 Scanning Electron Microscopy in Life Sciences

(i) Imaging with Highest Resolution at Low Voltages

Realised in the ZEISS Sigma and Gemini SEM families, the unique Gemini column, along with field emission (FE) technology, provides the best resolution and excellent contrast performance. The Gemini column produces good contrast images at low voltages, making it ideal for sensitive and non-conductive biological samples. The FE-SEMs can easily photograph ultrathin sections to produce TEM-like pictures with a resolution that can resolve even lipid bilayers. A huge range of sample carriers can be mounted in an SEM, overcoming the size and number limitations of a TEM grid and TEM grid holders, thus supporting the use of a large variety of samples. SEM-based imaging is well suited to investigating resin-embedded materials, which are common in many biological applications. Cutting the material into ultrathin slices is one method that could be used. Different types of SEM detectors, including the secondary electron (SE) detector, the backscattered electron (BSE) detector, and the STEM (scanning transmission electron microscopy) detector, may easily examine single or series ultrathin sections. Even at extremely low voltages, the SE and BSE detectors provide images with high resolution and contrast. With the limitation of TEM grids as sample carriers and the added benefit of loading up to 12 grids into the SEM, imaging sections on grids with a STEM detector provides the best resolution possible in a SEM. The use of indium tin oxide (ITO)-coated cover glasses or silicon wafers as sample carriers, on the other hand, allows for the imaging of huge numbers of serial sections in a FE-SEM at unparalleled speed for high throughput. Furthermore, the individual sections can be much larger, and typically, one section alone is similar in or even exceeds the size of a TEM grid. TEM grids are enabling access to much larger sample areas than ever before.

(ii) Topographical Imaging under Environmental Conditions

Modern scanning electron microscopes, such as the ZEISS EVO series, can image the surface topography of objects like insects and plants in real-world settings. The biological specimens can be examined in their original hydrated form, with increased pressures and water vapour revealing fine surface features without the artefacts typically come with dehydration.

(iii) 3D Imaging

Single pictures are two-dimensional snapshots of a complex three-dimensional situation. Volume data is required to completely comprehend compartmentalisation and functionality beyond the ultrastructure of the sample. ZEISS supports a wide range of methods for entering the 3D world. One option is ZEISS Array Tomography (AT): Here, a resin-embedded sample is cut into ultrathin serial sections. The thickness of the sections determines the z-resolution of this z-stack, and the sequencing of the sections determines the z-information of a future computationally rebuilt 3D data set. The pieces' thickness ranges from 40 to 100 nanometres. A tape-collecting ultramicrotome (ATUMtome) can be used to manufacture and collect sections automatically on a continuous tape, making life considerably easier. Likewise, data acquisition, i.e., the imaging of the resulting series of sections, is a highly automated process with ZEISS AT. After that, the 2D photos are converted into a 3D model. Furthermore, 3D SEM data sets can be connected with 3D light microscopic data sets produced with the ZEISS AT solution for fluorescence light microscopes of the same sample. The serial sections can be saved and used for other imaging and labelling investigations in the future.

(iv) Large Area Imaging

ZEISS offers a variety of large-area imaging systems that are both dependable and rapid. The ZEISS Atlas 5 software provides large-area imaging with high resolution and fast imaging speeds up to 32 k 32 k pixels (down to 25 ns dwell-time per pixel). Individual photos are then stitched together to create incredibly huge fields of vision. After image acquisition, the ZEISS Atlas 5 allows the user to effortlessly zoom through large image data from nanometres to centimetres, always at the highest resolution. If ultimate acquisition speed is required, the unique ZEISS MultiSEM—the world's fastest scanning electron microscope becomes the technology of choice. It is the first and so far, only commercially produced multibeam SEM that uses several electron beams and related detection channels in one electron optical column. When compared to single-beam SEMs, ZEISS MultiSEM accelerates the acquisition of SEM data by nearly two orders of magnitude. This meets the constantly growing demand for nanoscale-resolution imaging of huge and increasingly bigger areas or volumes, as well as the demand for fast electron microscopes that can photograph enormous areas or volumes at nanometre resolution.

(v) Imaging Under Near-to-Native Conditions

Freezing biological samples is an alternative to chemical fixation for sample preparation: The ultrastructure of cells and tissues is preserved during vitrification in liquid cryogens. There is no requirement for fixatives or resin embedding because the samples are entirely hydrated. ZEISS provides the essential equipment for transporting a cryo-preserved sample into an electron microscope. This method can also be used in conjunction with a cryo-light microscope. The stability of fluorophores under freezing conditions aids the correlative cryo-microscopy method. There's also no need to be concerned

about the loss of fluorescence or structural changes that heavy metals and chemical fixing, which are commonly employed to fix and stain specimens for electron microscopy.

(vi) Correlative Imaging

The use of a combination of imaging modalities, such as light and electron microscopy, can provide new knowledge of biological interdependencies. Functional data produced with a fluorescence microscope can be linked to structural data obtained with a scanning electron microscope. A sample's regions of interest can be recovered using different microscopes. The connection of ultrastructural information with analytical techniques such as Raman and EDX spectroscopy is one of the many conceivable combinations supported by ZEISS software solutions.

(vii) Application of Scanning Electron Microscopy in Microbiological Research

The research was done in order to find a promising vaccine for this sickness. To do so, the researchers matched proteins released by bacterial biofilms in vitro with human antibodies in vivo to develop a possible vaccine. The researchers next utilised a scanning electron microscope (SEM) to observe the growth of biofilm on human bone as well as cryo-SEM sections of Staphylococcus aureus isolation. This method facilitates understanding of the many interactions that take place between the bones and the biofilm, as well as between the bacteria themselves. While some researchers are working on a way to prevent biofilm formation, another group at Japan's National Institutes of Natural Sciences is utilising *Pseudomonas fluorescens* to identify the genes involved in biofilm formation. The researchers initially detected a messenger-secreting gene known as c-di-GMP, which plays a role in the formation of biofilm. They used a method based on transposons, which are sequences of DNA capable of changing their positions inside the genome. This allows them to alter genes and thus leads to silencing or overexpression of genes. Once the important gene was identified, it was muted and the biofilm-forming capacities of the modified bacterial strain were compared against the normal, Wild-type strain. The mutant-formed biofilm was found to be less than half the size of the Wild-type strain's biofilm, but there was no change in the number of cells. This meant that the reduction in biofilm size was related to the mutant bacterial cell's capacity to multiply and form a biofilm, rather than its ability to multiply and produce a biofilm. SEM imaging was used on both strains to further confirm this notion. The varied sizes of bacteria were then measured using ParticleMetric software, and a clear numerical comparison was made. The mutant strain was found to be 25–30% smaller than the Wild-type strain.

(viii) Application of scanning electron microscope in microbiology and diagnosis of infectious disease:

Electron microscopy proved crucial in identifying the causal agents of infectious illnesses in early research [25–27]. It is still an important technique for diagnosing diseases and testing for microorganism identification. Negative staining for transmission electron microscopy (TEM) has long been considered the 'gold standard' for imaging microbiological samples in diagnostic

virology. Negative-stain TEM, on the other hand, necessitates a sufficient concentration of bacterial cells or virus particles, as these are adsorbed to a thin support surface. As a result, bacteria must be grown to a higher level, which is often unachievable with patient specimens or agents that are not able to persist. As a result, for many sorts of microbiological investigations, electron microscopy has historically had low test sensitivity. For TEM4,5, a minimum concentration of 105–106 particles/ml is required for the detection of agents such as poxviruses or polyomaviruses in patient specimens. Virus identification employing culture or nucleic acid testing, on the other hand, typically ranges between 1 and 50 particles per assay. Because of recent advancements in filtration procedures, virus detection by TEM and SEM can now be done with as few as 5000 total particles per sample. Furthermore, electron microscopy can be used to determine the type of microbe present, typically down to the genus level, allowing additional specialised tests (such as primers or specific antibodies) to be used to fully identify the agents present. In circumstances when a novel or developing pathogen is being researched with no a priori knowledge of the sort of agent present, electron microscopy is an ideal 'catch-all' approach that provides a 'open view'. The scanning electron microscope (SEM) can be used to expose morphological aspects of isolated organisms as well as diagnose them, but difficulties with specimen preparation methods have limited its usage in routine microbiology in the past. Polycarbonate filters of extremely high quality are now available: the optimal pore size can be adjusted to collect any virus or bacterial species (the pores can be as small as 10 nm, less than the smallest viruses). SEM may observe viruses and bacteria on their surfaces with these filters. Obtaining high-resolution SEM pictures of bacteria has two major challenges. To begin, a conducting surface is required to obtain enough contrast and to decrease charge for minute organic particles such as bacteria and viruses at magnifications greater than 1000×. Second, for the optimum imaging performance in the SEM, biological specimens have historically needed to be dried. When a moist specimen is placed in the microscope, operation under high vacuum conditions tends to dry the specimen out quickly. Both of these conditions have the potential to degrade microscope performance by reducing contrast and resolution. Drying is a concern during SEM observation, as it frequently results in the specimen collapsing, shrinking, and distorting, even after chemical fixing. Previously, a variety of procedures for dehydrating specimens prior to SEM viewing were developed, including solvents, critical point drying, and freeze drying.

8.4.8 Miscellaneous Applications

- In the disciplines of industrial application and analysis, quality control at microscopic scales is becoming increasingly relevant. Magnified depictions of materials and artefacts aid in putting our environment into context.

- SEM is a type of analytical study that captures items as small as 15 nanometres using high-resolution pictures. In scanning electron microscopy, images are created by scanning samples with a focused electron beam. The electrons interact with the atoms on the surface of the sample, gathering data about its topography and composition. All use scanning electron microscopy to analyse the surface composition of components and products.
- Scanning electron microscopy should be used by companies involved in product development or manufacturing to understand more about the composition and topography of products and components. For example, certain items, such as stainless steel, must be uniformly coated with particular chemicals for optimal performance. Scanning electron microscopy can detect cracks, defects, and pollutants on the surfaces of coated items.
- Small particle industries, such as cosmetics, can employ SEM [24] to learn more about the form and size of the small particles they work with. Large or jagged particles, for example, may not flow or mix as well as small, round particles. The uniformity and performance of a product might be harmed by particles of the wrong size or shape.
- Scanning electron microscopy can be used to detect problems with particle size or form before items reach the consumer. Finally, scanning electron microscopy is frequently used to analyse small components such as fine filaments and thin films by companies that create goods with small or microscopic components. Weathering processes and sample morphology can be determined using geological sampling and a scanning electron microscope [11].
- Some versions of SEM are more realistic than others. In the creation of digital artworks, SEM micrographs were utilised. Landscapes with strange and familiar visual subjects are created using high-resolution three-dimensional photographs of various materials [28–30].

8.5 Conclusion

The ability of a scanning electron microscope (SEM) to produce high-resolution images can provide insight into a wide range of subjects, making SEMs invaluable resources in many fields. Scanning electron microscopy has helped scientists and non-scientists of all ages learn more about the world around them for decades. Scanning electron microscopy is used by scientists in a variety of domains to better analyse the structure and topography of man-made and naturally occurring materials. For example, Biologists now can understand a lot more about minute creatures like bacteria and viruses because of SEM. Scanning electron microscopy is frequently used by geologists to understand more about crystalline structures. Scanning electron microscopy produces crisp, clear, and stunning high-resolution images, making it a great tool for both teaching and scientific research. SEM is also used in a variety of industrial settings. Microelectronics, semiconductors, medical devices, general manufacturing, insurance, and litigation assistance, as well as food processing.

References

1. Stokes DJ (2008) Principles and practice of variable pressure environmental scanning electron microscopy (VP-ESEM). Wiley, Chichester. ISBN: 978-0470758748
2. McMullan D (2006) Scanning electron microscopy 1928–1965. Scanning 17(3):175–185. https://doi.org/10.1002/sca.4950170309
3. McMullan D (1988) Von Ardenne and the scanning electron microscope. Proc R Microsc Soc 23:283–288
4. Knoll M (1935) Aufladepotentiel und SekundäremissionelektronenbestrahlterKörper. ZeitschriftfürTechnischePhysik 16:467–475
5. vonArdenne M. Improvements in electron microscopes. GB 511204, convention date (Germany) 18 February 1937
6. vonArdenne M (1938) Das Elektronen-Rastermikroskop. TheoretischeGrundlagen. ZeitschriftfürPhysik (in German) 109(9–10):553–572. https://doi.org/10.1007/BF01341584
7. vonArdenne M (1938) Das Elektronen-Rastermikroskop. PraktischeAusführung. ZeitschriftfürTechnischePhysik (in German) 19:407–416
8. Zworykin VA, Hillier J, Snyder RL (1942) A scanning electron microscope. ASTM Bull 117:15–23
9. McMullan D (1953) An improved scanning electron microscope for opaque specimens. Proc IEE – Part II: Power Eng 100(75):245–256. https://doi.org/10.1049/pi-2.1953.0095
10. Oatley CW, Nixon WC, Pease RFW (1965) Scanning electron microscopy. Adv Electronics Electron Phys 21:181–247
11. Smith KCA, Oatley CW (1955) The scanning electron microscope and its fields of application. Br J Appl Phys 6(11):391–399. https://doi.org/10.1088/0508-3443/6/11/304
12. Wells OC (1957) The construction of a scanning electron microscope and its application to the study of fibres. PhD Dissertation, Cambridge University
13. Malick LE, Wilson RB, Stetson D (1975) Modified thiocarbohydrazide procedure for scanning electron microscopy: routine use for normal, pathological, or experimental tissues. Biotechnic Histochem 50(4):265–269. https://doi.org/10.3109/10520297509117069
14. Conrad C, Jones EL, Newsome SD, Schwartz DW (2016) Bone isotopes, eggshell and Turkey husbandry at Arroyo Hondo Pueblo. J Archaeol Sci Rep 10:566–574. https://doi.org/10.1016/j.jasrep.2016.06.016
15. Jeffree CE, Read ND (1991) Ambient- and low-temperature scanning electron microscopy. In: Hall JL, Hawes CR (eds) Electron microscopy of plant cells. Academic, London, pp 313–413. ISBN: 978-0-12-318880-9
16. Karnovsky MJ (1965) A formaldehyde-glutaraldehyde fixative of high osmolality for use in electron microscopy (PDF). J Cell Biol 27(2):1A–149A
17. Kiernan JA (2000) Formaldehyde, formalin, paraformaldehyde and glutaraldehyde: what they are and what they do. Microscopy Today 2000(1):8–12. https://doi.org/10.1017/S1551929500057060
18. Russell SD, Daghlian CP (1985) Scanning electron microscopic observations on deembedded biological tissue sections: comparison of different fixatives and embedding materials. J Electron Microsc Tech 2(5):489–495. https://doi.org/10.1002/jemt.1060020511
19. Chandler DE, Roberson RW (2009) Bioimaging: current concepts in light and electron microscopy. Jones and Bartlett Publishers, Sudbury. ISBN: 9780763738747
20. Faulkner C et al (2008) Peeking into pit fields: a multiple twinning model of secondary plasmodesmata formation in tobacco. Plant Cell 20(6):1504–1518. https://doi.org/10.1105/tpc.107.056903
21. Wergin WP, Erbe EF (1994) Snow crystals: capturing snow flakes for observation with the low-temperature scanning electron microscope. Scanning 16(Suppl. IV):IV88
22. Suzuki E (2002) High-resolution scanning electron microscopy of immunogold-labelled cells by the use of thin plasma coating of osmium. J Microsc 208(3):153–157. https://doi.org/10.1046/j.1365-2818.2002.01082.x

23. Goldstein GI, Newbury DE, Echlin P, Joy DC, Fiori C, Lifshin E (1981) Scanning electron microscopy and x-ray microanalysis. Plenum Press, New York. ISBN: 978-0-306-40768-0
24. Seligman AM, Wasserkrug HL, Hanker JS (1966) A new staining method for enhancing contrast of lipid-containing membranes and droplets in osmium tetroxide-fixed tissue with osmiophilicthiocarbohydrazide (TCH). J Cell Biol 30(2):424–432. https://doi.org/10.1083/jcb.30.2.424
25. Everhart TE, Thornley RFM (1960) Wide-band detector for micro-microampere low-energy electron currents (PDF). J Sci Instrum 37(7):246–248. https://doi.org/10.1088/0950-7671/37/7/307
26. Hitachi Launches World's Highest Resolution FE-SEM. Nanotech Now. 31 May 2011
27. Takaku Y, Suzuki H, Ohta I, Tsutsui T, Matsumoto H, Shimomura M, Hariyama T (2015) A 'NanoSuit' surface shield successfully protects organisms in high vacuum: observations on living organisms in an FE-SEM. Proc R Soc Lond B Biol Sci 282(1802):20142857. https://doi.org/10.1098/rspb.2014.2857
28. Barnes PRF, Mulvaney R, Wolff EW, Robinson KA (2002) A technique for the examination of polar ice using the scanning electron microscope. J Microsc 205(2):118–124. https://doi.org/10.1046/j.0022-2720.2001.00981.x
29. Hindmarsh JP, Russell AB, Chen XD (2007) Fundamentals of the spray freezing of foods—microstructure of frozen droplets. J Food Eng 78(1):136–150. https://doi.org/10.1016/j.jfoodeng.2005.09.011
30. Ultra-high Resolution Scanning Electron Microscope SU9000

9 Transmission Electron Microscopy: A Powerful and Novel Scientific Technique with Nanoscale Resolution for Characterization of Materials

Navneet Kaur

Abstract

The electron microscopy has brought a revolution in the field of nanotechnology. Various electron microscopy techniques with unique possibilities are used to study morphology, topography, structures and different phases present in the materials. Transmission electron microscope (TEM) is a remarkable scientific tool for the imaging of materials at nanoscale. Ruska and Knoll invented the first TEM consisted of only two electromagnetic lenses for which Ruska got the Nobel Prize. As a result of this invention, it was realized that such lenses are capable to get magnified images at nanoscales. Later on in 1970, the best electron microscopes achieved the resolution of 3.5 Å with several technical improvements and optimizations. This achievement could resolve many columns of metal atoms such as oxide structures. The high resolution of sub-Å has been achieved with the use of advanced aberrations-corrected lenses. The modern TEM's are capable of attaining resolution of 1 Å at around 300 kV or even less than it can be achieved by using high accelerated energy of electrons. The high-resolution transmission electron microscopes (HRTEM) with high energy and spatial resolution provide the deep insight into almost all the atomic structures. The most important feature of TEM is that it works in both real and reciprocal space. This makes it a unique technique for imaging nanostructures. All samples must be prepared before TEM analysis in order to obtain accurate results. The sample should be very thin and have thickness around 100 nm so that the interaction with electrons should be weak. Thus, the high accelerated electron beam cannot damage the sample. The sample preparation technique for biological and non-biological materials is different. TEM has many applications and one can easily find out the structure, particle size, particle size distribution, elemental

N. Kaur, Ph.D. (✉)
Department of Physics, Baba Farid College,
Baba Farid Group of Institutions, Bathinda, India

S.-K. Kamaraj et al. (eds.), *Microscopic Techniques for the Non-Expert*,
https://doi.org/10.1007/978-3-030-99542-3_9

compositions and particle shape under observation using it. This technique indeed proved a boon for nanostructures analysis.

Keywords

Electron beam · Microscope · Resolution · Nanomaterials · Diffraction

9.1 Introduction

The advancement in technology has brought a revolution in the field of nanotechnology by introducing new techniques. These techniques use electron beam of high energy to gain insight into the morphology, topology, elemental composition, and structure of materials with higher resolutions. Electron microscopes have been proved a boon to nanotechnology for the analysis of nanomaterials. Transmission electron microscope (TEM) is a significant scientific equipment that determines structures at the nanoscale, provides information about their elemental compositions and lattice parameters with excellent image quality. It mainly probes nanostructures of a perfect crystal, defective structures, and biological entities such as viruses, DNAs by generating their 2D images. E. Ruska and M. Knoll were the first who built a transmission electron microscope that consisted of two electromagnetic lenses [1]. In 1986, E. Ruska got a Nobel Prize for his discovery of microscope. This discovery proved that magnified images of small objects can be produced using an electron beam and it serves the same purpose as light in an optical microscope but the electromagnetic lenses used provided small magnifications, i.e. 17 times smaller than modern TEM. This technique has emerged over many years into a sophisticated tool with higher resolutions. The highly accelerated electron beam of energy 60–300 keV is used in the TEM. Depending on the accelerated voltage, the resolution of TEM can be adjusted. In general, the spatial resolution of TEM is about 1 Å at an accelerated voltage of 300 kV and has an energy resolution of about 10 meV. High resolution less than 1 Å can be attained by increasing accelerated voltages up to 1000 kV. The use of spherical and chromatic aberrations correctors in this instrument makes it more significant for analyzing nanostructures and helps in increasing resolution. The sample under investigation must be prepared before analysis and is the foremost step in the TEM. Sample preparation for biological materials is different from other non-biological specimens [2] and will be discussed later on. The thickness of the specimen should be around 1000 Å so that electron interactions with the sample should be very weak and highly accelerated electrons do not affect the sample. The appropriate combination of electromagnetic lenses with strong magnetic fields is used to focus the electron beam on the sample for the formation of final image. In TEM, one can work in real and reciprocal space to extract accurate information of the materials. By adjusting the lenses, one can obtain desirable information of the specimen in real and reciprocal space. The simultaneous working of TEM in real and reciprocal space makes it an amazing instrument for materials characterization. TEM instruments require high vacuum pumps to ensure better performance and maintain resolution for high-quality imaging. The electron

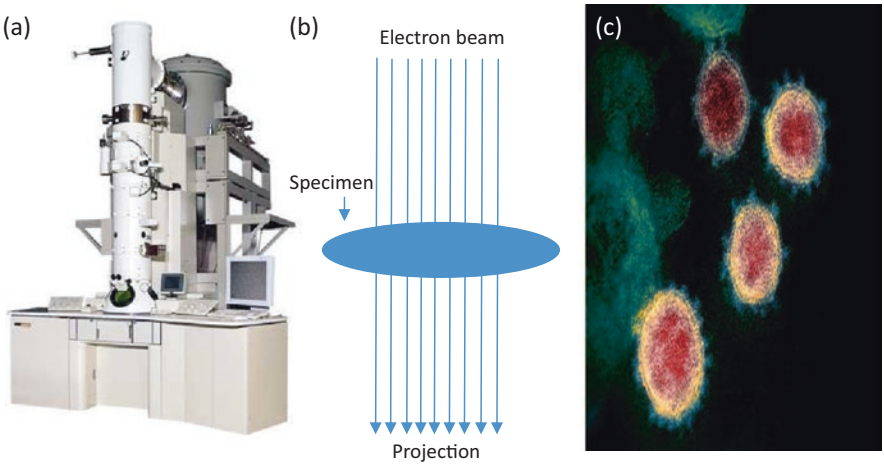

Fig. 9.1 (**a**) Model of a transmission electron microscope, (**b**) representation of imaging mode in a transmission electron microscope, (**c**) a transmission electron microscope image of coronavirus taken from a patient in the USA, the green spikes are seen around the surface of cells are virus particle (image credits: NIAID-RML and taken from the site of NIH (National Institute of Health), USA) [3]

microscopes require special rooms against disturbances from environmental factors like temperature, vibrations, electric/magnetic fields, and airflow for their proper functioning.

In this chapter, Sect. 9.2 covers the basics of electrons followed by electron–matter interactions that are important to understand the functioning of TEM, Sect. 9.3 demonstrates the principle, working, components of TEM instrumentation, and specimen preparation techniques used in TEM analysis along with some examples of the micrographs obtained from TEM. Section 9.4 describes the conclusion of the chapter (Fig. 9.1).

9.2 Basics of Electrons

Transmission electron microscopes make use of electron beam for imaging of specimens. The electrons are used because they can easily be generated and influenced by electric/magnetic fields. With the help of a different set of electromagnetic lenses, these electrons are allowed to focus along the optical axis or at one spot. A good vacuum system that generates pressure less than 10^{-5} mbar is used so that electrons do not scatter or be hindered. The interactions of electrons with thin specimens record images via computer control software. The images formed in the image plane provide information from the real space and the electron diffraction pattern provides information from the reciprocal space. Before we shed light on TEM instrumentation and the formation of images, some basics of electrons and their interactions with materials should be understood. The electron–matter interactions are quantum-mechanical in sense (wave-particle nature of electron). Therefore, the

image formed is a combination of scattering and interference, resulting in a change in amplitude, phase, and energy of electromagnetic wave associated with the electron.

In 1924, Louis de Broglie postulated the dualism of matter. The wavelength λ of the particle is given by,

$$\lambda = \frac{h}{mv}, \tag{9.1}$$

where h is Planck's constant given by 6.62×10^{-34} Js, m is mass and v is the velocity of the particle. This equation has fundamental importance for electron microscopy. We can calculate the wavelength of accelerated electrons using it. If an electron with mass m_e is moving in electric field U, the energy of the electron is given by $E = eU$ and the kinetic energy $E_{\text{kin}} = m_e v^2/2$. These equations give velocity v_e of an electron as,

$$v_e = \left(\frac{2eU}{m_e}\right)^{\frac{1}{2}}. \tag{9.2}$$

The momentum p of an electron is given by $m_e v_e$. Using Eq. (9.2) the momentum becomes,

$$p = \left(2m_e eU\right)^{\frac{1}{2}}. \tag{9.3}$$

Equations (9.1) and (9.3) give wavelength λ_e of an electron as

$$\lambda_e = \frac{h}{\sqrt{2m_e eU}}. \tag{9.4}$$

But at high voltages of more than 100 kV, the electrons are accelerated at high speeds almost approaching the speed of light. Therefore, a relativistic term must be added and given as

$$\lambda_e = \frac{h}{\sqrt{2m_e eU\left(1+\frac{eU}{2m_e c^2}\right)}}. \tag{9.5}$$

9.2.1 Electron–Matter Interactions

Let us understand, how electron–matter interactions take place. When the electrons hit the specimen, there occur interactions between the atoms of the specimen and incident electrons. These interactions of the electrons with the atoms of the material are explained in the diagram shown in Fig. 9.2. The electrons near to nucleus are deflected at higher angles are backscattered electrons, scattering of electrons at angles less than 90° are due to elastically scattered electrons, electrons scattered at

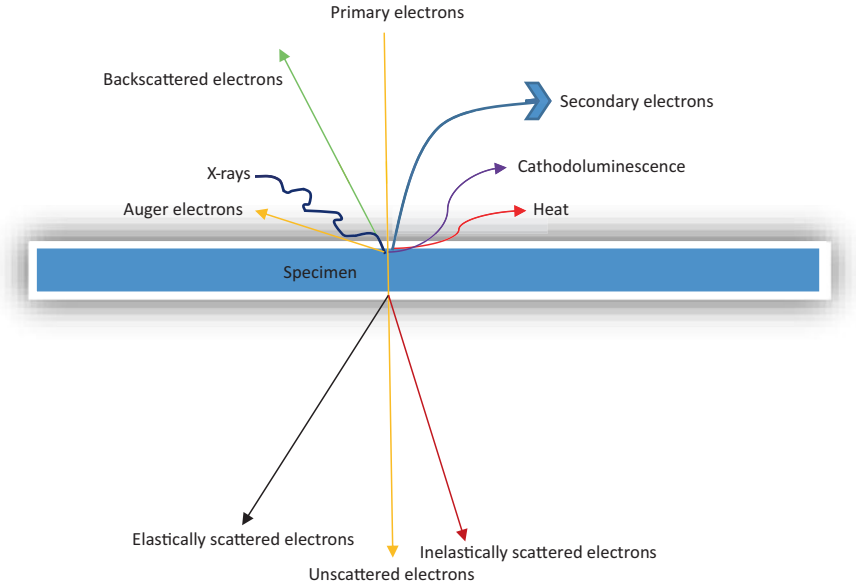

Fig. 9.2 The most important electron–matter interactions that arise on account of hitting the electron beam with the specimen

low angles are referred to as inelastically scattered electrons. The electron microscopes provide information of the samples by recording signals from various electron–matter interactions and can be discussed as follows.

9.2.1.1 Elastic Scattering

When electrons interact with the atoms of a specimen with no change in energy, then the scattering is elastic. There is no loss of energy of electrons occurs during this interaction. Also, the electrons which pass through the specimen without any interaction with the specimen, i.e. unscattered electrons, are the same case as well. The elastically scattered electrons deflected from their path due to the Coulomb interactions and with almost no measurable amount of loss in energy. The following effects are discussed:

Incoherent Scattering An electron beam when enters the electron cloud of an atom, the positive nucleus attracts the electron due to Coulombic interactions. Due to these electrostatic interactions, its path gets deflected at some angle. The more closely the electron to the positive nucleus, the larger is the Coulombic force and the higher is the deflection angle. In some rare cases, the deflection causes the electron to backscatter. Backscattered electrons deflect their path at an angle of more than 90° with the incident beam. These electrons have the same energy as the primary electrons. The Coulomb forces between an incident electron and the nucleus of an atom of the specimen increase with increasing the number of positive charges, i.e. protons. Therefore, the materials with higher Z have a higher force which increases

the backscattered events at high angles. Most electrons are scattered in the forward direction, there is a small probability of backward scattering.

Coherent Scattering When these scattering centres are well arranged, then coherent scattering takes place. On the other side, when the scattering centres are irregularly arranged as in amorphous materials it results in incoherent scattering. The constructive interference of the scattered electrons in certain different directions results in the formation of the diffracted beams. The diffraction of the beam from materials is described by Bragg's law. This law is given by the following equation:

$$n\lambda = 2d\sin(\theta), \tag{9.6}$$

where λ is the wavelength of the incident beam, d is the distance between the lattice planes and θ is the diffraction angle. Due to the small wavelength of high-energy electron used in TEM, the diffraction angles are quite small and are less than 1°.

9.2.1.2 Inelastic Scattering

If the electron loses energy after interacting with the specimen it results in an inelastically scattered electron. The electron transfers its energy to the specimen and different signals are obtained that depend on the material. The following effects take place in this case:

Inner-shell Ionization The incident electron knocked out an electron from the inner shell of an atom. This electron either occupies the empty electronic state or ejects in the vacuum space. It creates a vacancy in a low-energy shell. This vacancy is filled by the electron from the higher energy shell. The energy is released during this transition can be emitted as a characteristic X-ray or is transferred to another electron with the emission of Auger electron.

Bremsstrahlung Deceleration of the electron due to the Coulomb forces generates uncharacteristic X-rays carrying any amount of energy from the incident beam.

Secondary electrons The loosely bound electrons with lower work function can be easily ejected to vacuum with a little transfer of energy.

Phonons The generation of collective oscillations in crystal lattice due to the transfer of energy of an incoming electron. This may lead to heating of the sample and damage the beam.

Plasmon The collective oscillations of the free electrons.

Cathodoluminescence When an electron leaves the valence band and jumps into the conduction band, the electron-hole pairs generate. To fill the vacancy in the

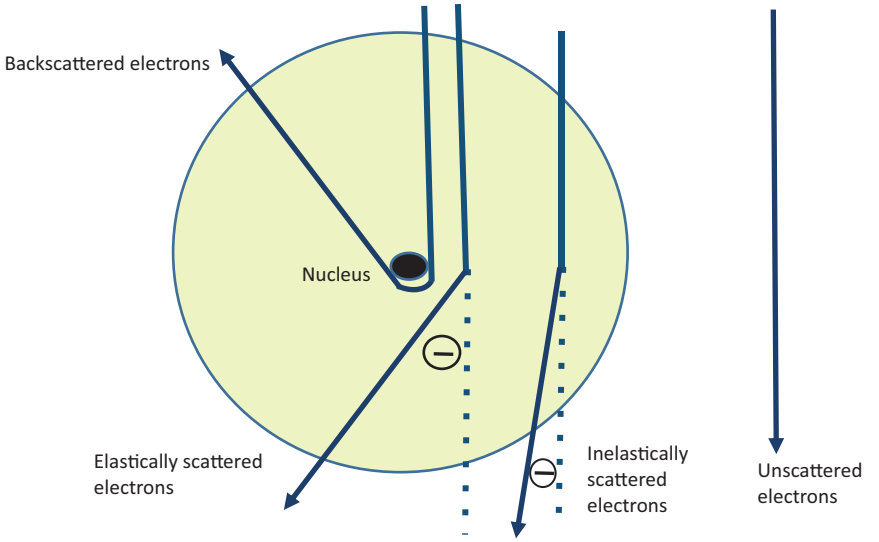

Fig. 9.3 Scattering of incident electrons inside the electron cloud of an atom

valence band, an electron from the conduction band falls into the valence band. This recombination process results in the emission of a photon of energy $h\nu$ (Fig. 9.3).

All kind of interactions provides specific information about the materials. The information about the topography, the elemental composition can be extracted based on the type of emitted electrons used for detection. The TEM mainly uses elastically or unscattered electrons for the imaging of the specimen. For biological samples, elastically scattered electrons are used. X-ray spectroscopy, electron energy loss spectroscopy and analytical electron microscopy use inelastically scattered electrons.

9.3 The TEM

The TEM work similar to light microscopes but with a difference that the light is replaced by an electron beam and electromagnetic lenses are used in place of glass lenses. Figure 9.4 depicts the similarity of light and transmission electron microscopes. In TEM, an electron beam is produced using a heating filament. These electrons are generally accelerated using voltages of 60–300 kV [4]. The speed of the electrons determines their wavelength. It is clear from Sect. 9.2, the wavelength of electrons depends upon the energy with which the electrons are accelerated. Therefore, the higher the voltage, the higher the speed of electrons leads to their smaller wavelength, and thus the resolution of the instrument increases. Generally,

100 kV voltage is used in TEM instrumentation with a resolution of 0.5 nm. This resolution can be exceeded by using high voltages.

The transmission electron microscope consists of the following parts: an electron source, set of condenser lenses, the main imaging lens called the objective lens, set of projective lenses that project images in image plane from real space or form a reciprocal image in diffraction mode on a screen. There is a lens above and below the sample called twin objective lenses. Along with seven more lenses, there are spherical and chromatic correctors which require independently controlled power supplies connected with a computer control system and specialized software. This larger arrangement of the instrument requires special rooms with proper control of environmental disturbances and it works well with no external disturbances. High vacuum systems are also required for an electron microscope and discussed later on. A simple schematic illustration of the TEM instrument and its comparison with a light microscope is shown in Fig. 9.4.

Now, to understand the imaging in TEM we will talk about its features separately one by one. But before that, we will discuss the sample holder and the specimen preparation which is the necessary and foremost step.

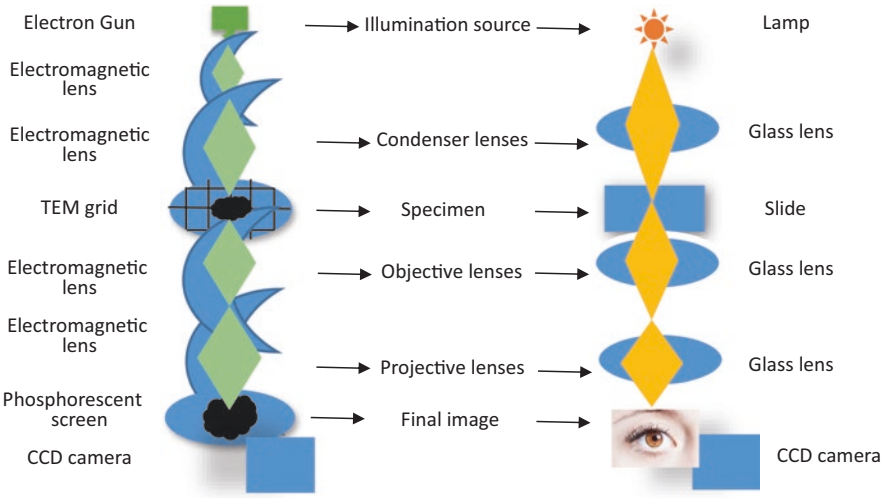

Fig. 9.4 Comparison of the transmission electron microscope (left) and light microscope (right) [5]

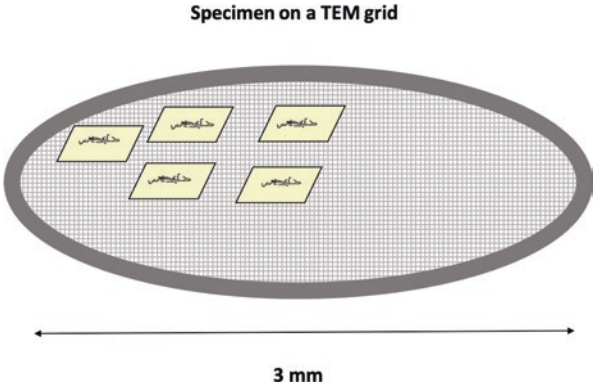

Fig. 9.5 TEM holder grid of size 3 mm used for sample analysis

9.3.1 Sample Holder and Stages

The specimen used for TEM analysis must be very thin so that it allows electrons to pass through it and form an image. Biological samples of thickness ~ 70–100 nm are used with a maximum acceleration voltage of 100 kV [6]. For higher acceleration voltages, the sample thickness should be more. The non-biological specimens (thickness less than 100 nm) in TEM are mounted on copper grids of a diameter of about 3 mm shown in Fig. 9.5 and are available with different mesh sizes and materials. The grid is attached to the sample holder and is introduced into the goniometer through a vacuum lock. The goniometer is a mechanical setup in the TEM instrumentation which enables the precise and stable control of the sample. The study of material along a certain orientation of the unknown oriented material is achieved by tilting the sample in two perpendicular directions using a sample holder and observing the electron diffraction pattern using double-tilt holders.

Electron microscopes require special care from the surroundings as they are very sensitive to vibrations and electromagnetic fields. To absorb these vibrations, an electron column is mounted on air cushions. The arrangement of the setup is managed in such a way that it is free from disturbances from the rest of the building.

9.3.2 Specimen Preparation

Sample preparation is the foremost step for the TEM analysis. A high vacuum system is required for imaging in TEM which will be discussed in Sect. 9.3.4. But, high vacuum is not suitable for biological specimens such as cells and tissues. Specimens with thickness less than 10 nm are suitable for HRTEM and TEM analysis samples should be 70–100 nm thin. The specimen under investigation should pose the following prerequisites:

1. Resistant in the vacuum.
2. Providing imaging contrast.
3. Electrons can penetrate through it.
4. Resistant in the electron beam.

Large biological samples do not fulfil any of the above conditions and have to be prepared first for the analysis. The sample is converted into solid-state and it becomes suitable for high vacuum and electron beam resistance. Moreover, very thin sections of the specimen of thickness 70–100 nm are cut for the analysis. The image contrast for the biological specimen is not formed because these materials have elements like C, H, N, O, P, S, which do not interact with electrons. Contrast formation in imaging can be done by selective staining and with heavy metals.

9.3.2.1 Preparation of Powdered Specimen

Crystalline samples are ground to a fine powder using an agate mortar and these powders are dispersed in suitable solvents for their dispersion in the TEM analysis. The suspension of particles is usually prepared in inert solvents like alkane and alcohol. A drop of suspension is then dried on a thin carbon-coated grid consists of several small meshes as shown in Fig. 9.5. This grid is then placed in a sample holder for the analysis.

9.3.2.2 Preparation of Cells and Tissues for TEM Analysis

Two types of specimen preparations can be done for biological materials. Classical preparation is done at room temperature and cryogenic preparation is performed at low temperature. The steps involved in both types of preparation are shown in Fig. 9.6. The first step is a chemical fixation, where the specimen is stabilized chemically, the fixatives like glutaraldehyde and osmium tetroxide are used. Fixation can lead to artifacts in the sample because it is a slow process and the specimen has enough time to react with the chemical and undergoes changes. The specimen is then completely dehydrated using a sequence of different concentrations of ethanol. The next step after dehydration is the embedding of the sample inside the block using monomers. This allows cutting of the blocked specimen into thin sections in ultramicrotomy. Dehydration and embedding both are conducted at room temperature which causes extraction and shrinkage of the sample. The interpretations are to be done with extreme care as the thinning of a sample can affect the structural chemistry of the sample and there is a risk of generating artifacts. The next step is staining of these thin sections which are done with uranyl acetate and lead citrate [2]. Uranium, and lead ions are selectively attached to proteins, lipids, and nucleic acid and provide the image of the specimen. The mechanism of negative staining is illustrated in Fig. 9.7. To ensure the prevention of artifacts, the cryogenic method is best. In this process, initially, the specimen is frozen without any chemical treatment. This process generally takes a few seconds. High-pressure freezing is preferred to avoid the formation of ice crystals. The chemical fixation and dehydration are done simultaneously at low temperatures. The rest steps embedding the sample in block, sectioning, and staining are done similar to the classical preparation.

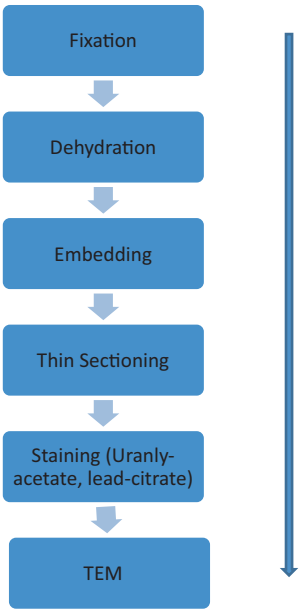

Fig. 9.6 Sample preparation steps for a transmission electron microscope

The cleanliness of the sample is also a necessary step. The contamination of the samples can interfere with the results during microscopy. The sample is treated under vacuum to prevent any contamination or an alternative approach to reduce it inside the microscope is done by a method "beam shower" [7]. In this method, the large area of the sample is exposed to an intense beam of electrons (Fig. 9.7).

9.3.3 The Electron Source

Electrons can be produced by two methods: thermionic emission or cooled field emission. During thermionic emission, a filament tip is heated using an electric current which produces electrons. Materials with low work function are preferred as electron sources. The heating element can be a tungsten filament, LaB_6 crystal, or Schottky emitter and requires heating temperatures up to 2700 K [8]. These electrons are of low energy and escaped to the electron column by accelerating them at desired high speeds using high voltages. These high voltages are applied between the cathode (electron source) and anode plate generating an electrostatic field that accelerated and guided the electrons. Cold field emission uses tungsten tip at room temperature for the generation of electrons. The cold field emission has an advantage over thermionic emission in a way that it yields a high number of electrons and has very low chromatic aberration results in high resolution of the instrument. Smaller energy spreads are achieved by using cold field emitters [9]. These electron sources require high vacuum systems and are cost-effective.

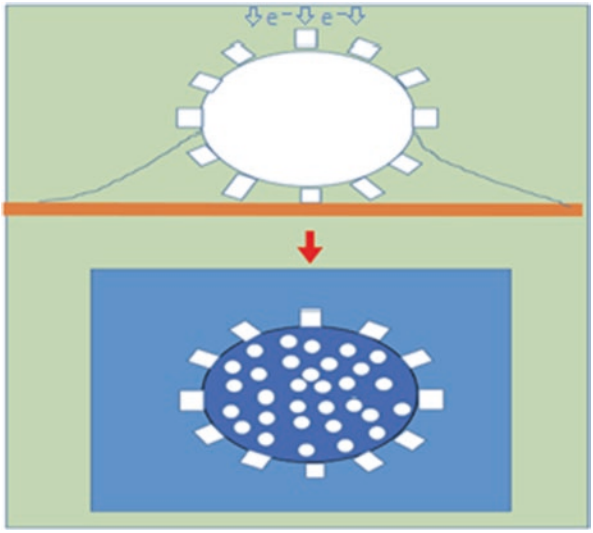

Fig. 9.7 Mechanism and image formation in negative staining

9.3.4 Vacuum System

The electron source was maintained at a high vacuum system of 10^{-7} to 10^{-10} mbar to prevent burning/oxidation of heated filament. A pressure of 10^{-5} to 10^{-7} mbar is required for the electron column and specimen area [10]. The collisions of electrons with the residual can interfere with the resolution and performance of the instrument. Therefore, these are evacuated steadily to avoid any collision of electrons with the residual gas in the system. A series of the setup of low and high vacuum pumps, i.e. rotary pump, diffusion pump, ion getter pumps are used as shown in Fig. 9.8.

9.3.5 Electromagnetic Lenses

The electron lenses are magnetic consisting of a huge bundle of copper windings around a soft iron cast and pole pieces as shown in Fig. 9.9. The electric current is passed through the windings and a magnetic field is generated. This electric field E is weak at the centre and becomes stronger radially outwards. Electron passing through the magnetic field B experiences the deflection having velocity v and the resultant force acts on it is given by Lorentz force as:

$$\left|F\right| = -e\ \left(E + v\,X\,B\right), \tag{9.6}$$

Electrons that move closer to the centre are less deflected than those passing far away from there because of the weak magnetic field. The focusing effect of the lens can be increased or decreased by changing the magnetic field. This magnetic field can be controlled by varying the current in the coil.

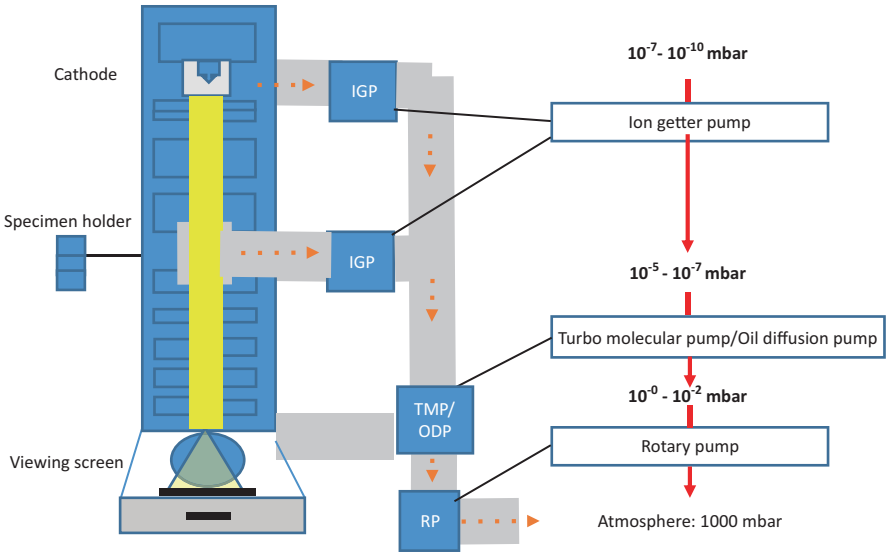

Fig. 9.8 Schematic illustration of a vacuum system for TEM [10]

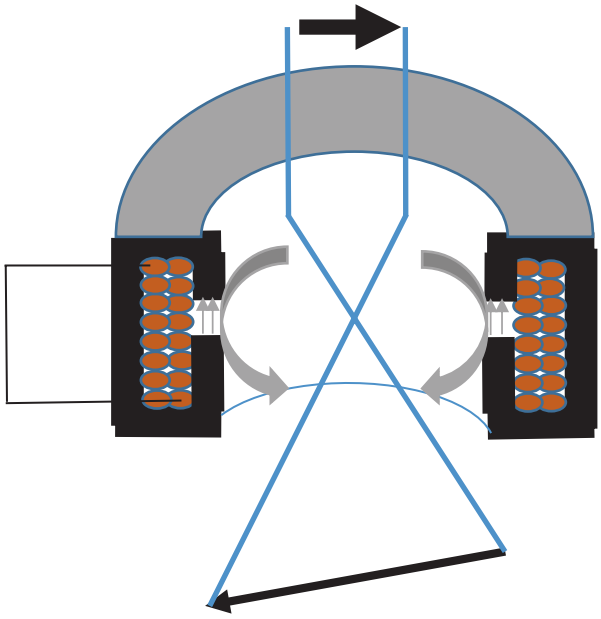

Fig. 9.9 Schematic illustration of a cross section of the magnetic lens. The brown colour shows coils of copper wire inside iron cylinders (black). Grey-coloured arrows show radially inhomogeneous magnetic field focussing electron beam (blue). Black arrows represent the rotation of the image due to the circular path of electrons

The transmission electron microscopes consist of a set of lenses. Three types of lens systems are used: condenser lenses, objective lenses, and projective lenses. The first set of lenses that guide the electrons and control the overall brightness of the electron beam is called condenser lenses. These lenses create a parallel electron beam. This electron beam transmits through the specimen and passes through an objective lens that forms the primary image as well as the diffraction pattern. The diffraction lens system set below the objective lens is allowed to switch between the imaging and diffraction mode. Figure 9.10 illustrates the imaging and diffraction mode. The switching from real to reciprocal space can be done by changing the strength of intermediate lenses. This system determines the selected mode for projective lenses to magnify. Electron diffraction studies are important to investigate new and defective structures. The NIST Materials Science and Engineering Laboratory, Gaithersburg, found new structures with the help of electron diffraction [11]. The information of the reciprocal space belongs to diffraction pattern and the image plane gives information about real space. This feature of the TEM to simultaneously image real and reciprocal space of the same area of sample makes it an outstanding technique. The conversion of real space into reciprocal space is mathematically done by Fourier transform. To obtain particular information from the same region, one can adjust the electron lenses in the TEM to form an image contrast. A selective aperture is placed in the plane of the first intermediate and allows to select a region for selected area electron diffraction pattern (SAED). We will extend our discussion about electron diffraction in Sect. 9.3.5.1 (Fig. 9.10).

Usually, TEM works in two imaging mode: bright field and dark field imaging. The image formed by transmitted electrons with less deflection angles is called a bright field image. The scattered electrons are used to construct a dark field image. In the Bright field image, the morphology of the specimen appears darker on bright background. Whereas in dark field imaging, the brighter image appears on dark background. The most specimen has high crystallinity or mass and results in to the darker appearance of the image. Some details and visualizations of the specimen can be missed in bright field imaging. Even, many staining techniques may harm the specimen used for the image contrast. To enhance the contrast, an objective aperture is inserted in the back focal plane of the objective lens. The metal plate objective consists of holes. The holes in the objective aperture allow the electrons to pass through it, but the electron fall on other areas of the metal objective aperture gets absorbed. If only the electron beam along the optical axis passes through the aperture then it results in the formation of a bright field TEM image. But if the electron beam is tilted at some angle to the sample by shifting the aperture then the electrons scattered at the same angle to the tilted beam moves down to the electron column and the transmitted beam is blocked gives a dark field TEM image as shown in Fig. 9.11. To ensure high-quality results of the imaging, the aperture should stay along the optical axis. The large apertures enable interference of the direct beam as well as several other diffracted beams with each other in the imaging plane, creating the lattice imaging of crystals and the set-up is called high-resolution transmission electron microscope (HRTEM). The images obtained from diffraction lenses are further magnified using a set of lenses. Therefore, a set of two or three lenses that

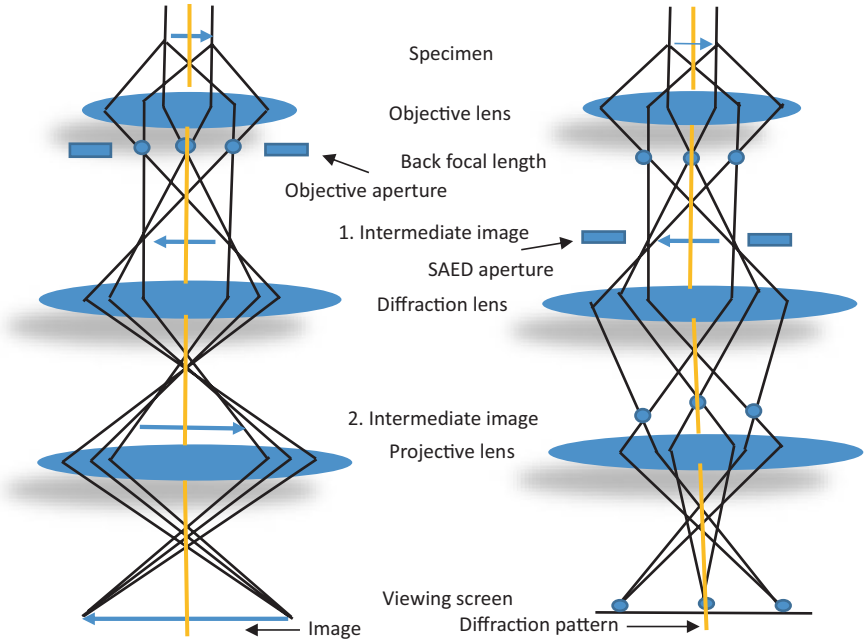

Fig. 9.10 Schematic ray diagram of imaging mode (left) and diffraction mode (right) in TEM [12]

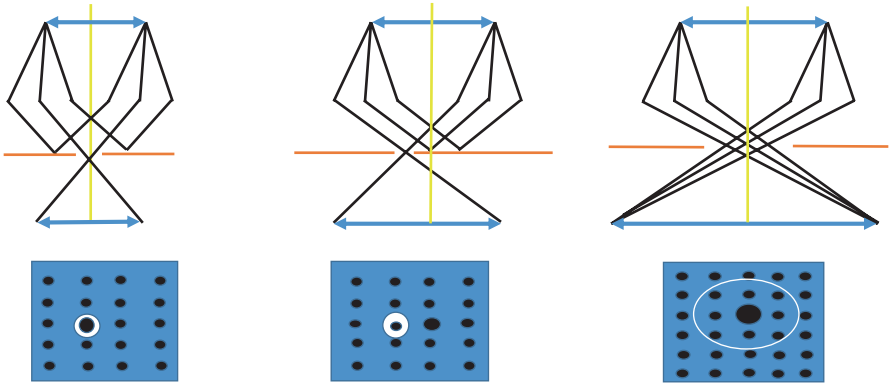

Fig. 9.11 Bright Field TEM image (left), dark field TEM image (centre), and HRTEM image (right)

act in a combination called projective lenses are used to project the final image on a fluorescent screen or a photosensitive film.

Alike a glass lens, the electromagnetic lens also creates the problem of chromatic or spherical aberrations, astigmatism, or distortion. The design for spherical corrector was proposed firstly by H. Rose [13] and the arrangement was used experimentally around the year 2000. This arrangement of corrector design consists of two

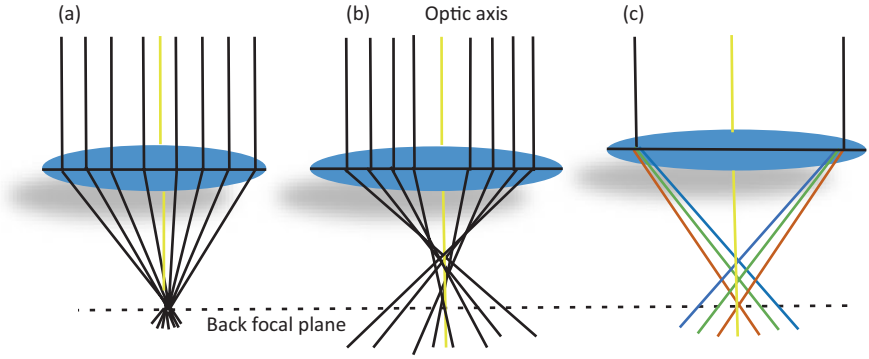

Fig. 9.12 Ray diagram representing an image formation of (**a**) an ideal lens, (**b**) lens with spherical aberration, and (**c**) lens with chromatic aberration

hexapoles and two transfer lenses which compensate for the spherical aberration by achieving a dispersion effect. This effect is analogous to light optics where concave lenses are used to correct spherical aberration of the convex lens. The high resolution of sub-Å is achieved using spherical correctors by reducing the diameter of the electron beam. Techniques and applications of aberration corrections are mentioned in some textbooks [14–16].

Astigmatism is caused by several factors such as contamination of lens and apertures, inhomogeneities of the lens, and charging of specimen. Axial astigmatism is very common and the inability of the electrons deriving from one point source to focus on one and the same point leads to image confusion (Fig. 9.12).

9.3.5.1 Selected Area Electron Diffraction

As we stated earlier, the reciprocal image of materials is formed in diffraction mode. The crystallographic information, elemental composition, information about the symmetry of the crystals, and the presence of defects can be gathered from the diffraction pattern. The schematic illustration of the diffraction pattern of a single crystal consists of well-defined points as well as a polycrystalline sample consisting of rings shown in Fig. 9.13. One can observe bright spots for a single crystal in a diffraction pattern and small spotty rings that are reflections from the small number of crystallites or grains in materials. For polycrystalline material, i.e. number of grains or crystallites is large, ring patterns obtain which is due to the superposition of small crystallites that leads to diffraction rings. All the diffracting planes which are at the same distance give too many small spots forming rings. The arrays of spots are the characteristics of crystal structure and its symmetry, and distances between them provide information about the lattice parameters. The diameter of the spots or rings gives the *d*-spacing values and is assigned with the indices. The description of the diffraction pattern can be obtained by constructing the Ewald sphere. The radius of the sphere is $1/\lambda$, which is very large due to the small wavelength of the electrons and it contains the reciprocal points. Each point is located on the Ewald sphere to satisfy Bragg's law and diffraction spots appear. For amorphous materials, diffused rings are formed in a diffraction pattern because of short-range atomic order.

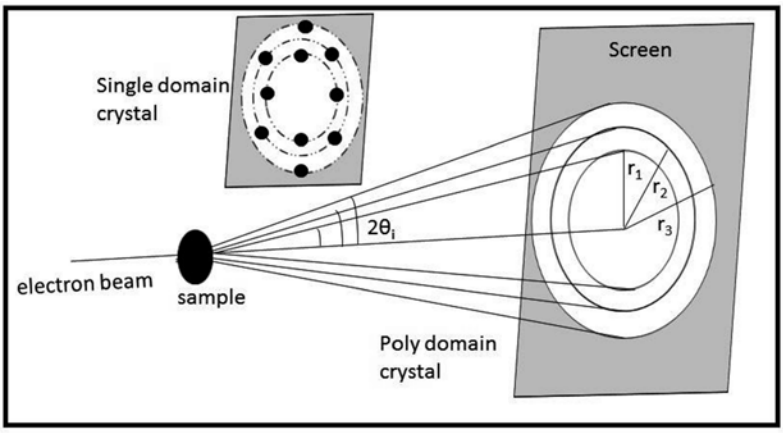

Fig. 9.13 Generation of rings by polycrystalline material and spots by the single crystal in the selected area diffraction pattern [17]

9.3.6 Discussions on Some Transmission Electron Micrographs of Inorganic Nanoparticles and Biological Specimens

The above discussion has demonstrated that a transmission electron microscope can probe structures of small inorganic materials and biological materials. Here are some micrographs of some biological and non-biological samples are discusses. The discussion is only confined to the information or observations drawn from their micrographs so that the readers can interpret the TEM images easily.

Figure 9.14 represents the TEM micrographs of the sample taken from equine spleen ferritin. Ferritin is a biological material that is mainly found in the blood of mammals and is responsible for the iron regulation inside body. The core-shell structure of ferritin has an antiferromagnetic core of around 7–8 nm in size which is shielded by a protein shell of 2–3 nm in thickness [18, 19]. This ferritin sample is purchased from Sigma Aldrich, USA and is supplied as a suspension in a saline solution of NaCl. For TEM analysis, two drops of ferritin suspension are dissolved in 2 ml of distilled water. This mixture is dried on a TEM grid. The TEM micrograph of ferritin in Fig. 9.14a, b taken at different resolutions only shows the ferritin core. The ferritin cores are seen to be almost spherical and uniform in size. These particles are well dispersed because of the presence of protein shell which shields the ferritin cores and reduces the strength of dipolar interactions among them. The average size of the most particles estimated from these micrographs is around 8 nm. The protein shell of ferritin core is not observed in these micrographs. To see the protein shell, negative staining of the sample has to be done which have already been discussed in Sect. 9.3.2.2. Figure 9.14c, d shows the micrographs of same ferritin sample (dried under vacuum to get powdered form) heated at 550° and 1050 °C, respectively. The size of the particle is clearly seen to be increased with the increasing temperature of the heating. Figure 9.15 shows the TEM image of negatively stained sample of human ferritin [20]. The black coloured cores are seen to be

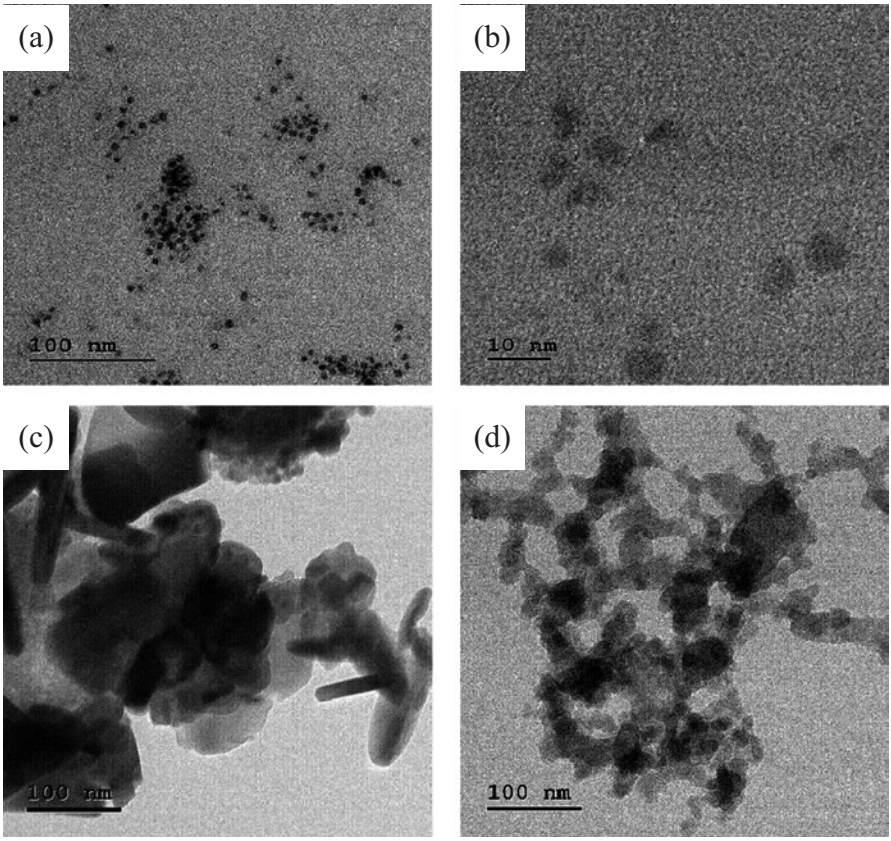

Fig. 9.14 Transmission electron micrographs of (**a**) and (**b**) ferritin core at two different magnifications. Ferritin sample heated at temperature (**c**) 550° and (d) 1050 °C

encapsulated inside their protein cages. Also, one can easily estimate the particle size distribution using transmission electron micrographs by measuring the size of each particle seen in the images manually or using different software such as image J, Axio vision etc. After measuring the particle size, the distribution of sizes can be estimated by plotting the histogram [18, 21]. Thus, the peak of the histogram gives the information about the average particle size. This method is more feasible for particles with spherical geometry. An example of particle size distributions is shown in Fig. 9.16. Figure 9.16 shows transmission electron micrographs and the corresponding particle size distributions of Ag^{+} (silver) nanoparticles fabricated by modifying on carboxyl functionalized bacterial cellulose (BC + Ag). These BC + Ag nanoparticles are reduced by $NaBH_4$ (Fig. 9.16a, c) and sodium citrate (Fig. 9.16b, d) [22]. The sample preparation for microscopy is done by obtaining thin slices in the presence of liquid nitrogen and dispersing on copper grids. It has been depicted from micrographs and histogram that the Ag nanoparticles formed on carboxyl-functionalized BC reduced with $NaBH_4$ are well-dispersed and have regular shapes

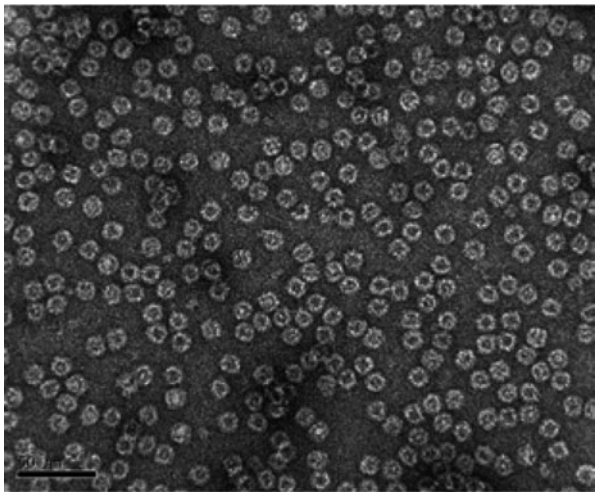

Fig. 9.15 TEM image of negatively stained human protein ferritin showing cage-like morphology at 50 nm scale bar [20]

with much smaller sizes. The peak of histogram gives average particle sizes and estimation of particle size distribution. One can conveniently compare the size distributions and shape of particles from TEM images. The spherical Ag + BC nanoparticles reduced by sodium citrate have larger diameters and standard deviations. These observations concluded that the reducing agent has affected the nucleation rate of particles to a greater extent. The transmission electron micrographs of nanoparticles of ferrimagnetic magnetite at two different resolution scale bars are shown in Fig. 9.17. Magnetite is the phase of iron oxide and can be easily synthesized in laboratories using ferric and ferrous salts in the ratio 2:1. The TEM images of magnetite nanoparticles are taken from transmission electron microscope model Jeol Jem 2100Plus. The nanoparticles are seen to be agglomerated because of the interactions between them. The agglomerations can be reduced by decreasing the influence of interactions among particles. It can be done by surface modifications of the nanoparticles using different coatings such as sodium citrate, sodium metasilicate, tetraethyl orthosilicate (TEOS), and oleic acid. One can also easily control the shape and size of particles using optimum synthesis conditions. Transmission electron micrographs of magnetite nanoparticles coated with oleic acid [23], TEOS [24] and FePt nanoparticles with Au shell further coated with silica [25] are shown in Fig. 9.18. The black coloured dots are the particles and the outer layer is the coating resulting in core-shell structures. The author has synthesized controlled sized nanoparticles of magnetite by using different amounts of coatings [23, 24]. Figure 9.19a shows the HRTEM image of magnetite nanoparticles. The lattice fringes are seen to correspond to the reflections from the planes of magnetite crystallites. The interplanar spacing *d* can easily be calculated by measuring the distance between two fringes. The marked circle 1 is a reflection from (311) plane of magnetite which corresponds to *d* equals to 0.23 nm and the marked circle 2 shows reflection from (220) plane, which corresponds to *d* value of 0.14 nm. The micrograph reveals that the sample consists of several small crystallites of arbitrary shape. Also,

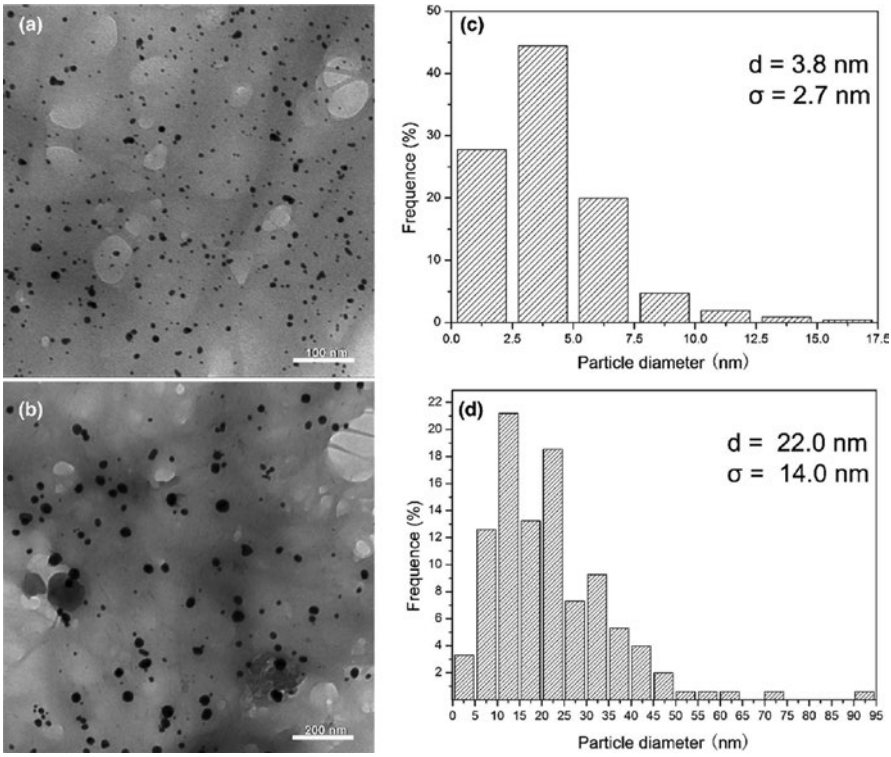

Fig. 9.16 TEM images and particle size distributions obtained for Ag nanoparticles obtained from BC-Ag reduced with (**a**), (**c**) $NaBH_4$ and (**b**), (**d**) sodium citrate [22]

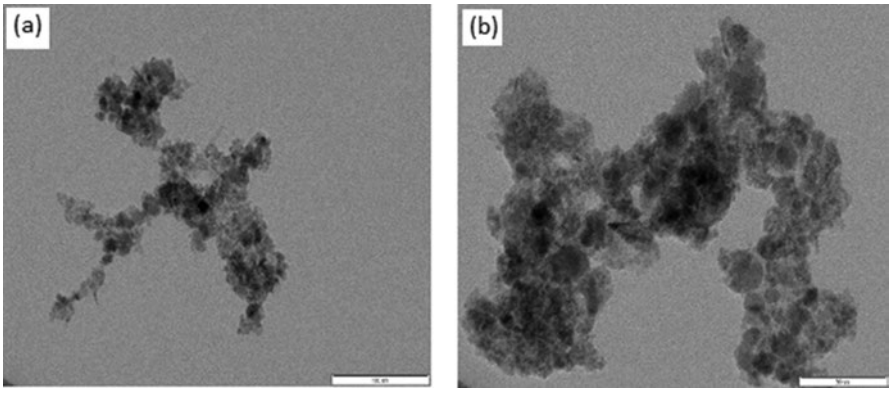

Fig. 9.17 TEM (Jeol Jem 2100Plus) images of magnetite nanoparticles at the two different resolutions (**a**) 100 and (**b**) 50 nm. Particles are seen to be of arbitrary shapes and agglomerated

the TEM and HRTEM images of gold nanorods are shown in Fig. 9.19b, c [26]. Figure 9.19b shows TEM micrograph of gold nanorods produced from seeds (in the

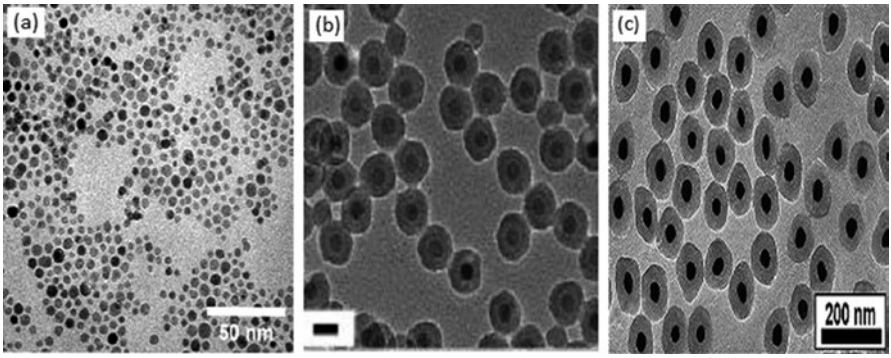

Fig. 9.18 TEM image of (**a**) oleic acid [23] (**b**) TEOS (Scale bar: 20 nm) [24] coated magnetite nanoparticles, (**c**) star shaped FePt@Au coated with silica [25]

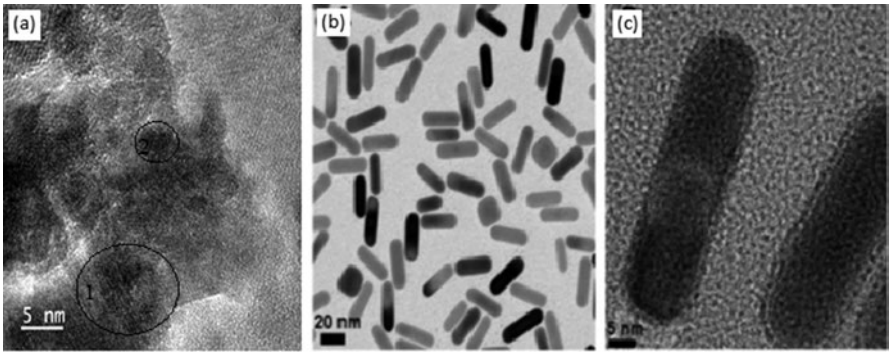

Fig. 9.19 (**a**) HRTEM image of magnetite nanoparticles, (**b**) and (**c**) shows TEM and HRTEM image of gold nanorods [26]

presence of 0.1 mM $AgNO_3$) irradiated with X-ray radiations. Figure 9.19c is the corresponding HRTEM image of those gold nanorods.

Figure 9.20 shows transmission electron micrographs of *E. coli* bacteria cells and the grown bacteria cells on Lauria-Bertani (LB) broth with aeration at temperature 37 °C. *E. coli* has an inner and outer membrane with thickness 8 and 12 nm, respectively. The effect of the antibacterial behaviour of ZnO on *E. coli* has been studied through these micrographs [27]. The *E. coli* bacteria is suspended in ZnO nanoparticles and the micrographs depicted that there is no traces of ZnO found in the interior of a cell.

The dark field and bright field images of TEM have their own roles to draw different information of the study of the materials. The TEM micrographs in Fig. 9.21 show the images taken in bright field and dark field modes. The dark field imaging proved to be more efficient for biological specimens. The micrograph in Fig. 9.21a, b shows the bright and dark field images of gold nanoparticles incubated with *B. subtilis* bacteria [28]. The arrow indicates the brighter spots of gold nanoparticles

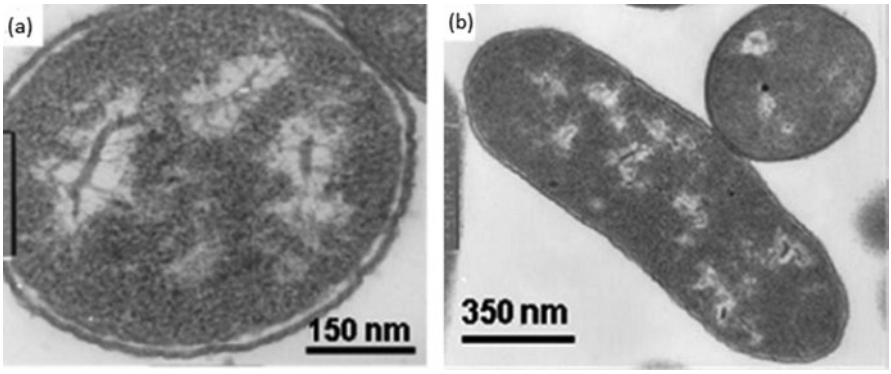

Fig. 9.20 Transmission electron micrograph of (**a**) *E. coli* bacteria cells (**b**) *E. coli* grown in Lauria-Bertani (LB) broth at 37 °C [27]

more clearly in dark field imaging. Some observations like nanoparticle clustering at the cellular membrane, the presence of gold nanoparticles in the interior of bacteria are left obfuscated with bright field imaging. Figure 9.21c, d shows large gold nanoparticles. The variety of facets of gold nanoparticles having same crystallinity appear in the dark field imaging mode at various diffraction angles that are not possible to be clearly visible with bright field imaging mode [28]. Dark field imaging provides the noise free and clear images of the particles as compared to bright field imaging.

Transmission electron microscopy also enables to study defects inside crystals such as planar, point, layered, anti-phase defects, twin defects, and dislocations that affects the properties of materials. Study of defects in materials is useful for their proper use in applications. TEM allows to image such defects. When the electron beam is parallel to the twin plane is incident then a dark twin line is seen across the twin boundary, i.e. dark image contrast is formed. A study of twin defect is explained here. Figure 9.22 (a) shows HRTEM image with two twin defects in cubic Si nanowires along [112] axis (the growth direction of Si nanowire) and (b) shows the HRTEM image after rotating the Si wire by 15° along [112] axis [29]. It is observed that after rotation the sharp twin planes disappeared and seems there is a defect free single crystal. The tilted angle images are sometimes deceptive in TEM studies and does not always mean that there is no defect.

The selected area diffraction pattern always gives information about crystalline planes. The interplanar spacing d from these crystalline planes can be calculated using this pattern. These SAED patterns also provides the information of other phases present in the samples. It means to check the phase purity the SAED images are reliable and gives the information of impurity phase less than 5%. Figure 9.23 shows SAED pattern of single crystals of gold nanoparticles [30] and Co_2P nanocrystals [31] with the corresponding indices of planes. These SAED patterns show the dots corresponding to Bragg's reflection of gold nanoparticles and Co_2P nanocrystals. The indices represents the (hkl) reflections from the planes. The interplanar

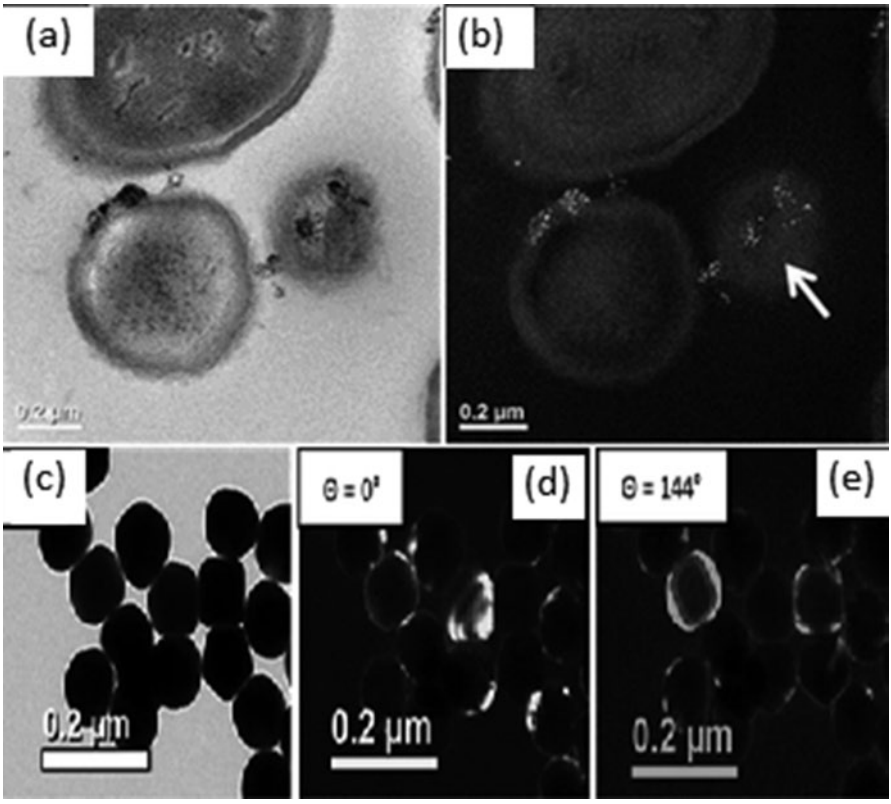

Fig. 9.21 (**a**) Bright and (**b**) dark field images of *Bacillus subtilis* bacteria incubated with 4 nm gold nanoparticles, (**c**) Bright and (**d**) and (**e**) dark field (at different tilt angles with respect to diffraction ring) images of gold nanoparticles. Dark field images reveals more information about specimen [28]

spacing can also be calculated using these patterns. Figure 9.24 represents the SAED pattern of ferritin and magnetite nanoparticles. It is clearly visible that sharp rings or dots are not formed for ferritin sample. There are diffused rings that reveal the sample is poorly crystalline or amorphous. On the other hand, there are some spots forming rings are seen in the SAED pattern of magnetite nanoparticles. This observation depicts that it is consist of a small number of crystallites. The corresponding Bragg's reflections from planes are indicated in the Fig. 9.24b confirms the single phase of magnetite.

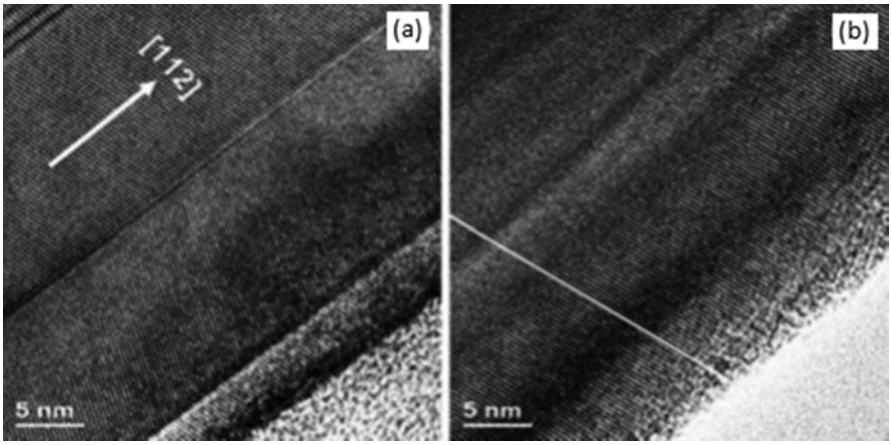

Fig. 9.22 HRTEM image of (**a**) Si nanowires with two twin defects (**b**) image taken after rotation of Si nanowire around [112] direction by 15^0 [29]

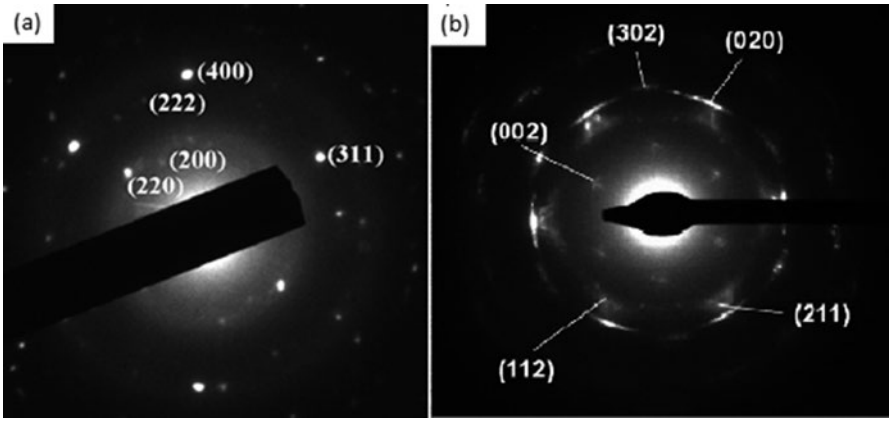

Fig. 9.23 Selected area diffraction pattern of single crystal (**a**) gold nanoparticles [30] and (**b**) Co_2P nanocrystals [31] with indices of planes

9.4 Conclusion

As the progress in the nanotechnology grows, there is a demand to accurately characterize the materials. Historically, the study of nanoscale structures has been difficult due to the need for high-resolution techniques. The above discussion concluded that transmission electron microscopy is the advance and novel technique of microscopy used to characterize nanostructures. It provides information about particle size, crystal structures, presence of impurity or other phases, particle size distribution, particle shape etc. Biological and non-biological samples can be characterize using this technique but their sample preparation before analysis is different. The proper sample preparation is considered to be the most important part of analysis

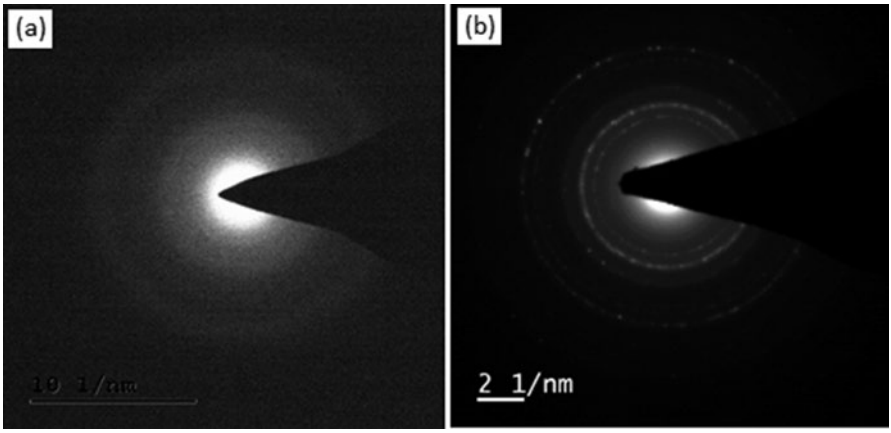

Fig. 9.24 Selected area diffraction pattern of (**a**) ferritin nanoparticles showing diffused rings due to their poorly crystalline nature (**b**) magnetite nanoparticles consisting of some spots making rings

otherwise it introduces artifacts and creates interference in the information. The different results and their interpretations have been discussed in this chapter. The study concluded that this technique has been easily adopted in research work and improves the visualization of small-scale particles which brings new insight in the topographical studies. This interesting technique provides an accurate analysis of nanoparticles and biological systems.

References

1. Ruska E (1987) The development of the electron microscope and of electron microscopy. Biosci Rep 7:607. https://doi.org/10.1007/BF01127674
2. Nagashima K, Zheng J, Parmiter D, Patri AK (2011) Biological tissue and cell culture specimen preparation for TEM nanoparticle characterization. Methods Mol Biol 697:83. https://doi.org/10.1007/978-1-60327-198-1_8
3. https://www.nih.gov/news-events/nih-research-matters/novel-coronavirus-structure-reveals-targets-vaccines-treatments
4. Egerton RF (2014) Choice of operating voltage for a transmission electron microscope. Ultramicroscopy 145:85. https://doi.org/10.1016/j.ultramic.2013.10.019
5. Ul-Hamid A (2018) Introduction. In: A beginners' guide to scanning electron microscopy. Springer, Cham. https://doi.org/10.1007/978-3-319-98482-7_1
6. Cosslett VE (1971) High voltage electron microscopy and its application in biology. Philos Trans R Soc Lond B 261:35. https://doi.org/10.1098/rstb.1971.0034
7. Mitchell DRG (2015) Contamination mitigation strategies for scanning transmission electron microscopy. Micron 73:36. https://doi.org/10.1016/j.micron.2015.03.013
8. Thompson RF, Walker M, Siebert CA, Muench SP, Ranson NA (2016) An introduction to sample preparation and imaging by cryo-electron microscopy for structural biology. Methods 100:3. https://doi.org/10.1016/j.ymeth.2016.02.017
9. Kimoto K (2014) Practical aspects of monochromators developed for transmission electron microscopy. Microscopy 63:337. https://doi.org/10.1093/jmicro/dfu027
10. Heinemann K, Poppa H (1986) An ultrahigh vacuum multipurpose specimen chamber with sample introduction system for in situ transmission electron microscopy investigations. J Vac Sci Technol A 4:127. https://doi.org/10.1116/1.573484

11. Bendersky LA, Gayle FW (2001) Electron diffraction using transmission electron microscopy. J Res Natl Inst Stand Technol 106:997. https://doi.org/10.6028/jres.106.051
12. Champness PE (2001) Electron diffraction in the transmission electron microscope. Garland Science, London. https://doi.org/10.1201/9781003076872
13. Haider M, Rose H, Uhlemann S, Schwan E, Kabius B, Urban K (1998) Towards 0.1 nm resolution with the first spherically corrected transmission electron microscope. Microsc 47:395. https://doi.org/10.1093/oxfordjournals.jmicro.a023610
14. Pennycook SJ, Nellist PD (2011) Scanning transmission electron microscopy. Springer, New York. https://doi.org/10.1007/978-1-4419-7200-2
15. Brydson R (2011) Aberration-corrected analytical transmission electron microscopy. Wiley, Chichester. https://doi.org/10.1002/9781119978848
16. Erni R (2015) Aberration-corrected imaging in transmission electron microscopy, 2nd edn. Imperial College Press, London. https://doi.org/10.1142/p703
17. Kaur N (2021) Effect of magnetic anisotropy and particle size distribution on magnetization of antiferromagnetic nanoparticles, Ph. D. Thesis, Thapar Institute of Engineering and Technology, Patiala
18. Kaur N, Tiwari SD (2018) Role of particle size distribution and magnetic anisotropy on magnetization of antiferromagnetic nanoparticles. J Phys Chem Solids 123:279. https://doi.org/10.1016/j.jpcs.2018.08.013
19. Kaur N, Tiwari SD (2019) Thermal decomposition of ferritin core. Appl Phys A Mater Sci Process 125:805. https://doi.org/10.1007/s00339-019-3104-9
20. Falvo E (2016) Improved doxorubicin encapsulation and pharmacokinetics of ferritin-fusion protein nanocarriers bearing PAS elements. Biomacromolecules 17:514. https://doi.org/10.1021/acs.biomac.5b01446
21. Kaur N, Tiwari SD (2020) Role of wide particle size distribution on magnetization. Appl Phys A Mater Sci Process 126:349. https://doi.org/10.1007/s00339-020-03501-w
22. Feng J et al (2014) Antimicrobial activity of silver nanoparticles in situ growth on TEMPO-mediated oxidized bacterial cellulose. Cellulose 21:4557. https://doi.org/10.1007/s10570-014-0449-2
23. Vitorino HA et al (2018) Magnetite nanoparticles coated with oleic acid: accumulation in hepatopancreatic cells of the mangrove crab Ucides cordatus. Environ Sci Pollut Res 25:35672. https://doi.org/10.1007/s11356-018-3480-2
24. Ding HL et al (2012) Fe3O4@SiO2 core/shell nanoparticles: the silica coating regulations with a single core for different core sizes and Shell thicknesses. Chem Mater 24:4572. https://doi.org/10.1021/cm302828d
25. Pérez NP, González BR, Hilgendorff M, Giersig M, Marzán LML (2010) Gold encapsulation of star-shaped FePt nanoparticles. J Mater Chem 20:61. https://doi.org/10.1039/B911175A
26. Cai X et al (2010) Tailored au nanorods: optimizing functionality, controlling the aspect ratio and increasing biocompatibility. Nanotechnology 21:335604. https://doi.org/10.1088/0957-4484/21/33/335604
27. Zhang L et al (2010) Mechanistic investigation into antibacterial behaviour of suspensions of ZnO nanoparticles against E. coli. J Nanopart Res 12:1625. https://doi.org/10.1007/s11051-009-9711-1
28. Klien ND et al (2015) Dark field transmission electron microscopy as a tool for identifying inorganic nanoparticles in biological matrices. Anal Chem 87:4356. https://doi.org/10.1021/acs.analchem.5b00124
29. Su Z et al (2010) Crystal growth of Si nanowires and formation of longitudinal planar defects. Cryst Eng Comm 12:2793. https://doi.org/10.1039/B925198G
30. Weng CH, Huang CC, Yeh CS, Lei HY, Lee GB (2008) Synthesis of hexagonal gold nanoparticles using a microfluidic reaction system. J Micromech Microeng 18:035019. https://doi.org/10.1088/0960-1317/18/3/035019
31. Zhang H, Ha DH, Hovden R, Kourkoutis LF, Robinson RD (2011) Controlled synthesis of uniform cobalt phosphide hyperbranched nanocrystals using tri-noctyl phosphine oxide as a phosphorus source. Nano Lett 11:188. https://doi.org/10.1021/nl103400a

Preparation of Biological Samples for SEM: Techniques and Procedures

10

M. Sreejith, S. Prashant, Sonu Benny, and T.P. Aneesh

Abstract

SEM analysis attains a special role and wide acceptance in biomedical researches as it is helping in the better imaging and analysis of different biological specimens. Preparation of the biological samples is one of the crucial steps which in turn affects the result. This chapter briefs the important techniques and procedures involved in the processing and preparation of the biological samples for the SEM analysis. The sampling process starts with fixation where it allows the sample to adhere properly to the following processes. Various types of chemicals, traditional chemical, physical fixatives are employed for the same along with vapour fixation techniques. The sample preparation will be then further proceeded with dehydration and drying methods to ensure the complete removal of water from the biological samples. Air drying, critical point drying, freeze-drying, chemical drying etc. are a few such processes before the mounting where it provides a firm binding of the sample to the holder. Then the biological samples can be analyzed for their features based on SEM images generated.

Keywords

Microscope · Sample preparation process · Resolution · Drying process · Freeze drying

M. Sreejith, M.Pharm, Ph.D
Nazerath College of Pharmacy, Pathanamthitta, Kerala, India

S. Prashant, M.Pharm, · S. Benny, M.Pharm, · T. P. Aneesh, M.Pharm, Ph.D (✉)
Amrita School of Pharmacy, Amrita Vishwa Vidyapeetham,
AIMS Health Sciences Campus, Kochi, Kerala, India
e-mail: aneeshtp@aims.amrita.edu

S.-K. Kamaraj et al. (eds.), *Microscopic Techniques for the Non-Expert*,
https://doi.org/10.1007/978-3-030-99542-3_10

10.1 Introduction

The Scanning Electron Microscope (SEM) has been widely employed in material, chemical, and physical sciences. However, it is getting wide acceptance and applicability in biological research, including medical sciences, biotechnology, and pharmaceutical sciences. This wide range of SEM utility in these biological areas has opened up more avenues and opportunities to understand and visualize the unknown facts and concepts in biomedicine. Moreover, the advancement of SEM has helped in the better imaging and analysis of various biological specimens [1, 2].

Different types of biological samples that can be analyzed using scanning electron microscopy include:

1. Liquid biological samples such as blood, urine, Cerebrospinal fluid (CSF) and synovial fluid.
2. Solid tissue samples such as brain, liver, spleen, lungs and kidney.
3. Cells of the living system like Red Blood Cells (RBC), White Blood Cells (WBC), Platelets, macrophages, dendritic cells, cancer cell lines and other tissue cells such as hepatocytes and neurons.
4. Microorganisms such as bacteria, viruses and parasites.
5. Miscellaneous (surface morphology of insect wings, ant eyes, antenna, hair follicles, tooth architecture etc.)

Sample preparation in SEM is a crucial step for better imaging and analysis. In this chapter, the different techniques and procedures for preparing biological samples for SEM analysis are explained. All the biological samples need to be processed and prepared for analysis using SEM except in the analysis using environmental SEM (ESEM). However, the use of ESEM cannot be utilized for all biological samples [3].

Various steps involved in specimen preparation are:

1. Fixation.
2. Dehydration.
3. Drying.
4. Mounting.
5. Sputter coating or surface conductivity.

Images are obtained in SEM by scanning the specimen using a high-energy beam of the electron. The scanning pattern is called a raster scan. The detailed information of the surface, as well as internal structures, can be obtained by this technique [4, 5].

The main problem dealing with biological specimens is that it is primarily composed of water, demanding additional preparatory steps to ensure that the native structure is retained and make the sample resistant to high vacuum and electron beam. An aqueous/hydrated sample is not suitable for SEM observations.

The major constituent of most of the biological specimens is the non-dense material. Hence, a very low number of secondary electrons are produced to be involved

in creating an image. That is why a very fine metallic coating layer is there for the specimens is facilitated to generate secondary electrons. In turn, the large and deep field area is leading to the production of three-dimensional images of great visual depth [6].

10.2 Preparation of Biological Samples

The highly dynamic living organisms contain the highest water levels and organic material. The ideal characteristic required for biological samples is they should be rigid, possess stability in the vacuum condition, be conductive and not contain any liquid. Every biological specimen should be chemically fixed, dehydrated, and dried at the critical point. However, for solid samples, only vapour fixation is done. SEM samples are not necessarily cut into thin sections since they usually visualize the surface of 3D objects. Nevertheless, to view thin sections, ultra-microtomes, and cryotomes can be used, which helps to get the ultra-thin sections of the biological specimen. A thin metallic layer coating is required for the samples to make them conductive and usually, gold or gold-palladium are preferred. It acts as an electric wire which is drawing away from the electrons and they are leading to the bombarding of the sample [6]. The samples will build up electrons without this coating and cause charging artefacts which give a false impression regarding the appearance of the sample (Figs. 10.1 and 10.2).

Fig. 10.1 Ultramicrotome (**a**) and cryotome (**b**) instrument used for ultra-thin and semi-thin sectioning for Electron microscopy (Model: RMC PowerTome PTPC, Picture Courtesy: ACNSMM, AIMS, Kochi)

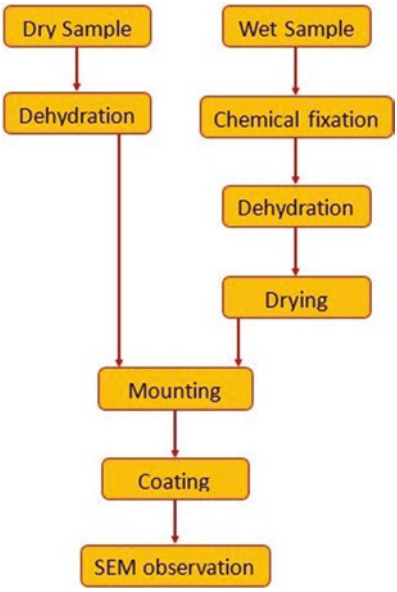

Fig. 10.2 General outline of sample preparation for SEM analysis

10.3 Fixation

The first and foremost procedure after the selection of a biological sample is rapid fixation. It should be done followed by the death of the organism and prior to the beginning of decomposition at a cellular level and immediately after the death of the organisms. The routine method of fixation composed of chemical cross-linking and water removal from the protein and further denaturation. The fixation process will help stop the cellular processes and help preserve the specimen with a maximum resemblance to its natural state [7].

10.3.1 Traditional Chemical Fixation

Stabilization is the primary goal of the step fixation to withstand the SEM examination and the subsequent steps involved in the process. It is of two types: Chemical fixation and physical fixation. The most commonly used method is chemical fixation, whereas primarily freezing, a physical fixation method, is attaining significance nowadays.

10.3.2 Chemical Fixation

Chemical fixation involves immersing biological specimens in chemical solvents for a short period. These chemical solvents are called chemical fixatives, which

include Formaldehyde, Glutaraldehyde, Osmium tetroxide and Protein crosslinking reagents. While the effect of this process is dependent upon various factors, including the nature of chemical properties of the fixating agent, the vehicle employed for dissolving fixative and the physical conditions in the process is also important.

While preparing the samples, one of the primary considerations will be the difference between fixing and killing. Fixing is sometimes referred to as killing, although both of them are not the same. The primary choices of the fixatives are aldehyde groups, which allow the cells to respond with the fixative solutions for a significant period before death.

10.3.3 The Fixatives

The chemical fixating agents can be broadly categorized into two such as:

- Fixed by denaturation or coagulation of biological macromolecules.
- Fixed by covalent crosslinking of macromolecules.

Denaturing fixatives are exclusively useful for the Light microscope (LM) and poorly preserve the ultra-structure. Acetone, methanol, and ethanol are a few examples of these fixatives. Simultaneously, crosslinking fixatives introduce either intermolecular or intramolecular crosslinks between the macromolecules and provide excellent preservation for the ultra-structures. Formaldehyde is the most widely applicable fixative for light microscope and glutaraldehyde (GA), osmium tetroxide (OT) for SEM analysis.

Formaldehyde (FA) Formaldehyde (CH_2O), a mono-aldehyde, reacts with the amine groups resulting in the crosslinking of adjacent proteins or macromolecules. This crosslinking is based on the methylene bridge formed between two FA molecules, and consequently, these crosslinks are short and can be reversed through hydrolysis. It is very much supportive of LM, while its utility for high resolutions works is limited. SEM fixation by FA requires an additional fixation in GA. Only freshly prepared FA from paraformaldehyde powder should be used. Commercially prepared FA contains preservative methanol, and therefore not recommended.

Glutaraldehyde (GA) Glutaraldehyde ($C_5H_8O_2$), a dialdehyde, forms two intra- and inter-molecular crosslinks with proteins through the simultaneous reaction with two amine groups. GA can also form long, branched, and multivalent crosslinks of the molecule through the reaction with itself. It can introduce essentially irreversible and multiple crosslinks that convert the cells' cytoplasm into a macromolecular gel. It will snap the spaces in-between the nearby proteins. GA is the choice of fixative as it preserves the macromolecular level resolution of the fine structure and possesses high resistance of the sample against various steps involved in SEM analysis. However, it cannot fix the lipids, but GA will provide well sufficient stability

to the biological membrane to resist the extraction by using the detergents. The cells which got fixed with GA will retain their osmotic activity for some time after the fixation.

Osmium tetroxide (OT) Osmium tetroxide (OsO_4) is a popular SEM fixative that can crosslink most lipids. It can help to render their resistance against the extraction by using the organic solvents, which dehydrate the samples before drying. OT helps to preserve the biological membranes as well as make them osmotically inactive and water permeable. In Transmission Electron Microscopy (TEM) analysis of the cell sections, osmium generated two black lines parallel to each other, which indicates the lipid bilayer location. Osmication of the samples will damage the proteins and other cellular components; hence, it is not advised to use OT if an alternative option is available.

10.3.4 Protein Crosslinking Reagents

Buffers Various types of buffers can be used as the vehicle that facilitates chemical fixation, where these gentle liquid mediums will facilitate the entry of fixatives to the cellular components. They will also help to maintain the normal pH levels during the fixation of cells to maintain osmotic conditions and to avoid shrinkage or swelling. For instance, Phosphate buffer, sodium cacodylate buffer, pipes etc. can be employed.

Vapour Fixation The principle and materials used for the vapour fixation are the same as that of the chemical fixation. However, the chemical fixation is not applicable for all types of samples as sometimes the immersion in those fixating agents or fluids may damage them. For instance, fungal hyphae and conidia, their fruiting bodies may get separated from their parent plants upon touching. A drop of the fixating agent will be placed near the sample in a well-sealed container. The sample will turn black upon the fixation, and this colour change will help to detect the progress of the process. Once the sample gets fixed, it will be subjected to freezing by placing it in a metal block that is cooled by employing liquid nitrogen and freeze-dried. Post fixation performed with OT is optional, and it can be omitted as the samples with 'charging problems' may lead to the image distortion in association with this osmication.

Physical Fixation (Cryofixation) As an alternative to chemical fixatives, heating and freezing are the two phenomena employed in the physical fixation to serve the same. Both these techniques have their unique contributions to the LM. However, cryofixation or freezing is regarded as the best alternative to chemical fixation to preserve the high-resolution microscopical evaluation of the biologically fine structures.

The rapid freezing technique of the biological specimens will be stopping all the molecular motions instantaneously. A wide variety of methods are available for this

rapid freezing. The major obstacle to this method is the damage of Ice crystals. This ice crystal growth is altered following the freezing speed, the heat transfer rate of the coolant and specimen size. To neglect the ultrastructural damage to the specimen that arises from the growth of large crystals, this method is very essential. Rapid freezing can be applied to individual cells and very thin samples, but the slower freezing rate for the tissues and other thicker samples will create a very limited layer free from ice crystals. It will be of a few micrometres and located near the freezing surface or medium.

10.4 Dehydration

The complete removal of the water and organic fluids from the sample is a requisite for the SEM analysis, where it also favours the process of immobilization before the examination and analysis. The term 'Dehydration' is indicating the removal of water. As water is being the major component of biological materials, the term dehydration is applicable for removing fluids. Potentially, it is a problematic process as it leads to several concerns such as:

- Extraction of molecules present in the sample favoured by the dehydrating solvent.
- Precipitation induced with the loss of water.
- Shrinkage of the sample occurred by the loss of water.
- Crushing of the sample aroused by the interface between solvent and air.

Among these issues, shrinkage cannot be avoided as it occurs due to the loss of surrounding solvents or water from the macromolecule, making it more tightly packed together. Hence, we need to allow the samples to undergo a gradual loss of water and shrinkage instead of rapid water loss and shrinkage. In order to combat this issue, various methods were introduced such as chemical dehydration and air drying. Ethanol, methanol, and acetone are some of the most commonly used chemical dehydrating agents. For preserving the original structure of peritoneal tissues and other biological samples, acetone and ethanol were employed in the process. The process of dehydration is performed by passing the sample tissue through a series of alcohol solutions with serially increasing concentrations. The tissue blocks will be transferred to various alcohol concentrations such as 30%, 50%, 70%, 80%, 90%, and finally 100% alcohol. Finally, the sample is placed in 100% ethanol solution to ensure the complete removal of water. Ethanol will absorb water vapour from the atmosphere as it is hygroscopic. Absolute ethanol will be absolute only if the water is completely removed off from it.

Dehydration is different from drying. Tissues are not supposed to be air-dried. Dehydration is the process where the water present inside the tissues will be slowly substituted with some organic solvents. The speed of the dehydration should be adjusted in such a way as of enough speed to prevent the excessive extractions of acetone soluble compounds and alcohol and slow enough to avoid the process of

plasmolysis. It is very much difficult to control the extraction of the specimen components. Commonly carbohydrates possess very poor cross-linking followed by the fixation, and hence these low molecular weight carbohydrates were found to be susceptible in particular. Proteins prefer GA-induced crosslinking during the primary fixation, and the lipids follow OT favoured cross-linking at the time of secondary fixation. Carbohydrates are essentially unfixed. The problem associated with the extraction is shrinkage. These problems were found to be serious at a low concentration during the dehydration series. The best solution to these problems is rapid dehydration. Through dehydration with 70% alcohol, the tissues will not shrink as much, but they may begin to harden. The prolonged dehydration with higher concentrations of alcohol may transform the tissues into a quite brittle texture. For the convenience of the practical experiment conditions, if it is required to pause at any stage during the dehydration process, mostly the histologists will prefer to stop at 70–100% alcohol concentrations. If the process of plasmolysis is found to be evident, meanwhile, then additional dehydration steps should be followed. There may be chances of developing osmotic activity by the cell membranes after the short period fixation processes. However, lengthy fixations with GA are found to be responsible for reducing osmotic sensitivity, i.e. insensitive osmotic alterations may be visible after 48 hours of GA fixations.

Living tissues are most sensitive to poor dehydration, and hence they prefer to have dehydration at the temperature of a refrigerator. The dehydration process recommended for the living tissues is as follows, rinse the samples in a fume hood with fresh buffer solution free from fixative and be repeated thrice. The buffer solution is to be then replaced with the least concentration of ethanol solution as per the dehydration alcohol concentrations fixed and do not disturb that for around 20 min. Continue the process until 100% ethanol is employed for the same.

10.5 Drying

The presence of water and other fluids in the biological sample is of major concern for the SEM analysis. The process of evaporation, which in turn favouring the escape of fluids, can negatively affect the machine operations and thus it is always suggested to make sure that the specimen is dry before being placed in the chamber for analysis. Mostly the sample becomes free of water at the end of dehydration itself without undergoing the drying process. If not, the surface tension of any drying artefacts can be introduced to serve the same. Some of the other approaches to perform drying are the usage of transitional fluids, critical point drying (CPD) which is a very common method, freeze-drying (FD), employing liquid CO_2 or a series of various chemical solvents such as freon 113, hexamethyldisilane (HMDS), tetramethylsilane (TMS), and PELDRI II. Through these processes, the high surface tension forces can be reduced and consequently the specimen cells will undergo collapse and shrinkage to aid drying.

The introduction of surface tension may be a problem to the biological samples as it may disturb the surface structures via collapse and shrinkage as it can be led to the complete collapse of the hollow specimens (Fig. 10.3).

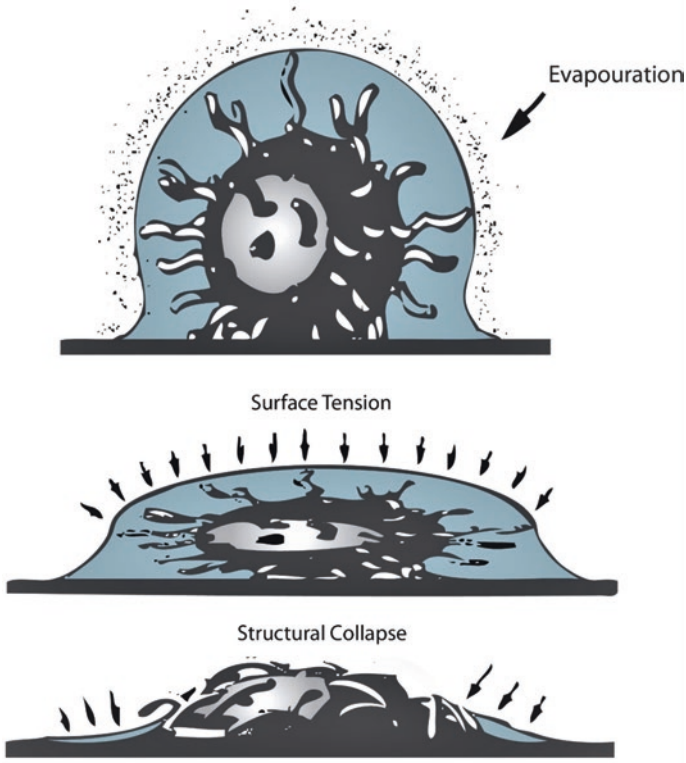

Fig. 10.3 Impact of surface tension on drying of the sample

Air Drying The water removal from the sample is initiated by drying in the air, and sometimes there may be a few problems associated with it. The water–air interface originated will be passed to the bulk from the initial surface, while the surface tension associated with it also will rise to high values. Finally, it may end up with nearly 45% shrinkage of the cell as it reaches the final phases of the air drying. This force will increase to larger figures as the drying make the cell smaller. This drastic variation in the surface tension of the specimen cell will distort the structural integrity of the soft specimen cells and create troubles for the specimens that consist of inorganic and organic solutes in the dissolved form [3, 4]. An example is illustrated in Fig. 10.4.

Critical Point Drying (CPD) Critical point drying (CPD) is a well-established drying method preferred for the biological tissues before the SEM analysis. This technique is exclusively introduced for the preparation of SEM specimens in 1970 by Polaron Ltd. It is one of the traditional approaches for processing the SEM specimen samples to avoid the shrinkage effect. Under certain conditions of pressure and temperature, a fluid will become indistinguishable from its overlying vapours. This point is termed as the critical point at which the surface tension on the specimen in

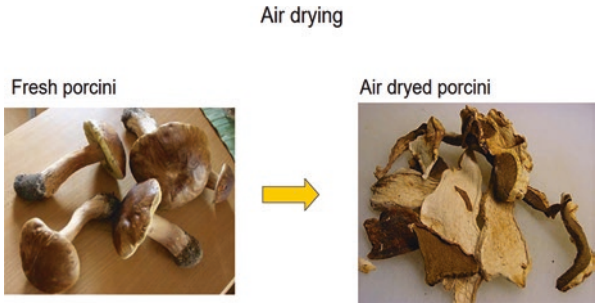

Fig. 10.4 Air drying of Porcini

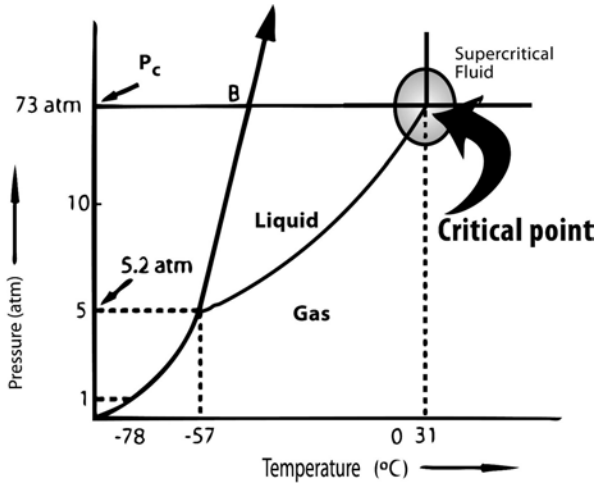

Fig. 10.5 Phase diagram

the fluid phase will become zero. This is the underlying principle of CPD. The phase diagram is depicted in Fig. 10.5.

The removal of water will become a major concern for the biological samples; however, the critical points of water is found to be inconvenient as it could damage the specimen thermally. The critical pressure point for water is 217.7 atm, and the critical temperature is +373.9946 °C. To omit these harsh conditions, a sample should be dehydrated to a point of 100% ethanol before placing it in a CPD chamber. Later the chamber will be purged with liquid CO_2 repeatedly till the ethanol present in it is completely replaced with CO_2. The chamber will then be sealed and cooled until it attains the critical point for CO_2 (31 °C and 72.8 atm).

The chamber is again heated to achieve the critical point where liquid–gas phases of CO_2 will be in equilibrium. The chamber temperature should be maintained above the critical temperature (36–38 °C) so that it can be vented out to expel CO_2 gas without allowing the re-condensation into the liquid state which produces a surface tension over the biological specimen. The venting speed should be adjusted

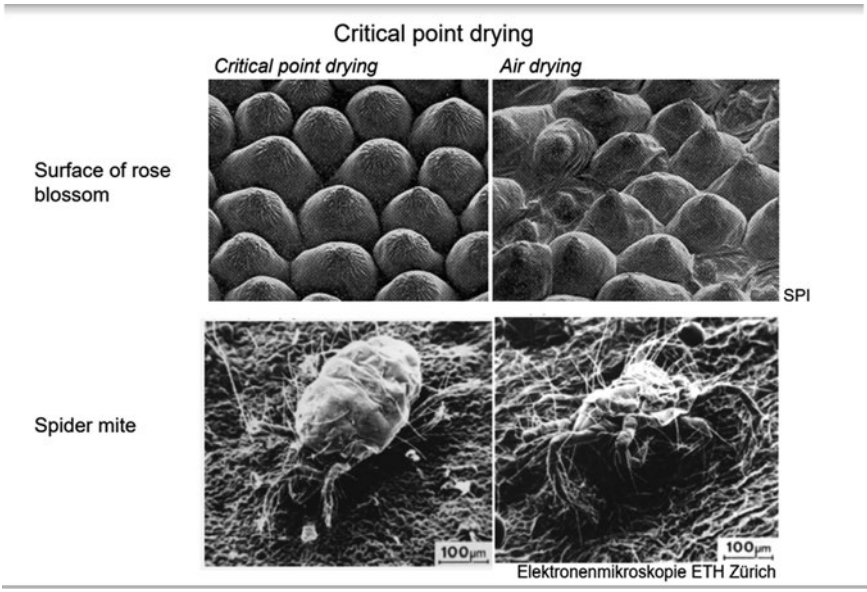

Fig. 10.6 Critical point drying of a sample

to low, and the temperature gauge should be monitored well. The exit of the gas through a small orifice or venting valve at a very high velocity will make a sudden fall or drop in temperature. If the temperature became lower than the critical point, it might lead to a rewetted surface where surface tension damages are experienced. There are chances for shrinking the specimen cells in association with the fixation and dehydration processes themselves. The further shrinkage observed due to CPD is not favourable, and hence CPD cannot be called a perfect technique (Fig. 10.6).

Freeze-Drying The fewer chances for the occurrence of shrinkage based on theoretical aspects is the attracting factor behind the introduction of the freeze-drying (FD) method. FD is identical to that of dehydration in terms of the processing schedules. Once the specimen is treated in 100% ethanol, it may be frozen in liquid nitrogen-cooled Freon TM 12 or subjected to cryofixation from its native state. The sample is placed in a pre-cooled specimen stage under a mild vacuum for a particular period. The disappearance of frost will indicate the completion of the sublimation process of the fluid present in it. Later the sample is undergoing gradual warming followed by venting. It is then mounted and examined at the earliest.

Chemical Drying Agents The need to have a capital investment in CPD or FD and the associated complications can be overcome with the utilization of chemical drying agents. The previous scientific studies showed HMDS and TMS as effective chemical agents to drying solutions. This method is a useful alternative option to the CPD for large samples which cannot fit into the CPD chamber. HMDS is not an

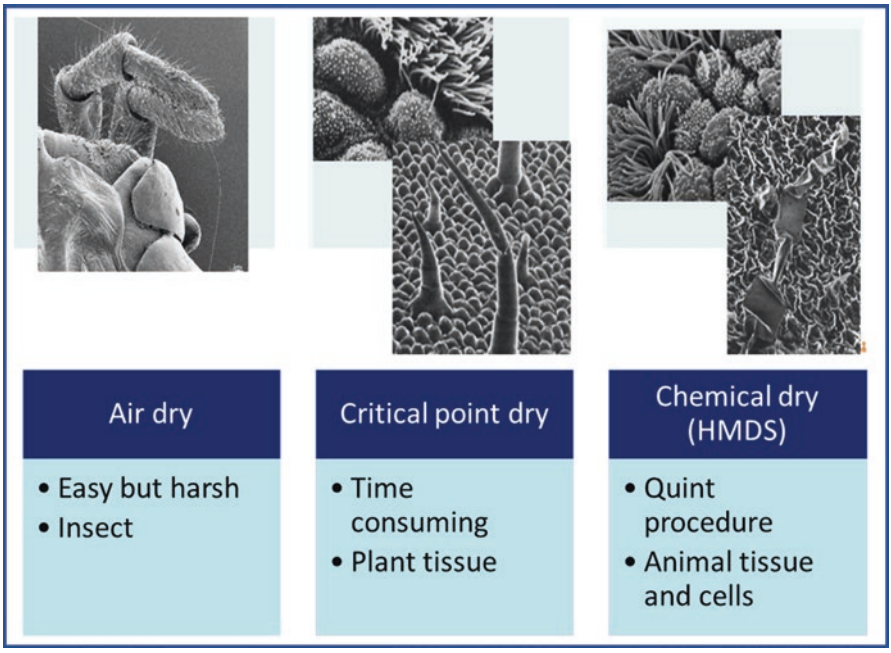

Fig. 10.7 Differences between Air dry, Critical point dry and Chemical dry methods

effective agent to induce drying in every sample; hence a trial process is required before the standard procedure. Even then, it was effective against many of the biological sample types and an economical method (Fig. 10.7).

10.6 Mounting

The samples should be mounted onto the holders for the SEM analysis, where most of the specimen holding mounts are made with brass or aluminium. Particulate samples and poly-L-lysine-coated coverslips are attached and then joined to stubs. Coverslips or the specimens were attached to the stubs with any adherent material or colloidal silver paste or paint, colloidal carbon tape or paint, and double-stick tape. Coverslips will be acting as insulators. Before being placed in the high-vacuum SEM analysis chamber, it should make sure that the pastes or paints are dried completely.

10.7 Sputter Coating or Surface Conductivity

The two major objectives of the sample coating are:

- To make electrically conductive samples while the excess electrons can be trapped by the atom and it can be drawn off to the ground.

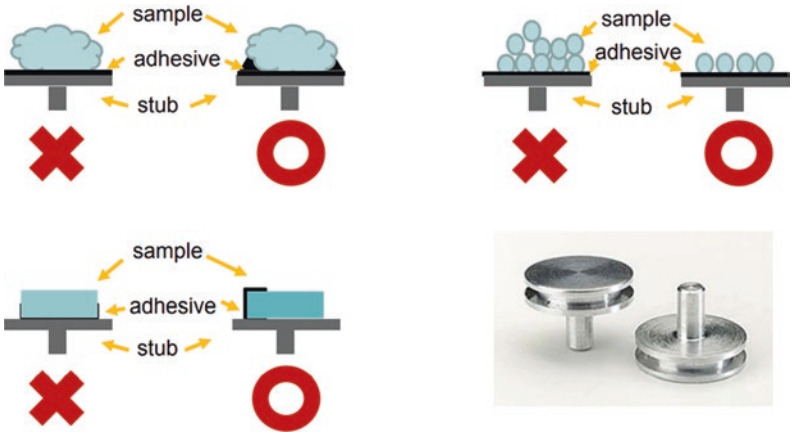

Fig. 10.8 Procedure of mounting process

- To induce the contrast to render them visible in the microscope.

Once the sample got dried, they should be then mounted onto the specimen stubs, coated, and examined at the earliest as possible. If the sample needs to be stored, it should be kept well inside the chamber to get rid of atmospheric humidity-associated problems and rehydration. The image quality of the specimen will be got affected as hygroscopic swelling of the samples may lead to the development of hairline fractures.

For the effective interpretation of the high-resolution images of the metal-coated specimens, a few major considerations are there such as the thickness of the metal coat, uniformity, and its granularity. The coating will add up material to the sample surface and thus make them thicker and larger under the microscopic view. The uniformity also will vary respectively with each of the microscopic methods. At the same time, a uniform coat is very essential to avoid electrical charges. In some cases, the granularity of the coast will distort the underlying structures and hence it should be considered during the interpretation of the image (Fig. 10.8).

To obtain a high-resolution SEM observation, it is crucial to have a thin and grain-free metal coat. Sputter coating is introduced as an alternative to solve all the problems. Sputter coating will increase these signals and contrast. Altogether, each of the steps during sample preparation for SEM analysis is found to be of significance [8].

Preparing Tissue for the SEM

- Materials Required
- Glutaraldehyde (25%) (cat# 18426 from Ted Pella).
- Osmium tetraoxide (cat#18451 from Ted Pella).
- NaH_2PO_4.

- Na_2HPO_4.
- Scintillation vials.
- Stock Solutions
  - 0.1 M phosphate buffer at pH 7.0 (200 ml).
    39 ml of 0.2 M NaH_2PO_4.
    61 ml of 0.2 M Na_2HPO_4.
    100 ml of dd water.
- Fixative Solution

Working Concentration	Amount (50 ml)	Stock Solution
25 mM Phosphate Buffer at pH 7	12.5 ml	
0.1 M Phosphate Buffer		
3% Glutaraldehyde	6.0 ml	
25% Glutaraldehyde	31.5 ml	
dd water		

Procedure

A. Fixation
   1. Prepare a fixative solution and fill the scintillation vials with a fixative agent.
   2. Cut the tissue and then place it in a tube that is filled with the fixative agent solution.
   3. Place the tissue on the sides of the tube, to keep the air away from the it.
   4. Incubate at 4 °C for 12–24 h. (Overnight is more preferable).

B. Osmium Tetroxide Step
   1. Buy 0.5 g capsules.
   2. Place 25 ml of water in a bottle.
   3. Put the capsule in a bottle and break it down with a glass pipet. This makes about a 2% solution.
   4. Keep the solution at room temperature.
   5. The solution can be stored in a cold room or freezer for about 1 month. If it is frozen, then keep it at room temperature. This solution should be straw coloured. If it is purple in colour then it indicates that the solution may be no longer good.
   6. Dilute it to 1% solution in 25 mM phosphate buffer (25 mM is the final concentration desired for PB).
   7. Pour off the fixative followed by the addition of 1% osmium tetroxide solution.
   8. Incubate it in a cold room for an overnight to several days. The osmium will turn black.

C. Dehydration of Tissue
   1. Pour off osmium solution and rinse 3 times with 25 mM PB. Be sure to put the first wash into the osmium waste.

2. Put the tissue through a series of various alcohol concentrations. Allow 15–30 min for each step. The various concentrations that can be considered as follows:

a. 30%	g. 100%
b. 50%	h. 100%
c. 65%	i. 100%
d. 75%	J. 100%
e. 89%	k. 2 more 100% soak next day
f. 95%	

The tissue can be stored in 100% alcohol permanently.

D. Critical Point Drying
   1. Put the tissue into baskets for analysis.
   2. Fix it with alcohol.
   3. Dry the specimen in the SEM facility.

References

1. Yuan J, Wang X, Zhou H, Li Y, Zhang J, Yu S et al (2020) Comparison of sample preparation techniques for inspection of leaf epidermises using light microscopy and scanning electronic microscopy. Front Plant Sci 11:133. https://doi.org/10.3389/FPLS.2020.00133/BIBTEX
2. Henini M (2000) Scanning electron microscopy: an introduction. III-Vs Review 13:40–44. https://doi.org/10.1016/S0961-1290(00)80006-X
3. Pathan AK, Bond J, Gaskin RE (2010) Sample preparation for SEM of plant surfaces. Mater Today 12:32–43. https://doi.org/10.1016/S1369-7021(10)70143-7
4. Moran P, Coats B (2012) Biological sample preparation for SEM imaging of porcine retina. Microscopy Today 20:28–31. https://doi.org/10.1017/S1551929511001374
5. Khosravi-Darani K, Pardakhty A, Honarpisheh H, Rao VSNM, Mozafari MR (2007) The role of high-resolution imaging in the evaluation of nanosystems for bioactive encapsulation and targeted nanotherapy. Micron (Oxford, England: 1993) 38:804–818. https://doi.org/10.1016/J.MICRON.2007.06.009
6. Kaech A (2013) An introduction to electron microscopy instrumentation, imaging and preparation introduction to electron microscopy table of content
7. Fischer ER, Hansen BT, Nair V, Hoyt FH, Dorward DW (2012) Scanning electron microscopy. Current protocols in microbiology, Chapter 2:Unit 2B.2.-Unit 2B.2. https://doi.org/10.1002/9780471729259.MC02B02S25
8. Barshack I, Kopolovic J, Chowers Y, Gileadi O, Vainshtein A, Zik O et al (2004) A novel method for "wet" SEM. Ultrastruct Pathol 28:29–31. https://doi.org/10.1080/01913120490275222

Index

S.-K. Kamaraj et al. (eds.), *Microscopic Techniques for the Non-Expert*,
https://doi.org/10.1007/978-3-030-99542-3